Changes of clay mineral and trace element characteristics of sinking particulate matter during transport into the Deep South China Sea

Dissertation

Zur Erlangung des Doktorgrades an der Fakultät für Mathematik, Informatik und Naturwissenschaften

Fachbereich Geowissenschaften

Universität Hamburg

vorgelegt von

Annette Schröder

geb. Heddaeus-Espenschied

aus

Hamburg

Hamburg, Mai 2015

Eidesstattliche Erklärung

Hiermit versichere ich, Annette Schröder, geboren am 02.04.1985 in Hamburg unter dem Namen Heddaeus-Espenschied, an Eides statt, dass ich die vorgelegte Dissertation mit dem Titel:

Changes of clay mineral and trace element characteristics in sinking particulate matter during transport into the Deep South China Sea

abgesehen durch die Beratung meiner Betreuer selbstständig ausgearbeitet und verfasst habe, bzw. keine anderen Quellen und Hilfsmittel als die angegebenen verwendet habe und die genutzten Quellen als solche kenntlich gemacht habe. Ich habe diese Arbeit zuvor weder gänzlich noch in Teilen einem anderen Fachbereich im In- oder Ausland im Rahmen eines Prüfungsverfahrens vorgelegt.

Hamburg, den

Annette Schröder,

geb. Heddaeus-Espenschied

Table of Contents

0. Abstract

0.1. Abstract

Clay mineral assemblages are used for over-regional weathering reconstruction, which contributes to the pressing topic of climatic change and to the question about human involvement in it. The sediments in and around the South China Sea (SCS) were carefully researched on their clay mineral properties during the last decades. Reconstruction studies are based on the sedimentary record and in order to know where the clay mineral signal came from, its provenance needs to be identified. Provenance analysis often includes several simplified assumptions about sedimentation history, contribution of various sources and alteration of particulate matter composition during transport. So far, most studies dealt with the recent clay mineral assemblages of dischargers and marine deposits, which left most of the marine trajectory of the source-to-sink transport with little observation. It is insufficiently known how particulate matter changes its composition during transport under recent conditions, which shall be the aim of this study. The observation gap was narrowed with clay mineral, geochemistry, grain size and flux data on sinking particulate matter (SPM). The samples were intercepted during the last 25 years from 1987 to 2012 by sediment trap systems, which were moored at eight stations along two trajectories parallel to the main axis of the direction of monsoonal winds across the SCS. SPM was sampled in 14- to 28- day intervals, which was tested on relative clay mineral abundances, grain size distributions and trace element concentrations. In combination with previously studied particle fluxes and main components analyses, clay mineral fluxes and specific element ratios were calculated.

Clay mineralogical and geochemical characteristics of SPM proved to be regionally divers and change down the water column. Lithogenic matter fluxes in the southwestern basin (8.5-68.5 g/m²/y) are much higher than in the northern basin (11.9-18.5 g/m²/y). Clay mineral assemblages are highly smectite enriched near Luzón (76-84%) at the northeastern margin of the SCS, illite and chlorite rich in the northern (62-64%), central (45-56%) and western (60%) basin and nearly proportional in the southwestern basin. Regional diversity and temporal variability of sinking particulate matter are high in the shallow traps and only moderate in the deep traps. Material reaching the shallow traps is mainly transported by monsoonally changing surface current. In the deep basin, a steady circulation homogenizes detrital particulate matter causing the clay mineral assemblages to homogenize. Additionally, smectite increases relatively and absolutely with depth. In the northern and central basin, higher lithogenic matter fluxes in the deep indicate lateral advection (+9-39%). This laterally advected, smectite-rich material from Luzón is suspected to be the major cause of the downward increasing relative smectite abundance (SCS-N: +26%; SCS-NC: +118%; SCS-C +41%). In the southwestern basin, strongly increased lithogenic matter fluxes also indicate lateral advection (+55-457%), but smectite enriches not nearly as much (+13-38%), because no comparably smectite-rich source exists near the southwestern basin.

Our findings on annual clay mineral abundances and fluxes show, that homogenization by deep circulation and general enrichment with smectite mask the regional clay mineral signals of the deep sea sediments. The deeper and farther offshore a sediment trap is deployed, the higher can the relative enrichment of smectite be. Accordingly, this means for the sediment below the traps, that the combination of material from different sources and differential fractionation effects may mask the riverine clay mineral signals. These masking effects augment with distance from the shore and with the variability of currents through the statistical funnel. As the statistical material collection funnel of a sediment trap widens with depth of the respective trap, so does, statistically, the transport distance of the material. With increasing transport distance SPM fractionation and enrichment with smectite get more effective.

In order to verify and specify provenance analysis results obtained by clay mineral assemblages we correlated them to additional trace element data of the same material. We compiled existing and new trace element data of important sources and analyzed the same sinking particulate matter samples on trace elements. Lanthanide patterns and specifically Europium anomalies, LREE/HREE and Zr/Sc ratios are useful to characterize material from Luzón (1.29-1.43; 0.03-0.07; 3.98-5.17), Taiwan (1.06-1.10; 0.9-1.26; 3.7-3.8/12.7-16.3), Hainan (1.43; 1.13; 7.34) and some smaller southern Vietnamese rivers (0.48-0.93; 0.48-1.07; n.d.) (Nha Trang, Dinh, Ninh Hoa and Long Song). The ratios are less useful to identify material from the larger drainage basins (Pearl River, Red River, Mekong), which discharge sediment with a similar, mixed signal from several lithologies. Trace element characteristics at stations SCS-NE, -N and -C confirm the provenance indications of clay mineral assemblages in the northern basin. SPM in the northern basin is mainly composed of material from Taiwan and Luzón. The contribution from South Chinese Rivers, to SPM could not be confirmed by trace elements. At SCS-NE and -N geochemical signals do not vary seasonally, but remain steady throughout the year. SPM reaches the deep central basin in low concentrations, with a diluted, but distinctive trace element signal of Luzón in both SPM and deep sea sediment. In the southwestern basin the major dischargers are not well distinctive, so the provenance indicator fails in this part of the basin. Only few examples of SPM with a strong negative Eu* proved that contribution of the smaller Vietnamese Rivers increases episodically at SCS-S and that the transport pathways are more variable than statistical means indicate.

Episodic contribution variations at SCS-C can only characterize changes of oceanographic conditions due to its remote location. The vertical changes of Lanthanide patterns and element ratios confirm that the cyclonic deep circulation passes between the 1200 m and 1800 m traps. Occasional variations of the Luzón signal intensity in middle and deep traps demonstrate that the circulation appears to shift up- and downwards or vary its lateral reach and intensity irregularly. Whether the negative Eu* and low LREE/HREE values at SCS-W in the Xisha trough originate from Luzón and Taiwan or Hainan Island, could not be resolved satisfactorily. The general Lanthanide distributions at SCS-W remain steady throughout the year, similar as those at the shore-near stations SCS-NE, -N and -SW. Though temporal variations of specific element ratios and relative clay mineral abundances are noteworthy, they cannot have been caused by the monsoon. At both stations, SCS-C and SCS-W, trace element ratios and clay mineral characteristic variations do not correlate, which suggests that clay minerals are not the main carriers of trace elements. At SCS-W the lack of correlation among the elemental ratios prohibits further deductions, as it can be a result of both source mixing and different fractionation during transport. Apparently, clay minerals and other carriers of trace elements are differently affected by transport processes.

Lanthanide distributions measured on SPM intercepted during 1987-1988 at SCS-N, which sampled an El Niño year, strongly resemble that of Taiwan, while during non-ENSO years 2009-2010 and 2011-2012 element distributions clearly show a mixture of SPM from Taiwan with significant contributions from Luzón. Either the availability of Luzón material is strongly reduced during El Niño years or a change in circulation causes that suspension does not reach station SCS-N. In any case, warm/normal/cool variations of the El Niño Southern Oscillation are enough to significantly alter contribution and dominant provenance of sinking particulate matter at this particular station. The periods are too short to leave an impact on the sediment, which resembles the signal of SPM during normal conditions, only in higher concentrations. But for longer phased warm/cold variations, like glaciation events, the impact could be enough to provide variations in the sedimentary record.

Concluding, we find that seasonal variations are limited to lithogenic matter fluxes, while relative clay mineral assemblages display only locally (SCS-SW, SCS-S) significant fluctuations that could be related to monsoonal changes. Whether these fluctuations are related to changes in weathering, discharge

rates or monsoonal surface current reversals, however, remains unresolved. At most stations (SCS-NE, SCS-N, SCS-W, SCS-NC, SCS-C, SCS-SC) changes of relative clay mineral abundances cannot be related to seasonal variations of weathering, even at the shallow traps. Despite previous assumptions, the most important mechanism determining SPM's clay mineral characteristics appears to be deep current activity, which controls both contribution and differential settling. However, trace element characteristics show, that these can vary interannually and episodically. These can indeed reflect climatic warm/cold conditions like the short-scaled ENSO, but it should be expected, that these refer mostly to changes of the marine environment rather than the terrestrial environmental changes.

0.2. Zusammenfassung

Die Zusammensetzung von Tonmineralvergesellschaftungen findet Anwendung in der überregionalen Rekonstruktion der Silikatverwitterung, die zum besseren Verständnis des Klimawandels und der Rolle des Menschen in ihm beitragen. Die Sedimente des Südchinesischen Meeres und dessen Lieferanten wurden innerhalb der letzten Jahrzehnte sorgfältig auf ihre Tonmineral-Vergesellschaftungen untersucht. Die vorherigen Studien basierten auf Analysen der Sedimentabfolge und beinhalteten häufig einige vereinfachte Annahmen über die Sedimentationsgeschichte, einschließlich der Sedimentprovenanz, das Zusammenspiel verschiedener Quellen und die Veränderung der Zusammensetzung des partikulären Materials durch sortierende Transportmechanismen. Bislang haben sich die Studien mit den Tonmineralzusammensetzungen der Lieferanten und denen der marinen Ablagerungen beschäftigt, was nur wenig Beobachtungen über den gesamten „source-to-sink" Transportweg zulässt. Es ist nur unzureichend bekannt, wie partikuläres Material rezent seine Zusammensetzung während des Transportes verändert. Ziel dieser Arbeit ist, die Beobachtungslücke mit Daten zu Tonmineralvergesellschaftungen, Geochemie, Korngrößen und Partikelflüssen von partikulären Sinkstoffen zu verschmälern. Die Proben wurde während der letzten 25 Jahre, von 1987 bis 2012, mit der Hilfe von Sedimentfallensystemen aufgefangen, die an acht Stationen entlang zweier Geraden parallel zur Hauptachse der monsunalen Winde über das Südchinesische Meer ausgesetzt wurden.

Charakteristika der Tonmineralzusammensetzung und Geochemie der partikulären Sinkstoffe erwiesen sich als regional spezifisch und veränderlich mit der Wassertiefe. Lithogene Partikelflüsse im südwestlichen Becken (8.5-68.5 g/m²/y) sind weit höher als die im nördlichen Becken (11.9-18.5 g/m²/y). Tonmineral-Vergesellschaftungen sind sehr smektitreich nahe Luzón (76-84%) am nordöstlichen Schelfrand, illit- und chloritreich im nördlichen (62-64%), zentralen (45-56%) und westlichen (60%) Becken, während die Verhältnisse im südwestlichen Becken nahezu ausgeglichen sind. Regionale Diversität und zeitliche Variabilität von partikulären Sinkstoffen sind in den oberen Fallen hoch und in den tiefen Fallen moderat. Material, dass die oberen Fallen erreicht ist mehr von den monsunalen Oberflächenströmungswechseln beeinflusst. Im Tiefseebecken homogenisiert eine stetige Zirkulation das detritische partikuläre Material, was dazu führt, dass die Tonmineralvergesellschaftungen nahezu uniform werden. Zusätzlich reichert sich Smektit mit zunehmender Tiefe relativ und absolut an. Im nördlichen und zentralen Becken weisen höhere Lithogen-Partikelflüsse in der Tiefsee (+9-39%) auf laterale Advektion hin. Das lateral advektierte, smektitreiche Material von Luzón wird als die Hauptursache für abwärts ansteigende Smektitgehalte vermutet (SCS-N: +26%; SCS-NC: +118%; SCS-C +41%). Im südwestlichen Becken steigen die Lithogenflüsse ebenfalls stark an (+55-457%); der Smektitanteil weist hingegen einen nicht annähernd so starken Anstieg auf (+13-38%), vermutlich, weil es keine vergleichbar smektitreiche Quelle im Einzugsbereich des südwestlichen Beckens existiert.

Unsere Erkenntnisse über mittlere jährliche Tonmineralvergesellschaftungen und -flüsse zeigen, dass die Homogenisierung durch die Tiefseezirkulation und die generelle Anreicherung mit Smektit das regionale Signal sowohl der partikulären Sinkstoffe als auch der Tiefseesedimente maskiert. Da sich der statistische Materialeinzugtrichter einer Sedimentfalle weitet, je tiefer die jeweilige Falle positioniert ist, vergrößert sich auch die statistisch mögliche Transportdistanz des Materials. Deswegen kann die relative Anreicherung des Materials mit Smektit in Sedimentfallen, die in größerer Wassertiefe und weiter entfernt von der Küste ausgesetzt wurden, besonders hoch sein. Entsprechend bedeutet das für die unter der Sedimentfalle gelegenen Tiefseesedimente, dass das ursprüngliche, flussspezifische Tonmineralsignal durch die Vermischung unterschiedlicher Materialien aus verschiedenen Liefergebieten und den Auswirkungen der gravitativen Sortierung

durch differenziertes Absinken maskiert wird. Der Grad der Maskierung steigt mit Distanz zur Küste und mit der Variabilität der Strömungen innerhalb des statistischen Materialeinzugstrichters.

Im Bestreben die Ergebnisse der vorangegangenen Provenanz-Analysen zu verifizieren und zu präzisieren wurden dieselben Proben mit zusätzlichen Spurenelementdaten korreliert. Die Gesamtverteilung der normalisierten Lanthanid-Konzentrationen, insbesondere Europium-Anomalien, LREE/HREE und Zr/Sc Verhältnisse erwiesen sich als nützliche Indikatoren um Material von Luzón (1.29-1.43; 0.03-0.07; 3.98-5.17), Taiwan (1.06-1.10; 0.9-1.26; 3.7-3.8/12.7-16.3), Hainan (1.43; 1.13; 7.34) und einiger geringerer vietnamesischer Küstenflüsse (0.48-0.93; 0.48-1.07; n.d.) (Nha Trang, Dinh, Ninh Hoa und Long Song) voneinander zu unterscheiden. Sie sind weniger nützlich um Material der großen Materialeinzugsgebiete (Pearl River, Red River, Mekong) zu unterschieden, deren Sedimente ein ähnliches, gemischtes Spurenelement-Signal verschiedener primärer Lithologien liefern. Spurenelementanalysen am Material der Stationen SCS-NE, -N, und -C bestätigen die Provenanzindikationen durch die Tonmineralvergesellschaftungen im nördlichen Becken. Die partikulären Sinkstoffe setzen sich hauptsächlich aus Material von Taiwan und Luzón zusammen. Die Zufuhr von Materialien südchinesischer Flüsse einschließlich des Pearl Rivers konnte über diese Methoden nicht bestätigt werden. An den Stationen SCS-NE und -N konnten keine saisonalen Veränderungen des geochemischen Signals festgestellt werden, stattdessen bleiben sie über das ganze Jahr hinweg konstant. Die Tiefsee erreichen partikuläre Sinkstoffe in niedrigen (Partikel-) Konzentrationen mit einem verdünnten, aber erkennbaren Spurenelement-Signal von Luzón, das sich auch im Sediment wiederspiegelt. Im südwestlichen Becken können die Hauptlieferanten nicht ausreichend voneinander unterschieden werden, weswegen auch Provenanzindikatoren durch Spurenelemente in dieser Region versagen. Lediglich während weniger Intervalle konnte ein verändertes Spurenelementsignal nachgewiesen werden, dessen intensive negative Europium-Anomalien auf episodisch (relativ) erhöhte Zufuhr von den vietnamesischen Küstenflüssen hindeutet und damit zeigt, dass die marinen Transportwege veränderlicher sind, als die Mittelwerte vermuten lassen.

Episodische Veränderungen der Beteiligung verschiedener Quellen zur Falle SCS-C können wegen seiner entlegenen Position nur Veränderungen der ozeanographischen Bedingungen charakterisieren. Die vertikalen Veränderungen in der Lanthaniden Verteilung und Element-Verhältnisse bestätigen, dass die zyklonale Tiefenzirkulation zwischen den Fallen in 1200 m und 1800 m passieren muss. Gelegentliche Variationen der Intensität des Luzónsignals in der mittleren und tiefen Falle zeigen an, dass sich die Zirkulation in unregelmäßigen Zeitabständen auf- und abwärts verlagern kann oder ihre laterale Reichweite und Intensität verändert. Ob die negative Europium Anomalie und niedrigen LREE/HREE Werte in SCS-W im Xisha Trog von Luzón oder Hainan abstammen, konnte nicht zufriedenstellend gelöst werden. Wie auch bei den anderen küstennahen Fallen SCS-NE, -N und -SW bleibt die Verteilung der Lanthaniden auch an Falle SCS-W über das ganze Jahr hinweg ähnlich. Obwohl es eine bemerkenswerte zeitliche Variabilität der spezifischen Elementverhältnisse und relativen Tonmineralvergesellschaftungen gibt, sind diese vom Monsun unabhängig. An beiden Stationen, SCS-C und SCS-W, korrelieren Spurenelementverhältnisse und Tonmineralcharakteristika nicht miteinander, was nahelegt, dass die Tonminerale nicht die Hauptträger der Spurenelemente sind. Die fehlende Korrelation der Elementverhältnisse zueinander an Falle SCS-W verbietet weitere Schlussfolgerungen, da sie sowohl ein Ergebnis vom Mischverhältnis verschiedener Quellen als auch von verschiedenen Fraktionierungsprozessen während des Transports sein können. Dies legt nahe, dass Tonminerale und weitere Träger von Spurenelementen unterschiedlich stark von Transportprozessen beeinträchtigt werden.

Lanthanidenverteilungen aus Sinkstoffen, die 1987-1988 während eines El Niño Jahres, beprobt wurden, ähneln stark denen der Sedimente von Taiwan, während die des Materials, das zwischen

2009-2010 und 2011-2012 während nicht-ENSO Jahren beprobt wurde, eine Mischung taiwanesischem Material mit bedeutendem Eintrag von Luzón zeigt. Entweder die Verfügbarkeit des Materials von Luzón ist während El Niño Jahren deutlich reduziert oder eine Veränderung der Zirkulation bewirkt, dass jene Suspension die Fallen an Station SCS-N nicht erreichen kann. In jedem Fall genügen die Veränderungen durch den warm/normal/kalt Wechsel der ENSO an dieser besonderen Station, um die Beteiligung der dominanten Sedimentquellen von partikulären Sinkstoffen bedeutend zu verändern. Allerdings sind die Phasen zu kurz um das El Niño Signal im marinen Sediment unter der Falle zu hinterlassen, welches das Signal der Sinkstoffe während der normalen Bedingungen wiederspiegelt, nur höher konzentriert. Für grob-skaligere warm/kalt Veränderungen, wie durch Vereisungszyklen, können die Auswirkungen stark genug sein um als Variationen in der Sedimentabfolge erkennbar zu werden.

Insgesamt konnten feststellt werden, dass sich die saisonalen Schwankungen auf die lithogenen Partikelflüsse beschränken, während Fluktuationen der Tonmineralvergesellschaftungen nur lokal (SCS-SW, SCS-S) im Zusammenhang mit dem Monsun stehen. Ob diese Fluktuationen in Verbindung mit Veränderungen der Verwitterung, Abflussraten oder monsunalen Oberflächenströmungsveränderungen stehen, bleibt jedoch ungelöst. Die Veränderungen der Tonmineralzusammensetzungen an den meisten Stationen (SCS-NE, SCS-N, SCS-W, SCS-NC, SCS-C, SCS-SC) kann nicht einmal in den oberen Fallen auf saisonalen Änderungen der Verwitterung im Liefergebiet zurückgeführt werden. Der ausschlaggebende Mechanismus, der die Tonmineralcharakteristika in Sinkstoffen bestimmt scheinen die Tiefseeströmungsverhältnisse zu sein, die sowohl die Beteiligung verschiedener Quellen als auch das fraktionierte Absinken steuert. Allerdings zeigen Abweichungen der Spurenelementverteilungen, dass sich diese Mechanismen interannuell und episodisch verändern können. Diese können tatsächlich warm/kalt Veränderungen des Klimas, wie durch kurz-skalige El Niño Ereignisse, anzeigen, aber es kann angenommen werden, dass sie sich eher auf Veränderungen des marinen, anstatt die des terrestrischen Milieus beziehen.

1. Introduction – From source to sink

Silicate weathering is one of the most important anorganic processes to remove CO_2 from the atmosphere. It is the reaction of fresh water and dissolved HCO_2^- with silicate minerals. Warm climate and high precipitation rates support the reaction and its durable products are clay minerals. These mineralize in soils, erode and get transported to a final sink, either lacustrine or marine, where they will form part of a sediment. Cores from these sediments can be studied for their clay mineral assemblages, which are the relative abundances of the four major clay mineral classes smectite, illite, chlorite and kaolinite, in order to reconstruct chemical weathering (Boulay et al., 2007; Colin et al., 2010; Liu et al., 2005; Trentesaux et al., 2003; H. Wang et al., 2011; Zhao et al., 2011).

Clay mineral assemblages of marine sedimentary records are also used for source identification of multiple dischargers (Gingele and De Deckker, 2004; Honjo et al., 1982; Khim and Park, 1992; Liu et al., 2014; Petschick et al., 1996; Xu et al., 2009), for sea level change reconstructions (Steinke et al., 2008) and as tracers for current routes (Fagel et al., 1997; Gingele et al., 2001). All of these studies interpret variations of the clay mineral record differently, but all are related to sediment transport in the marine environment. So, what are the dominant mechanisms to affect sedimentary composition during marine transport? Are these regionally different? Do they mask the desired weathering signal?

When sediment and suspension leave the turbulent riverine stream, they carry drainage basin specific clay mineral assemblages (Griffin et al., 1968) and trace element signatures (Piper, 1974). But already within the estuary, calming current velocity and salinity changes cause flocculation (Asper, 1987; Eisma, 1986; Kranck, 1973) and differential settling among clay minerals. Result of and proof for differential settling by flocculation is sediment zonation around estuaries (Gibbs 1977, Porrenga, 1966). Part of the material remains suspended; another part settles and forms transitory shelf sediments or bedload. Both fan up in the water column while they continue the journey across the shelves and into the deep sea in different compositions, at different velocities (McCave et al., 1995). Fine grained particles, floccs and aggregates of low density remain in the surface waters, while larger or denser particles, aggregates and floccs descend into the deeper strata and concentrate on thermohaline barriers, forming nepheloid layers. Occasionally, shelf sediments slide off the margin top, turn into gravity currents, rework slope sediments and get transported into the deep basin quickly.

The outgoing suspension is scavenged by plankton, transformed into feacal pellets (Honjo et al., 1982) or clusters abiogenically to aggregates (Alldredge & Silver, 1988; Asper et al., 1990; Pryor, 1975; Syvitski, 1980). Without the formation of floccs or fecal pellets, clay sized minerals would probably not sink through the thermohaline boundary layer (Honjo, 1980). Particles trapped in the upper layer enrich in suspension until vertical transport initiates after seasonal planktonic blooms, which adds seasonal flux peaks to the "background flux" of directly sinking particulate matter. Vertical transport was proven to be comparatively fast (Honjo, 1980; Wiesner et al., 1996). The altered drainage basin specific clay mineral assemblages are preserved within feacal pellets and aggregates until being deposited or breaking up again (Eisma, 1986). When aggregates decay, finer and individual particles are exposed to differential settling again, this time controlled by lateral transport at current velocities below 6 mph (Whitehouse et al., 1960; around 270 cm/sec), which depends then upon particle and sea water densities, surface charge and buoyancy of the minerals.

Sediments that are transported into the deep sea basin by gravity current have a different composition than the initial riverine suspended matter and re-work sediments of shelf margin and slope during their descent. During the slowdown of transport velocity in the deep sea plain, differential settling gets more effective again, which again produces mineral gradation. Also upwelling, which transports upward close to the slopes, re-suspend sediment and result in the

continuation of its transport. Part of the re-suspended sediments follows conturites, which carry material along the slope (vertical to the plane in Figure 1) and advect suspension laterally. Lateral advection contributes significantly to re-distribution of material (Honjo et al., 1982) and mixing with material from other, far away sediment sources. Eventually, all these differently transported materials, of different age and origin reunite and mix to form permanent deep sea sediments. So, the determining mechanisms to control clay mineral assemblages of marine sediments are dependent on transport mechanisms and they depend on the regional sedimentary basin morphology, on oceanographic currents, on number and characteristics of the sediment suppliers.

So what happens to the silicate weathering signal? How are clay mineral assemblages and sediment composition in general affected by all those transport mechanisms?
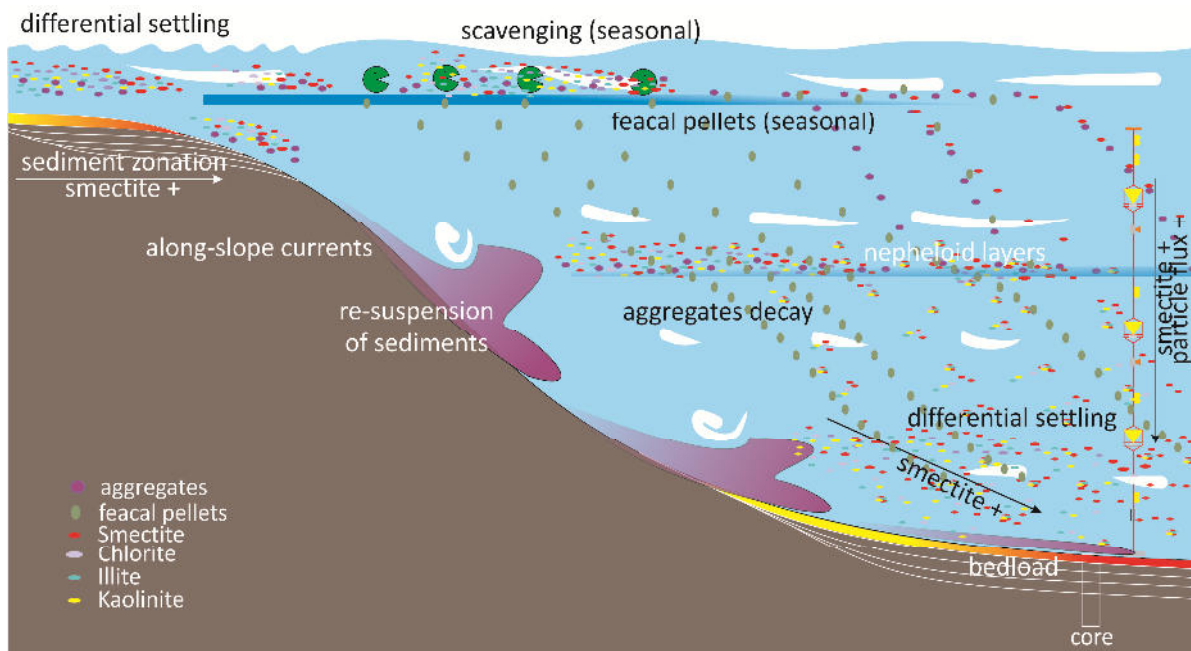
Figure 1: Processes during marine transport of particulate matter into the deep sea.

1.1. Research gaps and objectives

The sediments of and around the South China Sea (SCS) are particularly well-studied. They were cored and surface-sampled in high resolution during the last decade for various research aims, including weathering (Boulay et al., 2005; Liu et al., 2010; Liu et al., 2003; Liu et al., 2007), sea level (Steinke et al., 2008) and circulation reconstructions (Liu et al., 2013; Liu et al., 2010). As the SCS receives its sediments from many dischargers of very different climatic and geologic environments, the source identification and estimation of contribution from various sources are important factors to interpret the sedimentary record (Liu et al. 2013, Liu et al. 2010). These questions were approached by mapping clay mineralogical and geochemical characteristics of recent surface sediments of drainage basins, shelves, shelf slopes and the deep sea (Liu et al., 2013). Then, the sediment's provenance regions were identified by end-member modelling under the assumption that clay mineral assemblages do not change significantly during transport.

This study intends to close the observational gap between estuaries and final deposition using clay mineralogical and geochemical (REE) data obtained from sinking particulate matter collected by sediment traps to find out: **How does particulate matter distribute in the SCS? Which mechanisms**

have the most significant effect on sedimentary composition? How does particulate matter change its composition during transport? Are there spatial and temporal variations of these mechanisms?

1.2. Genesis and properties of clay minerals

Clay minerals are one of the most diverse mineral classes. They are part of the phyllosilicates, which have a layered crystalline structure in common and occur in sediments and sedimentary rocks. They can consist of an octahedral layer (eight oxygen-ions positioned around one Al^{3+}-, Mg^{2+}-, Fe^{2+}- or Fe^{3+}-cation) a tetrahedral layer (four O-ions around one Si^{4+}-, Al^{3+}- or Fe^{3+}-cation) and an interlayer (various alkaline cations and H_2O molecules). Clay mineral classes are defined by their sequence of layers. Among them, further subdivisions are defined by geochemical substitutions. In this study we applied the nomenclature used by Chamley (1989) (Figure 2):

Chlorites are composed of one octahedral layer sandwiched between one tetrahedral layer and another octahedral sheet, separated from them by a hydroxyl-filled interlayer. They are very regularly crystallized and only rarely include substituted cations, so their crystal cell thickness ranges very little around 14 Å. Chlorites are primary minerals, eroded from magmatic or metamorphic rocks or secondary minerals of a weak weathering degree (bisialitization). **Illites** are fine grained micas. They can be primary minerals or weakly weathered secondary minerals. They are composed of two tetrahedral layers with one octahedral layer and a slim interlayer which can absorb interlayer cations. Their crystallinity and cell-thickness (10 Å) are consistent. Illites are comparatively resistant to chemical weathering. **Smectites** are mostly secondary minerals, which consist of two octahedral, one tetrahedral and one hydrated interlayer. They substitute cations of the octahedral and tetrahedral layers and are able to absorb water and cations into the interlayer. Smectites are the chemically most variable group; therefore the cell thickness is also variable between 14 Å and 17 Å. Generally they result from incomplete hydrolysis (bisialitization). **Kaolinites** are well defined clay minerals, by only one octahedral and one tetrahedral layer, without any interlayer and nearly no substituting cations. The cell thickness is 7 Å with little variation. They appear mostly as secondary minerals and are of a higher weathering degree than smectite (monosialitization).
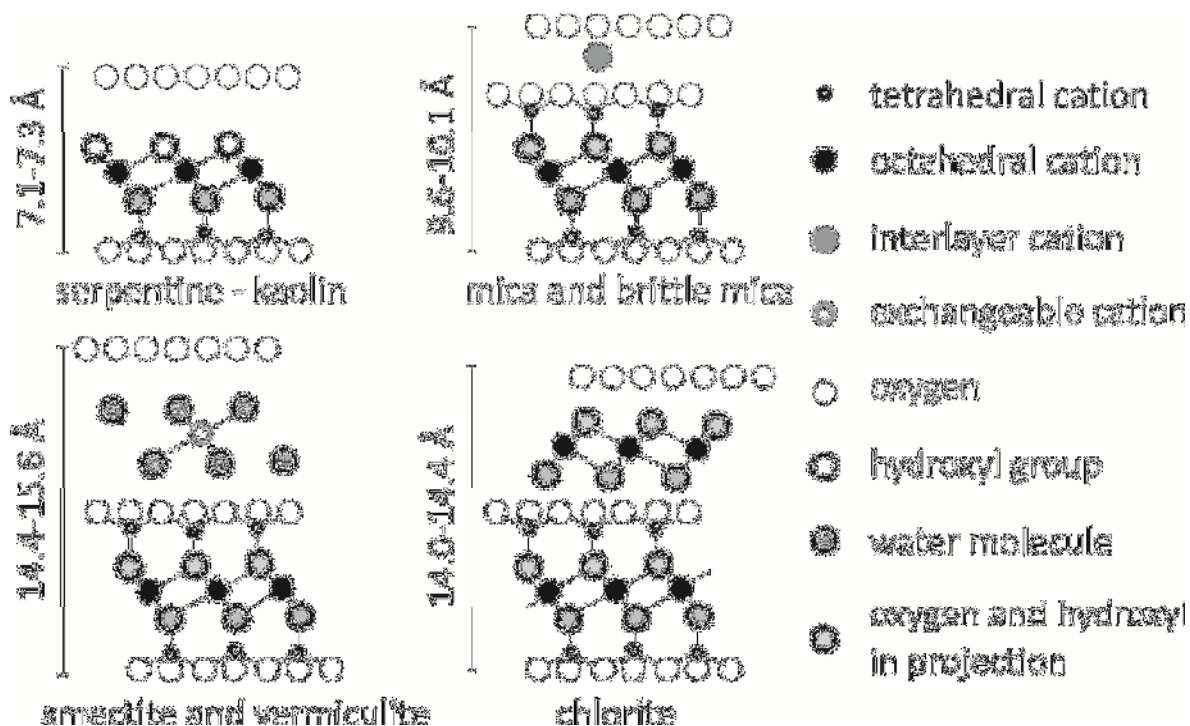
Figure 2: Molecular crystal grids of kaolinites, illites, smectites and chlorites (after Bailey, 1980**).**

1.2.1. Genesis

Secondary clay minerals form through silicate weathering. They are the product of the reaction of primary minerals, i. e. minerals that crystallize from the magmatic melt, with a cation depleted, often acidic 'attack solution', which desorbs cations and re-structures the silicates' crystal grids. This process is called hydrolysis or acidolysis and takes place in the deeper soil horizons (Chamley, 1989; Scheffer et al., 1982). Which clay mineral results, depends upon the degree of chemical weathering, morphology of the drainage basin and parental lithology (Griffin et al., 1968; Liu et al., 2012).

The degree of weathering is favorably increased by high temperatures, changing wet and dry seasons and fine particle size. It improves with increasing physical erosion rates, which are higher in regions of high relief and steep morphology. Good permeability of rock and soil, moderate to high pore-water circulation velocity, presence of organic acids, microbial activity and a low cation saturation of the pore water improve the effect of chemical weathering. The affinity for weathering of the parental rocks depends on their mineralogy. The sequence of leaching abilities of minerals is analogous with the magmatic crystallization sequence (Berner, 1971):

Olivine → Pyroxenes → Amphiboles →Biotites

Ca- → Na-Feldspars (Plagioclases)→ K-Feldspars → Muscovite →Quartz

Kaolinite is a pure aluminosilicate, which results from nearly complete weathering of silicates and leaching of surplus cations. The complete leaching is restricted to warm, humid, well flushed and terrestrial environments. They are associated to tropical weathering and only occur in low latitudes. Smectites are a product of incomplete weathering and are associated to volcanic rocks at all latitudes as well as changing arid and humid conditions. Chlorites and illites are the main clay minerals in cold and arid climates, especially at high latitudes and deserts.

Therefore, enrichment of clayey sediments with kaolinite and smectite most certainly derive from drainage basins in warm and humid, tropical to subtropical environment. If smectite is highly abundant, it may have weathered from volcanic rocks. A high ratio between smectite or kaolinite and chlorite + illite indicates a warmer and well flushed environment of the sediment provenance region, where silicate weathering was intense (Colin et al., 2010). The duration needed for a drainage basin specific clay mineralogical signal to be formed depends upon lithology, morphology, size of the drainage basin, water supply, exposure of fresh rock (including anthropogenic activity) and soil formation. It was estimated that the formation of a significant climatic clay mineral signal requires one to two million years (Thiry, 2000).

During terrestrial weathering, clay minerals can re-mineralize from one another. Remineralization is an advanced stage of cation depletion, which sequentially affects the layer structure (Figure 3). First to leach are cations of the interlayers, which are bound only by hydrogen bonds or electrochemical attraction. They can be replaced by other cations with the same charge and similar ionic radii or left vacant, which makes the crystal grid unstable and prone to ad- and desorption. Once the intermediate layer is removed completely, cations from the octahedral sheet get leached, which are held by ionic bonds within the center of the octahedra. First elements to desorb are substitution cations, Al^{3+} and Si^{4+} are leached last. The completion of this leaching step results in pure, substitution-free octahedral and tetrahedral layers and the transformation into kaolinite (kaolinitization). Thirdly, the silicate cations get leached from the tetrahedral sheets resulting in the pure aluminosilicate mineral gibbsite (Chamley, 1989; Millot, 1967).

During erosion, clay minerals pass through different environments and, depending of the drainage basin, are exposed to different attack solutions, which can slow down or accelerate re-mineralization through desorption. However, the saturation gradient between weathered minerals and attack

solution is not high enough for adsorption of cations into the crystal grid. Frequently mentioned chloritization or illitization, which requires the re-establishment of interlayers into the layer stack, is restricted to diagenetic processes and usually does not occur in normal fluvial, estuarine or marine environments (Chamley, 1989).
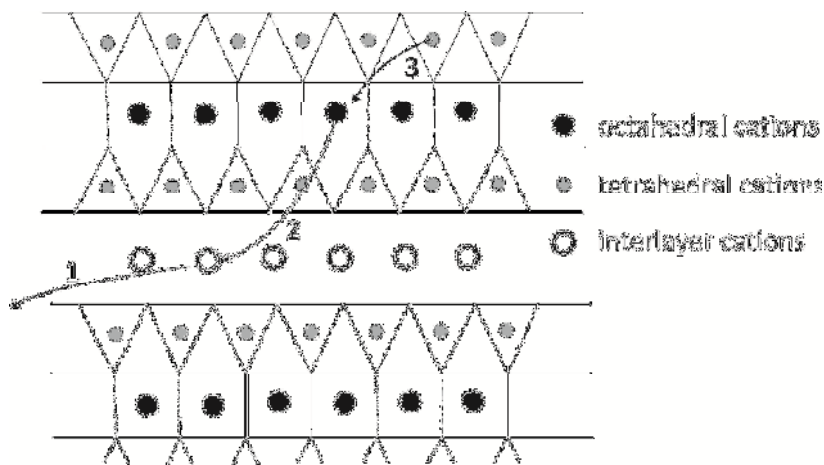
Figure 3: Leaching sequence of cations from clay minerals: 1- from the interlayer, 2 from the Octahedral sheet via the interlayer, 3 - from the tetrahedral layer via octahedral and interlayer (from (Chamley, 1989 after Millot, 1967)**.**

1.2.2. Properties of clay minerals and behavior during transport

Clay minerals develop with different ranges of grain size. As clay minerals' grain size strongly depends on size, weatherability and chemistry of the parental minerals, regional variations of the grain size spectra should be expected. The only study published about clay mineral grain sizes identified smectites (montmorillonite) to achieve the finest grain size (1.9 µm-0.2 µm), followed by kaolinite (10 µm-0.4 µm). Chlorite and illite (mica) have a broad and partly coarser range (100 µm-0.4 µm) (Figure 4) (Gibbs, 1977). Additionally, smectite (montmorillonite) has a significantly lower specific, hydrated density (1.40 g/cm³) than kaolinite (2.60 g/cm³), illite (2.72 g/cm³) and chlorite (2.94 g/cm³) (Osipov, 2012), mostly because smectites are the only minerals able to absorb water molecules into their interlayer (Figure 2).
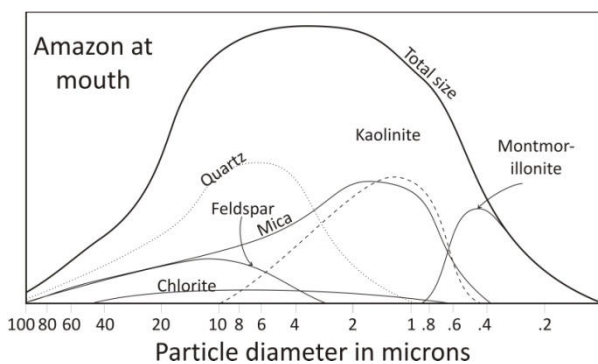
Figure 4: Grain size spectra of various clay minerals from Amazon River sediments show, that smectite and kaolinite develop finer grains than chlorite and illite (Gibbs, 1977).

All these differences among the clay mineral classes affect their dynamic behavior: As individual specimens, fastest clay mineral to sink in an immobile, marine environment are illite and chlorite with 15.8 m/d, second is kaolinite with 11.8 m/d and slowest to settle are smectites (which were classified as montmorillonites) with 1.3 m/d (Whitehouse et al., 1960). Furthermore, finer grained specimens flocculate preferentially in the estuary (Kranck, 1973), which results in coarser and dense kaolinite-rich floccs and coarser but lighter smectite-riche floccs. Accordingly, kaolinite, illite and chlorite settle faster than smectite, which has a tendency to enrich in suspension, which is

documented in clay mineral zonation around estuaries (Gibbs, 1977; Porrenga, 1966) (Figure 5). In lateral transport at velocities below 6 mph (9.7 km/h; 268 cm/sec) differential fractionation among clay minerals was observed (Whitehouse et al., 1960).
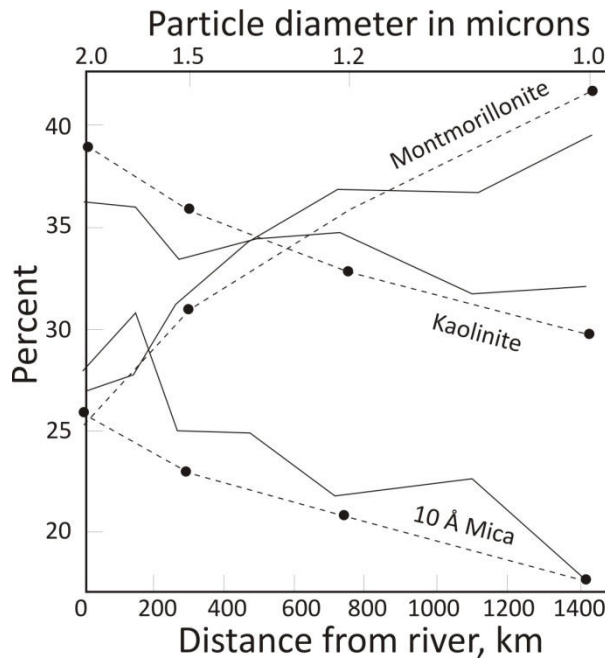
Figure 5: Clay mineral zonation around the Amazon River is proof of differential settling in suspension during transport across the shelves (Gibbs, 1977).

1.3. Chemical alterations in clay minerals

The trace element concentration and fractionation in clay minerals depend mainly upon the parental lithology. They are substituted into primary minerals during crystallization from magma (Okrusch and Matthes, 2009; Stosch, 2000) and depend on its chemical composition and origin. Silicate minerals are prone to substitute Ca^{2+} and Na^{2+} (and subordinately also Mg^{2+}, Fe^{2+} and Al^{2+}) with trivalent REE. Mafic minerals (especially Garnet (Grt), Orthopyroxene (Opx), Clinopyroxene (Cpx) and Amphibole (Amp)) absorb more HREE from the melt, so mafic minerals are enriched with them. These minerals spurn substitution with Eu^{2+}, which results in a strong (Grt) to weak (Opx, Cpx and Amp) negative Eu* (Okrusch and Matthes, 2009). Plagioclase and other Feldspars are the main felsic minerals that preferentially substitute LREE and especially Eu^{4+} as interspace cations (Stosch, 2000) (**Fehler! Verweisquelle konnte nicht gefunden werden.**). Other felsic minerals, especially micas and quartz, which are an abundant component of most acidic rocks, substitute cations with REE less frequently, mainly because the magma is already depleted with REE and especially HREE during the last stages of crystallization.

Generally, **mafic/basic plutonites** can be expected to contain higher concentrations of REE and are enriched with HREE, whereas felsic/acidic rocks contain a low REE concentration and are enriched with LREE. With increasing contents of plagioclase in mafic rocks an increasingly positive Eu* is to be expected. The later crystallizing **felsic plutonite** must then be depleted with Eu. Due to fast crystallization, **volcanic rocks** do not suffer fractionation (Stosch, 2000). Therefore they reflect the initial REE compositions of the magma. Generally, magma from the upper crust sports a negative Eu* and enrichment with LREE; magma from the lower crust a positive Eu* and also slight enrichment with LREE. Middle Oceanic Ridge Basalt magma from the mantle have no Eu* and a low LREE/HREE ratio, opposed to Ocean Island Basalts magma from the mantel-core boundary, that contain more

LREE than HREE (Stosch, 2000). **Sedimentary rocks** contain variable REE concentrations and patterns, which again depend upon the origin of the primary lithology from which they were eroded. Several accessory and main minerals like garnet, apatite, zircon and monazite enrich in sedimentary rocks. They are very resistant to weathering, contain high REE concentrations and specific Lanthanide distributions (Okrusch and Matthes, 2009). Nevertheless, drainage basins that drain vast sedimentary bodies will always produce a weak and mixed REE signal.

During hydrolysis, primary minerals are leached of their cations, including REE. Fresh waters' pH is neutral to acid and depleted of cations, which are characteristics of an efficient attack-solution to desorb cations from parent and clay minerals. The mobility of cations decreases with increasing ionic radius, which means that K^+, Na^{2+}, Mg^{2+}, Fe^{2+}, Fe^{3+} and Al^{3+} desorb faster than REE-cations. The latter are preserved comparatively well in the interlayer and octahedral layers of the resulting secondary clay minerals (Chamley, 1989). Only when the main elements are desorbed, REE get leached from the interlayer of smectite and chlorites and even from the octahedral layers during higher stages of hydrolysis (Figure 3).

Figure 6: Mafic minerals preferentially substitute HREE into their crystal grids, which results in sequential depletion of HREE in the melt and fractionated Lanthanide distributions in the rock-forming minerals. Plagioclase is the only mineral to enrich with Eu (Rollinson, 1993)**.**

Kaolinites result from intense hydrolysis and are therefore desorbed of nearly all their cations including REE. There are no interlayers and the octahedral layers, which are those with most frequent REE cation-substitutions apart from the interlayer, are already completely leached. **Illites** are fine micas, which are originally very poor in REE concentrations (Okrusch and Matthes, 2009) and therefore considered not to carry a relevant REE-signal. Nevertheless, micas can include accessory minerals like Zircon, which do carry REE in high concentrations (Stosch, 2000). **Chlorites** are a product of weak chemical weathering, so they are likely to maintain their parental minerals' REE concentrations and patterns in the octahedral and interlayers. **Smectites** are the product of incomplete hydrolysis, so they still possess their cation interlayer and octahedral sheet with a significantly lower degree of desorption than kaolinites. So, smectite and chlorites are the main carriers of REE among smectite, as kaolinite is highly depleted with cations and illite as a descendant of micas never contained significant concentrations of REE to begin with. As ionic radii among REE decrease from La to Lu, LREE are slightly more mobile than HREE, which can result in slight enrichment of HREE in clay minerals compared to their parent minerals.

Adsorption of cations into the clay mineral grid is limited to the marine environment, where cations, including REE cations are adsorbed from sea water with its high alkalinity. The different mineralogical grids of the four main clay mineral classes have, depending on the electrochemical fit of layers, irregularities that admit absorption of cations from the aquatic environment. Kaolinites and chlorites have simple and well-balanced layer structures without interlayers, which do not absorb cations and therefore have a low ion-exchange capacity (1-10 meq/100 g; 5-30 meq/100 g) (Berner, 1971). These classes are well defined, have only few varieties and a steady cell thickness. **Illites'** sheet structure is electrochemically well balanced and therefore has a higher cation exchange capacity (10-40 meq/100 g) than kaolinite and chlorite. The intermediate layer is rather thin and contains mainly potassium

cations, therefore the cell thickness is nearly invariably (Berner, 1971). Significant chemical variation is not to be expected of these clay mineral classes. With an ion exchange capacity of >80 meq/100 g (specifically for montmorillonites and vermiculite; Berner, 1971) **smectites** are most likely to substitute cations, as long as they do not transform into another mineral. They form the most variable clay mineral class (Chamley, 1989), therefore they are more likely to adsorb cations from the aquatic environment than other secondary minerals and cannot contain the geochemical signal of the parent rocks as well. Effectively, the main REE signal in outgoing suspension and riverine sediments reflects that of the main outcrops of magmatic rocks within the drainage basin. The signal may be relatively enriched with HREE compared to the parental lithology's REE distribution.

Sea water is slightly alkaline and more saturated with ions, mostly Na^+, Mg^{2+}, Ca^{2+} and K^+. Adsorption and desorption of cations, including REE, in the marine environment are known of (Elderfield and Greaves, 1982), but the adsorbed concentrations must be very low, as REE concentrations of trace elements in sea water of the SCS are 3 orders lower than that of sinking particulate matter (ppb instead of ppm) (Alibo & Nozaki 2000; Elderfield & Greaves 1982). The seawater of the SCS is generally enriched with HREE and increases its total concentration and relative HREE enrichment with depth. Minerals with interlayers like chlorite and smectite are more likely to absorb the sea waters' signal.

1.4. Thesis Outline

After a short introduction to the study area in Chapter 2, with emphasis on the characteristics of riverine dischargers and oceanography, Chapter 3 introduces sampling campaign, applied methods and data from previous studies are presented.

Discussion chapters are designed as manuscripts with each a short introduction to the topic, previous studies, material and methods. The topics were chosen to give a spatial overview over the entire SCS on the aspects of relative clay mineral abundances, -fluxes (Chapter 4) and trace element characteristics (Chapter 5) first. All data from each trap was statistically averaged and extrapolated to annual fluxes and distributions. Both come to the conclusion that a detailed provenance analysis is hindered by composition changing processes during transport. They aim to characterize these transport mechanisms (Chapter 4) and to find the most reliable method to identify the sources (Chapter 5). The averaged fluxes and compositions allow identifying temporal anomalies, which is the actual advantage of sampling by sediment traps. Temporal resolution of clay mineral and trace element data was displayed and analyzed in detail only at station SCS-N (Chapter 6), where data coverance was nearly complete. Several more studies, using the full temporal resolution could be performed in the future, using the produced database.

Closing remarks on spatial diversity and temporal variability of transport mechanisms and their impact on weathering signal masking are concluded in Chapter 7. Data, table of figures, abbreviations used and publications resulted and planned from this study are listed in Chapter 10.7.

2. Regional background

2.1. Climate

The drainage basins that deliver detrital matter to the South China Sea (SCS) lie in tropical to temperate climatic zones (Peel et al., 2007). Sumatra, Borneo, Malaysia and the southern Philippines are affected by rainforest-tropical conditions; Indochina to the Red River, Hainan and Luzón are affected by tropical monsoonal climatic conditions and the Southern Chinese Provinces including the Island of Taiwan are affected by temperate climatic conditions.

The main SCS basin lies under the influence of the South East Asian monsoon system, which strongly affects climate, weathering, soil formation and shallow oceanography. Its seasonality is most developed in the tropical monsoonal climate zone (Figure 7) and is a model region for a monsoonal system with dry winters, wet summers and typically reversing wind directions (Clift and Plumb, 2008). Winter monsoon is more intense and longer (Nov-Apr) than the weak summer monsoon (May-Sept) (Wang et al., 2009). As a marginal region to the Pacific, the monsoonal system of the SCS is affected by the El Niño Southern Oscillation (ENSO), which periodically decreases precipitation during summer in the tropical monsoon areas (Chao et al., 1997) (Figure 41). El Niño events are weaker and generally lag behind the Pacific 3.4 ENSO region with 4-6 months; La Niña events rarely affect the SCS.
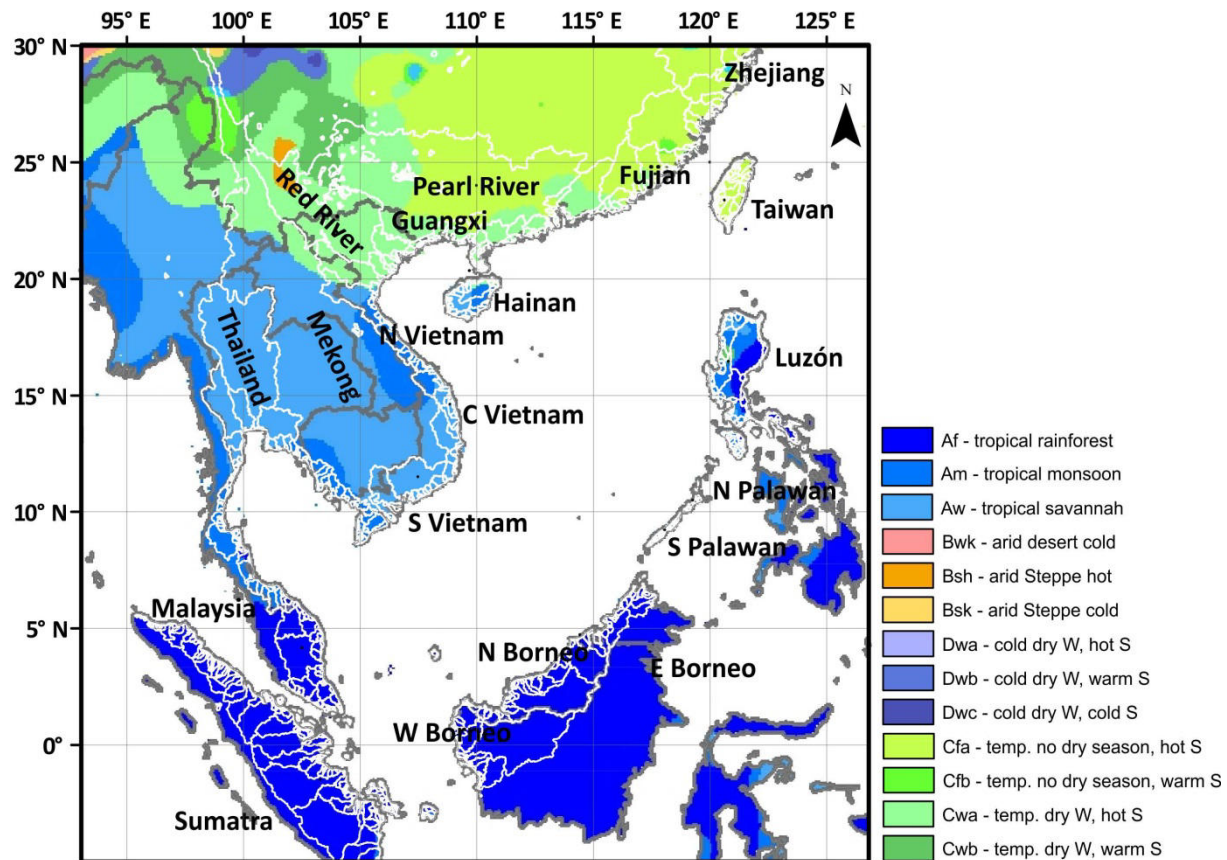
Figure 7: Climate zones (Peel et al., 2007) **are dominantly rainforest-tropical south of 10° N, monsoonal-tropical and Savannah from 10° N to Taiwan and the Red River, including Hainan Island. To the north lie regions of temperate climate.**

2.2. Geology

The formation of the deep SCS was triggered by the collision of India and Asia. The compressing force of the Himalayan uplift caused sinistral displacement along the Red River Ailao Shan shear zone (Wang et al., 2009). This caused extension in the former shelf south of the Yangzi block, which triggered rifting that opened the basin since the late cretaceous. Seafloor spreading between what are now the Islands of Taiwan and Palawan started from the late Eocene (33 Ma) and stopped during the early to middle Miocene (15 Ma), producing a semi-enclosed basin. To the north, west and south the SCS shelves have passive margins towards the Yangzi and Indochina blocks, which are counted as parts of the Eurasian plate, and the Island of Borneo (Wang and Li, 2009). At the eastern margin, the SCS is subducted below the Philippine volcanic Island arc.

Lithology of the surrounding drainage basins is diverse (Figure 8). Siliciclastic and carbonatic sedimentary rocks crop out in vat areas of all drainage basins, dominantly in the Pearly River, Guangxi, Red River, central Vietnamese, Mekong, Thai and Northern Borneo basins. Crystalline acidic and basic rocks crop out dispersed in all drainage basins. The Taiwanese Cordillera consists mainly of metamorphic rocks, mainly schist and gneisses (Brown et al., 2012). The South China granitoid massive consists of metamorphic, acidic and basin, plutonic and volcanic rocks and crops out in the Fujian, Guangdong and eastern part of the Pearl River drainage basin. Hainan consists mainly of acidic plutonic rocks, but large areas of basic volcanic rocks crop out in northern Hainan and southern Guangdong. Central and Southern Vietnamese rivers drain parts of the Annam Cordillera, which consist mainly of ultramafic and acidic plutonites or acidic and intermediate volcanic rocks. The Malayan Peninsula consists of metamorphic, carbonatic and acidic plutonites. Rivers of Sumatra drain mostly intermediate volcanic rocks and those of Borneo also acidic plutonites. Luzón and southern Palawan drain cordilleras of basic and ultramafic rocks (Hartmann and Moosdorf, 2012).

2.3. Sediment sources

Particulate matter reaches the SCS as fluvial and eolian detrital matter or forms as authigenic matter as chemicals sediments or from submarine exhalations. With annual fluxes of at least 409 Mt/y (statistically 116.86 g/m²/y) riverine input into the SCS is by far the highest transport medium from land to sea. Annual fluxes of dust fallout from the Gobi desert and loess Plateau were estimated to discharge annual fluxes range between 10-20 g/m²/y (S.-H. Wang et al., 2011; 2012) and 4.5 Mt/y (statistically 1.28 g/m²/y) (Gerbich, 2001). They are largely restricted to the South China shelf and slope (Lin et al., 2007). Its relative contribution is higher in pelagic sediments than in shelf sediments, as the dilution through fluvial sediments is lower. Fallout events of volcanic ashes from Philippine and Indonesian volcanoes are not considered in these calculations. Authigenic clay minerals can form from these volcanic ashes. Basaltic amorphous glasses of volcanic ash deposits in the eastern and central South China Sea from the Pinatubo eruption in 1991 (Wiesner et al., 2004) can transform into smectite (palagonitization (Honnorez, 1981). This transformation starts with temperatures as low as 0-5°C, which is the normal deep sea temperature, but is faster with higher temperatures up to 50°C. Palagonite-smectite can form already within less than two years at 3°C water temperature. The fluxes of neoformation of authigenic matter in submarine volcanic environments are unknown. Though they may play an important role in local deep sea sediments, we consider them not to play an important role in sinking particulate matter collected by out sediment trap sampling campaign (Chapter 3).
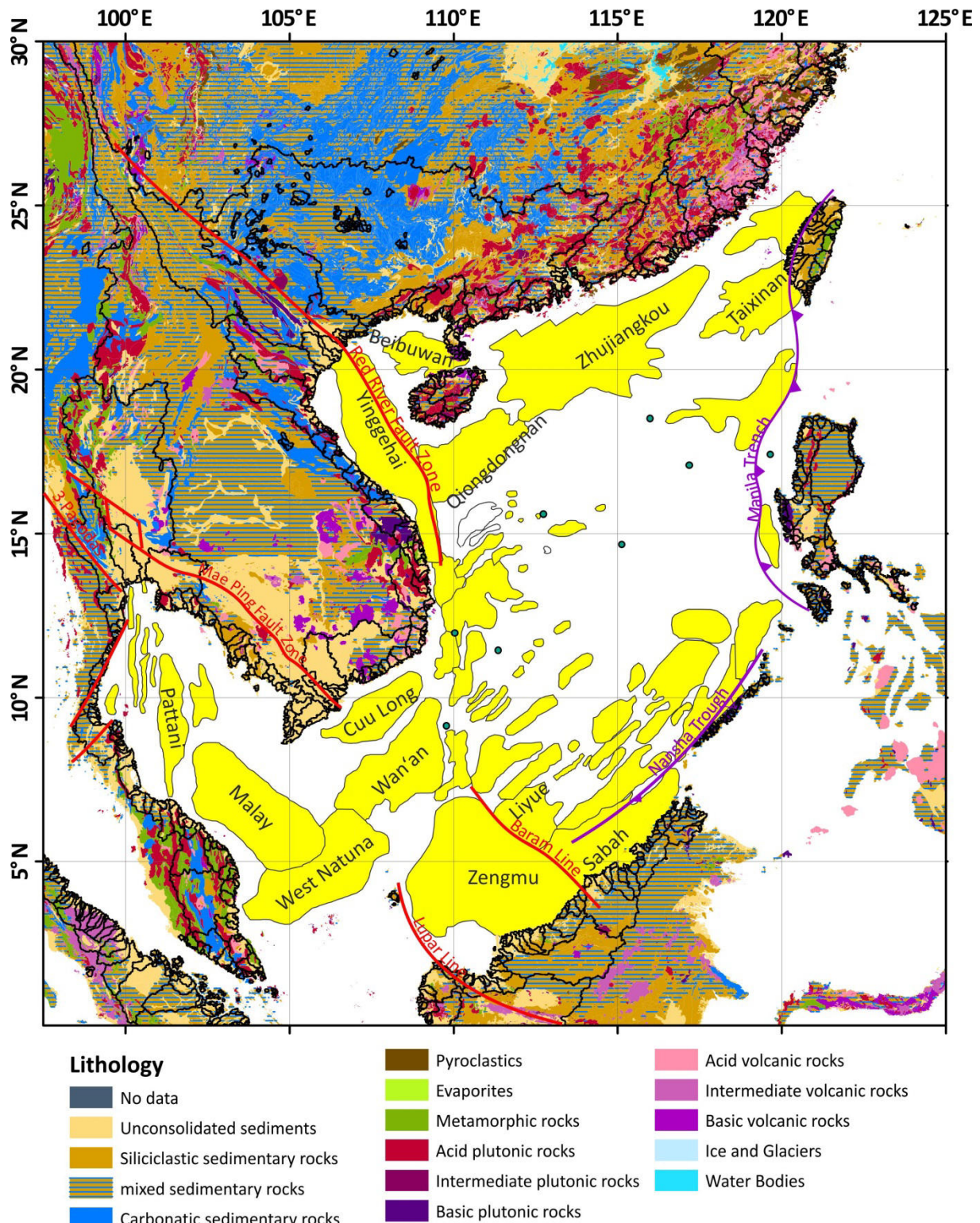
Figure 8: Lithology of the drainage basins (Hartmann and Moosdorf, 2012)**, major faults, subduction zones and sedimentary basins of the Quaternary** (Wang et al., 2009)**.**
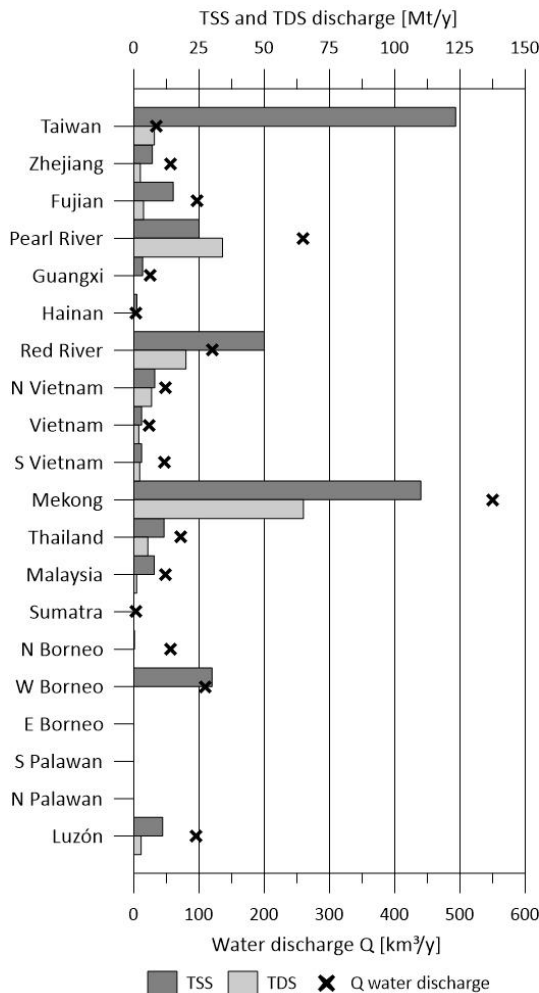
Figure 9: Total Suspended Solids (TSS), Total Dissolved Solids (TDS) and runoff of the 80 drainage basins listed in the Global River Database (Milliman and Farnsworth, 2011) as draining into the South China Sea or adjacent gulfs. More TSS from regions can be expected from drainage regions with a high runoff.

Among riverine sediment sources, Major Total Suspended Solids (TSS) dischargers are the Taiwanese Rivers (123 Mt/y; 30% of the known basin-wide TSS) the Mekong (110 Mt/y; 27%) and the Red River (50 Mt/y; 20%) (Figure 9). The Pearl River (25 Mt/y; 6 %) and South Chinese drainage basins (25.6 Mt/y; 6.25%) account for 50.6 Mt/y (12.3%). With the exception of Western Borneo (30 Mt/y; 7.3%), all other known dischargers into the SCS contribute less than 5% of the annual TSS into the SCS, including Thailand, Luzón and Hainan. Even the known, incomplete TSS discharge of Vietnamese coastal rivers sums up to 14 Mt/y (3.4%) (Milliman and Farnsworth, 2011). No recent sediments from the Yangtze are considered to reach the SCS (Liu et al., 2008; Xu et al., 2009). Currently collected observed suspended sediment discharges to the SCS from surrounding rivers add up to as much as 700 million tons annually, making the SCS the largest sink for fluvial sediments among enclosed or semi-enclosed marginal seas worldwide (Z. Liu et al. in review).

The Global River Database of Milliman and Farnsworth lists 69 rivers draining into the South China Sea. Unfortunately even the latest database update (Milliman and Farnsworth, 2011) is still fragmentary regarding Total Suspended Solids (TSS) and Total Dissolved Solids (TDS) in this region. Especially the smaller rivers in Vietnam, the Malayan Peninsula, Kalimantan and Philippine Islands are underrepresented - regions of tropical climate with intense weathering, which should be expected to deliver much more detrital matter than listed in Table 1. The riverine water discharge (Q) gives an estimate about the range of TSS to be expected in these drainage basins. Highest known TSS dischargers into the SCS are Rivers of Taiwan, Mekong and Red River (Song Hong), though, judging by

river runoff a lot more material could be expected from the smaller rivers of Luzón, Malaysia and Vietnamese Rivers (Figure 9).

Table 1: Extract from the Global River Database (Milliman and Farnsworth, 2011)**.**

Region	River name	Area	Q	TSS	TDS	TSS	TDS	Area
		[km²]	[km³/yr]	[Mt/yr]	[Mt/yr]	[%]	[%]	[%]
Taiwan	Chishui	0.41	0.52	2.1		0.51	0.00	0.02
	Choshui	3.10	4.30	40	1.6	9.76	1.04	0.13
	Erhjen	0.35	0.50	10	0.2	2.44	0.13	0.01
	Houlung	0.47	0.70	2.4	0.13	0.59	0.08	0.02
	Kaoping	3.30	7.40	21	2.3	5.12	1.50	0.14
	Linpien	0.34	0.86	1.8	0.19	0.44	0.12	0.01
	Pachang	0.47	0.74	2.5	0.23	0.61	0.15	0.02
	Peikang	0.64	0.80	1.4	0.29	0.34	0.19	0.03
	Potzu	0.43	0.55	0.83	0.21	0.20	0.14	0.02
	Taan	0.76	1.10	4	0.27	0.98	0.18	0.03
	Tachia	1.20	2.40	0.5	0.43	0.12	0.28	0.05
	Tanshui	2.70	7.00	11	0.32	2.68	0.21	0.11
	Touchien	0.60	0.80	1.1	0.17	0.27	0.11	0.02
	Tsengwen	1.20	1.00	12	0.49	2.93	0.32	0.05
	Tungkang	0.47	1.10	5.2	0.28	1.27	0.18	0.02
	Wu	2.00	3.70	5.3	0.74	1.29	0.48	0.08
	Yenshui	0.22	0.30	2.2		0.54	0.00	0.01
	sum	**18.66**	**33.77**	**123.33**	**7.85**	**30.09**	**5.12**	**0.77**
Zhejiang	Jiaoxi	5.50	6.90			0.00	0.00	0.23
	Oujiang	18.00	19.00	2.7		0.66	0.00	0.74
	Qiantangjiang	42.00	31.00	4.4	2.5	1.07	1.63	1.74
	sum	**65.50**	**56.90**	**7.10**	**2.50**	**1.73**	**1.63**	**2.71**
Fujian	Hanjiang	30.00	26.00	7.2		1.76	0.00	1.24
	Jinjiang	11.00	5.10	2.4		0.59	0.00	0.45
	Jiulongjiang	15.00	8.30	3.1	1.3	0.76	0.85	0.62
	Minjiang	61.00	58.00	2.4	2.4	0.59	1.57	2.52
	sum	**117.00**	**97.40**	**15.10**	**3.70**	**3.68**	**2.41**	**4.84**
	Pearl River	**490.00**	**260.00**	**25**	**34**	6.10	22.18	20.26
Guangxi	Jianjiang	9.50	5.50	1.5		0.37	0.00	0.39
	Moyangjiang	6.10	8.50	0.8		0.20	0.00	0.25
	Nanliujiang	6.60	5.10	1.1		0.27	0.00	0.27
	Tanjiang	5.30	6.30			0.00	0.00	0.22
	sum	**27.50**	**25.40**	**3.40**	**0.00**	**0.83**	**0.00**	**1.14**
Hainan	Changhuajiang	5.10	3.80	0.08		0.02	0.00	0.21
	Nandujiang	6.60	5.1	1.1		0.27	0.00	0.27
	sum	**11.70**	**3.80**	**1.18**	**0.00**	**0.29**	**0.00**	**0.48**
	Red River	**160.00**	**120.00**	**50**	**20**	12.20	13.05	6.62
N Vietnam	Ca	27.00	22.00	4	2.7	0.98	1.76	1.12
	Ma	28.00	17.00	3	2.2	0.73	1.44	1.16
	Nam San	11.00				0.00	0.00	0.45
	Thai Binh	15.00	9.00	1	1.9	0.24	1.24	0.62
	sum	**81.00**	**48.00**	**8.00**	**6.80**	**1.95**	**4.44**	**3.35**

Region	River name	Area	Q	TSS	TDS	TSS	TDS	Area
		[km²]	[km³/yr]	[Mt/yr]	[Mt/yr]	[%]	[%]	[%]
Vietnam	Ba	14.00	9.00	1		0.24	0.00	0.58
	Thu-Bon	10.00	14.00	2	1.9	0.49	1.24	0.41
	sum	**24.00**	**23.00**	**3.00**	**1.90**	**0.73**	**1.24**	**0.99**
S Vietnam	Cai	2.00	5.00			0.00	0.00	0.08
	Da Nhim	8.00				0.00	0.00	0.33
	Sai Gon	44.00	42.00	3	2.25	0.73	1.47	1.82
	sum	**54.00**	**47.00**	**3.00**	**2.25**	**0.73**	**1.47**	**2.23**
	Mekong	**800.00**	**550.00**	**110**	**65**	**26.84**	**42.40**	**33.08**
Thailand	Bangpakhlong	10.00	4.90		0.09	0.00	0.06	0.41
	Chao Phraya	160.00	30.00	3	5.3	0.73	3.46	6.62
	Khlong Phum Duang	3.00	3.40	0.12		0.03	0.00	0.12
	Mae Klong	31.00	13.00	8.1		1.98	0.00	1.28
	Pattani	4.00	3.00	0.35		0.09	0.00	0.17
	Petch	6.00	1.40			0.00	0.00	0.25
	Tapi	12.00	17.00			0.00	0.00	0.50
	sum	**226.00**	**72.70**	**11.57**	**5.39**	**2.82**	**3.52**	**9.35**
Malaysia	Endau	4.00				0.00	0.00	0.17
	Johore	4.30	2.40			0.00	0.00	0.18
	Kelantan	12.00	18.00	2.5	1.1	0.61	0.72	0.50
	Kinabatangan	16.00	20			0.00	0.00	0.66
	Langat	2.50	1.80	0.6		0.15	0.00	0.10
	Muda	7.40	3.60	0.09		0.02	0.00	0.31
	Murar	3.20	1.70	0.07		0.02	0.00	0.13
	Pahang	19.00	18	3		0.73	0.00	0.79
	Perak	13.00	12.00	0.9		0.22	0.00	0.54
	Selangor	3.20	3.00	0.09		0.02	0.00	0.13
	Trengganu	3.30	6.50	0.58		0.14	0.00	0.14
	sum	**87.90**	**49.00**	**7.83**	**1.10**	**1.91**	**0.72**	**3.63**
Sumatra	Asahan	7.50	3.00			0.00	0.00	0.31
	Inderagiri	22.00	18			0.00	0.00	0.91
	Kampar	36.00	33			0.00	0.00	1.49
	Panai	12.00				0.00	0.00	0.50
	Rokan	16.00				0.00	0.00	0.66
	Siak	16.00				0.00	0.00	0.66
	sum	**109.50**	**3.00**	**0.00**	**0.00**	**0.00**	**0.00**	**4.53**
N Borneo	Baram	23.00	44.00			0.00	0.00	0.95
	Belait	1.30	1.00			0.00	0.00	0.05
	Padas	5.00	7.10			0.00	0.00	0.21
	Tutong	2.30	4.40	0.25		0.06	0.00	0.10
	sum	**31.60**	**56.50**	**0.25**	**0.00**	**0.06**	**0.00**	**1.31**
W Borneo	Kidurong	5.40				0.00	0.00	0.22
	Lupar	7.00				0.00	0.00	0.29
	Rajang	51.00	110.00	30		7.32	0.00	2.11
	sum	**63.40**	**110.00**	**30.00**	**0.00**	**7.32**	**0.00**	**2.62**
Luzón	Abra	6.20	13.00			0.00	0.00	0.26
	Agno	6.90	6.70	5		1.22	0.00	0.29
	Angat	0.78		4.6		1.12	0.00	0.03

Region	River name	Area	Q	TSS	TDS	TSS	TDS	Area
		[km²]	[km³/yr]	[Mt/yr]	[Mt/yr]	[%]	[%]	[%]
	Cagayan	26.00	54.00		2.8	0.00	1.83	1.08
	Pampanga	10.00	21.00	1.4		0.34	0.00	0.41
	Pasig	0.60	0.08	0.06		0.01	0.00	0.02
	sum	**50.48**	**94.78**	**11.06**	**2.80**	**2.70**	**1.83**	**2.09**
	Yangtze	1800.00	900.00	470	180	114.68	117.42	74.43
	SUM	**2418.24**	**1651.25**	**409.82**	**153.29**	**100.00**	**100.00**	**100.00**

The rivers around the SCS discharge particulate matter of diverse compositions into the sedimentary basin (Figure 11): **Taiwanese** Rivers (30% of the basin-wide TSS) discharge material consisting nearly solely of chlorite and illite (92%) (Figure 10, Figure 11) in the clay sized fraction, which is a distinctive mineralogical signature in the SCS. It indicates strong physical weathering, which is in accordance with the low TDS/TSS ratio (Table 1,Figure 9). **South China Rivers** (12.6%), are the Rivers of Fujian (3.7%), Guanxi (0.8%), the Pearl River (6.1%), Zhejiang (1.7%) and Hainan (0.3). They share a common clay mineralogy characterized by dominant kaolinite abundance (46%-76%) and low contents of smectite (1%-6%). The **Red River** (12.2%), **Mekong** (26.8%) and **northern Vietnamese Rivers** (2.0%) contribute 41% of the known basin wide TSS. They discharge a similarly characterized clay sized fraction; enriched with illite and kaolinite (63%-87%) and depleted of smectite (<10%). **Central Vietnamese Rivers** (Ba and Thu Bon) carry a clay mineral signal similar to that of the South China and Malayan rivers, which is very rich in kaolinite (77%) and nearly no smectite (1%), but contributes only few material to the SCS (0.7%). **Southern Vietnamese** (0.7%) and **Thai Rivers** (2.8%) contribute 3.5% to the SCS TSS. Their sediments contain more smectite (28%-42%) than the other Indochine Rivers. **Malayan Rivers** are among those with the highest kaolinite contents (78%) and nearly no smectite (1%), because the chemical weathering on this tropical peninsula is very intense. With the discharge data available, Malayan Rivers contribute only 1.9% of the known TSS, but the river runoff and tropical climate suggest that higher TSS discharge amounts should be expected. TSS discharges are mostly unknown from **Sumatran** (n.d.), **Western** (0.1%) **and Northern Borneo Rivers** (7.3%) and should be expected to contribute much higher annual fluxes than 7.4% of the basin-wide TSS. They are rich with kaolinite (42%-57%) and Smectite (9%-19%) decreasing eastward in favor of increasing chlorite and illite. Clay mineral assemblages of sediments from Borneo are rich in illite and chlorite (77%-81%) and very scarce with smectite (0%-1%). **Southern Palawan** (n.d.) and Luzón Rivers (2.7%) are the only source regions that are mainly composed of smectite (54% and 87%) (Liu et al., 2003). Annual TSS contribution should be expected to be much higher than only 2.7% of the basin-wide TSS, as riverine water runoff is very high (Figure 9).
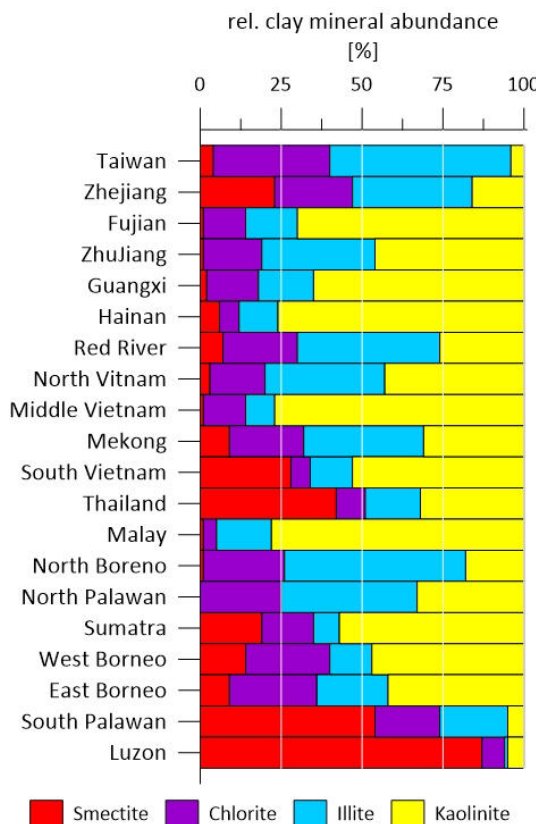
Figure 10: Relative clay mineral abundances of drainage basins that deliver sediments into the SCS (Liu et al., 2015)**.**

Table 2: Clay mineralogy of the drainage basins around the SCS (Liu et al., n.d.)**.**

Province	Smectite	Chlorite	Illite	Kaolinite
		[%]		
Taiwan	4	36	56	4
Zhejiang	23	24	37	16
Fujian	1	13	16	70
Pearl River	1	18	35	46
Guangxi	2	16	17	65
Hainan	6	6	12	76
Red River	7	23	44	26
North Vietnam	3	17	37	43
Central Vietnam	1	13	9	77
South Vietnam	28	6	13	53
Mekong	9	23	37	31
Thailand	42	9	17	32
Malaysia	1	4	17	78
Sumatra	19	16	8	57
North Borneo	1	25	56	18
West Borneo	14	26	13	47
East Borneo	9	27	22	42
South Palawan	54	20	21	5
North Palawan	0	25	42	33
Luzón	87	7	1	5
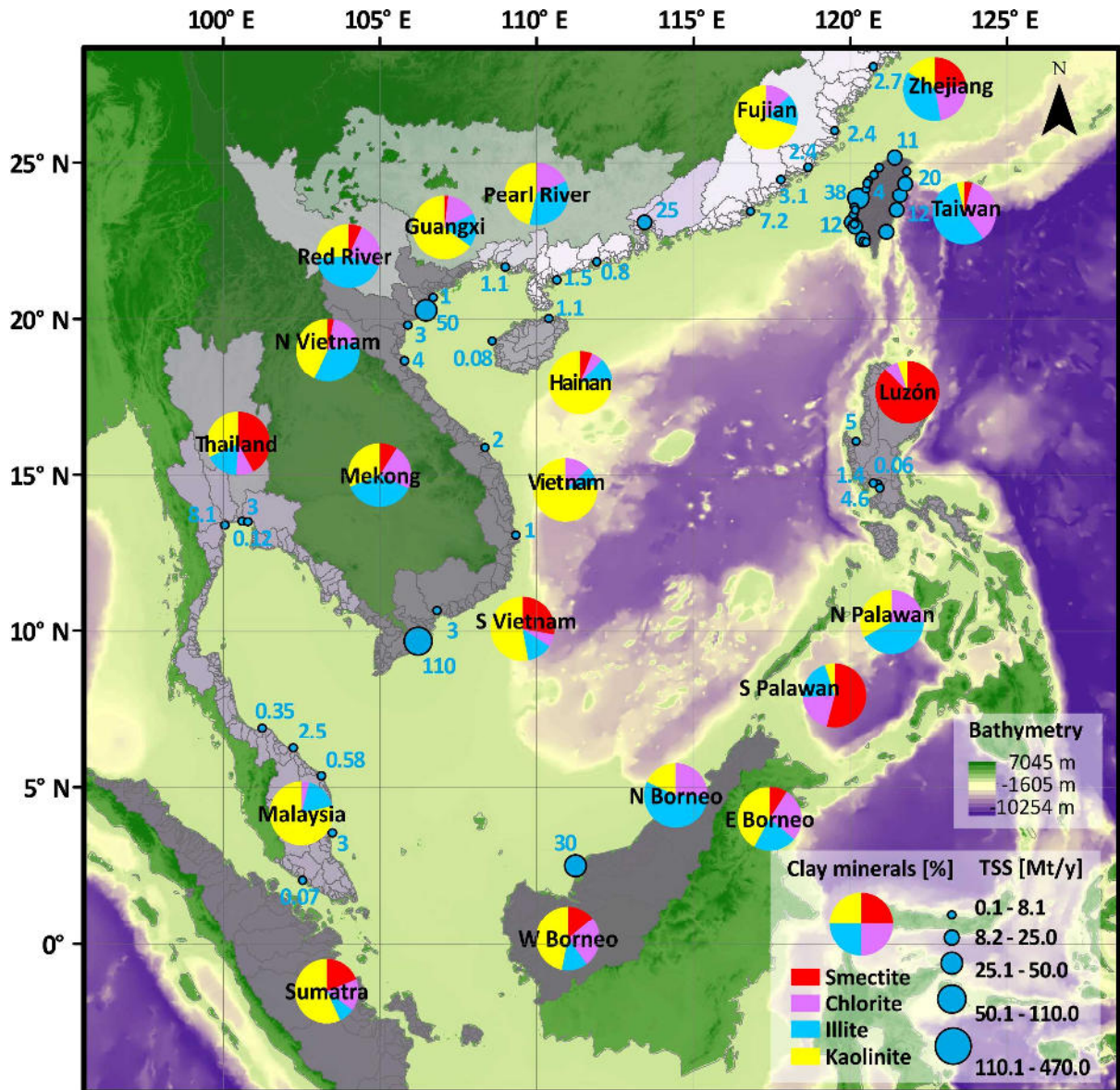
Figure 11: Map of clay mineral distributions in the major provinces according to Liu et al. (2015)**. Pie chart segments display relative clay mineral abundances (Table 2). Blue circles represent Total Suspended Solid (TSS) discharge [Mt/y] of fluvial sources according to** Milliman & Farnsworth (2011)**.**

2.4. Basin morphology and oceanography

The SCS basin is confined by broad shelves (less than 100 m water depth) in the north (the South China Shelf) and west (the Vietnamese and Sunda shelves) and by narrow shelves off Taiwan and Luzón. The central basin is 3500 to 5000 m deep and nearly completely enclosed. The only sill deep enough to affect basin wide deep circulation is the Luzón Strait in the east towards the Pacific Ocean (Wang and Li 2009; Chao et al. 1996).

Morphology and monsoonal wind stress determine the complex and variable circulation patterns at the surface, which include seasonal current direction reversals, gyres and mesoscale eddies. The monsoonal reversal impacts surface waters down to 100 m below the sea level surface (Chu et al., 1999; Huang et al., 2011) and causes NE-ward currents during summer (Figure 13) and SW-ward currents during winter (Figure 12) across the Sunda, Vietnamese and South China shelves (Bonjean and Lagerloef, 2002; Qu, 2000; Shaw and Chao, 1994).

Many small gyres and counter-currents develop as a response to the reversals. In the central basin, the general **summer** monsoonal NE-ward winds forces the so-called eastward offshore jet (Figure 13), which develops from the eastern cape of Vietnam into the central SCS. This NE-ward current forces bipolar gyres in the western SCS; a southern, anti-cyclonically rotating gyre and a northern cyclonic gyre (Figure 13). During **winter** monsoon the gyres unite into one basin wide cyclonic gyre (Shaw and Chao, 1994). With the general SW-ward currents, the Kuroshio Current often intrudes the SCS through the Luzón strait (Figure 12). Between Taiwan and Luzón eddies (Figure 14) result from the Luzón upwelling during late winter.
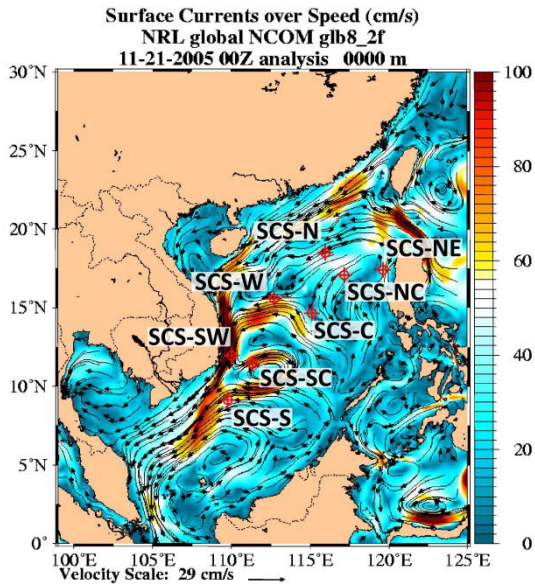
Figure 12: Strongly developed SW-ward currents during winter monsoon in December 2005 including Kuroshio intrusion, SW-ward Guangdong Coastal Current and East Vietnam S-current (Bonjean and Lagerloef, 2002).
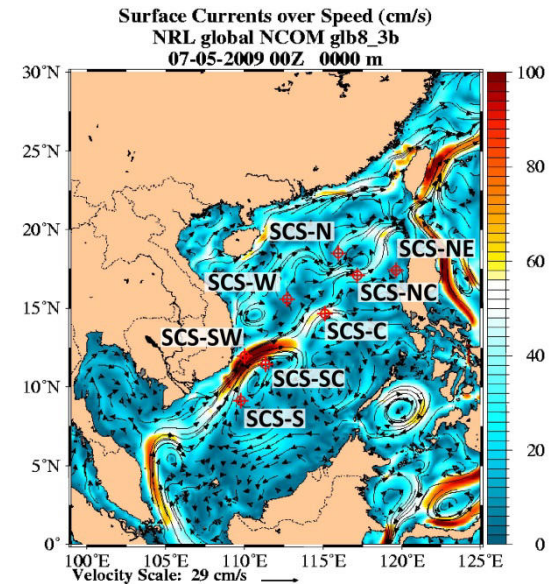
Figure 13: Weakly developed NE-ward currents during summer monsoon in July 2009, including Vietnam off-shore E-jet and rather weak NE-ward Guangdong Coastal Current.
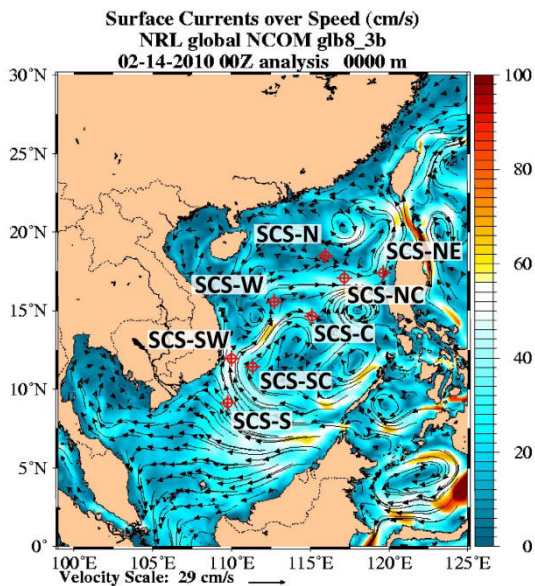
Figure 14: No predominant current direction and eddies in the northern SCS during late winter monsoon in February 2010 (Bonjean and Lagerloef, 2002)**.**
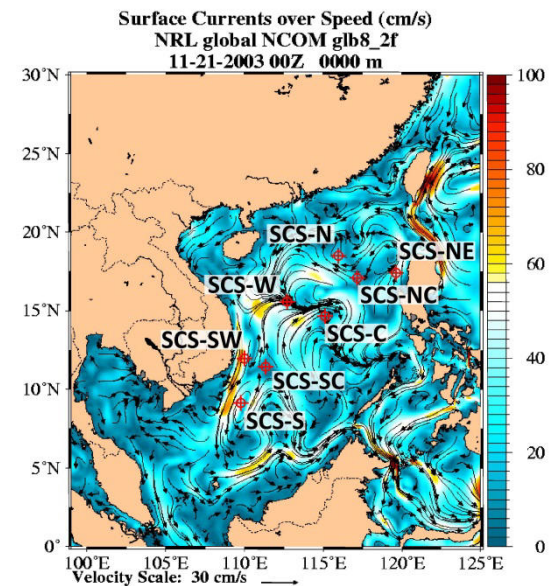
Figure 15: SE-ward currents meander through the central SCS during autumn intermonsoon in November 2003.

Coastal currents along the south-eastern shelf of the SCS are NE-ward during autumn intermonsoon (Figure 14) and W-ward during spring intermonsoon (Figure 15). During **intermonsoon** phases the steady wind stress recedes, slowing the coastal currents (Figure 15), but Taifuns often generate turbulences during this season. The predominant current directions weaken and change. The timing of these oceanographic features is not the same through the years; hence it would not be accurate to generalize the monsoonal seasons for all years to cover the same months. Surface currents weaken during El Niño years (Chao et al., 1997). Until today, deep circulation is investigated in less detail, but it is known to behave de-coupled from the monsoonal forcing of the surface waters (Wang et al., 2009). Main motor for deep circulation are the basin's morphology and the limited Luzón Strait overflow of Pacific intermediate and deep water. These force along-slope currents and a persistent, year-round basin-scale cyclonic gyre below 2000 m depth, with downwards weakening velocities (Figure 24)(Qu et al., 2006; G. Wang et al., 2011; Xie et al., 2013).

Vertical currents are driven by thermohaline gradients and sediment load, resulting from different water and suspension densities by temperature, salinity and particulate matter concentration. The downslope movement can be hindered and deflected by thermohaline boundaries and develop intermediate nepheloid layers, on which particulate matter concentrates. The presence of vertical currents has not been observed and described for recent sediments, but channels and submarine, quaternary sediment fans testify their occurrence in the past. Upwelling is a frequent phenomenon along all shelves of the SCS. Best developed and studied upwelling regions are west of Luzón during winter monsoon (Shaw et al., 1996) (Figure 14) and the east Vietnam upwelling area during summer (Hein, 2008).

2.5. Sediments of the SCS

Earliest sediments of the SCS are terrigenous Jurassic and Cretaceous pre-rift sediments. During rifting since the early Palaeocene several sedimentary basins opened and filled with terrigenous and lacustrine sediments (Figure 8). Oldest basins opened near the northern shelf, younger ones in the western and Southern SCS. Syn-rift sediments tend to shift more towards marine facies with increasing duration of rifting and distance from the terrigenous sources. Especially among syn-rift sediments of the northern basins, prograding siliciclastic sequence, turbidite and deep sea fan deposits document mass-wasting to be an important transport mechanism in the past. Post-rift sediments (after 15 Ma) were distinctively marine in the central regions (Wang et al., 2009).

Sedimentation varies spatially and temporally, as it still does today (Chapter 4), but with overall high sedimentation rates. These produced sedimentary sequences of up to 14 km thickness, with a very high temporal resolution, which makes the SCS an ideal study area for highly resolved environmental studies. In most of these basins, sedimentation continues until today.

3. Material, methods and previous data

3.1. Material

Materials used for this study are sinking particulate matter collected by sediment traps, marine sediment surface samples taken by boxcoring and riverine sediments.

3.1.1. Sinking particulate matter (SPM)

The main sample material used for this study was collected by sediment traps following the exemplary sampling setup of Honjo & Doherty (1988). These are plastic cones suspended in the water column on wires, kept in place by a heavy anchor and kept upright by a series of bouyancy bodies (Figure 16). The cones have openings of 0.5 m². Any trapped particle is funneled into sampling containers, which are filled with a poisonous HgCl solution, to inhibit any biological activity in the sample. In order to prevent diffusion of the poison, the solution is given a high NaCl concentration to give it a higher specific density. A small motor rotates the sampling cups below the lower opening of the funnel (Figure 17). Each trap is programmed to take samples in defined time intervals, through a whole year or a specific season, depending on the original purpose of the sampling campaign.

Sinking particles were collected by Mark VI and Mark VII time-series sediment traps which were deployed at eight locations according to major oceanographic and atmospheric features of the SCS (): in the centre of the SW-monsoon coastal upwelling region off Vietnam (SCS-SW), in the Vietnam offshore current (SCS-SC), in the NE-monsoon upwelling centre off the northern edge of the Sunda shelf (SCS-S), inside and outside the Luzón Upwelling cell (SCS-NE and SCS-NC, respectively), in the northern SCS below the major wind axis and dust veil of the NE-monsoon (SCS-N), south of the Xisha Islands where a branch of the SCS interoceanic through flow turns eastward (SCS-W), and in the oligotrophic central South China Sea (SCS-C) remote from continental sources (Figure 17). The traps were placed at water depths between 500 and 3700 m; collection intervals were between 16 and 28 days (Table 3). Surface sediments were taken with a standard box corer at stations SCS-SW, -C, -N and -NE. Sample names were given according: SCS-*station name**mooring number* *trap name**Cup number* (example: SCS-N03 SH01).

The sampled sinking particulate matter consists of a terrigenous, detrital, lithogenic matter fraction and of marine biogenic carbonate, opal and organic matter. This study focuses on the lithogenic matter fraction, more details about the biogenic fraction can be found in other studies (3.3). The content of organic matter is of some importance, as it supports the formation of aggregates and glues faecal pellets.

Macroscopic observations showed that most sinking particulate matter forms greenish-brown, loose and fluffy muddy silt in the sampling containers. Particle grain size is not distinguishable by the naked eye. Furthermore, particles are clustered into aggregates and faecal pellets of even more than 1 mm length. Carbonatic shells of foraminifers often constitute a major part of the particulate matter, but the content is spatially and temporally variable. Diatoms and silicate spiculae from unidentified algae form the opaline fraction of particles. Even copepods and other crustaceans, sometimes fish scales or entire fish get caught in the trap as well.
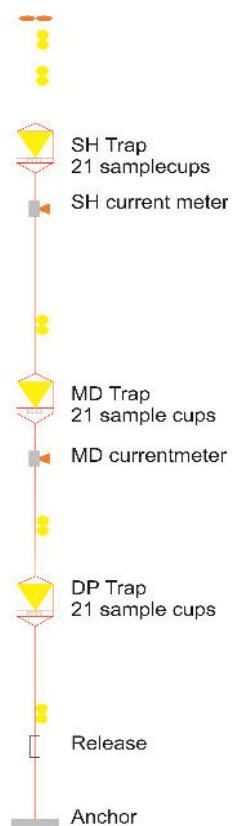
Figure 16: Sketch of a 3-trap sediment trap system (modified after technical sheet in (Wiesner, 2013)).
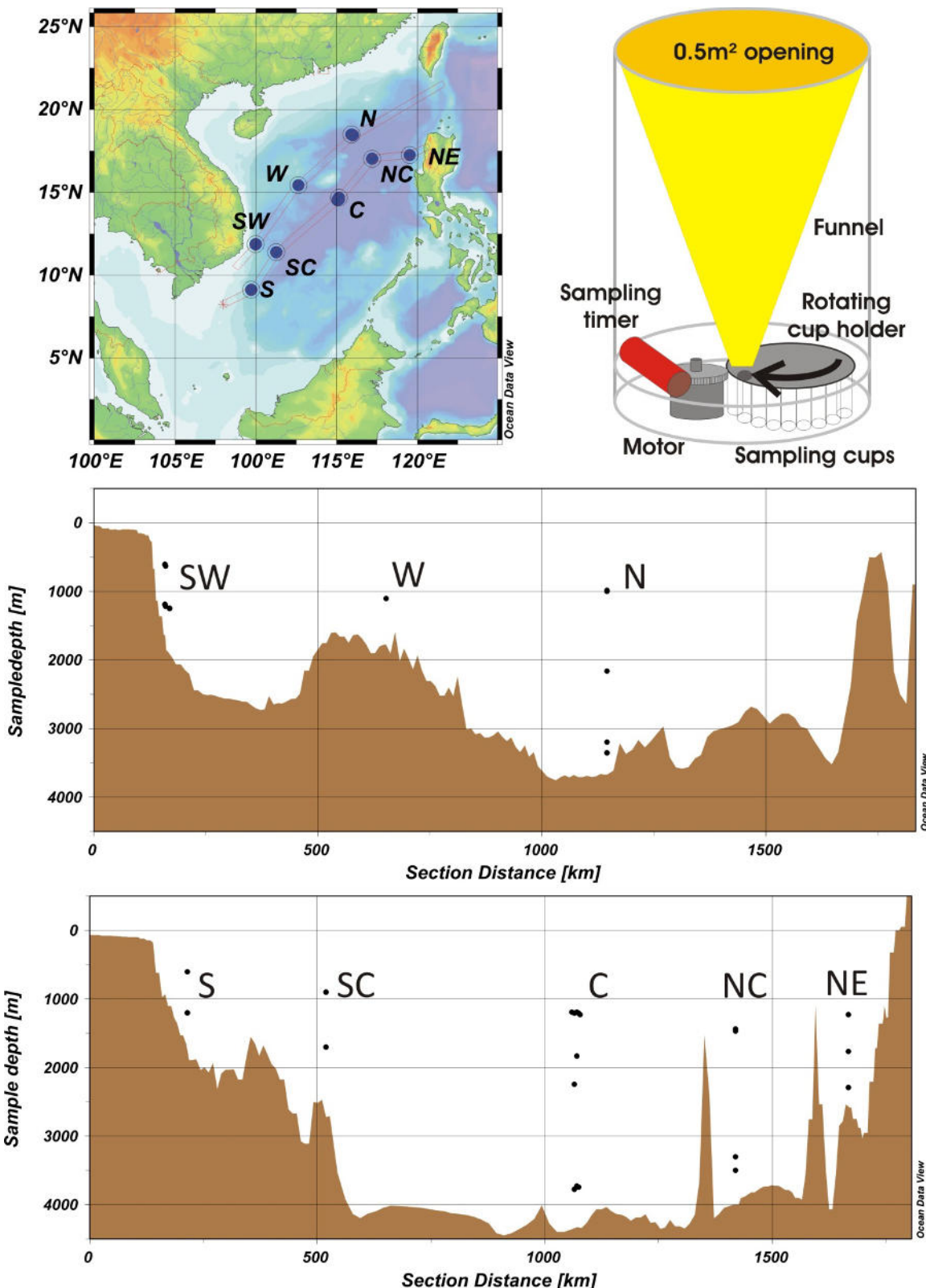
Figure 17: Map and sections of the positions of mooring stations. Each sediment trap collects sinking particulate matter, which falls through the funnel into the sampling cups. The motor moves the cup holder, so the cups rotate below the funnel-opening in pre-defined intervals, programmed in the sampling timer (top right).

Table 3: Positions and deployment times of the sampling campaign designs.

Mooring	Latitude [°N]	Longitude [°E]	Water Depth [m]	Start	End	Traps	Cups	interval duration [d]
SCS-N01	18.463	116.036	3766	10.09.1987	23.03.1988	2	13	15
SCS-N02	18.475	116.033	3766	13.04.1988	21.10.1988	2	13	15
SCS-N03	18.535	116.001	3736	27.06.2009	13.05.2010	3	21	16
SCS-N04	18.518	115.924	3736	20.05.2011	04.04.2012	3	21	16
SCS-NE01	17.420	119.529	2826	08.07.1998	30.04.1999	3	13	28
SCS-NE02	17.379	119.785	2951	15.05.1999	13.05.2000	2	13	28
SCS-NC01	17.075	117.192	4038	10.12.1996	26.11.1997	2	13	26
SCS-C01	14.604	115.110	4270	01.12.1990	03.12.1991	2	13	28
SCS-C02	14.583	115.050	4270	20.03.1992	09.05.1993	2	13	31
SCS-C03	14.597	115.143	4270	01.06.1993	31.05.1994	2	13	27
SCS-C04	14.600	115.131	4306	01.06.1994	05.04.1995	3	13	27
SCS-C05	14.617	115.117	4005	01.06.1995	24.06.1996	2	13	29
SCS-C06	14.719	115.156	4298	10.12.1996	26.11.1997	2	13	26
SCS-C07	14.840	115.249	4281	29.06.1998	25.04.1999	2	13	27
SCS-W01	15.696	112.866	2131	27.06.2009	13.05.2010	1	21	16
SCS-W02	15.472	112.619	2131	20.05.2011	04.04.2012	1	21	16
SCS-SC01	11.442	111.451	2250	10.05.2005	15.04.2006	2	21	16
SCS-SC02	11.421	111.282	2300	27.04.2006	15.04.2007	2	21	16
SCS-SW01	11.904	110.019	1881	01.06.1998	01.04.1999	2	21	28
SCS-SW02	11.904	110.019	1878	15.05.1999	09.07.1999	2	21	28
SCS-SW04	12.067	110.012	1825	10.06.2004	07.05.2005	2	21	16
SCS-SW05	12.064	110.144	1825	10.05.2005	15.04.2006	2	21	16
SCS-SW06	11.835	110.007	1850	27.04.2006	15.04.2007	2	21	16
SCS-S01	9.155	109.731	1740	30.06.2003	04.06.2004	2	21	16
SCS-S02	9.107	109.856	1725	10.06.2004	07.05.2005	2	21	15

3.1.2. Marine sediments

Though at most stations surface samples were taken with box corer, only four of them could be used for this study (Table 4). They are from stations SCS-C, -NE, -N and -SW. For box coring, a 0.5 x 0.5 x 1 m metal box is lowered to the sediment surface and driven by its own weight into the loose surface sediments. While pulling the box back up, a lid slides before the opening, locking the sediment inside. The boxed sediment is pulled up and opened at one side, which provides a good view at the deposits in their original habitat. Surface samples from these stations are also muddy silts with spatially diverse contents of TOC, carbonate and silicate. They are generally bioturbated by echinoids, mussles, crustaceans and worms, therefore deposited under oxic conditions and with low TOC contents. The depth of recent bioturbation in the box cores was approximately 20 cm.

Table 4: Positions of box core samples (Lahajnar et al., 2007)**.**

Station	Sample Name	Latitude [°N]	Longitude [°E]	Depth
SCS-NE	SO-95 17927-1	17.317	119.467	-2800 m
SCS-N	SO-50/27	18.433	116.017	-3750 m
SCS-C	SO-50/90	14.733	115.167	-4300 m
SCS-SW	SO-140/58	11.917	110.017	-1906 m

Table 5: Positions of fluvial sediment sampling locations (Stichel, 2007)**. Except for the Pearl River, all samples were taken in fluvial environments, landwards from tidal influence.**

Region	River name	Latitude [°N]	Longitude [°E]	Reference
Luzón	Abra	17.553	120.395	Z. Liu (personal)
	Abulug	18.338	121.426	Z. Liu (personal)
	Agno	15.980	120.226	Z. Liu (personal)
	Bucao	15.262	120.037	Wiesner (personal)
	Cagayan	18.123	121.673	Z. Liu (personal)
	Pampanga	14.902	120.819	Z. Liu (personal)
South China	Hainan	19.587	110.653	Ma (2007)
	Pearl River	23.000	113.000	Wiesner (personal)
	Pearl River East (Dong)	22.399	113.257	(Zhang & Wang 2001)
	Pearl River North (Bei)	23.105	113.432	(Zhang & Wang 2001)
	Pearl River West (Xi)	23.043	113.524	(Zhang & Wang 2001)
Taiwan	Cho Shui	23.833	120.433	Z. Liu (personal)
	Kao-Ping	22.637	120.442	Z. Liu (personal)
	Pei-Kang	23.515	120.179	Z. Liu (personal)
	Tseng-Wen	23.085	120.127	Z. Liu (personal)
Vietnam	Mekong 03	10.249	107.039	Stichel (2007)
	Mekong 05	10.249	107.039	Stichel (2007)
	Nha Trang	12.606	109.131	Stichel (2007)
	Song Ba	13.062	109.317	Stichel (2007)
	Song Cai Nin Hoa	12.486	108.727	Stichel (2007)
	Song Cai Phang Rang	11.604	108.936	Stichel (2007)
	Song Dinh	10.706	107.841	Stichel (2007)
	Song Hong	20.467	106.067	Stichel (2007)
	Song Long Song	11.239	108.563	Stichel (2007)
	Song Luy	11.172	108.563	Stichel (2007)

3.1.3. Fluvial sediments

Fluvial sediments of Vietnamese Rivers were previously sampled and analyzed on TOC, grain size, Nd isotopy and trace elements for a Diplom thesis (Stichel, 2007), which was not published (Table 3). Taiwanese River sediments were provided by Zhifei Liu and one sample from the Pearl River estuary was taken by box core during cruise SO-50/104. The data of Luzón Rivers was also provided by Zhifei Liu.

3.2. Methods

3.2.1. Fluxes

Prior to the deployment of the sediment traps sample cups were filled with sea water from the respective trap depths filtered over WHATMAN GF/F filters (precombusted at 450°C). NaCl (33.3 g/l) and $HgCl_2$ (3.33 g/l) were added to the cups to minimize diffusion and to retard decomposition of the trapped material. After recovery, the wet samples were passed through a 1 mm mesh nylon sieve to exclude pelagic macro organisms. Subsequently the <1 mm fractions were split into aliquots with a high-precision rotary splitter, then filtered over pre-weighed Nucleopore filters (0.45 µm pore size) and dried at 40 °C for 12 hours. The dry weights (Σm_{dry}) of these fractions were used for calculating the total mass fluxes (F_{total}) and for component analyses. The amount of lithogenic material was computed as the difference between the total mass of particulates and the sum of carbonate, organic matter and biogenic opal (Lahajnar et al. 2007). All analyses on main components were done at the anorganic laboratory of the Insitute for Geology at the University of Hamburg.
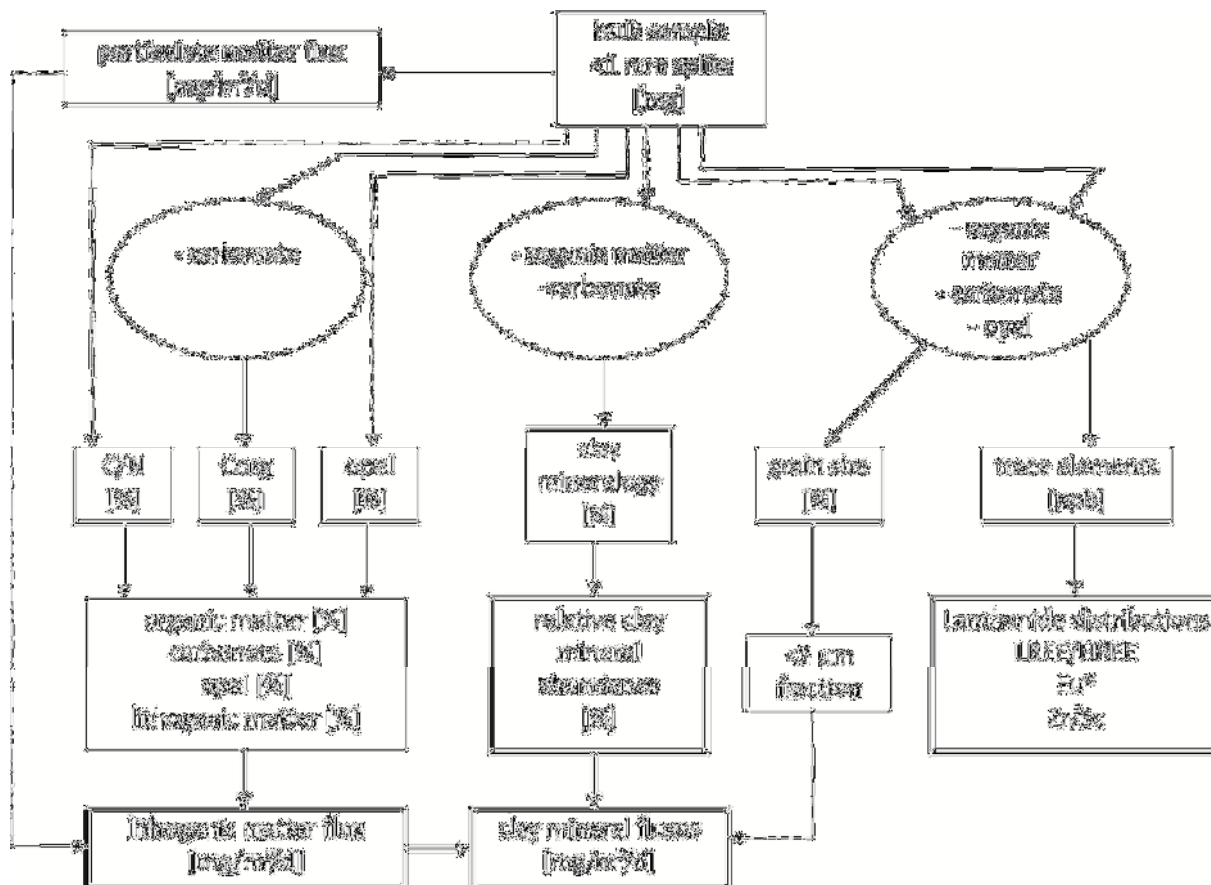
Figure 18: Box-diagram of the sample treatment and methods applied on sinking particulate matter <1 mm.

$F_{total}[mg/(m^2*d)] = \Sigma m_{dry} [mg] /(t [d] * 0.5 [m^2])$

$F_{org.m.} [mg/m^2/d] = C_{Corg}[\%] \times F_{total} [mg/m^2/d] \times 1.8$

$F_{CaCO3} [mg/m^2/d] = F_{total}[mg/m^2/d] \times C_{total\,C}[\%] - F_{org.m.} [mg/m^2/d]$

$F_{opal} [mg/m^2/d] = F_{total}[mg/m^2/d] \times opal \%$

$F_{Litho}[mg/m^2/d] = F_{total}[mg/m^2/d] - (F_{org.m}[mg/m^2/d] + F_{CaCO3}[mg/m^2/d] + F_{opal}[mg/m^2/d])$

3.2.2. Grainsize

Grainsize data of SCS-NC and SCS-C have been measured and evaluated by Glos (2002). Those of SCS-01, -02 and SCS-N01 by Rieger (1995), those of SCS-C02 and 03 by Gerbich (2001) and those from SW01 by Zaric (2001). Recent analyses on samples from SCS-SW, -S and -SC were carried out at Christian Albrechts University in Kiel and first used for the Diplom study of Xuan (2014) (Table 9).

Particles were brought into suspension in 20 ml distilled water and 2 ml 0.1 M sodium pyrophosphate ($Na_4P_2O_7$x 10 H_2O) in a centrifugation vial until the suspension began to develop flow marks/streaks. Grain size distribution analysis was carried out at Christian Albrechts University in Kiel with a Beckman Coulter LS 13 320 Laser Diffraction Particle size analyser ALM Aqueous Liquide Module. This device measures with a multi-wavelength system and detects a grain size range from 0.04-2000 µm with 0.1346 Φ steps. Among the multiple information grain size analyses provides about sediment, only the volume percentage of the fraction smaller than 2 µm was used in this study. Basic grain size statistics were calculated by the Excel Macro Gradistat (Blott and Pye, 2001) and used for the general classification of sinking particulate matter.

3.2.3. Clay mineralogy

Clay mineral analysis was done at the State Key Laboratory for Marine Geology at Tongji University in Shanghai, China. Basically, sample preparation follows the method of (Holtzapffel, 1985). The natural limitation of sample material made it necessary to prepare slides with the unfavorable drip method (Gibbs, 1968). The resulting data cannot be used for quantitative comparisons with analyses done with other preparation techniques.

Dried samples were separated from their filters, filled into an Erlenmeyer flask and dissolved in approximately 50 ml of distilled water, depending on the mass of sample material. To promote physical separation of the particles the suspension were only shaken by hand and stirred by a magnet rotator. Organic matter was oxidized by 5 ml 30% hydrogen peroxide (H_2O_2). To support the reaction, the suspension was stirred for 30 min and left to react for 5 days at room temperature. The reaction was considered to be finished when gas production subsided. Carbonate particles were dissolved by 50 ml of 0.5% hydrogenchloride (HCl) and again stirred for 30 min before adding distilled water up to 500 ml and another 30 min of stirring. The pH value should not be higher than 2, which was probed by universal pH indicator paper. Readjusting the pH by adding more acid was not necessary. To prevent the corrosion of lithogenic minerals, it was necessary to dilute the acid with distilled water as soon as possible. As centrifugation would promote cohesion of minerals, the suspension was left to sink down naturally before siphoning off the acid. The first time this takes six to eight hours, depending of the grain size distribution, the second and third time about 24 hours. Usually, three dilution steps of 500 ml to 600 ml were enough. Once the solution was neutral, most samples got split into two parts: One split was meant for clay mineral analysis, the other for grain size analysis.

From the split destined for clay mineral XRD the fraction smaller than 2 µm was extracted (Figure 19). We chose this method of mineralogical X-ray diffraction for better comparability to the existing data (Boulay et al., 2007; Liu et al., 2012, 2010a, 2009, 2008, 2007a; H. Wang et al., 2011). Taking advantage of Stokes' law of differential settling, the samples were stirred thoroughly and left to settle for 95 min at room temperature. Afterwards, the upper 2 cm of the suspension were siphoned off carefully with a syringe, put into plastic tubes and centrifuged for 15 min at 2000 rpm (Holtzapffel, 1985). This step needed to be repeated several times, depending on the content of lithogenic matter and grain size distribution of each sample. Even though the major part of opaline matter was estimated to be coarser than 2 µm, a fair amount of opaline fragments mixed with the <2 µm lithogenic matter fraction (Figure 20). Being amorphous, opal does not produce any interfering peaks, but cause a baseline hump in the 22°-29° 2Θ range. However, the resulting reduction of signal-to-noise ratios was low during most measurements. X-ray diffraction was done using a PANalytical X'Pert PRO Multipurpose Diffractometer. The slides were measured while rotating to provide best statistical coverage of the measurement area (r=0.5 cm). The 2Θ angle proceeds with 0.2 °/s and covers 2Θ=1° to 2Θ=30°.

Syringe

2 cm

<2 µm fraction

2 µm - 1 mm particles
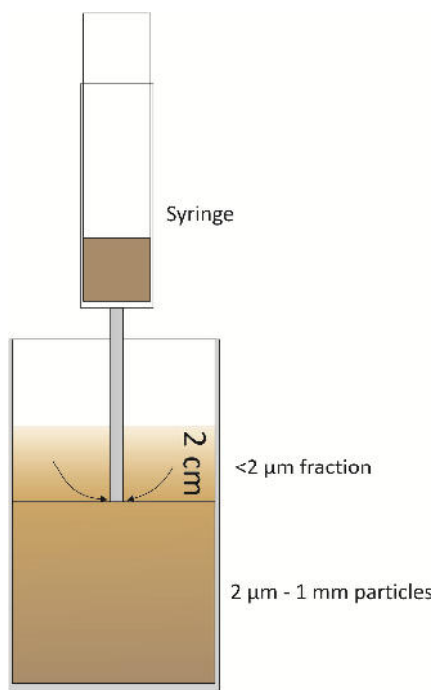
Figure 19: Sampling of the <2 µm fraction from suspension after 95 minutes of settling (re-drawn after (Holtzapffel, 1985)
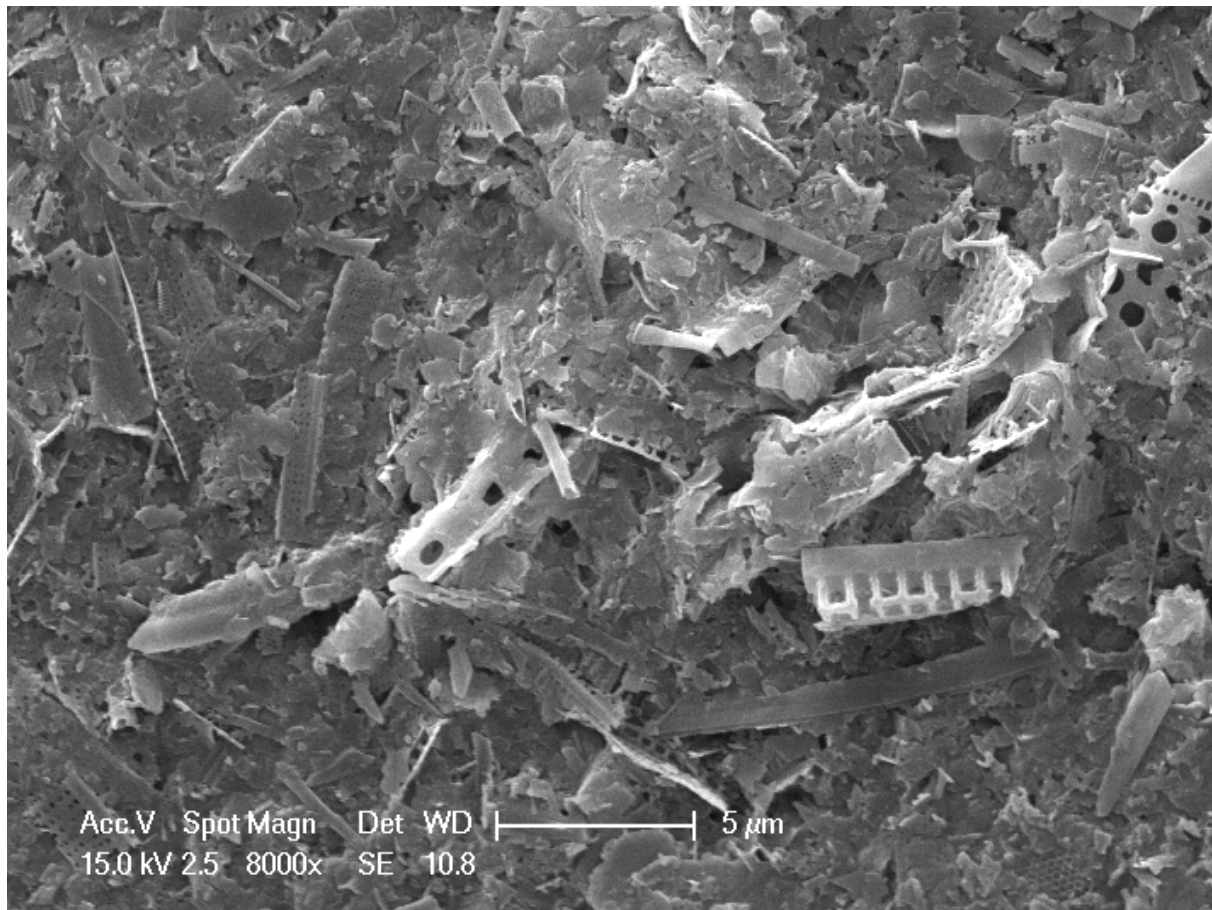
Figure 20: Scanning Electron Microscopy image of a drip-oriented slide. Several bulky opaline fragments remained in the <2 μm fraction and disturb the evenness of the XRD-slide surface.

Each sample was measured three times in a naturally dried state (N), a glycolated state (EG) and heated state (H). The N measurement shows the reflection of the minerals as they are. The saturation of the sample with ethylene glycol vapor causes smectite to swell, intensifies its reflection and increases its peak area. For glycolation the samples were put into a previously evacuated desiccator with an open pot of ethylene glycol at the bottom and left to absorb the vapor for 24 hours. The effect of the ethylene glycol vapor dissipates significantly after approximately 4 hours, therefore samples were measured within this time window. Heating irreversibly destroys smectite, making smectite and chlorite peaks easier to separate. The slides were heated with 490°C for 2 h and cool down slowly over night (approximately 10 h). Some slides got destroyed during heating, which results from high smectite contents.

The clay mineral groups of interest to this study are smectites, chlorites, illites and kaolinites. They were identified by the (001) and (002) plane reflections of the diffractogram in glycolated mode, which represent the layer thickness (smectite: 14-17 Å, chlorite: 14 Å, illite: 10 Å and kaolinite 7 Å) (Table 6, Figure 21). Before identification, the diffractogram was shifted into position with reference to the marker peak of Quartz (100) at 4.26 Å. Indeed, the four mineral groups are the main components the <2 μm fractions of all samples. Further accessory minerals present in most samples are K-Feldspars and Orthoclase, Quartz and occasionally Gibbsite.

Table 6: Parameters used for mineral identification.

mineral	reflection plane	thickness	angle
		[Å]	[2Θ]
Smectite	(001)	14-17	3.15-2.60
Chlorite	(001)	14.1	3.13
Illite	(001)	10	4.42
Chlorite+Kaolinite	(002)+(001)	7.1	6.23
Illite	(002)	5	8.86
Chlorite	(003)	4.72	9.39
Quartz	(100)	4.26	10.41
Kaolinite	(002)	3.57	12.46
Chlorite	(004)	3.54	12.56
Illite+Quartz	(003)+(101)	3.33	13.37
Feldspar	(110)	3.21	13.88
max		44.12	1
min		1.54	30
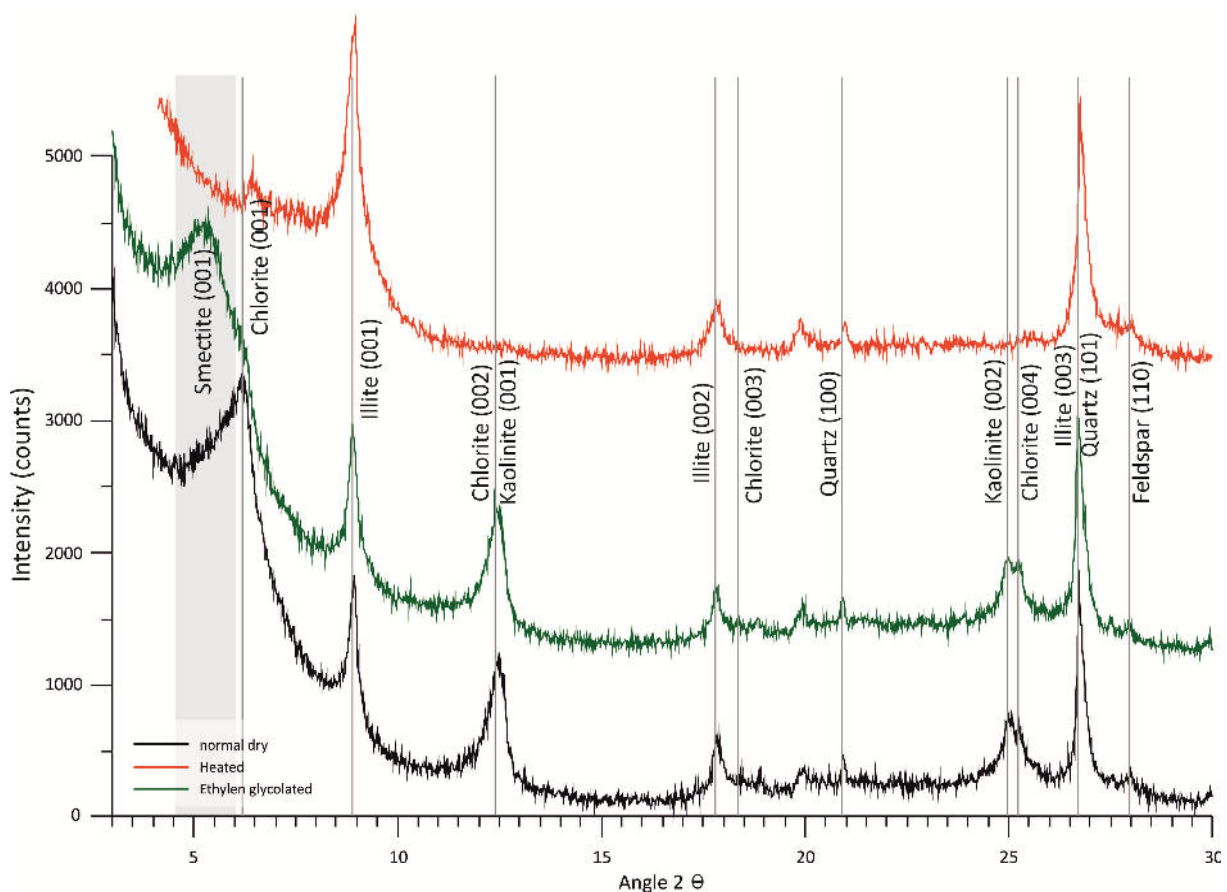
Figure 21: Exemplary diffractogram in normal, glycolated and heated modi, with markers at 2θ-angles of the most frequent reflecting planes.

Data output is as .xrdml and can be converted into .udv, .csv and .txt formats. Data evaluation was done using MacDiff 4.2.5. The calculation of the baseline was calculated by MacDiff with the standard settings used at Tongji. Definition of the peak limits was done manually. Relative minerals

abundances were calculated using the unweighted Peak Areas (PA) of the four mayor clay mineral classes according to the following equations.

$$PA_{sum} = PA_{Sm(001)} + PA_{Illite\ (001)} + PA_{Chl(002)\&Kao(001)} = 100\%$$

$$Sm\%^* = 100^* (PA_{Sm(001)}/ PA_{sum})$$

$$Chl\%^* = 100^* [PA_{Chl\ (002)}/(PA_{Chl\ (002)} + PA_{Kao\ (004)})] * PA_{Chl(002)\&Kao(001)}/ PA_{sum}$$

$$Ill\%^* = 100^* PA_{Ill(001)}/ PA_{sum}$$

$$Kao\%^* = 100^* [PA_{Kao(004)}/(PA_{Chl\ (002)} + PA_{Kao\ (004)})] * PA_{Chl(002)\&Kao(001)}/ PA_{sum}$$

Clay mineral fluxes were calculated with the lithogenic matter flux, the volume percent of the <2 μm fraction and the relative clay mineral abundance (Figure 18). It needed to be assumed that there is no significant difference between the Vol% and mass% of the <2 μm fraction, that the amount of clay sized minerals other than clay minerals is negligible and that the relative clay mineral abundance calculated from the peak areas of reflection intensities is conform with the real proportions.

$$f_{Sm} = (f_{Litho})x\ (Vol\%_{<2μm})\ x\ (relAb_{Sm})$$

$$F_{CM(y)} = \frac{\sum FCM(I) * 365}{\sum dI}$$

$$SR_{Litho} = \frac{\frac{FSm}{\varrho Sm} + \frac{FChl}{\varrho Chl} + \frac{FIll}{\varrho Ill} + \frac{FKao}{\varrho Kao}}{10000} + (1-Vol\%_{<2μm}) * \frac{\frac{FLitho}{\varrho Qz}}{10000}$$

Dripping suspension onto the glass slides is less favorable than the smeared oriented slide (Gibbs, 1968). Even during the less than twenty-four hours of drying in very little water with high density, the particles within the drop sink differentially according to their grain size. It is to be expected, that depending on grain size distribution and clay mineral contents of the suspension, the percentage of smectite and kaolinite accumulated in the upper layers of the slide is higher than in the total slide. If the drip slide results thicker than the X-ray perpetrates, the measured smectite and kaolinite contents results higher than the real content. Especially in samples with high suspension concentration and high contents of opaline fragments segregating clay minerals and opal developed a visible zonation while drying (Figure 22). Observation through the Scanning Electron Microscope (SEM) proved, that grain size diminishes from the center outward, so differentiation between clay mineral species might occur as well. The ring with smaller grain size can lie outside the measurement area, what sometimes caused low intensities of reflections.
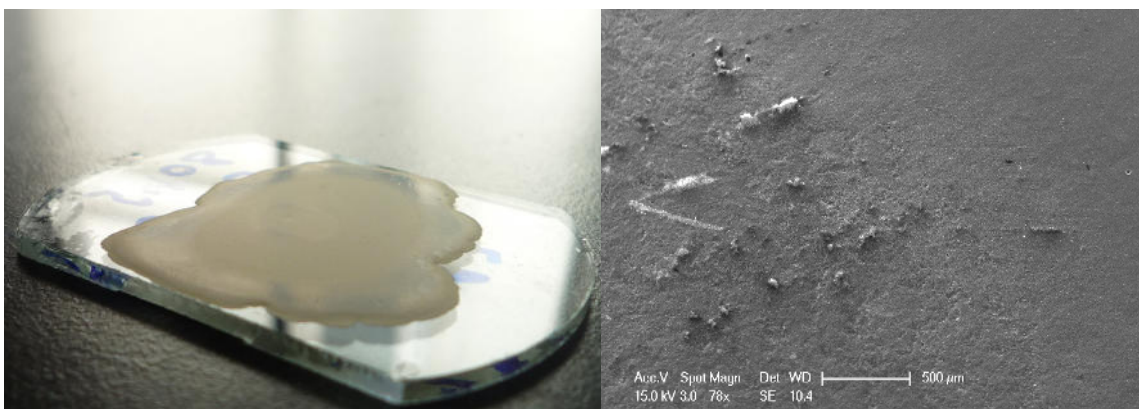
Figure 22: Some samples developed a visible zonation on the slides while they dried (left). Coarser grains concentrate in the center and finer grains at the rim of the dripped slide (right).

3.2.4. Trace elements

Preparation and analysis of trace elements were done at the Laboratory of Christian Albrechts University in Kiel (Garbe-Schönberg, 1993). Around 20 mg of the bulk <1 mm fraction of samples was moisturized with water and dissolved by hydroflouric acid and aqua regia. After boiling at 160°C for 2 hours, the solution was left to vaporize off at 180°C until near dryness. Perchloric acid was added as fluor blocker, cooked at 180-190°C and left to nearly dry. The residual liquid was rinsed with nitric acid and deionized water, boiled at 160°C/120°C and left to evaporate until near dryness. The residual liquid was diluted with nitric acid and deionized water before transfer into receptacles for analysis (Table 7).

Trace element measurements were done using an inductively coupled plasma mass spectrometer of the type VG Instruments PlasmaQuad PQ1 in 1996 (C02, C03, N01, N02) and 1998 (C04, C05) and using a AGILENT 7500cs during the measurement campaigns in 2001 (C07, NC01, NE01, SW01), 2005 (NE01, N01, S01, Vietnamese Rivers, Pearl River Estuary) and 2014 (N03, N04, W02, Taiwan Rivers). Standards used for calibration of the ICP-MS were BIR-1, BHVO-1, MAG-1. Only few samples could be measured twice or more times. As an example for internal error calculation SCS NE01 M09 has been measured six times with standard deviations for the RRE concentrations between 0.0015 and 0.007 which equals 0.25-1.14%. The concentrations of elements were normalized by the concentrations of the standard PAAS rock (McLennan, 1993)(Table 8). The Element ratios Eu* and LREE/HREE were calculated based on the normalized concentrations.

Table 7: Details of chemical agents used during sample preparation before ICP-MS analysis.

Step	Chemical agent	concentration	amount	duration	Temperature
Suspension	H_2O	(distilled, <0.05 µS)	500 µl		Room temperature
Dissolution of detrital fraction	hydrofluoric acid HF	40% (suprapur)	4 ml	2 h (vaporization to near dryness)	160°C hotplate (180°C)
	Aqua regia HCl + HNO_3	37% + 65% (P.A., distilled)	3 + 1 ml		
Rinse I (Fluor blocker)	Perchloric acid $HClO_4$	60%	1 ml	(vaporization to near dryness)	190°C hotplate (180°C)
Rinse II	Nitric acid HNO_3	65% (P.A., distilled)	2 ml	2 h (vaporization to near dryness)	160°C hotplate (180°C)
	H_2O	(distilled, <0.05 µS)	1 ml		
Rinse III	Nitric acid HNO_3	65% (P.A., distilled)	0.5 ml	2 h (vaporization to near dryness)	120°C hotplate (180°C)
	H_2O	(distilled, <0.05 µS)	5 ml		
Dilution, transfer	H_2O	(distilled, <0.05 µS)	<20 ml		

Table 8: Lanthanides concentrations of the Post Archaean Australian Sedimentary rocks (PAAS) used for normalization (in ppb) (McLennan, 1993)**.**

La	Ce	Pr	Nd	Sm	Eu	Gd	Tb	Dy	Y	Ho	Er	Tm	Yb	Lu
38.20	79.60	8.83	33.90	5.55	1.08	4.66	0.77	4.68	27.00	0.99	2.85	0.41	2.82	0.43

$$LREE = \frac{[La]}{[La]PAAS} + \frac{[Ce]}{[Ce]PAAS} + \frac{[Pr]}{[Pr]PAAS} + \frac{[Nd]}{[Nd]PAAS}$$

$$MREE = \frac{[Sm]}{[Sm]PAAS} + \frac{[Eu]}{[Eu]PAAS} + \frac{[Gd]}{[Gd]PAAS} + \frac{[Tb]}{[Tb]PAAS}$$

$$HREE = \frac{[Dy]}{[Dy]PAAS} + \frac{[Ho]}{[Ho]PAAS} + \frac{[Er]}{[Er]PAAS} + \frac{[Tm]}{[Tm]PAAS} + \frac{[Yb]}{[Yb]PAAS} + \frac{[Lu]}{[Lu]PAAS}$$

$$Eu* = \frac{2 \times [Eu]norm}{[Sm]norm + [Gd]norm}$$

3.3. Previous studies

Organic matter, carbonate, opal and lithogenic matter fluxes were measured on most samples. Whenever possible, analyses of grainsize, geochemistry, clay mineralogy, amino acids and nitrogen isotopes were carried through. Due to natural limitations of particulate matter, not all analyses could be done on all samples. The previously produced data also used in this study was taken from various thesis and publications listed in Table 9.

Table 9: References for data used in (previous) studies.

Mooring	Fluxes	Grainsizes	Clay mineralogy	Geochemistry
SCS-N01	(Chen et al., 1999) Lahajnar/Gerbich/Rieger	(Wiesner et al., 1996)	(Gerbich, 2001) (Rieger, 1995)	(This study)
SCS-N02	Lahajnar/Gerbich/Rieger		Gerbich/Rieger	(This study)
SCS-N03	This study	This study	This study	This study
SCS-N04	This study	This study	This study	This study
SCS-NE01	Lahajnar	-	This study	This study
SCS-NE02		-	This study	-
SCS-NC01	Lahajnar/Glos (Gaye et al., 2009)	(Glos, 2002)	This study	This study
SCS-C01	Chen/Gerbich/Rieger	Wiesner	Gerbich/Rieger	--
SCS-C02	Chen/Lahajnar/Gerbich/Rieger	Wiesner	Gerbich/Rieger/ This study	This study
SCS-C03	Chen/Lahajnar/Gerbich /Gaye		Gerbich This study	This study
SCS-C04	Chen/Lahajnar/Gerbich /Gaye		Gerbich This study	This study
SCS-C05	Lahajnar/Gaye		-	This study
SCS-C06	Lahajnar/Glos	(Glos, 2002)	This study	
SCS-C07	Lahajnar/Gaye	(Zaric, 2001)	This study	This study
SCS-W01	This study	-	-	-
SCS-W02	This study	This study	This study	This study
SCS-SC01	(Amann, 2008) Gaye/Xuan	(Xuan, 2014)	This study	-
SCS-SC02	Amann/Xuan	(Xuan, 2014)	This study	-
SCS-SW01	Gaye/Xuan/Lahajnar	Zaric/ Xuan	This study	-
SCS-SW02			-	-
SCS-SW04	Gaye/Xuan	(Xuan, 2014)	This study	(Stichel, 2007)/ This study
SCS-SW05	(Xuan, 2014)	(Xuan, 2014)	This study	-
SCS-SW06	(Xuan, 2014)	(Xuan, 2014)	This study	-
SCS-S01	Amann/Gaye/Xuan	(Xuan, 2014)	This study	Stichel/ This study
SCS-S02	Amann/Gaye/Xuan	(Xuan, 2014)	This study	-

4. Fluxes of clay minerals in the South China Sea

Annette Schroeder[1,2], Martin G Wiesner[2], Zhifei Liu[1]

[1]State Key Laboratory for Marine Geology, Tongji University, Shanghai 200092, China

[2]Institute of Geology, Hamburg University, 20146 Hamburg, Germany

Abstract - In order to assess dominant settling processes that change the composition of the detrital clay fraction during transport from neighbouring estuaries to a deep sea basin, we studied relative clay mineral abundances and absolute clay mineral fluxes of clay-sized sinking particulate matter collected by eight sediment trap systems deployed from shallow to deep water depth in the South China Sea. This is the first basin-wide study on recent sedimentation processes in the western Pacific marginal seas.

Annual averages of relative clay mineral abundances at the shallow traps are temporally more variable and regionally more diverse, resembling those of surrounding drainage basins. In contrast, higher fluxes of material reach the deeper traps. Their characteristics trend temporally and spatially towards uniformity and are enriched with smectite in the entire deep basin.

Sinking particulate matter that reaches the shallow traps spends less time in pelagic transport and is affected by monsoonal current reversals. The enrichment in smectite in the deeper traps is a result of longer duration in transport at low velocities, which may increase the effect of differential settling during transport. The trend is caused by lateral advection driven by the cyclonic deep circulation, and this is considered as the main transport process in the northern and central deep basin. The high fluxes in the south-western deep basin could be the result of laterally advected re-suspended sediments from the neighbouring shelves.

The effects on the composition of the detrital clay fraction caused by oceanographic control, which indirectly include those by differential settling, mask the climatic signal from surrounding drainage basins in the deep basin sediments. This strongly affects the interpretation of the clay mineralogical record in sediments deposited under recent conditions in the South China Sea deep basin.

Key words: clay minerals, provenance, transport processes, sediment traps, South China Sea, deep water settling

4.1. Introduction

Clay minerals in recent marine sediments are mainly detrital in origin (Griffin et al., 1968; Petschick et al., 1996; Velde, 1995) and as such have been widely used to trace the provenance of terrigenous particles in oceanic settings (Gingele and De Deckker, 2004), to constrain the intensity of continental weathering in the source region and hence climate changes on adjacent landmasses (Chamley, 1989) and to delineate the transport routes of suspended sediment loads from source to sink (Oliveira et al. 2002; Gingele et al. 2001). The relative abundances of the four major clay mineral groups (smectite, illite, chlorite and kaolinite) in sediments are used as proxies for silica weathering, sea level change and current intensities (Fagel et al. 1997). In the South China Sea (SCS) detailed and systematic clay mineral studies have been completed for much of the shelf, slope and basin sediments and adjacent rivers (Aoki, 1976; Chen, 1978; Tang and Wang, 1993; Z. Liu et al. 2008, 2010a, 2015; Li et al., 2012; J. Liu et al., 2013). They were cored and surface-sampled in high resolution to reconstruct weathering intensities (Boulay et al., 2005; Liu et al., 2007a, 2003a), sea level change (Steinke et al., 2008), provenance and contribution of sources (J. Liu et al., 2013, Z. Liu et al., 2010a).

The latter was calculated by clay mineral end member modelling under the assumption that the composition of sinking particulate matter is nearly unaffected by sorting or alteration during transport (Z. Liu et al., 2010b; J. Liu et al., 2013; 2014). However, the mapping clay of mineralogical characteristics of recent surface sediments of the north-eastern South China Sea revealed sediment zonation (Zhifei Liu et al., 2010a), which is likely the result of differential settling among clay minerals during transport across the shelf, as it had been proven for the Amazon River delta, the Niger delta and during laboratory studies (Gibbs, 1977; Porrenga, 1966; Whitehouse et al., 1960). Also in the South China Sea, clay minerals' depositional patterns may reflect rather transport routes of suspended sediment loads than source area characteristics, as it was demonstrated for other study areas (Fagel et al. 1997; Oliveira et al. 2002; Gingele et al. 2001). Therefore the role of segregation and redistribution processes during transport, which may modify suspension's composition, may need to be considered more carefully when interpreting proxies.

The aim of this study is to bridge the observation between the input of detrital particles at river mouths and their deposition in deep oceanic basin, to assess the processes apt to modify the clay mineral assemblages during transport in the open SCS. To achieve this we compare the fluxes and compositions of clay mineral assemblages intercepted by sediment traps in shallow, mid- and deep water across the basin with those of the surrounding rivers' sediments.

4.1.1. Study area

The South China Sea (SCS) is a semi-enclosed basin, which is connected to the open oceans by several shallow and narrow straits and the deeper Luzón strait (P. Wang et al., 2009). Its basin is confined by broad shelves of less than 100 m water depth in the north (the South China Shelf) and west (the Vietnamese and Sunda shelves) and by narrow shelves off Taiwan and Luzón (Figure 23). Morphology and monsoonal wind stress determine the complex and variable circulation patterns at the surface, which include seasonal current reversals from NE-wards during northern summer to SW-wards during northern winter (Bonjean and Lagerloef 2002; Shaw and Chao 1994; Qu 2000). The monsoonal reversal was also modelled for the water column down to 100 m (Chu et al., 1999; Huang et al., 2011) (Figure 23). According to their thermohaline characteristics, the monsoonally driven layers of surface and subsurface waters reach from 0-350 m water depth (Li et al., 2002). The intermediate, deep and bottom water layers are decoupled from the surface and subsurface waters and nearly unaffected by the monsoonal current reversals. They range regionally at different water depths. The central basin is 3500 to 5000 m deep and nearly completely enclosed. The only sill deep enough to affect basin wide deep circulation is the Luzón Strait in the east to the Pacific Ocean (Chao et al., 1996; Wang et al., 2009).

Bottom water forms through import of the Western Pacific Deep Water (WPDP) that enters the deep basin of the SCS though the Luzón strait at water depths below 1800 m. The water mass recurs the deep basin as an annually steady basin-scale cyclonic gyre (Figure 24) (Qu et al., 2006; G. Wang et al., 2011; Xie et al., 2013) with an effective SW-ward transport of water-masses (Wan and Jian, 2014). These well up at the south-western margin of the deep basin and pass the SCS as intermediate and deep waters at a water depth from 500 m down to even 3000 m water depth (Wan and Jian, 2014). These waters are advected across the SCS below the monsoonally affected surface and subsurface layers towards NE and exit again through the Luzón Strait at water depths between 500 m and 1800 m (Wan and Jian, 2014).

The rivers around the SCS discharge particulate matter of diverse compositions into the sedimentary basin (Z. Liu et al., 2015) (Figure 23). In the northern basin, clay mineral dischargers are the Taiwanese Rivers, which sediments are dominated by chlorite and illite (Z. Liu et al., 2008), Luzón Island, which sediments are dominated by smectite (Z. Liu et al., 2009) and the Southern Chinese

Rivers, which are dominated by kaolinite and contain smectite very scarcely (Z. Liu et al., 2015, 2007a). In the western part of the basin, Mekong, Red River and most of the Vietnamese coastal rivers discharge very similar kaolinite-rich assemblages, which contain less than 10% of smectite (Z. Liu et al., 2007a, 2015). Rivers draining southern central Vietnam with its basaltic terrains are enriched in smectite (>25%). In the south, along the Malay Peninsula and western Borneo fluvial sediments contain high relative abundances of kaolinite (H. Wang et al., 2011) while northern Borneo and northern Palawan river sediments are again rich in illite and chlorite. The river loads of southern Palawan on the other hand are characterized by comparatively higher smectite contents (Z. Liu et al., 2015).

Currently observed suspended sediment discharge to the SCS from surrounding rivers adds up to as much as 700 million tons annually, making the SCS the largest sink for fluvial sediments among enclosed or semi-enclosed marginal seas worldwide (Z. Liu et al., 2015; Milliman and Farnsworth, 2011). Major Total Suspended Solids (TSS) dischargers are the Taiwanese Rivers (123 Mt/y; 30% of the known basin-wide TSS) the Mekong (110 Mt/y; 27%) and the Red River (50 Mt/y; 12%) (Figure 23). The Pearl River (25 Mt/y; 6 %) and South Chinese drainage basins (26 Mt/y; 6.3%) account for 51 Mt/y (12.3%). With the exception of Western Borneo (30 Mt/y; 7.3%), all other known dischargers into the South China Sea contribute less than 5% of the annual TSS into the SCS, including Thailand, Luzón and Hainan. Even the known, incomplete TSS discharge of Vietnamese coastal rivers sums up to 14 Mt/y (3.4%) (Milliman and Farnsworth, 2011). No recent sediments from the Yangtze are considered to reach the South China Sea (Z. Liu et al., 2008; Xu et al., 2009), though they discharge into the adjacent East China Sea. Dust fallout from the Gobi desert and loess Plateau are largely restricted to the South China shelf and slope (Lin et al., 2007) and their annual fluxes range between 10-20 g m^{-2} y^{-1} (S.-H. Wang et al., 2011; 2012).

4.1.2. Materials and methods

Sinking particles were collected by Mark VI and Mark VII time-series sediment traps which were deployed at eight locations according to major oceanographic and atmospheric features of the SCS (Table 10): in the centre of the SW-monsoon coastal upwelling region off Vietnam (SCS-SW), in the Vietnam offshore current (SCS-SC), in the NE-monsoon upwelling centre off the northern edge of the Sunda shelf (SCS-S), inside and outside the Luzón Upwelling cell (SCS-NE and SCS-NC, respectively), in the northern SCS below the major wind axis and dust veil of the NE-monsoon (SCS-N), south of the Xisha Islands where a branch of the SCS interoceanic through flow turns eastward (SCS-W) and in the oligotrophic central South China Sea (SCS-C) remote from continental Sources (Figure 23).

The traps were placed at water depths between 500 and 3700 m; so all of them were positioned in intermediate and deep water layers; so all of them were positioned in intermediate and deep water layers, below the monsoonally affected surface and subsurface layers. Collection intervals were between 16 and 28 days (Table 10). The topmost centimetre of surface sediments were sampled from a standard box corer at stations SCS-SW, -C, -N and -NE at 1850, 4240, 3760 and 2900 m depth. There was no visible bioturbation; the fluffy layer was lost during recovery. Sedimentation rates are regionally different, but generally high in the SCS: During the Pleistocene, sedimentation rates were calculated from cores as: 46 cm/ky north of station SCS-N (ODP 1146; Z. Liu et al., 2003a); 40.7 cm/ky between stations SCS-S, SCS-SW and SCS-SC (MD01-2393; Z. Liu et al., 2005); 8 cm/ky near SCS-NE (17927-2; (L. Wang et al., 1999)); 7 cm/ky near SCS-W (17954-2; (L. Wang et al., 1999)); 5-8.5 cm/ky

Changes of clay mineral and trace element characteristics in the Deep South China Sea
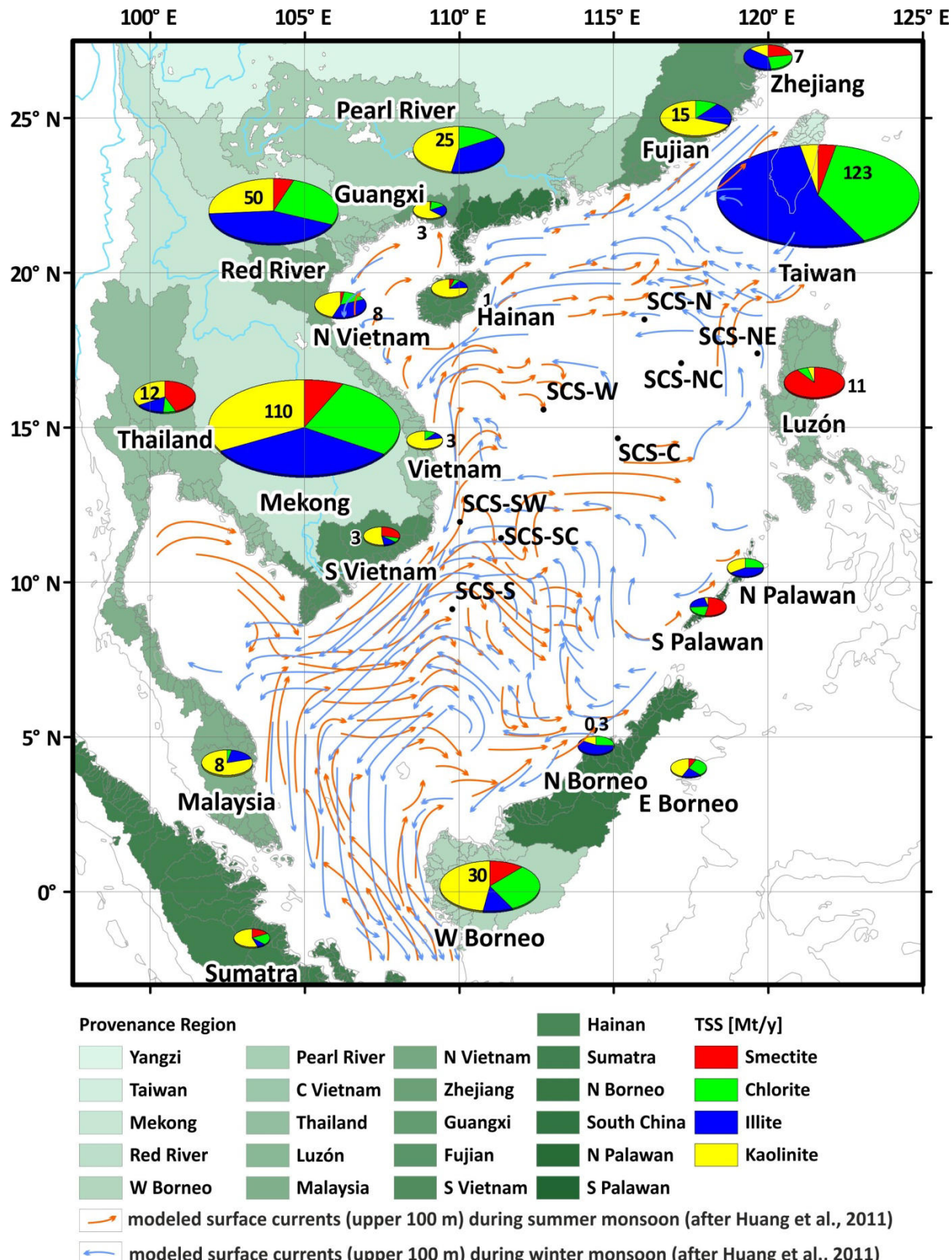
Figure 23: Locations of the sediment trap moorings (Table 1) in the SCS. Clay mineralogy of the surrounding drainage basins (Liu et al. in review). Red: smectite; purple: chlorite; blue: illite; yellow: kaolinite. Size of the pie charts represents the drainage basins' contribution to the basin wide total suspended solids (TSS) in percent calculated from the Global River Database (Milliman and Farnsworth 2011). Current directions in the upper 100 m water column reverse from NE-wards during summer monsoon to SW-wards during winter monsoon along the Indochina and Chinese Coasts; in the central basin currents are less variable (Huang et al., 2011)**.**
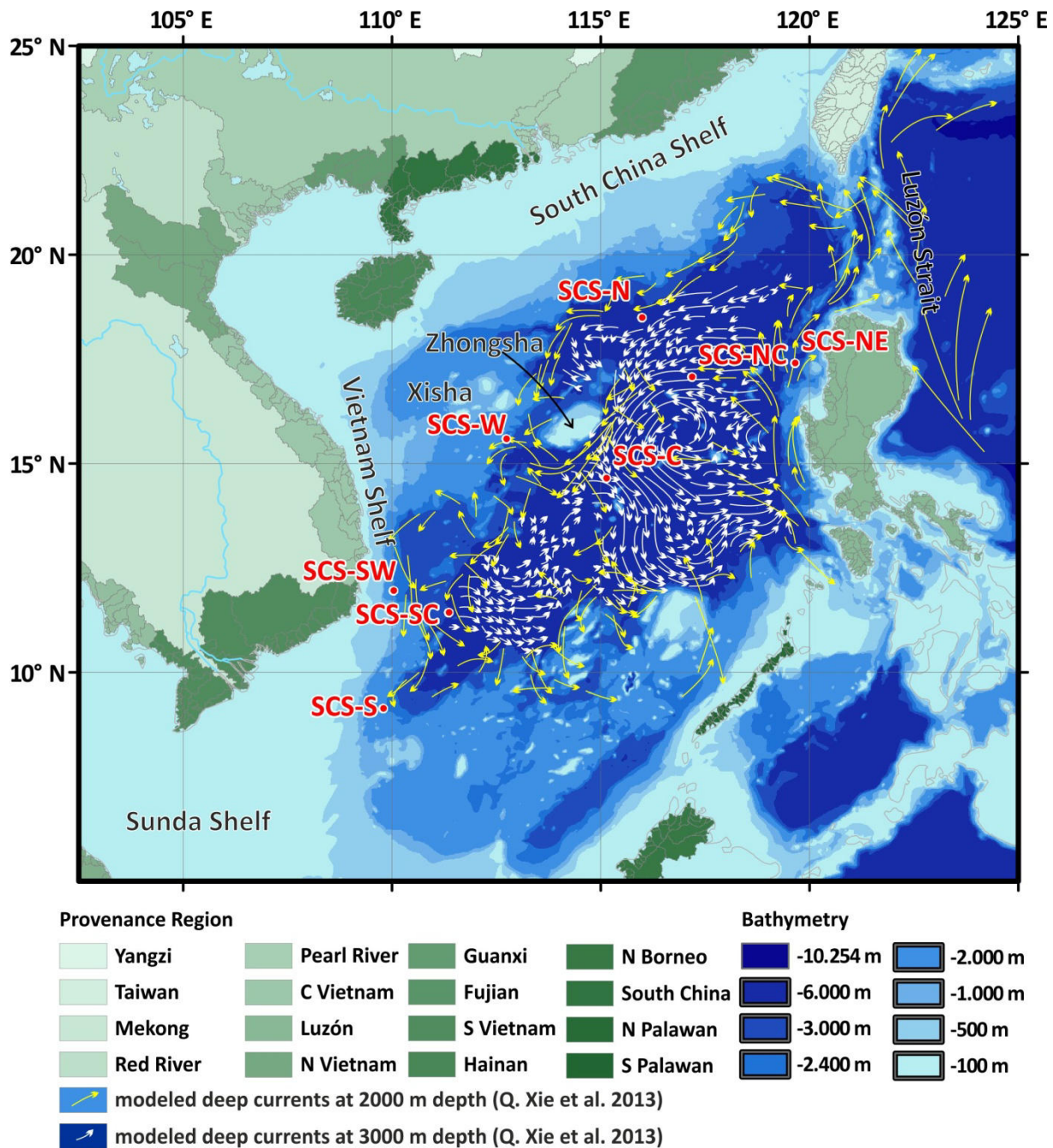
Figure 24: The modelled deep circulation at 2000 m, 3000 m (Xie et al., 2013) **and 2400 m depth** (G. Wang et al., 2011) **is consistently cyclonic.**

near SCS-C (17953-4; (Sarnthein et al., 1994)). These rates would produce 1 cm of sediment within 22 (SCS-N), 25 (SCS-S, -SW, -SC), 125 (SCS-NE), 167 (SCS-W) 200-118 (SCS-C) yrs.

Prior to the deployment of the sediment traps sample cups were filled with sea water from the respective trap depths filtered over WHATMAN GF/F filters (precombusted at 450°C). NaCl (33.3 g/l) and HgCl$_2$ (3.33 g/l) were added to the cups to minimize diffusion and to retard decomposition of the trapped material. After recovery, the wet samples were passed through a 1 mm mesh nylon sieve to exclude pelagic macro organisms. Subsequently the <1 mm fractions were split into aliquots with a high-precision rotary splitter, then filtered over pre-weighed Nucleopore filters (0.45 μm pore size) and dried at 40 °C for 12 h. The dry weights of these fractions were used for calculating the total mass fluxes and for component analyses. The amount of lithogenic material was computed as the

difference between the total mass of particulates and the sum of carbonate, organic matter and biogenic opal (Lahajnar et al. 2007).

Relative clay mineral abundances of the 0.45-2 μm fraction (relAb$_{CM}$) were measured at the State Key Laboratory of Marine Geology at Tongji University. To separate the bulk lithogenic fraction for clay mineral analyses both the surface sediment and bulk trap samples were treated sequentially with HCl (0.5%) and H_2O_2 (3%) to remove organic matter and carbonate, respectively. The clay fractions (0.45-2 μm) were separated from the bulk lithogenic matter by gravitational settling according to Stoke's law and centrifugation. Clay films were then prepared by pipetting 1 ml of the aqueous clay suspension onto glass slides and allowing the suspension to dry at room temperature (Holtzapffel, 1985). Whenever the calculated amount of 0.45-2 μm sized lithogenic matter on the glass slide fell short of 1 mg/cm², samples could not be used for clay mineral analysis, which resulted in 6.1% data loss. X-ray diffraction (XRD) was performed on a PANalytical X'Pert PRO diffractometer equipped with a nickel-filtered Cu-Kα radiation operating at 45 kV and 40 mA. The divergence slit was fixed at 0.38 mm. Three XRD runs were performed on the oriented mounts: untreated, glycolated (24 h in vapor of ethylene glycol) and heated at 490 °C for 2 h. Diffraction patterns were recorded from 1 to 30 °2Θ at a scan rate of 0.2 °2Θ/s. Most of the diffractograms revealed the presence of amorphous silica in the fine fraction, which caused unresolved baseline humps. Since these humps were small, they did not interfere significantly with the quantification of the individual clay minerals. Their relative abundance was calculated by measuring the peak areas (smectite (001): 15-17 Å, illite (001): 10 Å and kaolinite/chlorite: 7.1 Å) of the glycolated samples using MacDiff 4.2.5 software for the main clay mineral groups (Petschick, 2002). Relative proportions of kaolinite and chlorite were determined using the ratio of Kaolinite (002) and Chlorite (004) peak areas (3.57 Å and 3.54 Å) by the Pearson VII peak fit routine (Table 11). Smectite-chlorite mixed layer mineral peaks could not be differentiated from the smectite peaks. Only traces of quartz and feldspar were present in the 0.45-2 μm fraction. Correction factors (Biscaye, 1965) were not used in order to maintain the comparability to the existing data base (Z. Liu et al., 2015). The reproducibility error of the method is ±5%.

Part of the residue was leached with Na_2CO_3 (7%) at 85 °C for 5 hours to obtain opal-free subsamples for grain size analyses (Mortlock and Froehlich, 1989). They were then rinsed (H_2O dest.) into a vial and dispersed by tetrasodium diphosphate ($Na_4P_2O_7$ x 10 H_2O; 2 ml 0.1 M on 20 ml suspension). Grain size analyses were carried out at Christian Albrecht University in Kiel with a Beckman Coulter LS13 320 Laser Diffraction Particle Size Analyser. The laser was equipped with an Aqueous Liquid Module (ALM) to account for the small quantities of sample material available. Measurements were performed over the size range 0.04-2000 μm (14.542 to -0.932 Φ) in 0.1346 Φ resolution with a reproducibility error of less than 2 % on the remaining 0.45 μm to 1 mm fraction. The volume percent of the fraction 0.45-2 μm ($V_{0.45-2μm}$) was summed up and used to calculate the flux of clay-sized lithogenic matter.

Clay mineral fluxes of each sample interval ($F_{CM}(I)$) in [mg m^{-2} d^{-1}] were calculated for each of the four major mineral classes with $F_{litho}(I)$ as the lithogenic matter flux of the interval (I), $V_{0.45-2μm}$ the volume percent of the clay-sized fraction, and relAb$_{CM}$ the relative abundance of the clay mineral:

$$F_{CM}(I) = (F_{Litho}(I)) \times (V_{0.45-2μm}) \times (relAb_{CM})$$

As $V_{0.45-2μm}$ is nearly invariable at most stations, the average volume percent of each trap was used to calculate the clay mineral fluxes, whenever grain size data was missing in the dataset (Table 12). Annual Fluxes (F(Y)) in [mg m^{-2} y^{-1}] (Table 12), were extrapolated via the rule of proportion from the interval fluxes (F(I)) of the data-covered periods with d(I) representing the duration of the interval in days:

$$F(Y) = \Sigma F(I) \times (365/\Sigma d(I))$$

Table 10: Average positions, depths and deployment periods of all sediment traps and numbers of samples taken. SH: shallow, MD: middle, DP: deep.

Station	Trap	Latitude	Longitude	Trap Depth	Sampling Period		Samples
SCS-NC 01	SH	17.075° N	117.192° E	-1465 m	10.12.1996	26.11.1997	13
	DP	17.075° N	117.192° E	-3500 m	10.12.1996	26.11.1997	13
SCS-NE 01	SH	17.399° N	119.657° E	-1225 m	08.07.1998	30.04.1999	13
	MD	17.399° N	119.657° E	-1756 m	08.07.1998	30.04.1999	13
	DP	17.399° N	119.657° E	-2287 m	08.07.1998	30.04.1999	13
SCS-NE 02	SH	17.399° N	119.657° E	-1324 m	15.05.1999	13.05.2000	13
	DP	17.399° N	119.657° E	-2412 m	15.05.1999	13.05.2000	13
SCS-C 01	SH	14.651° N	115.136° E	-1191 m	01.12.1990	03.12.1991	13
	DP	14.651° N	115.136° E	-3730 m	01.12.1990	03.12.1991	13
SCS-C 02	SH	14.651° N	115.136° E	-1191 m	20.03.1992	09.05.1993	13
	DP	14.651° N	115.136° E	-3730 m	20.03.1992	09.05.1993	13
SCS-C 03	SH	14.651° N	115.136° E	-1191 m	01.06.1993	31.05.1994	13
	DP	14.651° N	115.136° E	-3769 m	01.06.1993	31.05.1994	13
SCS-C 04	SH	14.651° N	115.136° E	-1208 m	01.06.1994	05.04.1995	13
	MD	14.651° N	115.136° E	-2243 m	01.06.1994	05.04.1995	13
	DP	14.651° N	115.136° E	-3774 m	01.06.1994	05.04.1995	13
SCS-C 05	MD	14.651° N	115.136° E	-1830 m	01.06.1995	24.06.1996	13
	DP	14.651° N	115.136° E	-3467 m	01.06.1995	24.06.1996	13
SCS-C 06	SH	14.651° N	115.136° E	-1225 m	10.12.1996	26.11.1997	13
SCS-C 07	SH	14.651° N	115.136° E	-1208 m	29.06.1998	25.04.1999	13
	DP	14.651° N	115.136° E	-3744 m	29.06.1998	25.04.1999	13
SCS-SC 01	SH	11.432° N	111.366° E	-884 m	10.05.2005	15.04.2006	21
	DP	11.432° N	111.366° E	-1717 m	10.05.2005	15.04.2006	21
SCS-SC 02	SH	11.432° N	111.366° E	-1200 m	27.04.2006	15.04.2007	21
	DP	11.432° N	111.366° E	-1767 m	27.04.2006	15.04.2007	21
SCS-S 01	SH	9.131° N	109.794° E	-1205 m	30.06.2003	04.06.2004	21
SCS-S 02	SH	9.131° N	109.794° E	-610 m	10.06.2004	07.05.2005	21
	DP	9.131° N	109.794° E	-1193 m	10.06.2004	07.05.2005	21
SCS-SW 01	SH	11.955° N	110.040° E	-1246 m	01.06.1998	01.04.1999	21
SCS-SW 02	SH	11.955° N	110.040° E	-1243 m	15.05.1999	09.07.1999	21
SCS-SW 04	SH	11.955° N	110.040° E	-605 m	10.06.2004	07.05.2005	21
	DP	11.955° N	110.040° E	-1187 m	10.06.2004	07.05.2005	21
SCS-SW 05	SH	11.955° N	110.040° E	-604 m	10.05.2005	15.04.2006	21
SCS-SW 06	SH	11.955° N	110.040° E	-630 m	27.04.2006	15.04.2007	21
	DP	11.955° N	110.040° E	-1214 m	27.04.2006	15.04.2007	21
SCS-W 01	SH	15.584° N	112.742° E	-1100 m	27.06.2009	13.05.2010	21
SCS-W 02	SH	15.584° N	112.742° E	-1200 m	20.05.2011	04.04.2012	21
SCS-N 01	SH	18.498° N	115.999° E	-1000 m	10.09.1987	22.03.1988	21
	DP	18.498° N	115.999° E	-3350 m	10.09.1987	22.03.1988	21
SCS-N 02	DP	18.498° N	115.999° E	-3350 m	13.04.1988	21.10.1988	21
SCS-N 03	SH	18.498° N	115.999° E	-983 m	27.06.2009	13.05.2010	21

Station	Trap	Latitude	Longitude	Trap Depth	Sampling Period		Samples
	MD	18.498° N	115.999° E	-2158 m	27.06.2009	13.05.2010	21
	DP	18.498° N	115.999° E	-3196 m	27.06.2009	13.05.2010	21
SCS-N 04	SH	18.498° N	115.999° E	-983 m	20.05.2011	04.04.2012	21
	MD	18.498° N	115.999° E	-2158 m	20.05.2011	04.04.2012	21
	DP	18.498° N	115.999° E	-3196 m	20.05.2011	04.04.2012	21

4.2. Results

4.2.1. Seasonal variations

Annual lithogenic matter fluxes, the portion of the 0.45-2 µm grain size fraction and relative clay mineral abundances vary throughout the year at each station, but do not generally correlate. Monsoonal or seasonal connections between the parameters vary spatially and temporally and will be treated in more detail in a following study (Schröder et al. in review).

Lithogenic matter fluxes at the shallower traps peak during spring and autumn at all stations except SCS-W, but the peaks translate to the deeper traps only at SCS-N and -NE regularly. At Stations SCS-NC, -SW and -S lithogenic matter peaks in shallow and deep traps do not correlate; often peaks are higher and sharper in the deeper traps. Variations of the volume percentage of the 0.45-2 µm grain size fraction do not correlate to lithogenic matter flux peaks at stations SCS-N, -SW and -W, but they do correlate at SCS-SC and -S. Annual variations of relative clay mineral abundances are regionally different as well. At the traps of the northern stations SCS-N and -W variations are not immediately linked to the lithogenic matter peaks or seasonal variations. At stations SCS-SW and -S variations of relative clay mineral abundances appear to lag behind one interval after the lithogenic matter flux peaks. There appears to be no correlation between 0.45-2 µm fraction and relative clay mineral abundances at any station. At stations SCS-SC and -NE relative clay mineral abundances are nearly invariable throughout the year.

4.2.2. Regional variations of annual clay mineral abundances and fluxes

Clay mineral assemblages intercepted by the shallow and deep traps can be grouped into a northern and central (SCS-C, -W, -NC and -N), north-eastern (SCS-NE) and south-western regional signal (SCS-SW,-SC, and -S).

In the shallow traps in the northern and central SCS the clay-sized fractions account for about 22-27% of the annual lithogenic fluxes which average 6 g m^{-2} y^{-1} at SCS-C, 7 g m^{-2} y^{-1} at SCS-NC, 8 g m^{-2} y^{-1} at SCS-W and 14 g m^{-2} y^{-1} at SCS-N (Table 12). Clay mineral assemblages are dominated by illite and chlorite (SCS-C: 56%; SCS-NC: 65%; SCS-N: 62%; SCS-W: 60%) (Figure 26) with low smectite contents (32%; 23%; 25% and 24% respectively) (Figure 27). In the north-eastern SCS annual lithogenic matter fluxes are high at SCS-NE (12 g m^{-2} y^{-1}) (Table 12,Figure 27). Clay minerals are largely composed of smectite (76%) (Figure 27). In the south-western SCS, lithogenic matter fluxes are around 16, 8 and 22 g m^{-2} y^{-1}, respectively, at SCS-SW, SCS-S and SCS-SC (Table 12). The clay-sized fraction contributes 28-30% to the lithogenic matter and is characterized by relatively high smectite contents (49%; 34% and 43%) and moderate illite plus chlorite abundances (35%; 48% and 40%)(Figure 27).

Down column to the deep traps in the northern and central region annual lithogenic matter fluxes increase moderately and the relative smectite abundances increase strongly (SCS-C: 7 g m^{-2} y^{-1} and 45%; SCS-NC: 9 g m^{-2} y^{-1} and 51%; SCS-N: 15 g m^{-2} y^{-1} and 32%) (Figure 27, Figure 28, Table 11). This is paralleled by increases in the fluxes of the clay-sized fraction (Table 12). At the north-eastern station SCS-NE, lithogenic flux rates increase to 18 g m^{-2} y^{-1} in mid-water and 15 g m^{-2} y^{-1} in the deep water.

The clay mineral assemblages remain smectite dominated (85% and 79%, respectively). In the southwestern region, deep water fluxes of both lithogenic matter and clay minerals are significantly higher than in the shallow traps (60; 47 and 34 g m^{-2} y^{-1}) (Figure 27) and contain more smectite (55%; 46% and 51%). The abundance of 0.45-2 μm fraction remains nearly the same between shallow and deep traps at SCS-SC and SCS-SW (29.3% to 28.8% and 28.5% to 26.7%) and is unchanged at SCS-S (29.4%) at both depths (Figure 27, Table 11).

The topmost centimetre of seafloor sediments below the traps are rich in smectite at stations SCS-SW (46%), SCS-C (62%), SCS-N (55%) and SCS-NE (86%). These values are much higher than the previously presented basin-wide average of 12% relative smectite abundance in deep sea sediments (Chen, 1978).
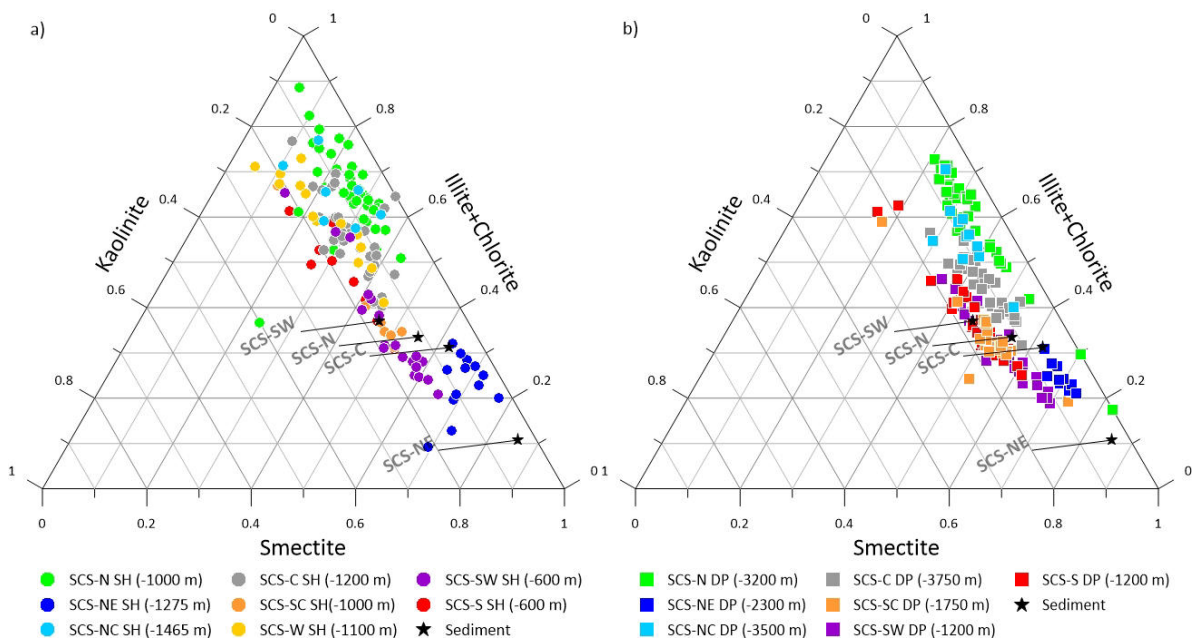
Figure 25: Relative clay mineral abundances in sinking particles intercepted in shallow (a) and deep water (b) at all sediment traps and in the surface sediments at stations SCS-N, NE, C and SW.
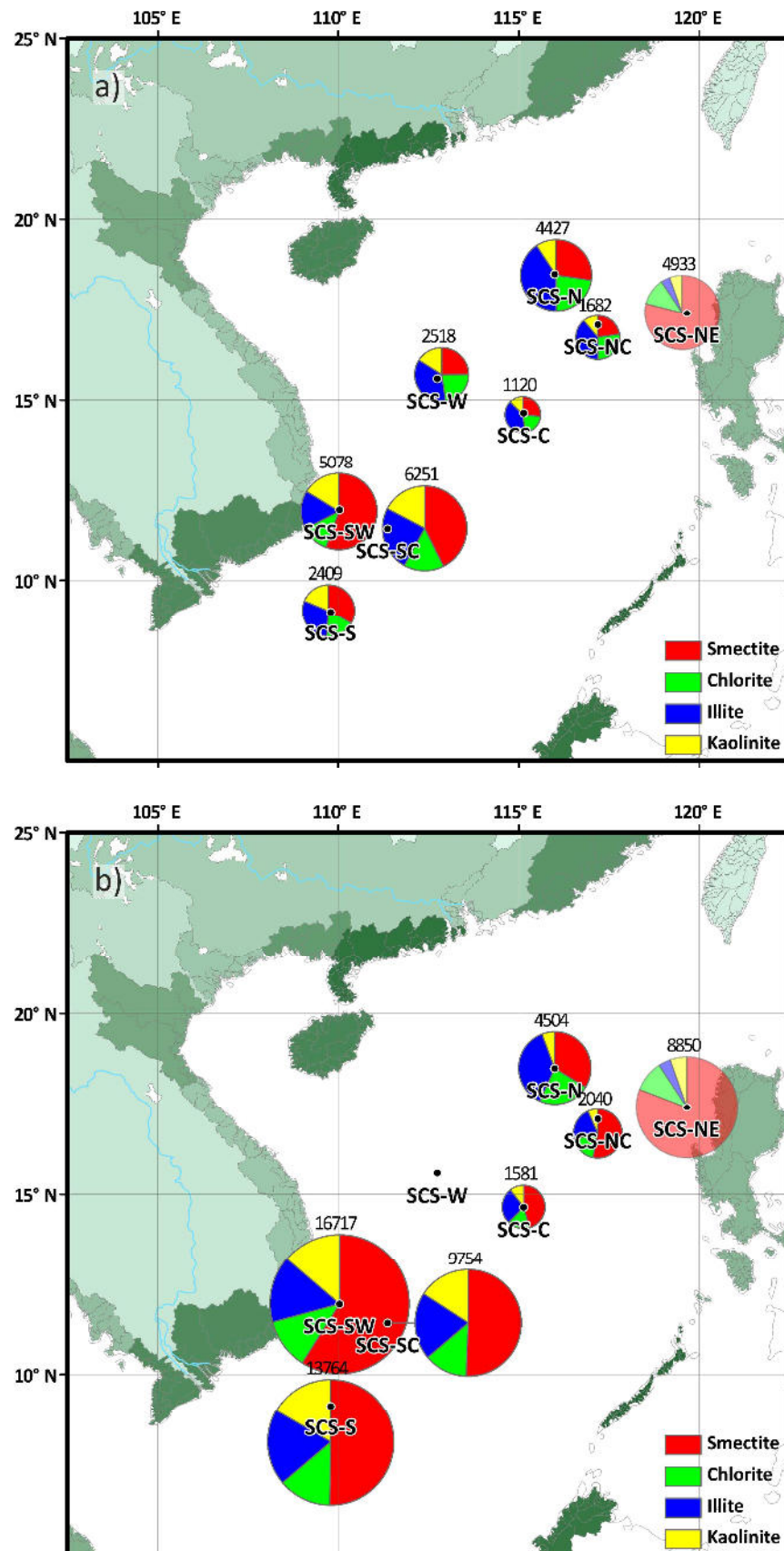
Figure 26: Annual fluxes of clay minerals in the shallow traps (a) and deep traps (b). Red: smectite; Purple: chlorite; Blue: illite; Yellow: kaolinite. Pie chart size represents the annual <2 μm fraction fluxes (mg/m²/y). Clay mineral assemblages are dominated by chlorite and illite in the north central basin and smectite dominated in the south-western basin. Clay fraction fluxes and relative smectite abundance increase with depth in the whole SCS.
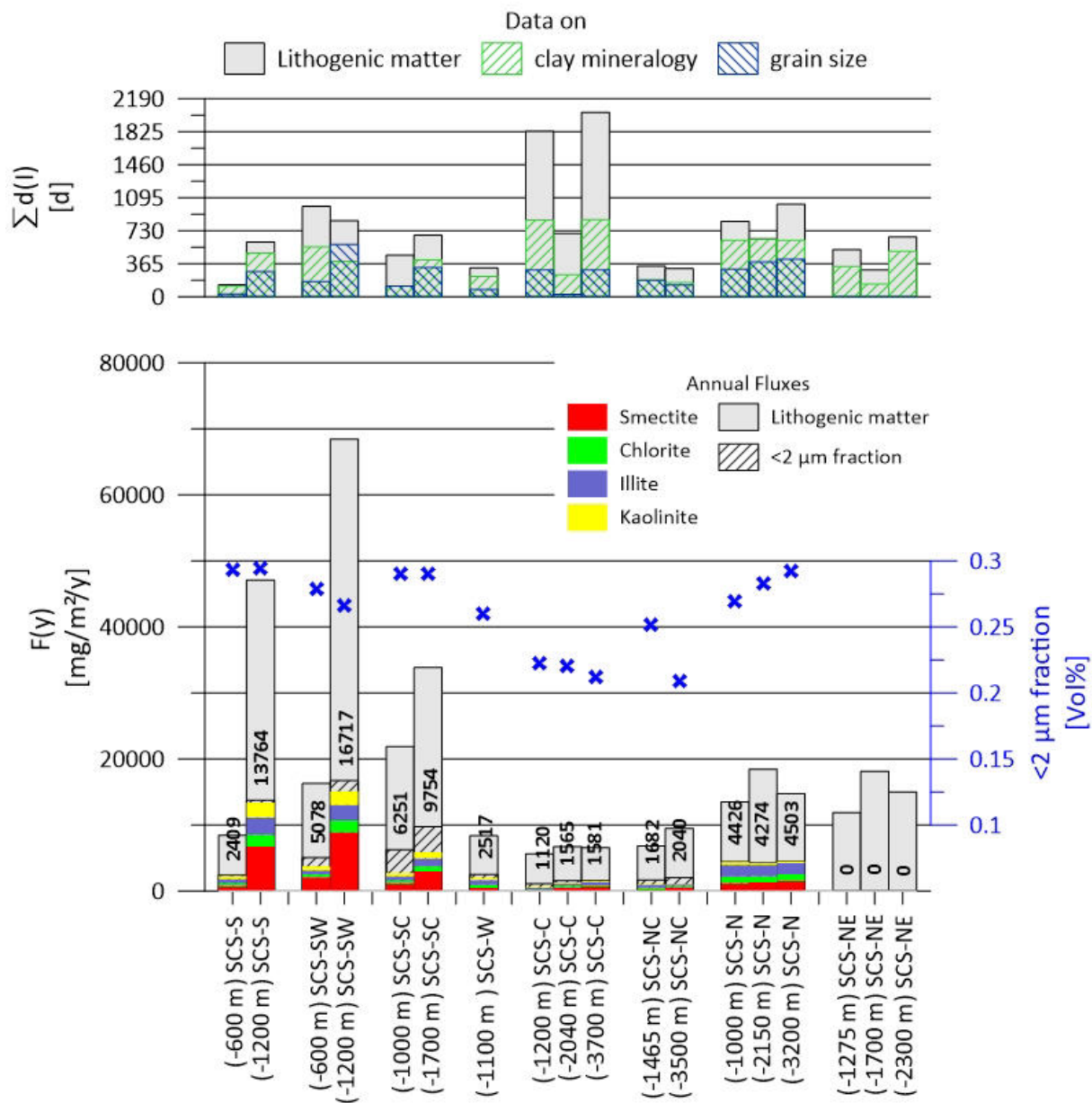
Figure 27: Annual fluxes of lithogenic matter and the four major clay mineral classes. Top: Days covered by analyses on components, grain size and clay mineralogy. Bottom: Annual fluxes of lithogenic matter and the four major clay mineral classes according. Numbers in the bottom figure show the sum of clay-sized matter fluxes, differences to the sum of clay mineral fluxes (slashed area) result from missing clay mineral data. Blue X: average volume percent of clay-sized lithogenic matter in the <1 mm fraction.

Changes of clay mineral and trace element characteristics in the Deep South China Sea

Table 11: Annual averages of clay-sized fractions, relative clay mineral abundances and their standard deviations of sinking particulate matter and seafloor sediments. N. d.: no data.

Trap Name	Depth	average <2 µm	average smectite	average chlorite	average illite	average kaolinite	Illite + Chlorite
	[m]	Vol [%]			[%]		
SCS-NC SH	-1456	25.4	23±9	26±4	39±5	11±5	65
SCS-NC DP	-3700	20.9	51±13	19±5	23±6	7±2	42
SCS-NE SH	-1273	n.d.	76±6	14±4	6±3	5±2	19
SCS-NE MD	-1755	n.d.	84±2	10±1	2±1	3±1	12
SCS-NE DP	-3500	n.d.	79±4	11±2	5±2	5±1	15
SCS-C SH	-1200	22.4	32±8	21±5	35±8	13±4	56
SCS-C MD	-2040	22.2	39±7	19±4	28±6	13±2	48
SCS-C DP	-3700	21.1	45±7	17±3	28±4	11±2	45
SCS-SC SH	-1000	29.3	43±14	15±3	25±9	17±2	40
SCS-SC DP	-1742	28.8	51±9	13±4	20±4	16±3	33
SCS-S SH	-600	29.4	34±11	17±4	30±7	19±3	48
SCS-S DP	-1200	29.4	46±10	15±3	22±6	17±2	37
SCS-SW SH	-600	28.5	49±13	15±5	21±8	16±2	35
SCS-SW DP	-1200	26.7	55±9	13±3	18±5	14±2	31
SCS-W SH	-1100	26.0	24±12	23±2	37±8	16±4	60
SCS-N SH	-1000	26.9	25±8	21±11	41±6	12±12	62
SCS-N MD	-2160	28.3	29±6	23±4	41±4	7±3	64
SCS-N DP	-3200	29.3	32±8	23±2	38±6	6±2	62
Sediments							
SCS-C	-4240	n.d.	62	13	18	7	
SCS-N	-3760	n.d.	55	13	20	11	
SCS-NE	-2900	n.d.	86	9	2	4	
SCS-SW	-1850	n.d.	46	15	22	17	

Table 12: Annual fluxes and data covered days of lithogenic matter, clay-sized fraction and each of the four clay mineral classes.

Trap	Depth	Annual Flux (F)						Data cover		
		Lithogenic	<2 µm	Smectite	Chlorite	Illite	Kaolinite	litho flux	grain size	clay mineral
	[m]	[mg/m²/y]						[d]		
SCS-NC SH	-1456	6832	1682	238	287	411	118	338	182	182
SCS-NC DP	-3700	9495	2040	584	196	246	74	312	130	156
SCS-NE SH	-1273	11882	n.d.	n.d.	n.d.	n.d.	n.d.	521	n.d.	334
SCS-NE MD	-1755	18158	n.d.	n.d.	n.d.	n.d.	n.d.	297	n.d.	140
SCS-NE DP	-3500	15000	n.d.	n.d.	n.d.	n.d.	n.d.	661	n.d.	502
SCS-C SH	-1200	5646	1120	151	122	225	72	1831	298	850
SCS-C MD	-2040	6737	1565	534	252	362	177	701	27	243
SCS-C DP	-3700	6581	1581	664	247	391	156	2039	299	851
SCS-SC SH	-1000	21863	6251	1153	417	667	469	459	119	119
SCS-SC DP	-1742	33851	9754	2992	783	1199	940	680	323	408
SCS-S SH	-600	8449	2409	745	398	674	419	135	30	120
SCS-S DP	-1200	47090	13764	6725	1821	2615	2229	605	280	483
SCS-SW SH	-600	16305	5078	2076	448	610	610	1000	167	552
SCS-SW DP	-1200	68449	16717	8931	1775	2344	2082	840	580	392
SCS-W SH	-1100	8374	2517	494	452	720	319	320	80	224

Trap	Depth	Annual Flux (F)						Data cover		
		Lithogenic	<2 µm	Smectite	Chlorite	Illite	Kaolinite	litho flux	grain size	clay mineral
	[m]	[mg/m²/y]						[d]		
SCS-N SH	-1000	13520	4426	1194	991	1789	409	835	304	624
SCS-N MD	-2160	18466	4274	1288	963	1730	294	640	384	640
SCS-N DP	-3200	14743	4503	1525	1028	1688	260	1025	416	624

4.3. Discussion

4.3.1. Regional transport mechanisms

For each sediment and sediment trap a 'catchment area' of particle provenance can be projected from a 'statistical funnel', which was developed to model the provenance of biogenic particulate matter (Siegel and Deuser, 1997). Lithogenic matter that is transported by vertical pelagic sinking is strongly dependent on pelletization during planktonic blooms and gets transported along with biogenic particulate matter, so the model also applies to the pelagically sinking portion of detrital particulate matter. The funnel's geometry depends upon vertical (particle sinking speed) and lateral (current direction and velocity fields) components of movement above the sediment or sediment trap (Waniek et al. 2000). The width of the statistical funnel depends on the sampling location and affects the accuracy of provenance analysis of sinking particulate matter and marine sediments. On the shelves, statistical funnels are narrower due to the shallower depth and less current direction fields above them. In the deep basin, the statistical funnel is larger and more layers of current fields work within it, which widens the catchment area of the statistical funnel and hence the probability to mix with other sources (Waniek et al. 2000). Therefore provenance analysis is less reliable for particulate matter and sediments in the deep basin than on the shelves. Off the shelves, the involvement of re-suspended sediments adds further uncertain variables, because their contribution is hard to quantify and adds previously deposited clay mineral assemblages to the recently discharged ones.

A rare case of well adaptable provenance analysis using clay mineral assemblages provides the material collected at station SCS-NE near the Philippine shelf. It is highly abundant with smectite (Figure 26) and nearly identical to the smectite-rich Luzón river sediments (Z. Liu et al., 2009)(Figure 23). Given the unique signal, proximity to Luzón and northward currents towards the trap (Figure 23, Figure 24) the material reaching there probably exclusively originates from Luzón (Figure 28).

In the north-central basin the annual statistical funnels of the traps are large, as the surface currents change according to the monsoon (Figure 23) and are underlain by the continuous cyclonic deep current (Chao et al., 1996; S.-H. Wang et al., 2011; Xie et al., 2013)(Figure 24). These current fields mix and direct water masses from Luzón and Taiwan towards this region (Figure 23, Figure 24). The material reaching SCS-N and SCS-NC is abundant with illite and chlorite (>50%) and also contains significant relative abundances of smectite (23-30%), therefore detrital matter from several drainage basins mixes during transport. Among them are material from Taiwan and Luzón, which both discharge material of distinguishable clay mineral assemblages (Figure 23)(Z. Liu et al., 2008, 2009). The known discharge of TSS originating from Luzón rivers recently is rather low (Figure 23), but the data cover in this region is not complete and probably underestimated (Milliman and Farnsworth, 2011). The rather irregular discharges (by typhoons, flooding and landslides) and the reworking of 1991 Pinatubo ash sediments (Wiesner et al., 1995) may further increase detrital material discharge by Luzón indirectly. The moderate relative kaolinite abundance indicates moderate contribution of material from the South Chinese Rivers including the Pearl River (Z. Liu et al. 2010b; J. Liu et al. 2013)

to the traps at station SCS-N. The absolute and relative differences between the shallow and deep traps are usually high: clay-sized lithogenic matter fluxes at SCS-N increase downwards by 2% and the relative smectite abundances increase by 26%. Also at SCS-NC both clay-sized lithogenic matter fluxes (+21%) and relative smectite abundance (+118%) increase towards the deep trap (3500 m), which is among the highest increase rates in the SCS (Figure 29). At both stations, the vertical change of composition is the effect of stronger influence of the cyclonic deep current and more contribution of Luzón derived matter in deeper water depths and below the shallow traps at 1000 m (SCS-N) and 1500 m depth (SCS-NC) (Figure 28). So there must be a boundary of particle transport conditions between 1000 and 2100 m at SCS-N and between 1500 and 3500 m at SCS-N, which may well relate to water stratification.

Material similarly characterized as that collected at SCS-N and -NC was obtained at stations SCS-W and SCS-C (Figure 26), suggesting, that peripheral zones of the cyclonic deep current could reach them. At SCS-C, the downward increase of both clay-sized lithogenic matter fluxes and relative smectite abundance are considerably high (+41%) between only 1200 m and 1830 m (SCS-C05 MD), indicating more contribution of Luzón derived material to the middle and deep traps (Figure 28) than to the shallow one. So the Luzón particle plume must pass between these two water depths. Variations from the signal found in the traps at SCS-N insinuate mixing with additional materials of uncharacterized origins. At SCS-W it may well derive from the Red River (J. Liu et al. 2013) and seasonally from the south-western region, whenever the Off-Vietnam East-Jet (Fang et al., 2002) elongates its axis towards the north and central basin.

Material collected by shallow traps at stations SCS-SW, -SC and -S in the south-western basin is rich in smectite (49%, 34% and 43%). Though the traps SCS-SW and -SC were both deployed at shallow depths (600 m and 1200 m), the statistical funnels of these traps are expected to be wide, as the surface currents are particularly strong across the Vietnam and Sunda shelves and reverse according to the monsoon (Figure 23). Therefore also provenance analysis, using clay mineral assemblages alone, is particularly difficult in this region. Furthermore none of the known surrounding drainage basins compares to the composition of the detrital clay fraction. The high relative abundance of smectite in the sediments of this region was formerly contributed to material from Luzón (J. Liu et al. 2013). Our observations contradict this interpretation. As the Luzón plume reaches even station SCS-C only at a water depth of 2000 m and below, it is highly unlikely that it can reach stations SCS-SC ,- S and -SW at 600 m and 1200 m depth. The increase of smectite fluxes could else be explained by contribution of material from Sunda shelf sediments (Figure 28). These contain 40% of relative smectite abundance (P. Wang et al., 2009, recalculated from Jagodzinski, 2005) which is similar to the relative abundances of smectite in the clay sized lithogenic matter fraction collected by our traps and within the error range between the different preparation methods applied in these studies.

The vertical gradients of clay-sized lithogenic matter fluxes are particularly high at SCS-SW and SCS-S (+229% and +471%) (Figure 28). Since SCS-SC was deployed farther off-shore (150 km) and deeper (1200 m and 1750 m), clay-sized lithogenic matter fluxes are lower and increase moderately (+56%), which is still high in basin-wide comparison. The reason for these high fluxes are the proximity to the Mekong with its high discharge rates and the Vietnam and Sunda shelf margins (80 km and 50 km), from which significant amounts of re-suspended sediments can be imported episodically. The clay mineral composition is similar in shallow and deep traps (downward increase of smectite: +13% and +20%) (Figure 29). The differences are lower, because the catchment areas of shallow and deep traps are similar, as they were deployed with only 600 m between the shallow and deep traps (Figure 28). Also, upwelling (Hein 2008; Kuo et al. 2000) and probable down-slope currents cause more vertical homogenization of suspension. Due to the lack of a smectite rich riverine source, lateral advection as in the north-central SCS is unlikely to explain the down column increase of smectite.

4.3.2. Basin-wide differential settling

Our observation shows, that at each station, relative and absolute clay mineralogical compositions differ between the traps, which prove that suspension composition changes down the water column. In the shallow traps, clay mineral assemblages are regionally more divers and temporally more variable (Figure 25). In the deep traps they are regionally and temporally more homogeneous and generally enriched with smectite in comparison to the shallow traps at the same station (Figure 29).

Considering the lateral clay mineral zonation documented in the northern South China Sea, namely around the Pearl River estuary, Taiwan and the Philippine shelf (Z. Liu et al. 2010a), the vertical enrichment of smectite can be explained with differential settling during lateral transport (Whitehouse et al. 1958; Gibbs 1977). Whether the differentiation is a result of smectite having a lower, individual density (Osipov, 2012), which can be decreased further by adsorption of organic acids (Satterberg et al., 2003) or preferential flocculation (Asper, 1987) cannot be resolved with this study. Among clay-sized lithogenic matter, differential settling functions at current velocities below <268 cm/s (6 mph) (Whitehouse et al. 1958). This condition is met during most of the year by the surface currents and always by the modelled deep currents.

With increasing depth of a sampling location, the statistical funnel and catchment area widen (Siegel and Deuser 1997; Waniek et al. 2000), which also augments the lateral transport distance and duration of transport. As current velocities tend to weaken down column from <100 cm/s (5-day averages of surface currents; Naval Research Laboratory, 2014) towards less than 20 cm/s (modelled velocities at 2400 m depth; G. Wang et al. 2011), the effectiveness of sorting, and consequentially smectite enrichment, increases with depth. Also the vertical component of sinking particulate matter transport (4000 m within <14 d ≈ <0.5 cm/s) (Wiesner et al., 1996) is well below the critical velocity for differential settling.

Also, clay minerals can sink though thermohaline density barriers only by increasing their size through forming aggregates and faecal pellets (Honjo 1980; Asper et al. 1992). As long as the aggregates remain intact, specific clay mineral signals remain preserved within them. This reduces the effectivity of segregation during transport. But with increasing depths more of the aggregates decompose (Eisma, 1986) and expose the individual minerals to differential settling at greater depths. The decomposition of aggregates at greater depths may further enhance the effectivity of clay mineral segregation in the deep basin.
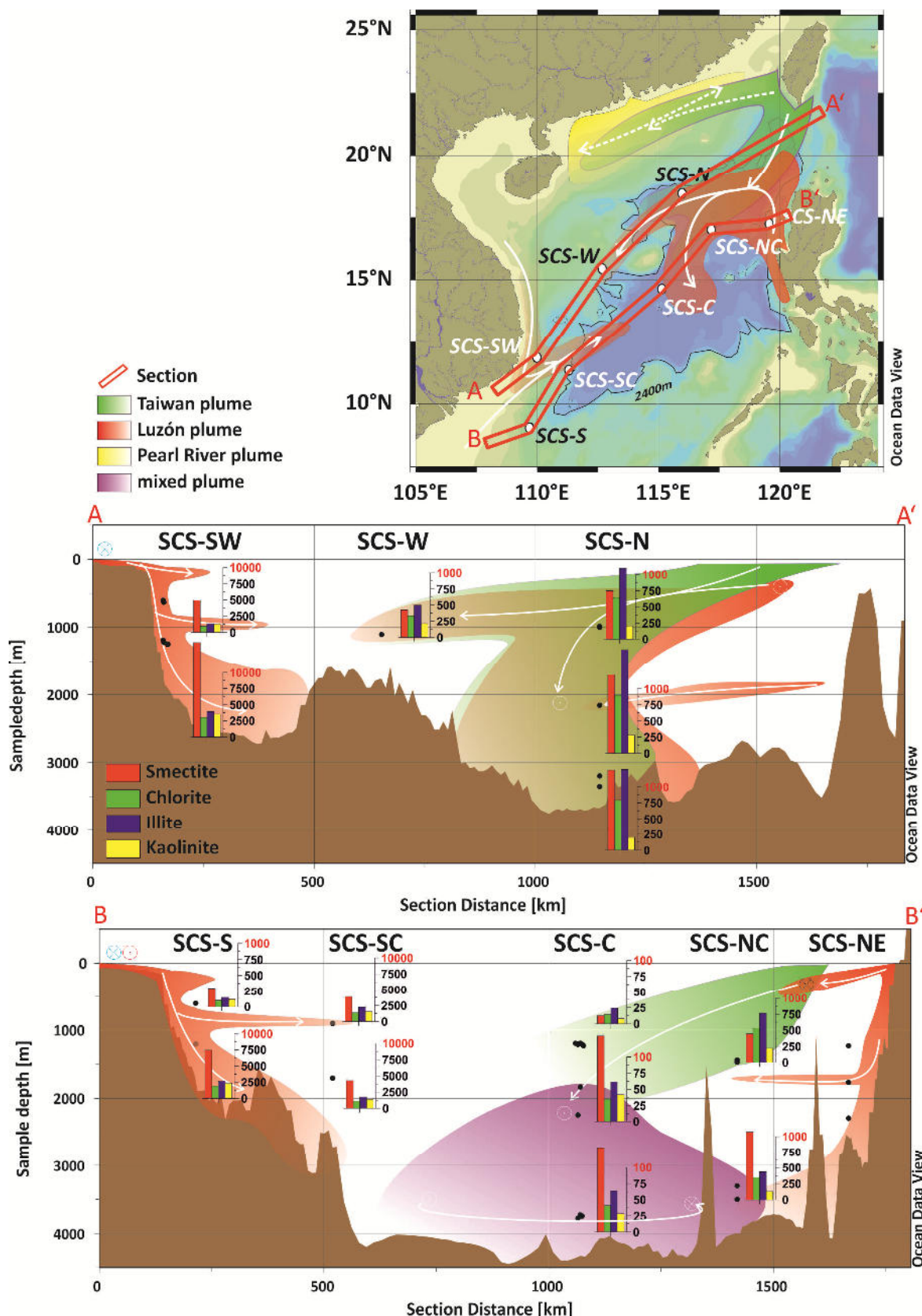
Figure 28: Top: Map with schematic suspension plumes, which follow the modelled deep currents at 2400 m depth (arrows) (G. Wang et al., 2011). **The fine red lines mark the trajectories of the sections. Below: Schematic sections through the SCS basin with an exaggerated vertical scale. Black dots represent the positions of the sediment traps, next to them are diagrams showing annual clay mineral fluxes. Note the difference in scale. Shaded areas are sketches of suspension plumes, encircled dots and X indicate current directions towards the reader and into the page.**
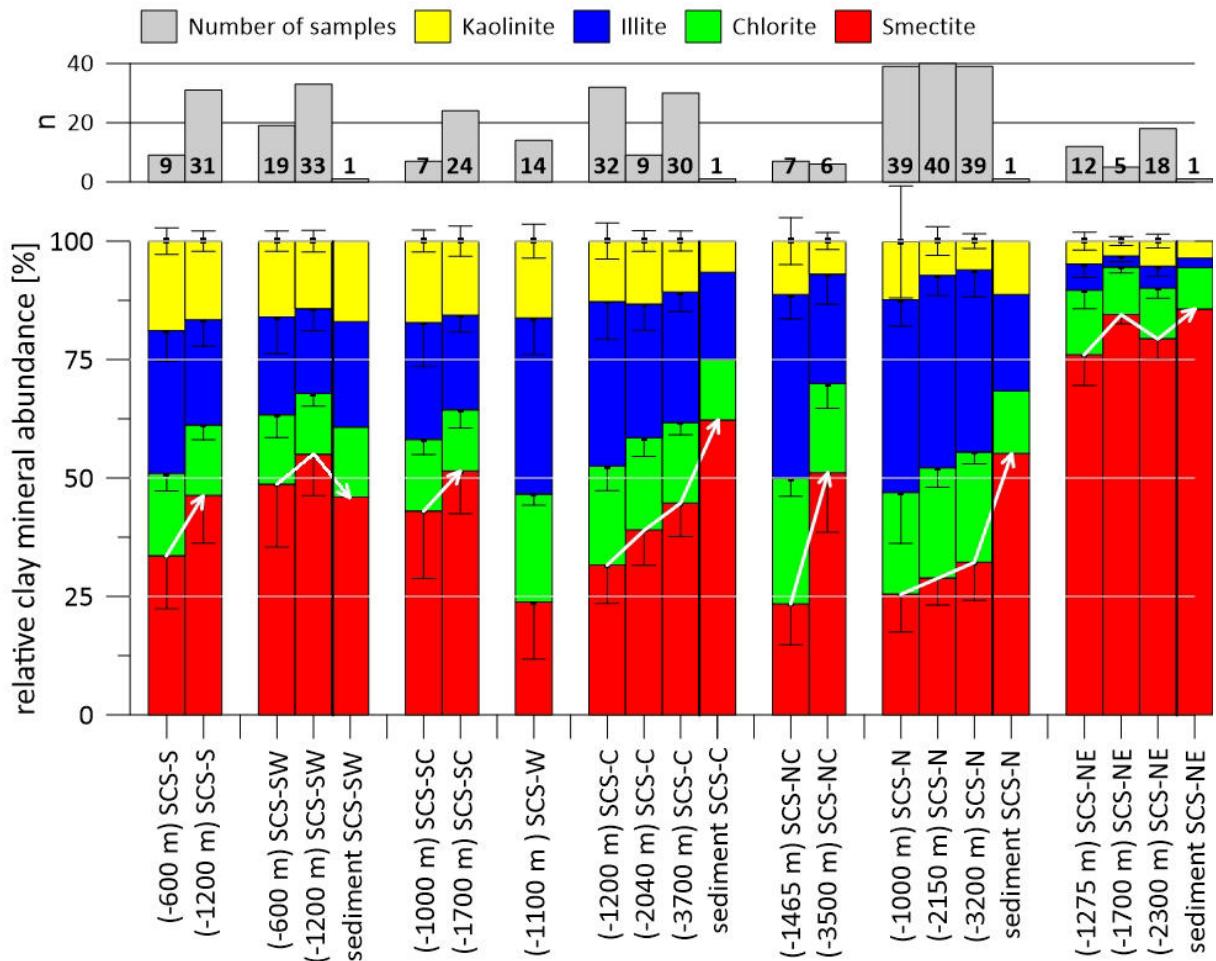
Figure 29: Average relative smectite abundances increase with depth at most stations. Error bars represent the standard deviation among the samples averaged.

4.4. Conclusions

Sinking particulate matter sampled by sediment traps at eight stations reveal regionally diverse clay mineral distributions in the shallow traps and more homogeneous, smectite enriched clay mineral assemblages in the deep waters. The modification of clay mineral assemblages during transport from the fluvial sources towards the final sinks depends strongly upon regional oceanographic conditions.

Clay mineral signals of riverine sources are better preserved in the shallow waters. The fluxes of clay-sized detrital matter are generally lower in the shallow traps than in the deep ones with 4.4 g m^{-2} y^{-1} in the northern basin, 1.1-1.7 g m^{-2} y^{-1} in the central basin and 2.4-6.3 g m^{-2} y^{-1} in the western and south-western basin, respectively. The clay-sized fraction of detrital matter in shallow waters is smectite dominated in the north-eastern region near Luzón (>75%), illite and chlorite dominated (>50%) in the north-central basin and smectite and kaolinite rich in the south-western region (30-50% and 16-18%). Temporal variations of clay mineral assemblages are likely caused by monsoonal current and therefore changes of contribution, which intensify with increasing transport duration.

Lithogenic matter fluxes are higher in the deep traps, indicating lateral advection at all stations. Furthermore, clay mineral compositions are generally less variable, less divers and basin-wide enriched in smectite. Generally, more transport mechanisms and different current layers are involved in the transport of material that reaches the deeper traps and basin floor, because the statistical funnel in which sinking particulate matter reaches the deep traps is larger.

Clay-sized lithogenic matter fluxes are high in the deep traps in the northern (4.3-4.5 g m^{-2} y^{-1}) and low in the central basin (1.6-2.0 g m^{-2} y^{-1}). The smectite contents (32-51%) increase relatively and absolutely in the clay mineral assemblages of those materials. These differences are mainly caused by lateral advection of smectite-rich material originating from Luzón, which were transported by the cyclonic deep circulation in the northern basin. Subordinately, further smectite enrichment is suspected to be caused by differential settling. In the deep traps of the south-western basin, near the Vietnam and Sunda shelves, clay-sized lithogenic matter fluxes (9.8-16.7 g m^{-2} y^{-1}) and relative smectite abundances are very high (46-55%). They increase with depth (+6-15%), but vertical differences in clay mineral assemblages are less intense than in the north-central basin. Down-slope currents provide additional material of re-suspended shelf sediments and better vertical mixing of the suspension-loaded water masses.

The farther off-shore and deeper a sampling location is, the more variables need to be considered for provenance analysis. Clay mineral assemblages are useful provenance indicators in the north-eastern and northern SCS, where Luzón and Taiwan provide very characteristic clay mineral signatures to the basin. The major central Asian rivers provide detrital matter carrying balanced clay mineral assemblages, which are less suitable for provenance analysis. In the south-western region, where there are barely distinguishable source signals and strong, seasonally variable currents, clay minerals are not useful provenance indicators.

In the northern basin, vertical increase of relative smectite abundance is mainly caused by lateral advection of smectite rich detrital matter from Luzón. In the south-western SCS the main cause of relative enrichment are longer lateral transport pathways to the deep traps. Smectite enriches in suspension during lateral transport through preferential settling of chlorite, illite and kaolinite. The effect of differentiation augments with longer duration of transport and slower current velocity. Clay mineral fractionation is more effective with increasing transport distance and by transportation on the slower deep currents. Preservation of clay mineral signals in aggregates restricts differential settling in the shallow water layers, whereas the probability of exposure to differential settling increases with depth, as aggregates tend to decompose while sinking.

In any case, significant modifications of clay mineral assemblages during transport are controlled by oceanographic factors, which mask the drainage basin specific signals. This strongly affects the interpretation of clay mineral assemblages used as proxies for provenance identification or environment indications in deep sea sedimentary records.

4.5. Acknowledgements

5. Regional diversity of geochemistry in the Deep South China Sea

[1,3]Annette SCHRÖDER, [2]Dieter GARBE-SCHÖNBERG, [3]LIU Zhifei, [1]Martin WIESNER

[1]Institute of Geology, Hamburg University, 20146 Hamburg, Germany

[2]Christian Albrechts University, Kiel, Germany

[3]State Key Laboratory for Marine Geology, Tongji University, 200092 Shanghai, China

Corresponding author: annette.heddaeus@zmaw.de

Abstract – The dischargers of particulate matter into the South China Sea (SCS) each provide a trace element signal carried within its primary and secondary minerals. These are regionally a comparatively reliable provenance indicator. Several of the smaller drainage basins, like Luzón, Hainan, Taiwan and Vietnamese rivers can be distinguished by their Europium anomaly, LREE/HREE and Zr/Sc ratios. The main contributors Mekong, Pearl River and Red River are less distinctive, as they drain different types of lithology.

Trace element signals in sinking particulate matter (SPM) intercepted by sediment traps rarely resemble those of the sediments of a singular drainage basin. The signals are affected by dilution, desorption, differential settling and mixing of various provenances. In some regions of the SCS trace element characteristics and clay mineral assemblages, which were used as provenance indicators in previous studies, do not always correlate, which we conclude to result from differential settling among the carrier minerals. We conclude that of the two provenance indicators, trace element characteristics are more reliable.

Key words: South China Sea, Sinking particulate matter, trace elements, REE, clay minerals, source identification

5.1. Introduction

Clay mineral assemblages respond to a variety of mechanisms, which alternate the composition of sinking particulate matter during marine transport (Schröder et al., n.d.). They were previously used as provenance indicators (Fagel and Boës, 2008; Gingele and De Deckker, 2004; Liu et al., 2014, 2013, 2010a; Petschick et al., 1996) but their reliability depends strongly upon the environment of the basin applied on. In this study we want to point out the advantages of provenance analysis by trace elements distributions and their ratios over clay mineral assemblages.

Source identification is one of the first essential steps when interpreting the sedimentary record on the purpose of environmental reconstructions. In the South China Sea (SCS), provenance analyses of marine sediments were previously based on clay mineralogy, trace elements and Neodymium isotopy (Liu et al., 2013, 2010a; Schimanski, 2002). It requires indicators that satisfy three conditions: Firstly, the sediment sources must discharge or supply **specific**, distinguishable **signals**. Secondly, the signal needs to be **temporally stable**. And thirdly, the signals must remain **intact during transport**.

In this study we summarize published and previously unpublished data on trace element characteristics of sediments around the SCS and establish the best indicators for provenance analysis by trace elements. We focus on Lanthanide distribution patterns, light and heavy rare earth element (LREE, HREE) ratios and the zirconium scandium ratio (Zr/Sc). In continuation of our previous study (Schröder et al., n.d.) we aim to test their reliability as a provenance indicator on sinking particulate matter (SPM) collected by sediment traps in a basin-wide long-term sampling campaign.

5.1.1. Clay minerals and Trace elements

The trace element concentration and fractionation in clay minerals depend mainly upon the parental lithology. The parent minerals' rare earth element (REE) concentrations and distributions result from

the chemical composition of the magma from which the parent minerals crystallized. During magmatic rise and crystallization, REE fractionate within the melt. Silicate minerals are prone to substitute Ca^{2+} and Na^{2+} (and subordinately also Mg^{2+}, Fe^{2+} and Al^{3+}) with trivalent REE. Mafic minerals (especially Garnet (Grt), Orthopyroxene (Opx), Clinopyroxene (Cpx) and Amphibole (Amp)) absorb more HREE from the melt. These minerals spurn substitution with Eu^{4+}, which results in a strong (Grt) to weak (Opx, Cpx and Amp) negative Eu* (Okrusch and Matthes, 2009). Plagioclase as the main felsic mineral preferentially substitutes LREE and especially Eu as crystal grid interspace cations (Stosch, 2000). Felsic minerals, especially micas and quartz, which are an abundant component of most acidic rocks, are less prone to substitute cations with REE, mainly because the magma is already depleted with REE and especially HREE during the last stages of crystallization.

All silicate minerals can weather into clay minerals. Into which class specifically depends partly upon the degree of chemical weathering, parental lithology and morphology of the drainage basin (Chamley, 1989; Liu et al., 2012). The degree of weathering is favorably increased by high temperatures, changing wet and dry seasons and fine particle size. Clay minerals and ion-enriched mineral waters are the product of silica weathering and form from parent minerals, which are leached by an 'attack solution' (Chamley, 1989). Therefore clay minerals are prone to contain less REE than their parent minerals, depending on their grade of hydrolysis. Generally, **mafic/basic plutonites** can be expected to contain higher concentrations of REE and are enriched with HREE, whereas felsic/acidic rocks contain a low REE concentration and are enriched with LREE. With increasing contents of plagioclase in mafic rocks an increasingly positive Eu* is to be expected. The later crystallizing **felsic plutonite** must then be depleted with Eu. Due to fast crystallization, **volcanic rocks** do not suffer fractionation (Stosch, 2000). Therefore they reflect the initial REE compositions of the magma. Generally, magma from the upper crust sports a negative Eu* and enrichment with LREE, magma from the lower crust a positive Eu* and also slight enrichment with LREE. Middle Oceanic Ridge Basalts magma from the mantle have no Eu* and a low LREE/HREE ratio, opposed to Ocean Island Basalts magma from the mantel-core boundary, that contain more LREE than HREE (Stosch, 2000). **Sedimentary rocks** contain variable REE concentrations and patterns, which again depend upon the origin of the primary minerals from which they had weathered. Several accessory and main minerals like garnet, apatite, zircon and monazite are very resistant to weathering, contain high REE concentrations and specific Lanthanide distributions (Okrusch and Matthes, 2009). Drainage basins that drain vast sedimentary bodies will always produce a weak and mixed REE signal.

REE cations belong to the most immobile ones, so during weathering, they are the least affected and likely to be preserved in the octahedral layer of the resulting secondary minerals (Chamley, 1989). Nevertheless, if the weathering is very intense, also REE cations can be leached, preferentially LREE, which are slightly more mobile than HREE. This can result in enrichment of HREE in clay minerals compared to their parent minerals.

Illites are fine micas, which themselves are very poor in REE concentrations and are therefore considered not to carry a relevant REE-signal. Nevertheless, micas often include accessory minerals like Zircon, which do carry REE in high concentrations. **Kaolinites** weather from silicate minerals and have suffered a high degree of weathering. They do not contain interlayers to store REE cations and the octahedral layer, which is the one with highest REE cation-substitutions, is already completely leached. If there are REE spared by leaching, they reside in the tetrahedral layer and are probably enriched with HREE. **Chlorites** weather from silicates, but do rather suffer from physical weathering, than from chemical weathering (Chamley, 1989). They are likely to maintain their parental minerals' REE concentrations and patterns. **Smectites** are the product of incomplete weathering; they still possess their cation interlayer and octahedral sheet.

To conclude, chlorite and smectite are the clay minerals which contain most REE. Weathering could enrich the mineral slightly with HREE, which would be more effective in smectite than in chlorite. Nevertheless, the main REE signal in outgoing suspension and riverine sediments reflects that of the main outcrops of magmatic rocks within the drainage basin of the respective river or stream.

5.2. Material and Methods

5.2.1. Sampling

Sinking particles were collected by Mark VI and Mark VII time-series sediment traps which were deployed at eight locations according to major oceanographic and atmospheric features of the SCS (Table 13): in the centre of the SW-monsoon coastal upwelling region off Vietnam (SCS-SW), in the Vietnam offshore current (SCS-SC), in the NE-monsoon upwelling centre off the northern edge of the Sunda shelf (SCS-S), inside and outside the Luzón upwelling cell (SCS-NE and SCS-NC, respectively), in the northern SCS below the major wind axis and dust veil of the NE-monsoon (SCS-N), south of the Xisha Islands where a branch of the SCS interoceanic through flow turns eastward (SCS-W), and in the oligotrophic central South China Sea (SCS-C) remote from continental sources. The traps were placed at water depths between 500 and 3700 m; collection intervals were between 16 and 28 days (Table 13). Surface sediments were taken with a standard box corer at stations SCS-SW, -C, -N and -NE.

Prior to the deployment of the sediment traps sample cups were filled with sea water from the respective trap depths filtered over WHATMAN GF/F filters (precombusted at 450°C). NaCl (33.3 g/l) and $HgCl_2$ (3.33 g/l) were added to the cups to minimize diffusion and to retard decomposition of the trapped material. After recovery, the wet samples were passed through a 1 mm mesh nylon sieve to exclude pelagic macro organisms. Subsequently the <1 mm fractions were split into aliquots with a high-precision rotary splitter, then filtered over pre-weighed Nucleopore filters (0.45 μm pore size) and dried at 40 °C for 12 hours. The dry weights of these fractions were used for calculating the total mass fluxes and for component analyses. The amount of lithogenic material was computed as the difference between the total mass of particles and the sum of carbonate, organic matter and biogenic opal (Lahajnar et al. 2007).

Sediment trap samples were wash sieved (1 mm mesh), split, pump-filtered (Polycarbonate, Nucleopore, 0.45 μm pore size, 0.8 bar), rinsed (H_2O dest), dried on the filters and weighted. Due to the natural limitations of sinking particulate matter the material obtained was not always sufficient for all analyses; therefore during several series only a few samples were selected as representatives.

Vietnamese river sediments were sampled during fieldtrips in 2003 and 2007 from their estuaries. These were analyzed with the method described below and evaluated in an unpublished graduate thesis (Stichel, 2007). The Pearl River estuary sediment was taken by a box core during 'Sonne' - cruise SO-50/104; Taiwanese River sediments sampled during a Field trip in 2007 and analyzed the same way. Philippine River samples were taken during another field trip in 2005 and analyzed at Tongji University.

Table 13: Positions, depths, deployment periods and numbers of samples originally taken of all sediment traps. SH: shallow, MD: middle, DP: deep.

station	trap	latitude	longitude	trap depth	sampling period		samples
SCS-NC 01	SH	17.075° N	117.192° E	-1465 m	10.12.1996	26.11.1997	13
	DP	17.075° N	117.192° E	-3500 m	10.12.1996	26.11.1997	13
SCS-NE 01	SH	17.399° N	119.657° E	-1225 m	08.07.1998	30.04.1999	13
	MD	17.399° N	119.657° E	-1756 m	08.07.1998	30.04.1999	13
	DP	17.399° N	119.657° E	-2287 m	08.07.1998	30.04.1999	13
SCS-NE 02	SH	17.399° N	119.657° E	-1324 m	15.05.1999	13.05.2000	13
	DP	17.399° N	119.657° E	-2412 m	15.05.1999	13.05.2000	13
SCS-C 01	SH	14.651° N	115.136° E	-1191 m	01.12.1990	03.12.1991	13
	DP	14.651° N	115.136° E	-3730 m	01.12.1990	03.12.1991	13
SCS-C 02	SH	14.651° N	115.136° E	-1191 m	20.03.1992	09.05.1993	13
	DP	14.651° N	115.136° E	-3730 m	20.03.1992	09.05.1993	13
SCS-C 03	SH	14.651° N	115.136° E	-1191 m	01.06.1993	31.05.1994	13
	DP	14.651° N	115.136° E	-3769 m	01.06.1993	31.05.1994	13
SCS-C 04	SH	14.651° N	115.136° E	-1208 m	01.06.1994	05.04.1995	13
	MD	14.651° N	115.136° E	-2243 m	01.06.1994	05.04.1995	13
	DP	14.651° N	115.136° E	-2774 m	01.06.1994	05.04.1995	13
SCS-C 05	MD	14.651° N	115.136° E	-1830 m	01.06.1995	24.06.1996	13
	DP	14.651° N	115.136° E	-3467 m	01.06.1995	24.06.1996	13
SCS-C 06	SH	14.651° N	115.136° E	-1225 m	10.12.1996	26.11.1997	13
SCS-C 07	SH	14.651° N	115.136° E	-1208 m	29.06.1998	25.04.1999	13
	DP	14.651° N	115.136° E	-3744 m	29.06.1998	25.04.1999	13
SCS-SC 01	SH	11.432° N	111.366° E	-884 m	10.05.2005	15.04.2006	21
	DP	11.432° N	111.366° E	-1717 m	10.05.2005	15.04.2006	21
SCS-SC 02	SH	11.432° N	111.366° E	-1200 m	27.04.2006	15.04.2007	21
	DP	11.432° N	111.366° E	-1767 m	27.04.2006	15.04.2007	21
SCS-S 01	SH	9.131° N	109.794° E	-1205 m	30.06.2003	04.06.2004	21
SCS-S 02	SH	9.131° N	109.794° E	-610 m	10.06.2004	07.05.2005	21
	DP	9.131° N	109.794° E	-1193 m	10.06.2004	07.05.2005	21
SCS-SW 01	SH	11.955° N	110.040° E	-1246 m	01.06.1998	01.04.1999	21
SCS-SW 02	SH	11.955° N	110.040° E	-1243 m	15.05.1999	09.07.1999	21
SCS-SW 04	SH	11.955° N	110.040° E	-605 m	10.06.2004	07.05.2005	21
	DP	11.955° N	110.040° E	-1187 m	10.06.2004	07.05.2005	21
SCS-SW 05	SH	11.955° N	110.040° E	-604 m	10.05.2005	15.04.2006	21
SCS-SW 06	SH	11.955° N	110.040° E	-630 m	27.04.2006	15.04.2007	21
	DP	11.955° N	110.040° E	-1214 m	27.04.2006	15.04.2007	21
SCS-W 01	SH	15.584° N	112.742° E	-1100 m	27.06.2009	13.05.2010	21
SCS-W 02	SH	15.584° N	112.742° E	-1200 m	20.05.2011	04.04.2012	21
SCS-N 01	SH	18.498° N	115.999° E	-1000 m	10.09.1987	22.03.1988	21
	DP	18.498° N	115.999° E	-3350 m	10.09.1987	22.03.1988	21
SCS-N 02	DP	18.498° N	115.999° E	-3350 m	13.04.1988	21.10.1988	21
SCS-N 03	SH	18.498° N	115.999° E	-983 m	27.06.2009	13.05.2010	21
	MD	18.498° N	115.999° E	-2158 m	27.06.2009	13.05.2010	21
	DP	18.498° N	115.999° E	-3196 m	27.06.2009	13.05.2010	21
SCS-N 04	SH	18.498° N	115.999° E	-983 m	20.05.2011	04.04.2012	21
	MD	18.498° N	115.999° E	-2158 m	20.05.2011	04.04.2012	21
	DP	18.498° N	115.999° E	-3196 m	20.05.2011	04.04.2012	21

5.2.2. Trace element analysis

Preparation and analysis of trace elements were done at the Laboratory of Christian Albrecht University in Kiel (Garbe-Schönberg, 1993). Around 20 mg of the bulk <1 mm fraction of samples was moisturized with water and dissolved by hydroflouric acid and aqua regia. After boiling at 160°C for 2 hours, the solution was left to vaporize off at 180°C until near dryness. Perchloric acid was added as fluor blocker, cooked at 180-190°C and left to nearly dry. The residual liquid was rinsed with nitric acid and deionized water, boiled at 160°C/120°C and left to evaporate until near dryness. The residual liquid was diluted with nitric acid and deionized water before transfer into receptacles for analysis (Table 14).

Trace element measurements were done using an inductively coupled plasma mass spectrometer of the type VG Instruments PlasmaQuad PQ1 in 1996 (C02, C03, N01, N02) and 1998 (C04, C05) and using a AGILENT 7500cs during the measurement campaigns in 2001 (C07, NC01, NE01, SW01), 2005 (NE01, N01, S01, Vietnamese Rivers, Pearl River Estuary) and 2014 (N03, N04, W02, Taiwan Rivers). Standards used for calibration of the ICP-MS were BIR-1, BHVO-1, MAG-1. Only few samples could be measured twice or more times. As an example for internal error calculation SCS NE01 M09 has been measured six times with standard deviations for the RRE concentrations between 0.0015 and 0.007 which equals 0.25-1.14%. The concentrations of elements were normalized by the concentrations of the standard PAAS rock (McLennan, 1993)(Table 8). The Element ratios Eu* and LREE/HREE were calculated based on the normalized concentrations.

Table 14: Details of chemical agents used during sample preparation before ICP-MS analysis.

Step	Chemical agent	concentration	amount	duration	Temperature
Suspension	H_2O	(distilled, <0.05 µS)	500 µl		Room temperature
Dissolution of detrital fraction	hydrofluoric acid HF	40% (suprapur)	4 ml	2 h (vaporization to near dryness)	160°C hotplate (180°C)
	Aqua regia HCl + HNO_3	37% + 65% (P.A., distilled)	3 + 1 ml		
Rinse I (Fluor blocker)	Perchloric acid $HClO_4$	60%	1 ml	(vaporization to near dryness)	190°C hotplate (180°C)
Rinse II	Nitric acid HNO_3	65% (P.A., distilled)	2 ml	2 h (vaporization to near dryness)	160°C hotplate (180°C)
	H_2O	(distilled, <0.05 µS)	1 ml		
Rinse III	Nitric acid HNO_3	65% (P.A., distilled)	0.5 ml	2 h (vaporization to near dryness)	120°C hotplate (180°C)
	H_2O	(distilled, <0.05 µS)	5 ml		
Dilution, transfer	H_2O	(distilled, <0.05 µS)	<20 ml		

Table 15: Lanthanides concentrations of the Post Archaean Australian Sedimentary rocks (PAAS) used for normalization (in ppb) (McLennan, 1993)**.**

La	Ce	Pr	Nd	Sm	Eu	Gd	Tb	Dy	Y	Ho	Er	Tm	Yb	Lu
38.20	79.60	8.83	33.90	5.55	1.08	4.66	0.77	4.68	27.00	0.99	2.85	0.41	2.82	0.43

$$\text{LREE} = \frac{[La]}{[La]PAAS} + \frac{[Ce]}{[Ce]PAAS} + \frac{[Pr]}{[Pr]PAAS} + \frac{[Nd]}{[Nd]PAAS}$$

$$\text{MREE} = \frac{[Sm]}{[Sm]PAAS} + \frac{[Eu]}{[Eu]PAAS} + \frac{[Gd]}{[Gd]PAAS} + \frac{[Tb]}{[Tb]PAAS}$$

$$\text{HREE} = \frac{[Dy]}{[Dy]PAAS} + \frac{[Ho]}{[Ho]PAAS} + \frac{[Er]}{[Er]PAAS} + \frac{[Tm]}{[Tm]PAAS} + \frac{[Yb]}{[Yb]PAAS} + \frac{[Lu]}{[Lu]PAAS}$$

$$\text{Eu*} = \frac{2 \times [Eu]norm}{[Sm]norm + [Gd]norm}$$

5.3. Results and discussion

5.3.1. Specific source signals

Trace element signals preserved in minerals discharged into the SCS are divers (Figure 30). The best characteristics to distinguish drainage basin specific geochemical signals are elemental ratios of LREE/HREE, Zr/Sc ratios and Europium anomalies (Eu*) (Figure 32, Figure 33).

Sediments from **Taiwanese Rivers** have the highest LREE/HREE ratio (0.9 to 1.26) in basin wide comparison. PAAS-normalized concentrations of Samarium, Europium and Gadolinium are nearly equally high and even higher than LREE, therefore there is a low positive, but insignificant Europium anomaly (1.06-1.10) present in these sediments. This signal is typical for felsic crystalline rocks. As the high contents of chlorite and illite implies, chemical weathering (Liu et al., 2008) and subsequent leaching of LREE must be insignificant. Zr/Sc ratios are very high in sediments of the Pei-Kang and Tseng-Wen (12.7-16.3) rivers, which drain the central cordillera, and low in Kao-Ping and Cho Shui (3.7-3.8) sediments.

The main signal emitted from continental Asia (drained Pearl River and South Chinese Rivers) is of slightly higher LREE than HREE contents (resulting in LREE/HREE ratios of 0.10-0.37) and enrichment with MREE. This is typical for felsic rocks of South China and northern Indochina. Additional to this regional background pattern, the **Pearl River** (Xi, Bei and Dong (Zhang et al., 2002)) contains a slightly negative Eu* (0.92). This can develop by crystallization of a residual, Eu depleted melt, which are usually acidic and plagioclase impoverished plutonites (Figure 31)**.**

Hainan rivers that drain the basalt area in the north deliver a positive Eu* (1.43), intermediate LREE/HREE (1.13) and a high Zr/Sc (7.34) ratio into the South China sea (Ma et al., 2007). The central and southern acidic granitoids (Figure 31) are expected to contribute lower concentrations of trace elements. The high LREE/HREE ratio is owed to the very high concentration of Ce in Hainan soils, which is likely to be absorbed in the marine environment by microbial activity (Moffett, 1990). With a 'regular' Ce concentration, the three proxies would all be very similar to those emitted by Luzón Rivers, which have a similar lithology.

Indochine lithology is very divers, containing metamorphic rocks, acid and basic magmatites in the north, basic plutonites in the central region and acidic plutonites, vulcanites and basic vulcanites in the south (Figure 31). Several of the southern, smaller **Vietnamese coastal rivers**, Song Dinh, Song Ninh Hoa, Song Long Song and Song Nha Trang (Figure 30) carry a negative Europium anomaly (0.48-0.93) and a high LREE/HREE ratio (0.48-1.07), which can only result from acidic rocks or vulcanites originating from the upper crust (Stosch, 2000). However the Lanthanide patterns of Mekong, Red River, Ba, Luy and Phang Rang, which include the biggest drainage areas, contain no Eu*, but a high LREE/HREE ratio.

For the southern contributors **Malaysia, Sumatra** and **Kalimantan,** no trace element characteristics are known yet. Based on the main outcrops of acidic Plutonites and volcanic rocks (Hartmann and

Moosdorf, 2012) (Figure 31) it can be assumed, that material from Malaysia and eastern Kalimantan is low in trace element contents with high LREE/HREE ratios and low or negative Eu*. Material from central Kalimantan outcrops of intermediate plutonic rocks and basic vulcanites could be enriched with HREE and significant for the trace element characteristics of sediments in the southern SCS. The significance of contribution of material from Sumatra is still not clarified, but it would carry a slightly HREE enriched signal, probably with a positive Eu* and low Zr/Sc values.

On the eastern side of the basin, namely in sediments of **Luzón** rivers, the signal is characterized by a very low LREE/HREE ratio (0.03-0.07), because they are enriched with HREE, which is typical for the ultramafic rocks and andesitic, plagioclase rich andesites that crop out in western Luzón (Figure 31). Furthermore they are one of the rare riverine sources that contain a strong positive Europium anomaly (1.29-1.45). Another distinctive feature is the very low Zr/Sc ratio (3.98-5.17) (Figure 33), which is unique among SCS sediment dischargers. Among the Luzón sediments, the REE-Signal of the Bucao River has the highest LREE/HREE ratio. As the Bucao river drains the Pinatubo Mountain Region, its signal also represents the Pinatubo 1991 ash layer, that covers vast areas of the central SCS, the Scarborough Seamounts and the Macclesfield bank (Wiesner et al., 2004).

In basin-wide comparison of these features, the fluvial sediments of Luzón, Taiwan, Hainan and small Vietnamese coastal rivers and are the only ones to produce a distinguishable trace element signal (Figure 32). Those of large drainage basins are a mixture of several geochemical signals, as they can drain several types of lithology. Therefore the most important rivers referring to sediment discharge amounts, as the Mekong, Red and Pearl Rivers, have unspecific characteristics in comparison to smaller ones.

Table 16: Specific rare earth element ratios of the river sediments discharging into the SCS.

Region	River name	Latitude [°N]	Longitude [°E]	Reference	Eu*	LREE/HREE	Zr/Sc
Luzón	Abra	17.553	120.395	Z. Liu (personal)	1.280	0.046	4.575
	Abulug	18.338	121.426	Z. Liu (personal)	1.448	0.071	4.281
	Agno	15.980	120.226	Z. Liu (personal)	1.328	0.037	4.295
	Bucao	15.262	120.037	Wiesner (personal)	0.283	34.287	
	Cagayan	18.123	121.673	Z. Liu (personal)	1.435	0.112	5.172
	Pampanga	14.902	120.819	Z. Liu (personal)	1.340	0.023	3.979
South China	Hainan	19.587	110.653	Ma (2007)	1.433	1.134	7.340
	Pearl River Estuary	23.000	113.000		0.921	0.243	8.859
	Pearl River East (Dong)	22.399	113.257	(Zhang & Wang 2001)	0.166	182.080	
	Pearl River North (Bei)	23.105	113.432	(Zhang & Wang 2001)	0.181	128.166	
	Pearl River West (Xi)	23.043	113.524	(Zhang & Wang 2001)	0.207	123.340	
Taiwan	Cho Shui	23.833	120.433		1.095	1.259	3.684
	Kao-Ping	22.637	120.442		1.104	1.139	3.781
	Pei-Kang	23.515	120.179		1.074	0.898	16.278
	Tseng-Wen	23.085	120.127		1.065	1.181	12.681
Vietnam	Mekong 03	10.249	107.039	Stichel (2007)	0.990	0.167	
	Mekong 05	10.249	107.039	Stichel (2007)	1.073	0.189	
	Nha Trang	12.606	109.131	Stichel (2007)	0.483	0.241	
	Song Ba	13.062	109.317	Stichel (2007)	1.004	0.368	
	Song Cai Nin Hoa	12.486	108.727	Stichel (2007)	0.773	0.158	
	Song Cai Phang Rang	11.604	108.936	Stichel (2007)	0.983	0.132	
	Song Dinh	10.706	107.841	Stichel (2007)	0.825	0.161	
	Song Hong	20.467	106.067	Stichel (2007)	1.036	0.210	
	Song Long Song	11.239	108.563	Stichel (2007)	0.931	0.099	
	Song Luy	11.172	108.563	Stichel (2007)	0.979	0.160	

Table 17: River sediments' PAAS-normalized concentrations of Lanthanides.

River name	La PAAS	Ce PAAS	Pr PAAS	Nd PAAS	Sm PAAS	Eu PAAS	Gd PAAS	Tb PAAS	Dy PAAS	Ho PAAS	Er PAAS	Tm PAAS	Yb PAAS	Lu PAAS
Abra	0.307	0.489	0.503	0.644	1.104	1.747	1.624	1.635	1.722	1.702	1.821	1.736	1.728	1.705
Abulug	0.438	0.563	0.550	0.646	0.910	1.497	1.158	0.953	0.935	0.877	0.893	0.898	0.874	0.863
Agno	0.269	0.338	0.346	0.418	0.645	1.021	0.893	0.829	0.863	0.840	0.841	0.841	0.828	0.857
Bucao	18.564	32.978	3.737	13.571	2.546	0.649	2.045	0.312	1.746	0.337	0.995	0.144	0.972	0.154
Cagayan	0.595	0.830	0.735	0.868	1.179	1.879	1.438	1.112	1.024	0.954	1.021	0.944	0.934	0.908
Pampanga	0.169	0.274	0.239	0.299	0.518	0.844	0.742	0.725	0.798	0.809	0.854	0.890	0.902	0.925
Hainan	0.793	1.439	0.746	0.790	1.003	1.439	1.003	0.867	0.752	0.612	0.586	0.552	0.535	0.609
Pearl River	1.458	1.433	1.533	1.472	1.698	1.577	1.728	1.532	1.419	1.285	1.228	1.278	1.218	1.138
Pearl River East (Dong)	74.600	140.000	16.500	60.000	11.480	1.880	11.120	1.450	7.260	1.400	3.900	0.605	3.110	0.522
Pearl River estuary	1.527	1.422	1.481	1.472	1.680	1.597	1.917	1.534	1.279	1.197	1.140	1.238	0.942	1.067
Pearl River North (Bei)	53.100	105.000	12.000	46.000	8.540	1.490	7.890	1.060	5.340	1.060	2.900	0.455	2.410	0.422
Pearl River West (Xi)	54.200	106.000	12.200	47.800	8.840	1.810	8.610	1.150	5.820	1.170	3.180	0.484	2.610	0.461
Cho Shui	1.202	1.215	1.189	1.169	1.330	1.391	1.210	0.972	0.803	0.669	0.610	0.607	0.564	0.542
Kao-Ping	1.078	1.051	1.050	1.029	1.187	1.250	1.079	0.901	0.766	0.656	0.593	0.599	0.550	0.531
Pei-Kang	1.020	1.063	1.081	1.107	1.340	1.329	1.135	0.919	0.811	0.746	0.745	0.823	0.813	0.817
Tseng-Wen	1.140	1.113	1.074	1.036	1.133	1.140	1.008	0.827	0.706	0.620	0.593	0.611	0.586	0.578
Mekong 03	0.981	0.966	1.031	0.966	1.139	1.131	1.146	1.022	0.922	0.837	0.806	0.830	0.793	0.748
Mekong 05	1.093	1.073	1.140	1.075	1.278	1.374	1.284	1.153	1.027	0.937	0.894	0.919	0.880	0.820
Nha Trang	1.475	1.575	1.704	1.287	1.573	0.749	1.525	1.373	1.260	1.141	1.129	1.224	1.217	1.197
Song Ba	2.066	1.789	1.742	1.616	1.873	1.872	1.856	1.629	1.425	1.241	1.158	1.162	1.093	1.017
Nin Hoa	0.908	0.953	0.954	0.856	1.025	0.782	1.000	0.893	0.811	0.730	0.701	0.731	0.701	0.660
Phang Rang	0.788	0.767	0.846	0.788	0.921	0.894	0.898	0.787	0.705	0.624	0.615	0.654	0.646	0.623
Song Dinh	1.054	1.088	1.084	0.982	1.110	0.914	1.106	0.981	0.895	0.815	0.818	0.899	0.905	0.910
Red River	1.153	1.141	1.196	1.116	1.291	1.306	1.231	1.072	0.946	0.848	0.813	0.840	0.811	0.766
Song Long Song	0.654	0.648	0.692	0.645	0.771	0.732	0.802	0.736	0.691	0.632	0.618	0.661	0.643	0.616
Song Luy	0.912	0.977	0.991	0.928	1.115	1.081	1.093	0.977	0.885	0.787	0.767	0.803	0.773	0.728

5.3.2. Temporal stability of the signal at the source

As the geochemical signal depends mostly on the parental minerals' composition, it is not likely to change until the outcrops are weathered off. During weathering, Lanthanide cations can be leached from the parent minerals. They are considered to be nearly immobile cations, which leach from their parent minerals only during bisiallitization under most intense weathering conditions (Chamley, 1989). Nevertheless, a slight fractionation can occur during weathering, as LREE are slightly more mobile than HREE. This depends on the acidity of the attack solution, the enlargement of surface area through physical weathering and the length of the river. Even in regions of active volcanism (Philippines, Indonesia) the initial source of the signal does not change as the drainage basins are dominated by rocks of the same magmatic source.

5.3.3. Integrity of signals during transport by current

The geochemical signal in sinking particulate matter that reaches the sediment traps is not identical with any of the sources (except at station SCS-NE). Within them a composite signal from various sources is preserved. Accordingly, the particles reaching a trap are nearly always mixed from different sources.
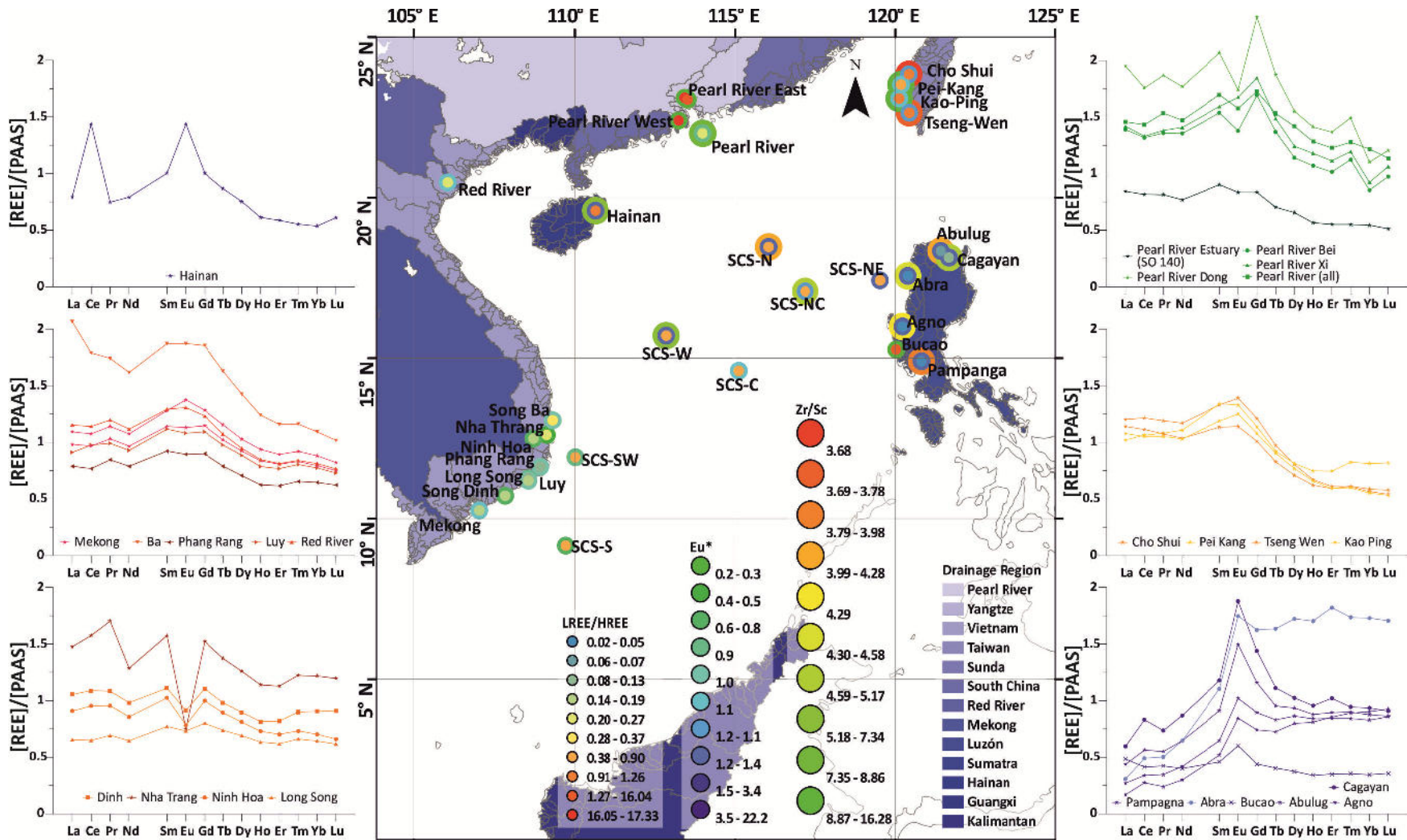
Figure 30: Regional overview of the Lanthanides signals in sediments from the drainage basins around the SCS. Reference-data of the Pearl River by Zhang & Wang (2001**), that of Hainan soils by** Ma et al. (2007)**. The geochemical properties of Luzón, Taiwan and specific smaller Vietnamese coastal rivers are more characteristic and therefore better provenance indicators than those of the Mekong, Pearl and Red River.**
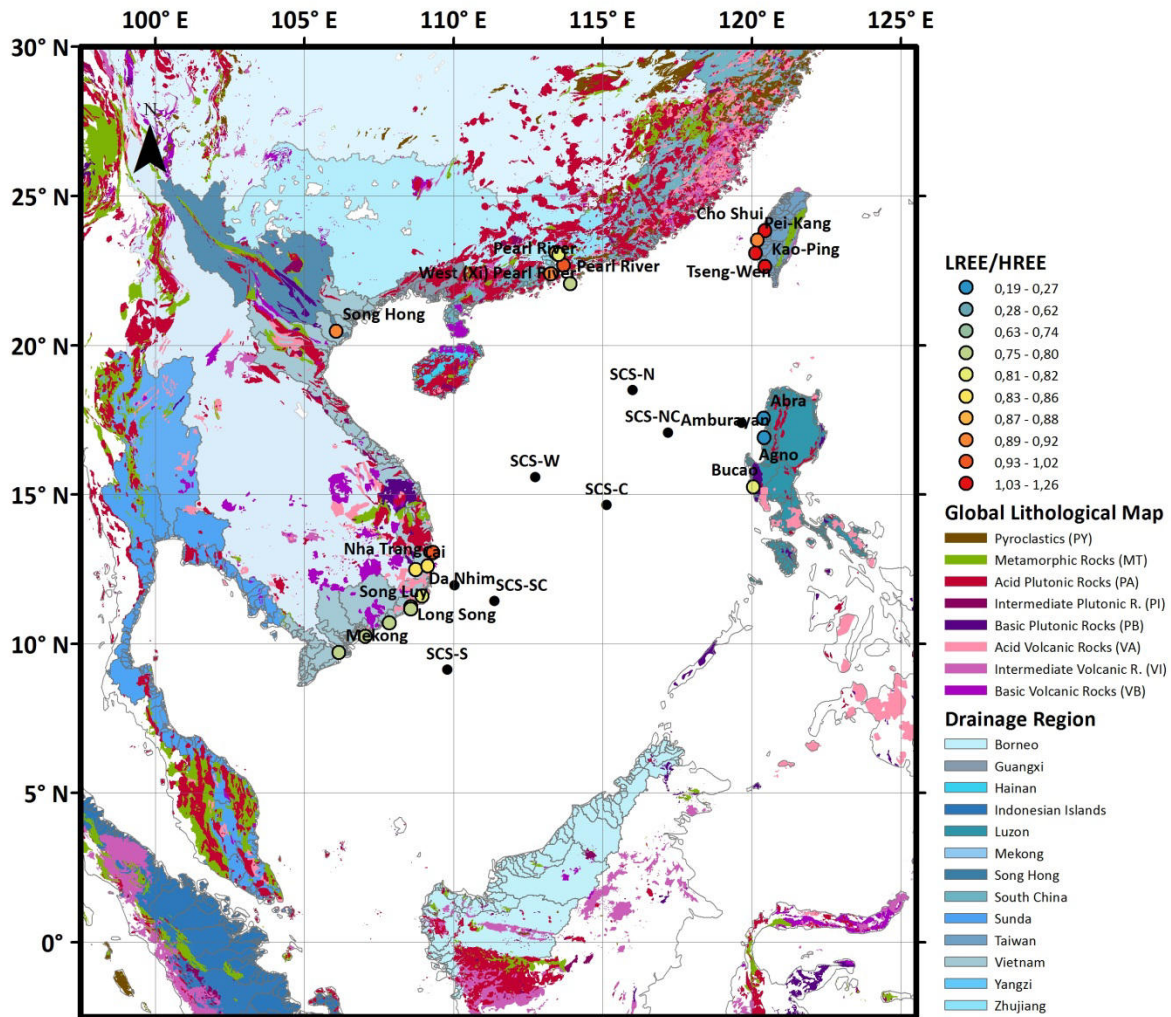
Figure 31: Outcrops of magmatic rocks (Hartmann and Moosdorf, 2012) **located in the drainage basins discharging into the SCS. Their rivers' sediments contain different LREE/HREE ratios, which are low on Luzón intermediate in central Asia and high on Taiwan.**

Element ratios of sinking particulate matter (in temporal resolution, Figure 32) cluster according to the regions (circles of the same color) and nearest to or between the contributing sediment dischargers (stars). The basin wide diversity (clusters of differently colored circles) and regional signals orient along two parallels stretching from the Luzón signal to the Mekong, Pearl, Vietnamese and Taiwanese element ratios. The scatter at each station resembles temporal variations and is reduced at stations near the shelf slopes with few probable riverine contributors and wider if the station is located farther off-shore and receives material from more sources.

5.3.3.1. Re-distribution by currents

The geochemical properties of question are similar at all depths (SH, MD, DP) and during the sampled intervals (mainly October – December) at station **SCS-NE** (Figure 34). The only significant differences between the single measurements affect the general concentrations; the pattern of element concentrations remains nearly identical. LREE concentrations are notably lower than those of the HREE and a distinctive positive Europium anomaly is always present. The Zr/Sc ratio (1.6-2.8) is comparatively low. Concentrations in the sediment are higher than in sinking particulate matter. These characteristics strongly resemble those of Luzón Rivers; particularly on a basin wide

comparison (Figure 32). These observations match those previously made on clay mineralogy and lead to the same deduction that the material reaching SCS-NE derives purely from the Luzón Rivers and is not modified significantly during transport.

Main features of the geochemistry of lithogenic sinking particulate matter at **SCS-N** are a distinctive positive Europium anomaly a LREE/HREE ratio below 1 and intermediate Zr/Sc rates, in basin-wide comparison (Figure 33). The simultaneous occurrence of higher relative smectite abundances, positive europium anomalies, enrichment with HREE and low Zr/Sc ratios is an indicator for significant contribution of material from Luzón Rivers, high relative illite and chlorite abundances indicate the presence of material from Taiwan sediments (Schröder et al., n.d.). Even though station **SCS-N** lies proximate to the South China Shelf and the closest fluvial source, the Pearl River, lies 465 km to the north, geochemical and mineralogical properties do not resemble the characteristics of the
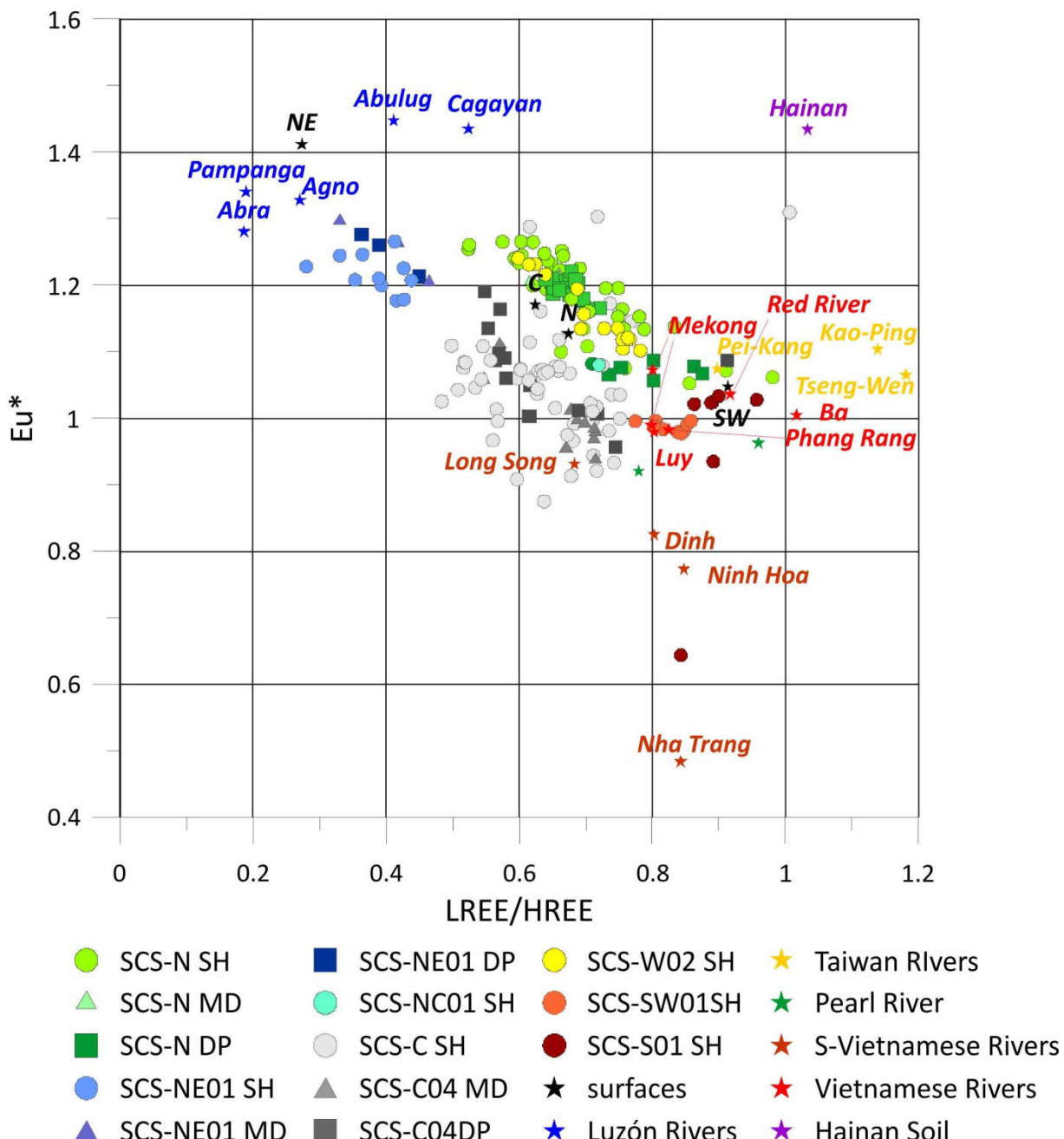
Figure 32: LREE/HREE ratios versus Europium anomaly of all river sediments and sinking particulate matter. Element ratios of sinking particulate matter form regional clusters near or between the contributing sediment dischargers.

Pearl River (Zhang and Wang, 2001). Nevertheless, material mainly composed of minerals that are low in REE concentrations, like quartz or kaolinite, may contribute to SCS-N as well.

Lanthanides' PAAS normalized profiles of SPM at **SCS-W** are very similar to those at SCS-N, only in lower concentrations and a lower Eu*. Also in the sediments at **SCS-C** the Europium anomaly shows, though the trace element characteristics of sinking particulate matter vary in depth and time. At none of the shallow traps (1200 m depth) any contribution of material from Luzón was detected, but during C05 (1995-1996) the Luzón signal was present in all sampled intervals at 1800 m depth. During C04 (1994-1995) the signal was present episodically at 2200 m depth and during most of sampled intervals at 3770m depth with episodic interruptions (Figure 35).

We previously interpreted (Schröder et al., n.d.) the material from Luzón to be transported and mixed through the deep cyclonic circulation in the northern SCS (G. Wang et al., 2011; Xie et al., 2013). Material from Luzón reaches station SCS-NE, travels farther north, collects material from Taiwan and South China and distributes the mixture into the central basin, reaching stations SCS-N regularly and stations SCS-C and probably also SCS-W occasionally (Figure 36). The farther the plume
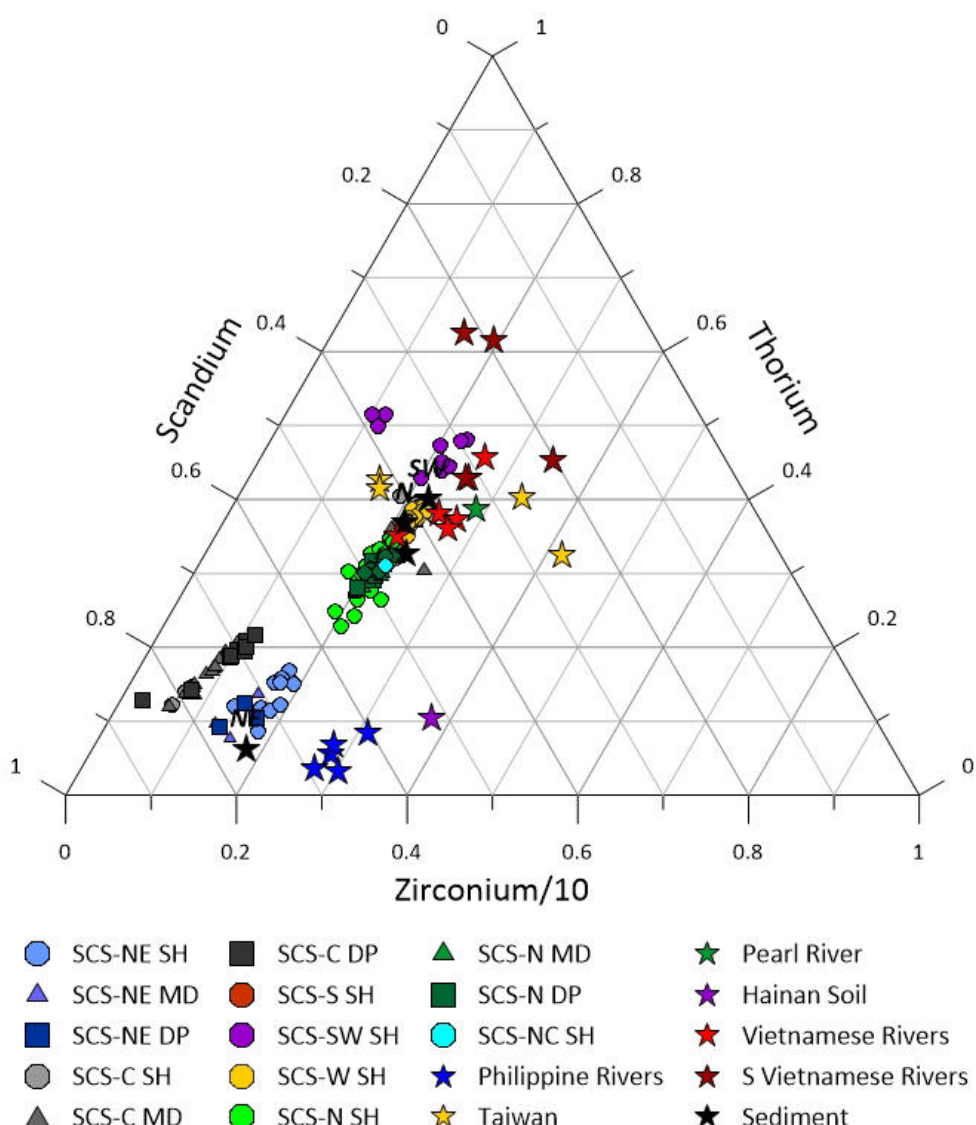
Figure 33: The Zr/Sc ratio is a good marker for particulate matter deriving from Luzón Rivers. The signal is present in all SCS-NE samples, most C04DP and C05SH samples and some, apparently random samples at C04MD.

travels, the weaker is the Luzón-signal, which indicates more contribution from the central Asian signals or dilution with minerals that are low in REE concentrations. However, a contribution from Hainan sediments to SCS-W between the shelf and Macclesfield bank should be considered an alternative or additional cause for the positive Europium anomaly at that particular station. At SCS-N and SCS-C the geochemical signal from Luzón strengthens towards the bottom, with such a strong effect in the central SCS that the Europium anomaly is negligible at the shallow traps, episodically high in the middle and deep traps and high in the sediment (Figure 34). The recursion of the cyclonic deep current strongly controls the sediment distribution and their characteristics.

Only one sample of the shallow trap at **SCS-NC** was used for element analysis. Sinking particulate matter is slightly depleted with LREE (LREE/HREE = 0.72), but does not show a real positive Europium anomaly (1.08) as the general MREE contents is high. Zr/Sc elemental ratio is intermediate (4.68) (Table 20). The Lanthanide pattern resembles that of Taiwanese sediments in a strongly diluted version (Figure 34). This is perplexing, as SCS-NC is located close to Luzón and at least some contribution of those sediments should be expected, but also the clay mineral assemblages indicated, that sinking particulate matter in the shallow trap derived mainly from Taiwan and that of the deeper trap contained more particulate matter from Luzón (Schröder et al., n.d.). From this we inferred, that the cyclonic deep current passes below the upper trap and above/through the lower trap.

In the southwestern part of the basin the deep circulation is seasonally more variable and the models are not quite as clear about them. The PAAS-normalized Lanthanides' concentration pattern is nearly invariable at **SCS-SW.** LREE/HREE ratios are high (0.77-0.85). A slight negative Europium anomaly (0.98-1.00) is present during all intervals (Figure 32). The sediment below the trap system contains a low positive Eu* (1.05) and even higher enrichment of the LREE (0.91). So, further lateral SPM or sediment input should be expected below the trap. The general Lanthanide distribution at **SCS-S** is characterized by high LREE/HREE ratios and enrichment with MREE, which develop a negative Neodymium anomaly. Europium anomalies are low, mostly positive, but negative during rare specific intervals (Figure 34, Figure 32). The concentrations of trace elements within the collected material are variable and occasionally very high at **SCS-S** during aforesaid intervals.

The PAAS-normalized concentration patterns at **SCS-SW and SCS-S** are relatively similar to the majority of adjacent rivers (Mekong, Phang Rang, Luy and Red River) and nearly invariable most of the year. Nevertheless, we observe negative Europium anomalies during specific sampling intervals at SCS-S (January and April 2004, Figure 32), which indicate occasionally enhanced contribution of Dinh, Nha Trang and Ninh Hoa rivers. As the geochemical signal of the main contributors are not differentiable from each other, it should be expected, that the dominating contribution of sediments may actually shift from the Mekong to Vietnamese coastal rivers or the Red River. The geochemical characteristics presented cannot solve the provenance problem in this region. No element analyses were performed on **SCS-SC** series.

The geochemical signals at stations SCS-NE, SCS-N, SCS-W and SCS-SW were steady, disregarding their variations in concentrations. Therefore, the provenance and blend of materials must be (statistically) regular and rather underlies the control of deep current distribution than monsoonal surface currents. At stations SCS-C and -S significant episodical changes of the geochemical indicate either variations in contribution by redirected deep currents or alterations in the material composition by physical sorting or chemical reactions. At SCS-N interannual variations of the signal were observed, which will be elaborated in a following study.
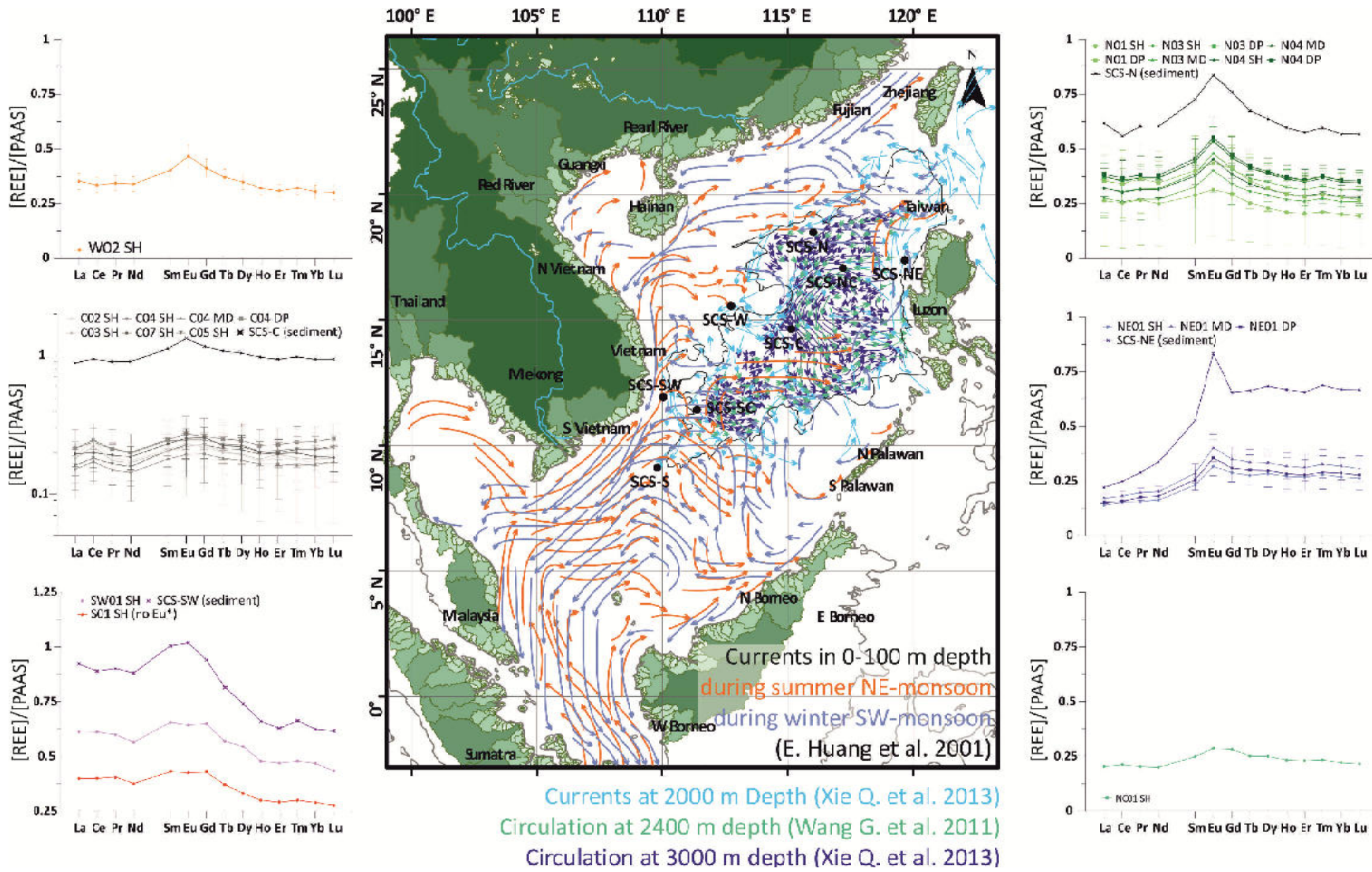
Figure 34: PAAS normalized Lanthanide pattern mean values at the traps during various moorings partly resemble the patterns from the drainage basins, but are often mixed by various sources through surface and deep currents.

Table 18: Mean values of PAAS-normalized concentrations at all stations/traps.

Station	La PAAS	Ce PAAS	Pr PAAS	Nd PAAS	Sm PAAS	Eu PAAS	Gd PAAS	Tb PAAS	Dy PAAS	Ho PAAS	Er PAAS	Tm PAAS	Yb PAAS	Lu PAAS
NC01 SH	0.204	0.212	0.204	0.201	0.250	0.287	0.283	0.253	0.252	0.234	0.230	0.235	0.221	0.216
NE01/02 SH	0.142	0.154	0.157	0.165	0.234	0.319	0.289	0.277	0.286	0.272	0.270	0.279	0.269	0.264
NE01 MD	0.173	0.183	0.199	0.204	0.287	0.403	0.351	0.337	0.335	0.320	0.313	0.329	0.320	0.308
NE01 DP	0.153	0.157	0.177	0.182	0.257	0.357	0.310	0.300	0.299	0.285	0.278	0.291	0.287	0.278
N01 SH	0.264	0.253	0.267	0.250	0.289	0.314	0.294	0.253	0.230	0.210	0.205	0.211	0.202	0.193
N01/02 DP	0.353	0.341	0.364	0.345	0.402	0.436	0.413	0.354	0.320	0.292	0.282	0.291	0.280	0.267
N03 SH	0.276	0.260	0.271	0.271	0.328	0.401	0.340	0.305	0.288	0.269	0.260	0.275	0.259	0.260
N03 MD	0.322	0.305	0.319	0.321	0.389	0.480	0.406	0.366	0.348	0.325	0.315	0.332	0.313	0.313
N03 DP	0.370	0.359	0.368	0.368	0.443	0.538	0.459	0.413	0.391	0.367	0.355	0.374	0.356	0.354
N04 SH	0.321	0.301	0.315	0.315	0.377	0.454	0.384	0.340	0.316	0.294	0.283	0.298	0.281	0.279
N04 MD	0.375	0.353	0.370	0.370	0.443	0.537	0.460	0.412	0.388	0.363	0.348	0.366	0.348	0.346
N04 DP	0.385	0.369	0.381	0.381	0.457	0.554	0.473	0.422	0.398	0.372	0.358	0.377	0.358	0.354
C02 SH	0.191	0.239	0.183	0.173	0.210	0.233	0.218	0.199	0.191	0.172	0.183	0.177	0.168	0.164
C03 SH	0.180	0.222	0.175	0.169	0.204	0.221	0.231	0.201	0.194	0.178	0.195	0.182	0.178	0.182
C04 SH	0.151	0.171	0.149	0.143	0.179	0.194	0.195	0.181	0.175	0.165	0.165	0.161	0.164	0.171
C04 MD	0.214	0.237	0.212	0.197	0.244	0.247	0.247	0.231	0.227	0.203	0.207	0.213	0.209	0.217
C04 DP	0.215	0.245	0.213	0.200	0.247	0.272	0.262	0.250	0.243	0.224	0.228	0.237	0.240	0.252
C05 SH	0.161	0.182	0.165	0.158	0.206	0.227	0.227	0.213	0.209	0.194	0.199	0.210	0.211	0.221
C07 SH	0.195	0.199	0.192	0.186	0.231	0.253	0.257	0.225	0.220	0.201	0.196	0.198	0.187	0.184
S01 SH	1.536	1.599	1.701	1.375	1.640	1.251	1.597	1.423	1.294	1.168	1.145	1.222	1.203	1.168
SW01 SH	0.615	0.614	0.600	0.566	0.657	0.645	0.651	0.570	0.546	0.479	0.471	0.480	0.470	0.435
W02 SH	0.353	0.335	0.344	0.340	0.403	0.468	0.413	0.371	0.349	0.322	0.309	0.322	0.304	0.301

Table 19: Standard deviations of PAAS-normalized concentrations indicate the intensity of temporal variations.

Station	La PAAS	Ce PAAS	Pr PAAS	Nd PAAS	Sm PAAS	Eu PAAS	Gd PAAS	Tb PAAS	Dy PAAS	Ho PAAS	Er PAAS	Tm PAAS	Yb PAAS	Lu PAAS
NC01 SH														
NE01/02 SH	0.018	0.021	0.021	0.024	0.043	0.062	0.055	0.057	0.062	0.060	0.061	0.065	0.064	0.059
NE01 MD	0.003	0.001	0.014	0.022	0.047	0.083	0.063	0.070	0.075	0.072	0.072	0.077	0.071	0.067
NE01 DP	0.038	0.044	0.053	0.059	0.092	0.137	0.113	0.116	0.117	0.109	0.108	0.115	0.112	0.103
C02 SH	0.060	0.077	0.057	0.054	0.065	0.073	0.073	0.062	0.057	0.052	0.060	0.058	0.047	0.046
C03 SH	0.059	0.054	0.057	0.054	0.064	0.061	0.075	0.061	0.058	0.054	0.073	0.055	0.052	0.049
C04 SH	0.024	0.028	0.025	0.024	0.029	0.038	0.031	0.025	0.027	0.025	0.029	0.038	0.024	0.026
C04 MD	0.080	0.077	0.081	0.074	0.092	0.093	0.093	0.082	0.077	0.070	0.073	0.071	0.071	0.070
C04 DP	0.054	0.057	0.050	0.044	0.048	0.047	0.046	0.047	0.047	0.044	0.048	0.051	0.050	0.053
C05 SH	0.038	0.044	0.038	0.036	0.041	0.044	0.048	0.047	0.045	0.040	0.036	0.042	0.038	0.039
C07 SH	0.032	0.031	0.031	0.030	0.036	0.043	0.042	0.038	0.036	0.033	0.033	0.035	0.031	0.031
S01 SH	2.434	2.614	2.841	2.109	2.594	1.563	2.511	2.267	2.086	1.889	1.874	2.039	2.033	2.006
SW01 SH	0.210	0.207	0.206	0.193	0.222	0.214	0.211	0.180	0.171	0.147	0.146	0.152	0.154	0.136
N01 SH	0.159	0.155	0.161	0.147	0.159	0.160	0.147	0.123	0.107	0.094	0.093	0.095	0.090	0.087
N01/02 DP	0.092	0.090	0.094	0.089	0.098	0.101	0.094	0.079	0.070	0.063	0.062	0.063	0.058	0.056
N03 SH	0.112	0.107	0.109	0.106	0.118	0.122	0.110	0.095	0.087	0.078	0.076	0.080	0.077	0.074
N03 MD	0.054	0.051	0.052	0.051	0.058	0.064	0.054	0.048	0.043	0.041	0.040	0.040	0.040	0.038
N03 DP	0.040	0.040	0.040	0.038	0.041	0.048	0.044	0.038	0.037	0.032	0.030	0.030	0.032	0.029
N04 SH	0.100	0.095	0.097	0.094	0.103	0.105	0.095	0.081	0.072	0.064	0.060	0.062	0.060	0.056
N04 MD	0.026	0.023	0.025	0.024	0.025	0.026	0.025	0.025	0.024	0.023	0.022	0.024	0.024	0.024
N04 DP	0.037	0.035	0.036	0.035	0.041	0.049	0.041	0.037	0.034	0.030	0.030	0.033	0.029	0.031
W02 SH	0.129	0.126	0.126	0.122	0.137	0.137	0.131	0.116	0.106	0.095	0.091	0.095	0.089	0.085

Table 20: Mean values, standard deviations of specific element ratios in sinking particulate matter and number (n) of samples.

Station	means								Standard deviations								n
	Eu*	La/Lu	LREE HREE	Tm*	LREE	MREE	HREE	Zr/Sc	Eu*	La/Lu	LREE HREE	Tm*	LREE	MREE	HREE	Zr/Sc	
NC01 SH	1.08	0.95	0.59	1.04	0.82	1.07	1.39	4.68									1
NE01/02 SH	1.22	0.54	0.38	1.04	0.62	1.12	1.64	2.51	0.03	0.09	0.05	0.02	0.08	0.22	0.37	0.28	11
NE01 MD	1.26	0.56	0.39	1.04	0.76	1.38	1.93	1.91	0.05	0.12	0.07	0.01	0.04	0.26	0.43	0.31	3
NE01 DP	1.26	0.55	0.39	1.03	0.67	1.23	1.72	2.06	0.03	0.08	0.04	0.01	0.19	0.46	0.66	0.32	3
C02 SH	1.09	1.17	0.74	1.01	0.79	0.86	1.06		0.13	0.18	0.09	0.09	0.25	0.27	0.32		13
C03 SH	1.02	0.99	0.67	0.97	0.75	0.86	1.11		0.06	0.10	0.05	0.09	0.22	0.26	0.33		13
C04 SH	1.04	0.88	0.61	0.98	0.61	0.75	1.00	0.91	0.08	0.13	0.07	0.10	0.10	0.12	0.16		11
C04 MD	1.01	0.99	0.67	1.02	0.86	0.97	1.28	3.17	0.05	0.14	0.06	0.04	0.31	0.36	0.43	1.66	11
C04 DP	1.07	0.85	0.61	1.01	0.87	1.03	1.42	1.68	0.07	0.13	0.07	0.06	0.20	0.18	0.29	1.83	12
C05 SH	1.05	0.73	0.54	1.03	0.67	0.87	1.24	1.08	0.04	0.06	0.03	0.05	0.16	0.18	0.24	0.18	13
C07 SH	1.04	1.06	0.65	1.03	0.77	0.97	1.19	5.37	0.03	0.08	0.04	0.02	0.12	0.16	0.20	0.41	11
S01 SH	0.77	1.32	0.86	1.04	6.21	5.91	7.20		0.14	0.11	0.04	0.01	10.00	8.93	11.93		7
SW01 SH	0.99	1.41	0.83	1.02	2.40	2.52	2.88	5.88	0.01	0.05	0.03	0.02	0.82	0.83	0.91	1.95	10
N01 SH	1.08	1.37	0.83	1.04	1.03	1.15	1.25		0.03	0.20	0.12	0.01	0.62	0.59	0.57		8
N01/02 DP	1.07	1.32	0.81	1.04	1.40	1.60	1.73		0.01	0.10	0.06	0.01	0.36	0.37	0.37		6
N03 SH	1.20	1.06	0.67	1.06	1.08	1.37	1.61	4.33	0.04	0.14	0.08	0.01	0.43	0.44	0.47	0.49	19
N03 MD	1.21	1.03	0.65	1.06	1.27	1.64	1.95	4.16	0.02	0.06	0.03	0.01	0.21	0.22	0.24	0.23	9
N03 DP	1.19	1.04	0.67	1.05	1.46	1.85	2.20	4.20	0.01	0.03	0.02	0.01	0.16	0.17	0.19	0.23	8
N04 SH	1.19	1.15	0.72	1.06	1.25	1.56	1.75	4.24	0.05	0.12	0.07	0.01	0.39	0.38	0.37	0.29	10
N04 MD	1.19	1.09	0.68	1.05	1.47	1.85	2.16	4.44	0.02	0.05	0.02	0.00	0.10	0.10	0.14	0.22	6
N04 DP	1.19	1.09	0.68	1.05	1.52	1.91	2.22	4.42	0.02	0.04	0.02	0.00	0.14	0.17	0.19	0.31	5
W02 SH	1.15	1.17	0.72	1.05	1.37	1.65	1.91	5.58	0.05	0.11	0.06	0.01	0.50	0.52	0.56	0.36	14

5.3.3.2.   Effects of differential settling

On rough observation, geochemical characteristics remain steady within the year at most stations. Zooming more into temporal detail, episodical changes of contribution at several stations reveal significant mismatches between clay mineral and geochemical provenance indications. These are best visible at SCS-C (Figure 35).

Material from Luzón carries high relative smectite abundance and Europium anomaly and low LREE/HREE and Zr/Sc ratios. While the corresponding signal indicates low contribution to the shallow and middle traps at SCS-C, it is generally higher in the deep trap, which means that the plume passes mainly below 2243 m water depth in the **central SCS** (Figure 35). Strong increase of Luzón material contribution in the middle trap can be inferred from higher Eu*, lower LREE/HREE and lower Zr/Sc ratios during November and December 1994.

During these intervals, the plume must have temporarily shifted upwards. In the deep trap an abrupt drop of these indicators during September 1994, January and March 1995 indicates irregular reductions of contribution from Luzón material to this trap. Partly, these drops coincide with lithogenic matter flux peaks, which indicate contribution of advected material from other sources. However, the change of signal does not correlate smectite variations, which are the main clay minerals from Luzón. Therefore the main carriers of trace elements are not the clay minerals, even in the far offshore central SCS. The other way around, this means that rises in relative smectite abundance during October 1994 in the middle trap are not necessarily a result of more sediment contribution from Luzón.

A similar misfit between the supposed provenance indicators was observed at **SCS-W** in the northwestern SCS (Figure 36). While relative smectite abundances increased abruptly during September 2011, geochemical Luzón indicators increased gradually and peaked after a sharp decrease of relative smectite abundance. So, either smectite is not the main carrier of the geochemical signal or it originates from a different source, with a different, weak signal.

Previous studies on mineralogy in the same sinking particulate matter identified significant amounts of plagioclase, amphibole, feldspars and pyroxenes that reached even the off-shore located sediment traps at station SCS-C (Gerbich, 2001; Rieger, 1995). As these minerals preferentially incorporate Lanthanide elements differently, fractionation of the riverine trace element sediment signal should be expected. We previously reported differential settling to be an important mechanism to sort the clay mineral signal (Schröder et al., n.d.), which will be more intense among bulk minerals than among clay minerals, as it depends on sorting by different densities and grain size, which depends on the minerals' weatherability. Using clay mineral and geochemical characteristics as provenance indicators does not lead to the same conclusions, which must mean that they respond differently to transport mechanisms. Differential settling among clay minerals is to be expected to alternate the signal, but this could well affect the trace elements, which are incorporated in significant concentration in primary minerals as well.

5.3.3.3. *Chemical alterations*

At all stations, bulk SPM shares the common feature that trace element concentrations are lower than in fluvial and marine sediments (compare Figure 32 and Figure 34), but locally resemble the terrigenous REE signals very closely. At the near-shore stations (SCS-NE, -NC, -SW, -S) the resemblance is so good that so no signal interference by adsorption, desorption or distortion by a marine REE-signal needs to be suspected.

Lower concentrations are most probably the result of loss of the main REE carriers or dilution with material of low REE concentrations. Minerals with highest REE concentrations are the primary minerals, which often have higher specific densities than secondary clay minerals. These settle fastest, so suspension enriches with clay minerals and fine detrital quartz grains, therefore outgoing suspension depletes its total REE concentration. At most stations, lithogenic matter constitutes less than 50 % of the total sinking particulate matter, with spatial and seasonal variations (Gaye et al., 2009; Wiesner et al., 1996). The total REE concentration in biogenic matter is considerably lower: In pelagic sediments of the Pacific ocean, REE-concentrations of total lithogenic matter are 19-91 times higher than those of biogenic carbonate and opal (Table 22); those of smectite (Montmorillonite) 3-15 times higher than biogenic carbonate and opal (Piper, 1974). Sedimentation rates of the main components organic matter, carbonate, opal and lithogenic matter are, assuming 5% of organic matter in the Pacific ocean as well, comparable to the sedimentation rates in the south-western SCS (Gaye et al., 2009). So, authigenic marine particles, which are mostly of biogenic origin, further dilute the bulk SPM. Once particulate matter sinks below the respective compensation depths, carbonate and opaline particulate matter dissolve. The lack of diluting particles results in higher general REE concentration in marine sediments (Figure 34).

Biogenic matter absorbs REE directly from the seawater and therefore mostly incorporates the same elemental distribution. In case of the SCS the sea water is slightly depleted with Ce, which is preferentially scavenged by microbial organisms (Moffett, 1990), and enriched with HREE (Alibo and Nozaki, 2000). As negative Cerium anomalies are rarely found in sinking particulate matter, the effects of Ce scavenging through microbes in the marine environment or desorption by depleted sea water, appear to be insignificant in comparison to the total bulk REE concentrations.
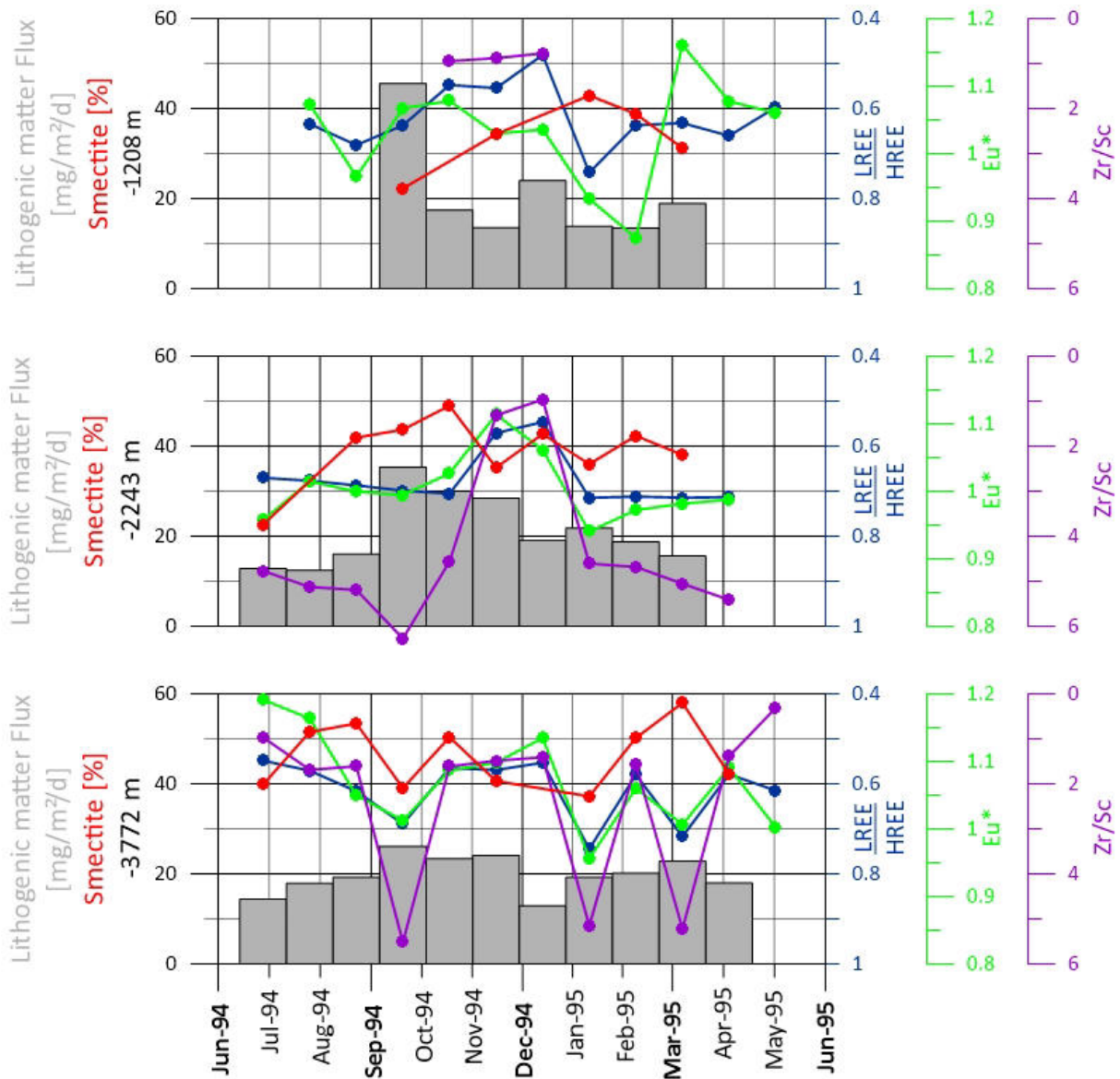
Figure 35: Temporal variations of Lithogenic matter (grey), relative smectite abundance (red), Eu* (green), LREE/HREE (blue) and Zr/Sc ratios (purple) at station SCS-C during mooring C04. The geochemical properties do, the clay mineralogical properties do not correlate with each other to indicate more contribution from Luzón.

Nevertheless, carbonate producers adsorb preferentially LREE, while opaline organisms enrich with HREE (Elderfield and Greaves, 1982). The chemical properties of seawater vary with depth and so do adsorption and desorption of REE from and to particulate matter (Elderfield and Greaves, 1982). Concentrations in the seawater enrich with depth (Alibo and Nozaki, 2000) and specifically with the less compatible HREE cations (Elderfield and Greaves, 1982; Piper, 1974). The leaching abilities of REE cations from clay minerals' crystal grids in a slightly alkaline pH range environment like sea water are generally low (Chamley, 1989). At stations SCS-N, -W and -C REE distributions do not resemble the REE signal of one specific source. Despite the probability that SPM with long transport distance and duration could be affected more by adsorption and desorption, we conclude that the REE concentrations in detrital particles are so high, that chemical alterations during transport affect the REE distribution negligibly.

Vertical transport time is spatially dependent, too. While vertical settling velocity was calculated to be faster than 3860 m per 60 days in the Pacific (Honjo, 1980), higher temporal resolution of the sampling intervals refined the velocity to be faster than 36-38 m/d in the northern and central basin

and faster than 49 m/d in the southwestern basin. This leaves 74 to 112 days of reaction time in the deeper north-central basin and 46 days in the shallower south-western basin. This is plenty of time for adsorption from and desorption to the sea water. Additionally, our recent findings about long lateral displacement of SPM owed to the complex layered circulation indicate, that sinking duration may actually take longer. At stations SCS-NC, -W, -SW and -S settling velocities and vertical transport time could not be calculated, as there were no flux peaks that coincided at shallow and deep traps at the same station.
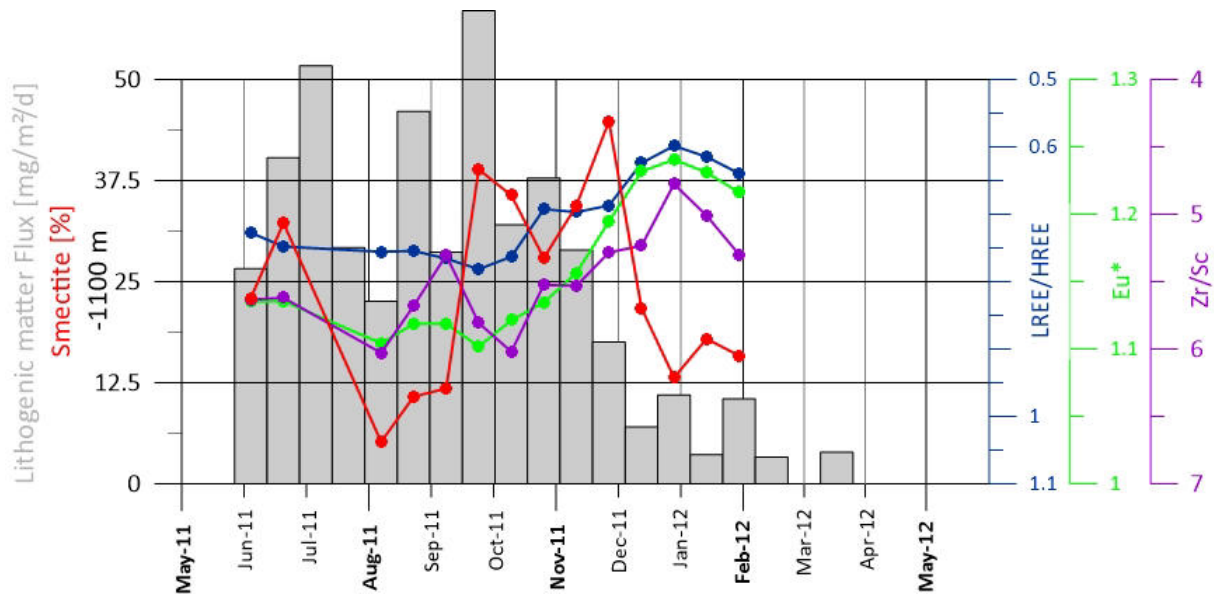
Figure 36: Geochemical and clay mineralogical variations at SCS-W during mooring W02 do not correlate.

Table 21: Lithogenic matter [mg/m²/d], relative clay mineral abundances [%] and element ratios of sinking particulate matter in full temporal resolution.

sample name	interval start	interval end	lithogen flux	Sm	Chl	Ill	Kao	Eu*	LREE HREE	Zr/Sc
SCS-W02 SH1	20.05.2011	04.06.2011	26.57	23	22	37	18	1.135	0.728	5.635
SCS-W02 SH2	05.06.2011	20.06.2011	40.30	32	22	34	12	1.135	0.748	5.621
SCS-W02 SH3	21.06.2011	06.07.2011	51.68							
SCS-W02 SH4	07.07.2011	22.07.2011	29.19							
SCS-W02 SH5	23.07.2011	07.08.2011	22.55	5	24	47	24	1.104	0.756	6.030
SCS-W02 SH6	08.08.2011	23.08.2011	46.05	11	26	44	20	1.119	0.755	5.681
SCS-W02 SH7	24.08.2011	08.09.2011	28.62	12	24	43	21	1.119	0.766	5.305
SCS-W02 SH8	09.09.2011	24.09.2011	58.47	39	22	27	12	1.102	0.782	5.808
SCS-W02 SH9	25.09.2011	10.10.2011	32.02	36	19	31	15	1.121	0.763	6.021
SCS-W02 SH10	11.10.2011	26.10.2011	37.80	28	23	36	14	1.134	0.693	5.524
SCS-W02 SH11	27.10.2011	11.11.2011	28.89	34	24	29	12	1.156	0.697	5.532
SCS-W02 SH12	12.11.2011	27.11.2011	17.50	45	17	24	14	1.194	0.687	5.284
SCS-W02 SH13	28.11.2011	13.12.2011	7.01	22	24	37	18	1.232	0.624	5.235
SCS-W02 SH14	14.12.2011	29.12.2011	10.97	13	24	49	14	1.240	0.599	4.777
SCS-W02 SH15	30.12.2011	14.01.2012	3.58	18	25	40	17	1.231	0.615	5.011
SCS-W02 SH16	15.01.2012	30.01.2012	10.48	16	23	44	17	1.216	0.640	5.300
SCS-W02 SH17	31.01.2012	15.02.2012	3.29							
SCS-W02 SH18	16.02.2012	02.03.2012								
SCS-W02 SH19	03.03.2012	18.03.2012	3.88							
SCS-W02 SH20	19.03.2012	04.04.2012								
SCS-C04 SH05	19.10.1994	15.11.1994	13.52	34	24	29	13	1.029	0.555	0.881
SCS-C04 SH09	08.02.1995	07.03.1995	18.90	31	18	34	17	1.161	0.632	
SCS-C04 SH08	11.01.1995	07.02.1995	13.44	39	21	27	13	0.875	0.637	

sample name	interval start	interval end	lithogen flux	Sm	Chl	Ill	Kao	Eu*	LREE HREE	Zr/Sc
SCS-C04 SH03	24.08.1994	20.09.1994	45.56	22	29	39	10	1.067	0.637	
SCS-C04 SH07	14.12.1994	10.01.1995	13.79	43	17	24	16	0.933	0.742	
SCS-C04 MD07	16.11.1994	13.12.1994	19.05	43	15	26	16	1.061	0.546	0.965
SCS-C04 MD10	08.02.1995	07.03.1995	15.60	38	22	28	12	0.982	0.715	5.053
SCS-C04 MD09	11.01.1995	07.02.1995	18.75	42	18	27	13	0.972	0.712	4.684
SCS-C04 MD08	14.12.1994	10.01.1995	21.82	36	25	24	15	0.940	0.715	4.607
SCS-C04 MD05	21.09.1994	18.10.1994	30.04	49	13	23	15	1.026	0.706	4.565
SCS-C04 MD05	21.09.1994	18.10.1994	30.04	49	13	23	15	1.026	0.706	4.565
SCS-C04 MD04	24.08.1994	20.09.1994	35.34	44	21	25	11	0.994	0.699	6.272
SCS-C04 MD03	27.07.1994	23.08.1994	16.02	42	19	29	10	0.999	0.687	5.193
SCS-C04 MD01	01.06.1994	28.06.1994	12.82	23	23	41	12	0.957	0.670	4.771
SCS-C04 MD06	19.10.1994	15.11.1994	28.44	35	19	31	15	1.114	0.571	1.313
SCS-C04 DP06	19.10.1994	15.11.1994	24.04	41	20	28	12	1.098	0.569	1.489
SCS-C04 DP11	08.03.1995	04.04.1995	17.96	42	19	26	13	1.091	0.579	1.389
SCS-C04 DP10	08.02.1995	07.03.1995	22.80	58	13	19	10	1.006	0.717	5.221
SCS-C04 DP09	11.01.1995	07.02.1995	20.13	50	16	21	12	1.060	0.580	1.567
SCS-C04 DP09	11.01.1995	07.02.1995	20.13	50	16	21	12	1.060	0.580	1.567
SCS-C04 DP05	21.09.1994	18.10.1994	23.37	50	14	25	11	1.086	0.565	1.612
SCS-C04 DP04	24.08.1994	20.09.1994	26.12	39	17	31	12	1.012	0.689	5.518
SCS-C04 DP03	27.07.1994	23.08.1994	19.26	53	15	23	8	1.050	0.616	1.610
SCS-C04 DP02	29.06.1994	26.07.1994	17.90	52	15	25	9	1.163	0.571	1.689
SCS-C04 DP01	01.06.1994	28.06.1994	14.34	40	18	32	10	1.191	0.549	0.970
SCS-C04 DP08	14.12.1994	10.01.1995	19.20	37	21	27	14	0.956	0.745	5.150

Table 22: Fluxes of components and select REE in pelagic sediments of the Pacific Ocean and their ratios with REE-fluxes of lithogenic matter (Piper, 1974)**.**

x	La	Sm	Yb	La (Litho) La (x)	Sm (Litho) Sm (x)	Yb (Litho) Yb (x)	La (Mont) La (x)	Sm (Mont) Sm (x)	Yb (Mont) Yb (x)	sedimentation rates	
	[µg/cm²/y]									[mg/cm²/y]	[%]
Lithogen	9.1	1.67	0.76	1.00	1.00	1.00	0.14	0.17	0.29	0.2	57.14
Montmorillonit	1.26	0.28	0.22	7.22	5.96	3.45	1.00	1.00	1.00	0.05	
Bio. carbonate	0.49	0.08	0.04	18.57	20.88	19.00	2.57	3.50	5.50	0.13	37.14
Bio. opal	0.1	0.026	0.015	91.00	64.23	50.67	12.60	10.77	14.67	0.02	5.71

Table 23: Vertical settling velocities, as calculated from trap distance and interval duration during simultaneous high Flux lithogenic matter Peaks at various stations, are spatially variable. Due to higher temporal resolution settling velocities appear to be slower than in the Pacific Ocean.

	Reference Peaks	Velocity [m/d]	Duration [d] for settling to	
			4000 m	respective water depth
(Honjo, 1980)		>44.50	<89.9	
SCS-N	N03 SH10/MD11	>36.72	<108.9	<101.7
SCS-NE	NE01 SH/DP 04	>38.07	<105.1	<74.2
SCS-NC		n.d.		
SCS-C	C04 SH/MD 04	>38.41	<104.1	<112.1
SCS-W		n.d.		
SCS-SC	SC01 SH/DP 09	>49.00	<81.6	<45.9
SCS-SW		n.d.		
SCS-S		n.d.		

5.4. Conclusions

The comparatively small drainage basins of Taiwanese, Luzón and Vietnamese coastal rivers provide distinctive geochemical signals. Hainan and Luzón rivers contribute originally low LREE/HREE (0.19-0.41; 1.03, higher due to microbial enrichment of Ce) and Zr/Sc (4.28-4.58; 7.34) ratios as well as high positive Europium anomalies (1.28-1.45; 1.43) to the SCS, whereas Vietnamese coastal rivers Dinh, Nha Trang, Ninh Hoa and Long Song contribute high LREE/HREE ratios (0.68-0.85) and negative Europium anomalies (0.48-0.93). Taiwanese Rivers are enriched with MREE, have a very high LREE/HREE ratio (0.90-1.26) and do not contain a significant Europium anomaly (1.07-1.10). The larger drainage basins of Mekong, Red and Pearl River share a similar continental Asian 'background signal', which is characterized by high LREE and MREE concentrations without significant Europium anomaly (Figure 32). The geochemical signals are mixed of various lithologies within the vast drainage basins, which leave them unsatisfactorily distinguishable by these criteria (Figure 31).

Near Luzón at SCS-NE, the geochemical signal within sinking particulate matter resembles the signal of the sediments of the Luzón Rivers, which are characterized by the low LREE/HREE (0.38-0.39) and Zr/Sc (1.91-2.51) ratios and a high Eu* (1.22-1.26). The total REE concentration is lower, than in the sediment, but as the LREE/HREE ratio did not increase above the sediments' ratios, dilution by REE depleted SPM may be the explanation rather than desorption of REE from lithogenic SPM. This signal also reaches the seafloor and accumulates in the sediment. The geochemical signals remain constant down the water column and temporally throughout the year (Figure 33, Figure 34).

In the north-central basin at SCS-NC and at SCS-N, during mooring N01 and N02, PAAS-normalized Lanthanides' concentration patters resemble those of the Taiwanese rivers, though slightly depleted in their LREE contents, which may either be an effect of desorption or the mixture with HREE enriched material from Luzón. At SCS-NC and -N the signal is characterized by high LREE/HREE (0.59; 0.81-0.83) and Zr/Sc (n.d; 4.68) ratios and a very low Eu*(1.08; 1.07-1.08). These particles are mostly of (direct or indirect) Taiwanese origin with minor contributions of Luzón and Pearl River derived material. This signal does not compose that of the sediment below SCS-N. The signal is the same at both water depths at SCS-N. No temporal variations of the geochemical signal were observed. In the north-central basin at SCS-C, SCS-W and at SCS-N, during moorings N03 and N04, sinking particulate matter is characterized by high LREE/HREE (0.54-0.74; 0.72; 0.65-0.68) and variable Zr/Sc (0.91-5.88; 5.58; 4.16-4.44) ratios, as well as a variably intense positive Eu* (1.01.-1.09; 1.15; 1.19-1.21). REE-concentrations at SCS-C are very low. The positive Eu* at SCS-W could be contributed by both Hainan and Luzón Rivers. The higher contribution of LREE could derive from various sources, including Taiwan, South China and Red Rivers and re-suspended material from the South China shelf. At SCS-N the geochemical signal is the nearly the same at all three depths, but with downward increasing HREE concentrations. Temporal variations are of minor significance. Though the main signal appears invariable through the year, variations of elemental ratios are notable at SCS-W. At SCS-C, trace element signals change down the watercolumn and vary irregularly within the year. Tendencially, contribution of Luzón derived material, represented by lower LREE/HREE and Zr/Sc ratios, increases downwards.

In the southwestern basin at stations SCS-SW and -S, sinking particulate matter is generally characterized by high trace element concentrations, enriched with MREE, high LREE/HREE (0.83; 0.86) and Zr/Sc (5.88; n.d) ratios and negative Europium anomalies (0.99; 0.77). As these characteristics are common in Indochina, it is not possible to differentiate between the Mekong, Red and Vietnamese coastal Rivers and the Vietnamese and Sunda shelves as sources of these materials. Episodical variations were observed at SCS-S, which indicate temporal variations of re-distribution.

The reliability of provenance analysis based on trace element characteristics depends strongly on the regional settings of source characteristics and oceanographic re-distribution of SPM. Differential settling and mixing of various sources should be expected to affect the reliability of trace element provenance analysis negatively, but less heavily than it does on provenance analysis by clay mineral assemblages.

5.5. Acknowledgements

6. ENSO-variations of trace elements in the northern SCS

[1,2]Annette SCHRÖDER, [2]LIU Zhifei, [1]Martin WIESNER

[1]Institute of Geology, Hamburg University, 20146 Hamburg, Germany

[2]State Key Laboratory for Marine Geology, Tongji University, 200092 Shanghai, China

Corresponding author: annette.heddaeus@zmaw.de

Abstract: Trace element signatures of sinking particulate matter intercepted during El Niño-years 1987/88 and non-ENSO-years 2009/10 and 2011/12 by sediment traps in the northern South China Sea indicate weak monsoonal, but strong interannual correlation of sediment contribution to warm/cool variations. During non-ENSO conditions, sinking particulate matter deriving from Luzón, Taiwan and South China Rivers contribute material to the sediment trap and underlying sediment. We correlate contribution changes of relatively more material from Taiwan during El Niño warm periods to reduced precipitation on Luzón Island and variations of the cyclonic deep current, which is responsible for the re-distribution of sinking particulate matter. The effective sediment below the sediment trap mooring (1 cm) is characterized by the signals of sinking particulate matter during non-ENSO conditions, which means that under recent conditions the warm-intervals are underrepresented in the sedimentary record. Nevertheless, the warm/cool environmental condition changes of sediment availability and distribution should be considered for sediment records, deposited during longer termed warm/cool cycles, like glaciations.

Keywords: Warm/cold conditions; Trace element signatures; REE; sinking particulate matter; sediment traps; northern SCS; sedimentation processes.

6.1. Introduction - ENSO effects in the SCS

The ongoing discussion about climatic changes is supported by weathering-reconstructions based on clay mineral assemblages and other proxies. The changes of warm/cool conditions caused by the El Niño Southern Oscillation (ENSO) enable us to monitor these proxies' behaviour on a shorter time scale and correlate them to directly measured environmental changes. The ENSO is an atmospheric cycle that causes short scaled (4-7 years) warming and cooling conditions in the Pacific region. The cause of El Niño variations lies in atmospheric changes, which affect precipitation rates, cloud formation, insolation, sea surface temperature, thermohaline variations and surface current conditions.

The South China Sea (SCS) as a marginal Sea to the western Pacific is only peripherically affected by the El Niño Southern Oscillation. The timing of an El Niño year in the SCS lags 3-5 months behind ENSO area 3.4 (Figure 37). El Niño conditions were recorded, but no distinguishable La Niña conditions (Chao et al., 1997). 1987 and 1997 were the last strong El Niño years in the SCS (Zhou and Chan, 2007). During El Niño years, rainfall is generally reduced (Chao et al., 1997) and even lower on the southern and central SCS drainage basins, including Luzón (Xu et al., 2004) (Figure 41). Therefore, already high discharges from Taiwan (123 Mt/y; 30% of basin wide TSS, calculated from Milliman and Farnsworth, 2011) increase even further during El Niño years, relative to those of Luzón (11 Mt/y; 3% of basin-wide TSS, calculated from Milliman and Farnsworth, 2011). Oceanographic conditions are affected by El Niño conditions, too: surface currents weaken, while the Kuroshio intrusion and the inflow through the Luzón Strait in general increase during El Niño conditions (Chao et al., 1997; Gordon et al., 2012a). The pacific water enters mainly above 400 m water depth and sinks rapidly due to its relative coldness and higher density (Qu et al., 2004).

Do these small scaled cold/warm variations also affect the deep sea currents and the sedimentary record? To find out more about how cold/warm events affect the sediment record, we deployed sediment trap systems during El Niño and non-ENSO-years and tried to reconstruct the lithogenic matter's provenance with their clay mineral and trace element characteristics.

Our results demonstrate significant changes of source contributions during transport of sinking particulate matter to the deep sea, which can be related to changes in erosion and marine transport routes. The results show both that the ENSO locally affects even deep sea currents and that strong variations of sediment composition can be caused rather by erosion and contribution changes than by changes in weathering.
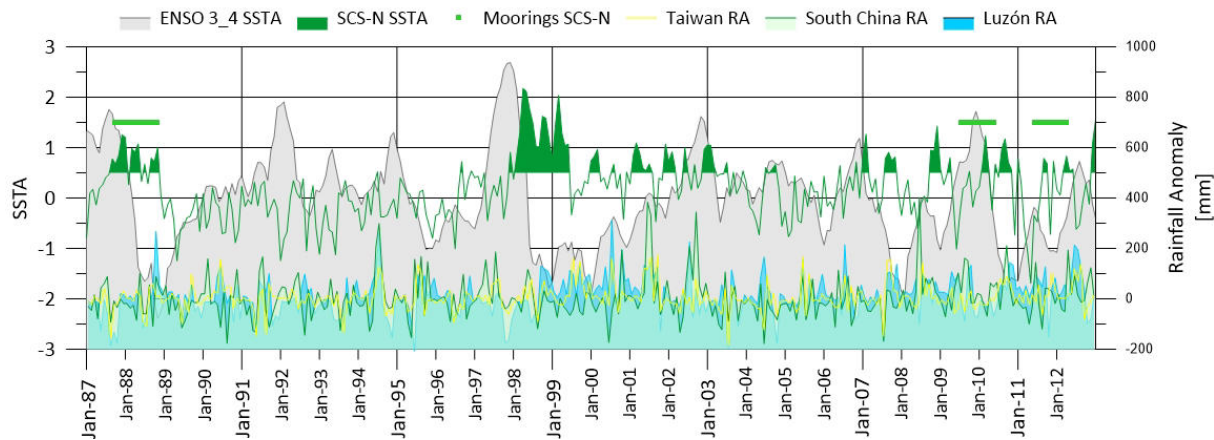
Figure 37: SSTA at stations SCS-N lags behind the Pacific ENSO induced SSTA. El Niño conditions are given when SSTA rise above 1; La Niña conditions are given when SSTA drop below -1. Both El Niño and La Niña conditions are notably weaker in the northern SCS than in the ENSO 3_4 zone.

Table 24: Positions and deployment times of the sediment traps deployed in the northern SCS.

Station name	Mooring Number	Trap Name	Mooring Start	Mooring End	Latitude	Longitude	Water Depth	Trap Depth
SCS-NC	1	SH	10.12.1996	26.11.1997	17 .075° E	117 .192° E	4038 m	-1465 m
SCS-NC	1	D	10.12.1996	26.11.1997	17 .075° E	117 .192° E	4038 m	-3500 m
SCS-NE	1	SH	08.07.1998	30.04.1999	17 .399° E	119 .657° E	2826 m	-1225 m
SCS-NE	1	M	08.07.1998	30.04.1999	17 .399° E	119 .657° E	2826 m	-1756 m
SCS-NE	1	D	08.07.1998	30.04.1999	17 .399° E	119 .657° E	2826 m	-2287 m
SCS-NE	2	SH	15.05.1999	13.05.2000	17 .399° E	119 .657° E	2826 m	-1324 m
SCS-NE	2	D	15.05.1999	13.05.2000	17 .399° E	119 .657° E	2826 m	-2412 m
SCS-N	1	SH	10.09.1987	22.03.1988	18 .498° E	115 .999° E	3766 m	-1000 m
SCS-N	1	D	10.09.1987	22.03.1988	18 .498° E	115 .999° E	3766 m	-3350 m
SCS-N	2	D	13.04.1988	21.10.1988	18 .498° E	115 .999° E	3766 m	-3350 m
SCS-N	3	SH	27.06.2009	13.05.2010	18 .498° E	115 .999° E	3766 m	-983 m
SCS-N	3	M	27.06.2009	13.05.2010	18 .498° E	115 .999° E	3766 m	-2158 m
SCS-N	3	D	27.06.2009	13.05.2010	18 .498° E	115 .999° E	3766 m	-3196 m
SCS-N	4	SH	20.05.2011	04.04.2012	18 .498° E	115 .999° E	3766 m	-983 m
SCS-N	4	M	20.05.2011	04.04.2012	18 .498° E	115 .999° E	3766 m	-2158 m
SCS-N	4	D	20.05.2011	04.04.2012	18 .498° E	115 .999° E	3766 m	-3196 m

6.2. Material and Methods

Sinking particles were collected by Mark VI and Mark VII time-series sediment traps which were deployed at station SCS-N in the northern SCS, 465 km south of the Pearl River Estuary. The traps were placed at water depths between 500 m and 3700 m; collection intervals were between 16 and

28 days (Table 24). The surface sediment was taken with a standard box corer and the upper 1 cm was sampled with a spoon.

Prior to the deployment of the sediment traps, sample cups were filled with sea water from the respective trap depths filtered over WHATMAN GF/F filters (precombusted at 450°C). NaCl (33.3 g/l) and $HgCl_2$ (3.33 g/l) were added to the cups to minimize diffusion and to retard decomposition of the trapped material. After recovery, the wet samples were passed through a 1 mm mesh nylon sieve to exclude pelagic macro-organisms. Subsequently the <1 mm fractions were split into aliquots, then filtered over pre-weighed Nucleopore filters (0.45 μm pore size) and dried at 40 °C for 12 hours. The dry weights of these fractions were used for calculating the total mass fluxes and for component analyses. The amount of lithogenic material was computed as the difference between the total mass of particles and the sum of carbonate, organic matter and biogenic opal (Lahajnar et al. 2007).

6.2.1. Trace element analysis

Preparation and analysis of trace elements have been carried out at the Laboratory of Christian Albrechts University in Kiel (Garbe-Schönberg, 1993). Element analysis was done on bulk sinking particulate matter and then prepared with the following steps:

Table 25: Preparation steps before element analysis according Garbe-Schönberg (1993).

Step	Chemical agent	concentration	amount	duration	Temperature
Dissolution of detrital fraction	hydrofluoric acid HF	40% (suprapur)	4 ml	>10 h On a hot-plate	160°C
	Aqua regia HCl + HNO_3	37%+ 65% p.a. →distilled	4 ml		
Fluor blocker	Perchloric acid $HClO_4$	60%	1 ml	Evaporate to near dryness	190°C
rinse	Nitric acid HNO_3	65% p.a. →distilled	1 ml	Evaporate to near dryness	190°C
	water	deionized	Few ml		
Dilution and transfer	Nitric acid HNO_3	65% p.a. →distilled	1 ml	Dilution factor 200	
	water	deionized	5 ml		

Trace element measurements have been done using an inductively coupled plasma mass spectrometer (ICP-MS) of the type VG Instruments PlasmaQuad PQ1 in 1996 and 1998 (N01 and N02) and the AGILENT 7500cs during the measurement campaigns in 2013 (N03 and N04). Standards used for calibration of the ICP-MS were BIR-1, BHVO-1, MAG-1.

For the plotting of Lanthanide profiles, concentrations of elements were normalized by the concentrations of the standard PAAS shale (McLennan, 1989).

Table 26: Lanthanides concentrations of the PAA-Shale used for normalization [ppb] (McLennan, 1989).

La	Ce	Pr	Nd	Sm	Eu	Gd	Tb	Dy	Y	Ho	Er	Tm	Yb	Lu
38.20	79.60	8.83	33.90	5.55	1.08	4.66	0.77	4.68	27.00	0.99	2.85	0.41	2.82	0.43

LREE is the sum of PAAS-normalized concentrations of the light rare earth elements (La, Ce, Pr, Nd), HREE the sum of PAAS-normalized concentrations of the last six elements (Dy, Ho, Er, Tm, Yb, Lu) according:

$$[LREE] = \frac{[La]}{[La]PAAS} + \frac{[Ce]}{[Ce]PAAS} + \frac{[Pr]}{[Pr]PAAS} + \frac{[Nd]}{[Nd]PAAS}$$

$$[MREE] = \frac{[Sm]}{[Sm]PAAS} + \frac{[Eu]}{[Eu]PAAS} + \frac{[Gd]}{[Gd]PAAS} + \frac{[Tb]}{[Tb]PAAS}$$

$$[HREE] = \frac{[Dy]}{[Dy]PAAS} + \frac{[Ho]}{[Ho]PAAS} + \frac{[Er]}{[Er]PAAS} + \frac{[Tm]}{[Tm]PAAS} + \frac{[Yb]}{[Yv]PAAS} + \frac{[Lu]}{[Lu]PAAS}$$

Few samples could be measured twice or more times. As an example for internal error calculation SCS NE01 MD09 has been measured six times with standard deviations for the REE concentrations between 0.0015 and 0.007 which equals 0.25-1.14%.

6.3. Results

6.3.1. Riverine Trace element signals of Taiwan, Luzón, Pearl River

Trace element signals preserved in minerals discharged into the SCS are divers (5.3.1). The best characteristics to distinguish drainage basin specific geochemical signals are elemental ratios of LREE/HREE, Zr/Sc ratios and Europium anomalies (Eu*). In basin-wide comparison of these features, the fluvial sediments of several drainage regions are well distinguishable: Sediments from **Taiwanese Rivers** have the highest LREE/HREE ratio (0.9 to 1.26) in basin wide comparison. PAAS-normalized concentrations of Samarium, Europium and Gadolinium are nearly equally high and even higher than LREE, therefore there is a low positive, but insignificant Europium anomaly present in these sediments. The material is rich with illite and chlorite (Liu et al., 2008), from intense physical and weak chemical weathering. On the eastern side of the basin the **Luzón** Rivers discharge a signal that is characterized by a very low LREE/HREE ratio (0.03-0.07), because they are enriched with HREE. Furthermore they provide a strong positive Europium anomaly (1.29-1.45). Another distinctive feature is the very low Zr/Sc ratio (3.98-5.17) (Table 16). Among the Luzón sediments, the REE-Signal of the Bucao River has the highest LREE/HREE ratio. As the Bucao river drains the Pinatubo Mountain Region, its signal also represents the Pinatubo 1991 ash layer, that covers vast areas of the central SCS, including the Scarborough Seamounts and the Macclesfield bank (Wiesner et al. 2004). The **Pearl River** is characterized by a moderate to high LREE/HREE ratio and a negative Eu*, which are characteristic for the South China granitoids and felsic endmember parent rocks of a plagioclase rich magmatic suite.

6.3.2. Sinking particulate matter

6.3.2.1. Lithogenic matter fluxes

Lithogenic matter flux peaks with 80 mg/m²/d (120 mg/m²/d) during November (December) and February (April) during mooring N01 and N02 (N03 and N04; non-ENSO years) in the shallow traps. During late summer and autumn lithogenic matter fluxes range below 20 mg/m²/d. The fluctuations are higher in the shallower trap than in the deeper traps (Figure 40).

As previously described, fluxes increase with depth through lateral advection (Schröder et al., n.d.). During the non-ENSO years, a high-flux phase from November to May transports up to 100 mg/m²/d at the middle trap and 75 mg/m²/d at the DP trap. During the low flux phase from July to October less than 25 mg/m²/d sink down (Figure 40). So, lithogenic matter fluxes are highest during winter monsoon and display a seasonal signal.

Table 27: Lithogenic matter fluxes and normalized trace element concentrations of all sampled intervals at SCS-N.

sample	interval		duration	Lithogen flux	Eu*	LREE/HREE	Zr/Sc
	start	end	[d]	[mg/m²/d]			
SCS-N01 SH01	10.09.87	25.09.87	15	15.03			
SCS-N01 SH02	25.09.87	10.10.87	15	3.54			
SCS-N01 SH03	10.10.87	25.10.87	15	8.88			
SCS-N01 SH04	25.10.87	09.11.87	15	11.46			
SCS-N01 SH05	09.11.87	24.11.87	15	88.71	1.06	0.98	
SCS-N01 SH06	24.11.87	09.12.87	15	71.12	1.07	0.91	
SCS-N01 SH07	09.12.87	24.12.87	15	43.83	1.05	0.86	
SCS-N01 SH08	24.12.87	08.01.88	15	45.87	1.08	0.76	
SCS-N01 SH09	08.01.88	23.01.88	15	76.39	1.10	0.66	
SCS-N01 SH10	23.01.88	07.02.88	15	49.48	1.13	0.70	
SCS-N01 SH11	07.02.88	22.02.88	15	41.97	1.11	0.70	
SCS-N01 SH12	22.02.88	08.03.88	15	29.73	1.08	0.71	
SCS-N01 SH13	08.03.88	23.03.88	15	15.22			
SCS-N01 DP01	10.09.87	25.09.87	15	24.44			
SCS-N01 DP02	25.09.87	10.10.87	15	50.05			
SCS-N01 DP03	10.10.87	25.10.87	15	48.53			
SCS-N01 DP04	25.10.87	09.11.87	15	46.46			
SCS-N01 DP05	09.11.87	24.11.87	15	50.39	1.08	0.86	
SCS-N01 DP06	24.11.87	09.12.87	15	46.57	1.07	0.87	
SCS-N01 DP07	09.12.87	24.12.87	15	27.07	1.09	0.80	
SCS-N01 DP08	24.12.87	08.01.88	15	5.72			
SCS-N01 DP09	08.01.88	23.01.88	15	15.84			
SCS-N01 DP10	23.01.88	07.02.88	15	41.17			
SCS-N01 DP11	07.02.88	22.02.88	15	53.94			
SCS-N01 DP12	22.02.88	08.03.88	15	61.60			
SCS-N01 DP13	08.03.88	23.03.88	15	28.22			
SCS-N02 SH01	13.04.88	27.04.88	14	54.58			
SCS-N02 SH02	27.04.88	12.05.88	15	51.67			
SCS-N02 SH03	12.05.88	27.05.88	15	48.12			
SCS-N02 SH04	27.05.88	11.06.88	15	64.14			
SCS-N02 SH05	11.06.88	25.06.88	14	69.92	1.08	0.75	
SCS-N02 SH06	25.06.88	10.07.88	15	59.44	1.07	0.73	
SCS-N02 SH07	10.07.88	25.07.88	14	50.22	1.06	0.80	
SCS-N02 SH08	25.07.88	09.08.88	15	18.32			
SCS-N02 SH09	09.08.88	23.08.88	14	12.13			
SCS-N02 SH10	23.08.88	07.09.88	15	8.09			
SCS-N02 SH11	07.09.88	22.09.88	15	11.88			
SCS-N02 SH12	22.09.88	07.10.88	15	10.27			
SCS-N02 SH13	07.10.88	21.10.88	14	8.56			
SCS-N03 SH01	27.06.09	13.07.09	16	16.02	1.24	0.60	4,92
SCS-N03 SH02	13.07.09	29.07.09	16	15.57	1.23	0.65	4,53
SCS-N03 SH03	29.07.09	14.08.09	16	22.41	1.22	0.66	4,70
SCS-N03 SH04	14.08.09	30.08.09	16	12.95	1.24	0.59	5,23
SCS-N03 SH05	30.08.09	15.09.09	16	6.45	1.27	0.60	4,54
SCS-N03 SH06	15.09.09	01.10.09	16	12.00	1.24	0.64	4,34
SCS-N03 SH07	01.10.09	17.10.09	16	9.39			
SCS-N03 SH08	17.10.09	02.11.09	16	21.67	1.23	0.60	4,32
SCS-N03 SH09	02.11.09	18.11.09	16	62.66	1.17	0.70	4,63
SCS-N03 SH10	18.11.09	04.12.09	16	125.34	1.13	0.79	4,77
SCS-N03 SH11	04.12.09	20.12.09	16	54.51	1.20	0.62	3,90
SCS-N03 SH12	20.12.09	05.01.10	16	59.73	1.19	0.64	4,01

Changes of clay mineral and trace element characteristics in the Deep South China Sea

sample	interval		duration	Lithogen flux	Eu*	LREE/HREE	Zr/Sc
	start	end	[d]	[mg/m²/d]			
SCS-N03 SH13	05.01.10	21.01.10	16	14.68	1.23	0.69	4,77
SCS-N03 SH14	21.01.10	06.02.10	16	13.52	1.25	0.52	4,04
SCS-N03 SH15	06.02.10	22.02.10	16	24.51	1.26	0.52	3,69
SCS-N03 SH16	22.02.10	10.03.10	16	26.40	1.27	0.57	3,42
SCS-N03 SH17	10.03.10	26.03.10	16	18.64	1.19	0.68	4,33
SCS-N03 SH18	26.03.10	11.04.10	16	118.97	1.13	0.76	4,62
SCS-N03 SH19	11.04.10	27.04.10	16	61.78	1.16	0.75	4,26
SCS-N03 SH20	27.04.10	13.05.10	16	46.07	1.20	0.75	3,48
SCS-N03 MD01	27.06.09	13.07.09	16	25.63			
SCS-N03 MD02	13.07.09	29.07.09	16	25.27	1.21	0.65	4,52
SCS-N03 MD03	29.07.09	14.08.09	16	25.55	1.22	0.66	4,38
SCS-N03 MD04	14.08.09	30.08.09	16	20.69	1.24	0.60	4,36
SCS-N03 MD05	30.08.09	15.09.09	16	21.54			
SCS-N03 MD06	15.09.09	01.10.09	16	17.52			
SCS-N03 MD07	01.10.09	17.10.09	16	15.11			
SCS-N03 MD08	17.10.09	02.11.09	16	7.66			
SCS-N03 MD09	02.11.09	18.11.09	16	52.93			
SCS-N03 MD10	18.11.09	04.12.09	16	73.46	1.20	0.65	4,35
SCS-N03 MD11	04.12.09	20.12.09	16	100.25	1.17	0.70	4,24
SCS-N03 MD12	20.12.09	05.01.10	16	94.04			
SCS-N03 MD13	05.01.10	21.01.10	16	54.19	1.19	0.69	4,18
SCS-N03 MD14	21.01.10	06.02.10	16	54.86	1.21	0.62	4,01
SCS-N03 MD15	06.02.10	22.02.10	16	55.65	1.23	0.62	3,86
SCS-N03 MD16	22.02.10	10.03.10	16	69.53	1.21	0.65	3,89
SCS-N03 MD17	10.03.10	26.03.10	16	56.69	1.21	0.66	4,12
SCS-N03 MD18	26.03.10	11.04.10	16	99.82			
SCS-N03 MD19	11.04.10	27.04.10	16	69.19			
SCS-N03 MD20	27.04.10	13.05.10	16	36.80			
SCS-N03 DP01	27.06.09	13.07.09	16	0.66			
SCS-N03 DP02	13.07.09	29.07.09	16	31.89	1.21	0.66	4,62
SCS-N03 DP03	29.07.09	14.08.09	16	29.04	1.21	0.68	4,16
SCS-N03 DP04	14.08.09	30.08.09	16	29.62	1.20	0.67	4,56
SCS-N03 DP05	30.08.09	15.09.09	16	27.47			
SCS-N03 DP06	15.09.09	01.10.09	16	27.63			
SCS-N03 DP07	01.10.09	17.10.09	16	21.41			
SCS-N03 DP08	17.10.09	02.11.09	16	25.87			
SCS-N03 DP09	02.11.09	18.11.09	16	20.44			
SCS-N03 DP10	18.11.09	04.12.09	16	44.46			
SCS-N03 DP11	04.12.09	20.12.09	16	58.62	1.18	0.68	4,36
SCS-N03 DP12	20.12.09	05.01.10	16	71.42	1.19	0.68	4,16
SCS-N03 DP12	20.12.09	05.01.10	16	71.42			
SCS-N03 DP13	05.01.10	21.01.10	16	69.92			
SCS-N03 DP14	21.01.10	06.02.10	16	75.34	1.19	0.65	4,39
SCS-N03 DP15	06.02.10	22.02.10	16	59.74	1.21	0.65	3,88
SCS-N03 DP16	22.02.10	10.03.10	16	66.33			
SCS-N03 DP17	10.03.10	26.03.10	16	66.57			
SCS-N03 DP18	26.03.10	11.04.10	16	58.74			
SCS-N03 DP19	11.04.10	27.04.10	16	57.66			
SCS-N03 DP20	27.04.10	13.05.10	16	42.38			
SCS-N04 SH01	20.05.11	05.06.11	16	27.49			
SCS-N04 SH02	05.06.11	21.06.11	16	43.28			
SCS-N04 SH03	21.06.11	07.07.11	16	20.73	1.25	0.64	3,85

sample	interval		duration	Lithogen flux	Eu*	LREE HREE	Zr/Sc
	start	end	[d]	[mg/m²/d]			
SCS-N04 SH04	07.07.11	23.07.11	16	13.62	1.25	0.66	3,93
SCS-N04 SH05	23.07.11	08.08.11	16	12.16	1.24	0.67	4,35
SCS-N04 SH06	08.08.11	24.08.11	16	18.90	1.26	0.62	4,01
SCS-N04 SH07	24.08.11	09.09.11	16	11.33			
SCS-N04 SH08	09.09.11	25.09.11	16	4.97			
SCS-N04 SH09	25.09.11	11.10.11	16	62.82	1.14	0.83	4,61
SCS-N04 SH10	11.10.11	27.10.11	16	38.28	1.15	0.75	4,19
SCS-N04 SH11	27.10.11	12.11.11	16	44.81	1.15	0.78	4,12
SCS-N04 SH12	12.11.11	28.11.11	16	64.22			
SCS-N04 SH13	28.11.11	14.12.11	16	21.47			
SCS-N04 SH14	14.12.11	30.12.11	16	18.73			
SCS-N04 SH15	30.12.11	15.01.12	16	38.90			
SCS-N04 SH16	15.01.12	31.01.12	16	101.68			
SCS-N04 SH17	31.01.12	16.02.12	16	27.61	1.16	0.70	4,27
SCS-N04 SH18	16.02.12	03.03.12	16	33.33	1.20	0.73	4,05
SCS-N04 SH19	03.03.12	19.03.12	16	47.36	1.18	0.68	4,78
SCS-N04 SH20	19.03.12	04.04.12	16	68.25			
SCS-N04 MD01	20.05.11	05.06.11	16	47.82			
SCS-N04 MD02	05.06.11	21.06.11	16	62.30			
SCS-N04 MD03	21.06.11	07.07.11	16	52.78	1.18	0.67	4,59
SCS-N04 MD04	07.07.11	23.07.11	16	29.29	1.20	0.65	4,60
SCS-N04 MD05	23.07.11	08.08.11	16	30.56	1.19	0.66	4,22
SCS-N04 MD06	08.08.11	24.08.11	16	28.68	1.22	0.68	4,11
SCS-N04 MD07	24.08.11	09.09.11	16	34.12			
SCS-N04 MD08	09.09.11	25.09.11	16	33.45			
SCS-N04 MD09	25.09.11	11.10.11	16	46.40			
SCS-N04 MD10	11.10.11	27.10.11	16	85.19			
SCS-N04 MD11	27.10.11	12.11.11	16	53.83			
SCS-N04 MD12	12.11.11	28.11.11	16	61.28			
SCS-N04 MD13	28.11.11	14.12.11	16	51.56			
SCS-N04 MD14	14.12.11	30.12.11	16	46.85			
SCS-N04 MD15	30.12.11	15.01.12	16	46.58			
SCS-N04 MD16	15.01.12	31.01.12	16	57.50			
SCS-N04 MD17	31.01.12	16.02.12	16	108.03			
SCS-N04 MD18	16.02.12	03.03.12	16	68.20	1.16	0.72	4,44
SCS-N04 MD19	03.03.12	19.03.12	16	50.54	1.18	0.69	4,62
SCS-N04 MD20	19.03.12	04.04.12	16	52.30			
SCS-N04 DP-01	20.05.11	05.06.11	16	35.43			
SCS-N04 DP-02	05.06.11	21.06.11	16	47.75			
SCS-N04 DP-03	21.06.11	07.07.11	16	52.32			
SCS-N04 DP-04	07.07.11	23.07.11	16	33.01	1.19	0.69	4,37
SCS-N04 DP-05	23.07.11	08.08.11	16	33.91	1.20	0.69	4,17
SCS-N04 DP-06	08.08.11	24.08.11	16	19.79	1.21	0.68	4,03
SCS-N04 DP-07	24.08.11	09.09.11	16	30.42	1.21	0.64	4,50
SCS-N04 DP-08	09.09.11	25.09.11	16	29.17			
SCS-N04 DP-09	25.09.11	11.10.11	16	36.93			
SCS-N04 DP-10	11.10.11	27.10.11	16	53.08			
SCS-N04 DP-11	27.10.11	12.11.11	16	20.82			
SCS-N04 DP-12	12.11.11	28.11.11	16	57.87			
SCS-N04 DP-13	28.11.11	14.12.11	16	46.03			
SCS-N04 DP-14	14.12.11	30.12.11	16	35.65			
SCS-N04 DP-15	30.12.11	15.01.12	16	46.40			
SCS-N04 DP-16	15.01.12	31.01.12	16	45.67			

Changes of clay mineral and trace element characteristics in the Deep South China Sea

sample	interval		duration	Lithogen flux	Eu*	LREE/HREE	Zr/Sc
	start	end	[d]	[mg/m²/d]			
SCS-N04 DP-17	31.01.12	16.02.12	16	63.02			
SCS-N04 DP-18	16.02.12	03.03.12	16	52.92	1.16	0.70	4,89
SCS-N04 DP-19	03.03.12	19.03.12	16	44.36	1.18	0.70	4,62
SCS-N04 DP-20	19.03.12	04.04.12	16	23.09			
SCS-N	sediment				1.13	0.67	5.08

Table 28: PAAS-normalized Lanthanide concentrations of each sample.

sample	La PAAS	Ce PAAS	Pr PAAS	Nd PAAS	Sm PAAS	Eu PAAS	Gd PAAS	Tb PAAS	Dy PAAS	Ho PAAS	Er PAAS	Tm PAAS	Yb PAAS	Lu PAAS
SCS-N01 SH01														
SCS-N01 SH02														
SCS-N01 SH03														
SCS-N01 SH04														
SCS-N01 SH05	0.48	0.47	0.48	0.44	0.49	0.52	0.48	0.40	0.36	0.32	0.31	0.32	0.31	0.29
SCS-N01 SH06	0.54	0.52	0.55	0.51	0.57	0.61	0.56	0.48	0.43	0.39	0.38	0.39	0.37	0.36
SCS-N01 SH07	0.29	0.28	0.29	0.27	0.31	0.33	0.32	0.27	0.24	0.22	0.22	0.22	0.21	0.21
SCS-N01 SH08	0.18	0.18	0.19	0.18	0.21	0.23	0.22	0.19	0.17	0.16	0.16	0.16	0.15	0.14
SCS-N01 SH09	0.14	0.13	0.14	0.13	0.16	0.18	0.17	0.16	0.15	0.14	0.13	0.14	0.13	0.13
SCS-N01 SH10	0.16	0.14	0.16	0.15	0.19	0.22	0.20	0.17	0.16	0.15	0.14	0.15	0.14	0.14
SCS-N01 SH11	0.17	0.16	0.17	0.17	0.20	0.23	0.21	0.19	0.18	0.16	0.16	0.16	0.16	0.15
SCS-N01 SH12	0.15	0.14	0.16	0.15	0.18	0.20	0.19	0.16	0.15	0.14	0.14	0.14	0.14	0.13
SCS-N01 SH13														
SCS-N01 DP01														
SCS-N01 DP02														
SCS-N01 DP03														
SCS-N01 DP04														
SCS-N01 DP05	0.39	0.38	0.40	0.38	0.44	0.48	0.44	0.38	0.34	0.30	0.30	0.30	0.29	0.28
SCS-N01 DP06	0.50	0.48	0.51	0.48	0.56	0.60	0.56	0.47	0.42	0.38	0.37	0.38	0.36	0.35
SCS-N01 DP07	0.23	0.21	0.23	0.22	0.26	0.29	0.27	0.23	0.21	0.19	0.18	0.19	0.18	0.17
SCS-N01 DP08														
SCS-N01 DP09														
SCS-N01 DP10														
SCS-N01 DP11														
SCS-N01 DP12														
SCS-N01 DP13														
SCS-N02 SH01														
SCS-N02 SH02														
SCS-N02 SH03														
SCS-N02 SH04														
SCS-N02 SH05	0.34	0.33	0.35	0.33	0.39	0.43	0.41	0.36	0.33	0.30	0.29	0.30	0.29	0.28
SCS-N02 SH06	0.30	0.29	0.31	0.30	0.34	0.38	0.37	0.32	0.30	0.27	0.27	0.27	0.27	0.25
SCS-N02 SH07	0.36	0.35	0.37	0.35	0.42	0.44	0.42	0.37	0.33	0.30	0.29	0.30	0.29	0.28
SCS-N02 SH08														
SCS-N02 SH09														
SCS-N02 SH10														
SCS-N02 SH11														
SCS-N02 SH12														
SCS-N02 SH13														
SCS-N03 SH01	0.22	0.21	0.22	0.22	0.28	0.36	0.30	0.27	0.26	0.24	0.23	0.24	0.23	0.23
SCS-N03 SH02	0.26	0.24	0.25	0.25	0.31	0.39	0.33	0.29	0.28	0.26	0.25	0.26	0.24	0.25
SCS-N03 SH03	0.26	0.25	0.26	0.26	0.32	0.39	0.33	0.30	0.28	0.26	0.25	0.27	0.25	0.24
SCS-N03 SH04	0.15	0.14	0.15	0.15	0.18	0.24	0.20	0.19	0.17	0.16	0.16	0.17	0.16	0.16
SCS-N03 SH05	0.20	0.19	0.20	0.20	0.25	0.34	0.28	0.25	0.24	0.22	0.21	0.22	0.21	0.21
SCS-N03 SH06	0.23	0.21	0.22	0.23	0.28	0.36	0.30	0.27	0.25	0.23	0.22	0.24	0.22	0.22

sample	La PAAS	Ce PAAS	Pr PAAS	Nd PAAS	Sm PAAS	Eu PAAS	Gd PAAS	Tb PAAS	Dy PAAS	Ho PAAS	Er PAAS	Tm PAAS	Yb PAAS	Lu PAAS
SCS-N03 SH07														
SCS-N03 SH08	0.18	0.17	0.18	0.18	0.23	0.28	0.24	0.22	0.21	0.20	0.19	0.21	0.19	0.19
SCS-N03 SH09	0.34	0.32	0.33	0.33	0.39	0.46	0.40	0.36	0.34	0.32	0.31	0.32	0.30	0.30
SCS-N03 SH10	0.51	0.49	0.50	0.50	0.58	0.65	0.57	0.50	0.47	0.43	0.41	0.43	0.41	0.40
SCS-N03 SH11	0.23	0.21	0.22	0.22	0.27	0.33	0.28	0.26	0.25	0.24	0.23	0.24	0.23	0.23
SCS-N03 SH12	0.31	0.29	0.30	0.30	0.36	0.44	0.38	0.34	0.33	0.31	0.30	0.32	0.31	0.31
SCS-N03 SH13	0.28	0.26	0.28	0.28	0.34	0.42	0.35	0.31	0.29	0.27	0.26	0.27	0.25	0.25
SCS-N03 SH14	0.12	0.11	0.12	0.12	0.16	0.20	0.17	0.16	0.15	0.15	0.14	0.16	0.15	0.15
SCS-N03 SH15	0.18	0.17	0.18	0.18	0.23	0.31	0.26	0.24	0.23	0.22	0.22	0.23	0.22	0.22
SCS-N03 SH16	0.20	0.19	0.20	0.21	0.26	0.34	0.28	0.26	0.25	0.23	0.23	0.24	0.22	0.23
SCS-N03 SH17	0.33	0.31	0.33	0.33	0.40	0.48	0.41	0.36	0.34	0.32	0.31	0.32	0.31	0.31
SCS-N03 SH18	0.53	0.50	0.51	0.51	0.58	0.66	0.58	0.51	0.48	0.45	0.43	0.46	0.44	0.44
SCS-N03 SH19	0.42	0.39	0.41	0.40	0.47	0.55	0.48	0.42	0.39	0.36	0.35	0.36	0.34	0.34
SCS-N03 SH20	0.30	0.28	0.29	0.29	0.35	0.41	0.35	0.30	0.28	0.26	0.25	0.26	0.25	0.25
SCS-N03 MD01														
SCS-N03 MD02	0.31	0.29	0.30	0.31	0.38	0.47	0.39	0.35	0.33	0.31	0.30	0.32	0.30	0.30
SCS-N03 MD03	0.33	0.32	0.33	0.33	0.41	0.50	0.42	0.38	0.36	0.34	0.32	0.34	0.32	0.32
SCS-N03 MD04	0.24	0.23	0.24	0.24	0.30	0.39	0.33	0.30	0.29	0.27	0.26	0.27	0.26	0.26
SCS-N03 MD05														
SCS-N03 MD06														
SCS-N03 MD07														
SCS-N03 MD08														
SCS-N03 MD09														
SCS-N03 MD10	0.37	0.36	0.36	0.37	0.44	0.55	0.47	0.42	0.40	0.37	0.36	0.38	0.36	0.37
SCS-N03 MD11	0.35	0.34	0.35	0.35	0.41	0.49	0.42	0.38	0.36	0.33	0.32	0.34	0.32	0.32
SCS-N03 MD12														
SCS-N03 MD13	0.39	0.37	0.39	0.39	0.46	0.55	0.47	0.42	0.40	0.37	0.36	0.38	0.36	0.36
SCS-N03 MD14	0.26	0.25	0.26	0.26	0.32	0.40	0.34	0.31	0.30	0.28	0.27	0.29	0.27	0.27
SCS-N03 MD15	0.30	0.28	0.30	0.30	0.37	0.47	0.39	0.35	0.34	0.32	0.31	0.33	0.31	0.31
SCS-N03 MD16	0.31	0.29	0.31	0.31	0.37	0.46	0.39	0.35	0.33	0.31	0.30	0.32	0.30	0.30
SCS-N03 MD17	0.40	0.38	0.39	0.39	0.48	0.59	0.49	0.45	0.42	0.40	0.39	0.40	0.38	0.38
SCS-N03 MD18														
SCS-N03 MD19														
SCS-N03 MD20														
SCS-N03 DP01														
SCS-N03 DP02	0.37	0.36	0.37	0.37	0.45	0.55	0.47	0.42	0.40	0.37	0.36	0.37	0.36	0.36
SCS-N03 DP03	0.39	0.37	0.39	0.39	0.47	0.58	0.48	0.44	0.41	0.38	0.37	0.38	0.36	0.37
SCS-N03 DP04	0.38	0.37	0.38	0.38	0.46	0.56	0.48	0.43	0.41	0.38	0.37	0.38	0.36	0.36
SCS-N03 DP05														
SCS-N03 DP06														
SCS-N03 DP07														
SCS-N03 DP08														
SCS-N03 DP09														
SCS-N03 DP10														
SCS-N03 DP11	0.43	0.42	0.42	0.42	0.50	0.61	0.52	0.47	0.45	0.41	0.40	0.42	0.40	0.40
SCS-N03 DP12	0.37	0.36	0.36	0.36	0.44	0.52	0.44	0.40	0.38	0.36	0.34	0.37	0.35	0.34
SCS-N03 DP12														
SCS-N03 DP13														
SCS-N03 DP14	0.34	0.33	0.34	0.34	0.41	0.50	0.43	0.38	0.36	0.34	0.33	0.35	0.33	0.33
SCS-N03 DP15	0.35	0.33	0.35	0.35	0.42	0.52	0.44	0.40	0.38	0.35	0.35	0.36	0.34	0.34
SCS-N03 DP16														
SCS-N03 DP17														
SCS-N03 DP18														
SCS-N03 DP19														
SCS-N03 DP20														
SCS-N04 SH01														
SCS-N04 SH02														
SCS-N04 SH03	0.27	0.25	0.26	0.27	0.33	0.42	0.35	0.31	0.30	0.27	0.27	0.28	0.26	0.26

sample	La PAAS	Ce PAAS	Pr PAAS	Nd PAAS	Sm PAAS	Eu PAAS	Gd PAAS	Tb PAAS	Dy PAAS	Ho PAAS	Er PAAS	Tm PAAS	Yb PAAS	Lu PAAS
SCS-N04 SH04	0.30	0.28	0.29	0.30	0.36	0.46	0.38	0.34	0.31	0.30	0.29	0.30	0.28	0.28
SCS-N04 SH05	0.22	0.21	0.22	0.22	0.27	0.35	0.28	0.25	0.24	0.22	0.21	0.23	0.21	0.21
SCS-N04 SH06	0.23	0.21	0.22	0.23	0.28	0.37	0.30	0.27	0.26	0.24	0.23	0.24	0.23	0.23
SCS-N04 SH07														
SCS-N04 SH08														
SCS-N04 SH09	0.56	0.53	0.55	0.54	0.63	0.71	0.61	0.53	0.49	0.44	0.42	0.44	0.42	0.41
SCS-N04 SH10	0.27	0.26	0.27	0.27	0.32	0.37	0.32	0.28	0.25	0.23	0.23	0.24	0.23	0.23
SCS-N04 SH11	0.41	0.39	0.40	0.40	0.47	0.54	0.46	0.40	0.37	0.34	0.33	0.35	0.33	0.33
SCS-N04 SH12														
SCS-N04 SH13														
SCS-N04 SH14														
SCS-N04 SH15														
SCS-N04 SH16														
SCS-N04 SH17	0.31	0.29	0.30	0.30	0.37	0.43	0.37	0.33	0.31	0.29	0.28	0.29	0.28	0.28
SCS-N04 SH18	0.33	0.31	0.32	0.32	0.38	0.46	0.39	0.34	0.32	0.29	0.28	0.30	0.28	0.28
SCS-N04 SH19	0.31	0.29	0.31	0.31	0.37	0.44	0.38	0.34	0.32	0.30	0.29	0.31	0.29	0.29
SCS-N04 SH20														
SCS-N04 MD01														
SCS-N04 MD02														
SCS-N04 MD03	0.39	0.37	0.39	0.39	0.46	0.56	0.48	0.43	0.41	0.38	0.36	0.39	0.37	0.37
SCS-N04 MD04	0.39	0.37	0.38	0.38	0.46	0.56	0.48	0.44	0.42	0.39	0.38	0.40	0.38	0.37
SCS-N04 MD05	0.34	0.32	0.34	0.34	0.41	0.50	0.43	0.38	0.36	0.34	0.33	0.34	0.33	0.33
SCS-N04 MD06	0.34	0.32	0.34	0.34	0.41	0.51	0.43	0.38	0.36	0.34	0.32	0.34	0.32	0.32
SCS-N04 MD07														
SCS-N04 MD08														
SCS-N04 MD09														
SCS-N04 MD10														
SCS-N04 MD11														
SCS-N04 MD12														
SCS-N04 MD13														
SCS-N04 MD14														
SCS-N04 MD15														
SCS-N04 MD16														
SCS-N04 MD17														
SCS-N04 MD18	0.39	0.37	0.39	0.38	0.45	0.54	0.47	0.41	0.39	0.36	0.34	0.36	0.34	0.34
SCS-N04 MD19	0.39	0.37	0.39	0.39	0.46	0.55	0.47	0.42	0.40	0.37	0.36	0.37	0.36	0.35
SCS-N04 MD20														
SCS-N04 DP-01														
SCS-N04 DP-02														
SCS-N04 DP-03														
SCS-N04 DP-04	0.42	0.40	0.41	0.41	0.49	0.59	0.50	0.45	0.42	0.40	0.38	0.41	0.38	0.38
SCS-N04 DP-05	0.43	0.41	0.42	0.42	0.51	0.62	0.53	0.47	0.44	0.41	0.40	0.42	0.39	0.39
SCS-N04 DP-06	0.35	0.34	0.35	0.35	0.42	0.52	0.44	0.39	0.37	0.35	0.33	0.35	0.33	0.32
SCS-N04 DP-07	0.35	0.34	0.35	0.35	0.42	0.53	0.45	0.40	0.38	0.36	0.35	0.37	0.35	0.35
SCS-N04 DP-08														
SCS-N04 DP-09														
SCS-N04 DP-10														
SCS-N04 DP-11														
SCS-N04 DP-12														
SCS-N04 DP-13														
SCS-N04 DP-14														
SCS-N04 DP-15														
SCS-N04 DP-16														
SCS-N04 DP-17														
SCS-N04 DP-18	0.41	0.39	0.41	0.40	0.48	0.57	0.50	0.44	0.42	0.39	0.37	0.39	0.37	0.37
SCS-N04 DP-19	0.35	0.33	0.35	0.35	0.41	0.50	0.43	0.38	0.36	0.33	0.32	0.34	0.32	0.31
SCS-N04 DP-20														

sample	La PAAS	Ce PAAS	Pr PAAS	Nd PAAS	Sm PAAS	Eu PAAS	Gd PAAS	Tb PAAS	Dy PAAS	Ho PAAS	Er PAAS	Tm PAAS	Yb PAAS	Lu PAAS
SCS-N	0.62	0.56	0.61	0.60	0.73	0.84	0.76	0.67	0.64	0.60	0.57	0.60	0.57	0.57
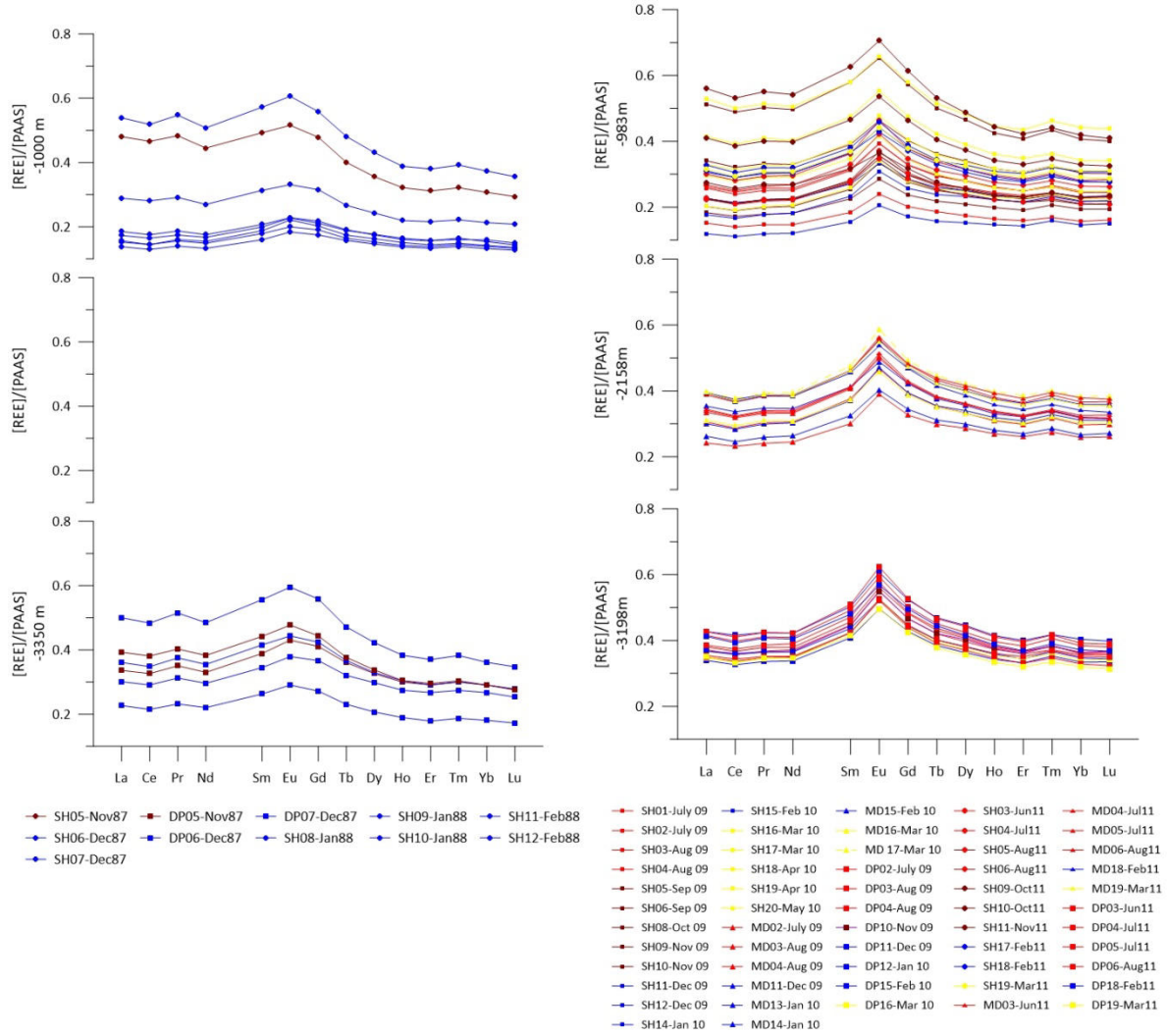
Figure 38: Lanthanides patterns during ENSO-moorings SCS-N01 and N02 are, similar to sediments of Taiwanese rivers, enriched with LREE and do not contain a positive Eu* during autumn inter- and winter monsoons (left). The patterns during non-ENSO-moorings SCS-N03 and N04 sport a positive Eu* and higher concentrations of HREE during most of a year. Within the sampled mooring intervals, the main variations between summer monsoon (red), autumn intermonsoon (purple), winter monsoon (blue) and spring intermonsoon (yellow), concern the general concentration of trace elements.
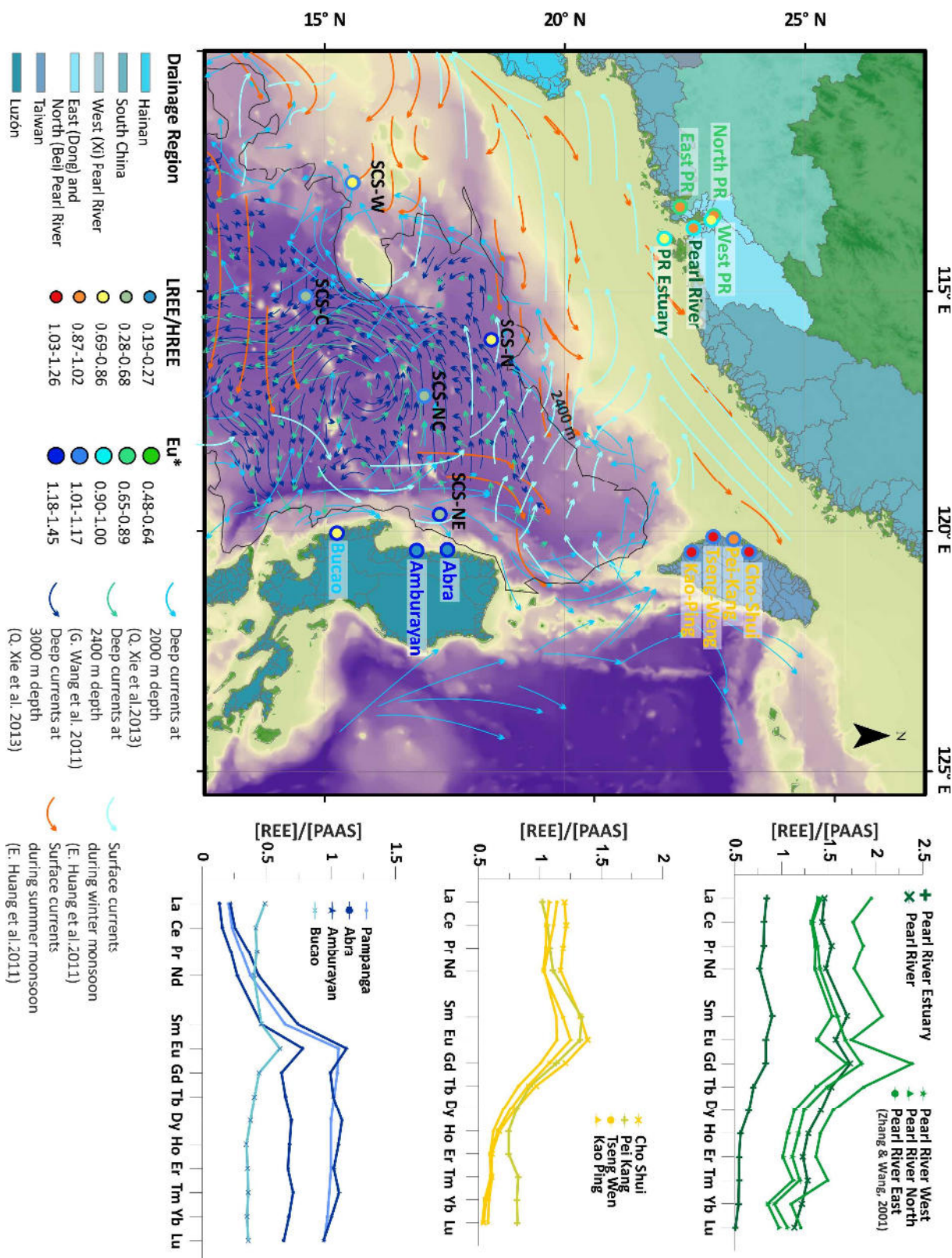
Figure 39: Regional overview of the Lanthanide signals in sediments from the drainage basins around the northern SCS. Reference-data of the Pearl River by Zhang & Wang (2001) **and of the Pampanga by** Goldstein & Jacobsen (1988)**. Map of the Eu* and LREE/HREE ratios of the dischargers and non-ENSO mean values at the shallow (-1000 m) sediment traps. Arrows indicate the modelled current directions within the upper 100 m, at 2000 m, 2400 m and 3000 m depths** (Huang et al., 2011; G. Wang et al., 2011; Xie et al., 2013)**.**

6.3.2.2. Geochemistry

Trace element signatures during winter monsoon of ENSO moorings N01 and N02 were characterized similar as the Taiwan signal with a high LREE/HREE ratio and a low Eu* at both depths (Figure 38). During non-ENSO moorings N03 and N04, sinking particulate matter is always characterized by a distinctive positive Eu* and intermediate to low LREE/HREE ratio, which both intensify slightly towards the middle and deep traps (Figure 38). This downward trend was previously interpreted to result from laterally advected material from Luzón by the cyclonic deep circulation (Schröder et al., n.d.).

During both ENSO and non ENSO-years the main geochemical signals did not change seasonally. Temporal variations concern the general concentration of trace elements and details of the Lanthanide patterns. Changes in concentration result from dilution through detrital or biogenic minerals that contain low concentrations of trace elements (Piper, 1974). These are most intense at the shallow trap, above the respective compensation depths, where carbonate and opaline shells are still intact, resulting in wider gaps between the Lanthanides' profiles.

Slight variations among Lanthanides concern the Eu*, LREE/HREE and Zr/Sc ratios. The variations are most intense at the shallow traps and reduce downwards to the middle and deep trap. Higher relative smectite abundance and Eu* and lower LREE/HREE and Zr/Sc should correlate as an indication for contribution from Luzón. The correlation is best in the shallow trap, but also there, the coincidence of peaks is not always given. These signal disturbances may result from interfering Lanthanide signals from the Pearl River, other South China Rivers or from mineral fractionation (Chapter 5).

6.4. Discussion

Main contributors of material to SCS-N are the rivers of Luzón and Taiwan with minor contributions of material from the Pearl River and South China Rivers (Chapter 5). Particle transport is influenced strongly by the cyclonic deep current in the northern SCS (Schröder et al., n.d.). During sinking, the cyclonic deep current transports the characteristic material from Luzón north- and westward, where it mixes with the plume of material from Taiwan. Further along the transport route, minor amounts of material from the Pearl River add to the mix. However, as the LREE/HREE ratio and Eu* are not well discernible, the Pearl River signal is masked easily by the more characteristic Luzón and Taiwan signals. Therefore the contribution of Pearl River material to the SCS-N traps can be underestimated.

The averaged signals that reach SCS-N during the El Niño-year 1987-1988 are all without Eu*, of high LREE/HREE ratio (Figure 38). The only effects of the Pearl Rivers' contribution of material to SCS-N may be the negative Eu* to extinguish the positive Eu* from Luzón, and contribute to the balancing of the LREE/HREE ratio. During non-ENSO years 2009-2010 and 2011-2012 the geochemical signal always contains a significant positive Eu* and low LREE/HREE ratios (increasing towards the bottom) (Figure 42). Trace element data indicates more influence from Taiwanese (and Pearl River) material rather than from Luzón material during ENSO years. During non-ENSO years the contribution of Luzón derived material is more abundant. The reason for this shift in contribution may be caused by higher availability of Luzón material during non-ENSO years or by changes of the main distribution mechanism, which is the cyclonic deep circulation.

Generally, precipitation is lower during El Niño years in the SCS (Chao et al., 1997). Lower precipitation rates produce lower erosion rates and therefore lower discharge of total suspended solids. This is reflected by reduced lithogenic matter fluxes (-40 mg/m²/d; -30%) during the N01/N02 moorings (Figure 40). During non-ENSO years, precipitation on monsoonal-tropical Luzón is higher than on temperate Taiwan and South Chinese drainage basins (Figure 41). Nevertheless, Taiwanese rivers deliver more detrital material to the ocean. During El Niño-years, precipitation on Luzón

diminishes greatly, which augments the difference between the discharge fluxes of the two main dischargers. This entrains different proportions of available material shifting the balance towards material from Taiwan.

During El Niño years, more water enters through the Luzón strait (Gordon et al., 2012b), which may deviate the cyclonic deep circulation so that it does not reach the station SCS-N during these years. The surface currents are considered to be the motor of the deep currents (Chao et al., 1996) and these generally weaken. This could result in the cyclonic deep current failing to reach the station SCS-N during El Niño-years. Along a north to south transect, salinity, density and thermal gradient of the water decreases towards the basin. The thermohaline heterogeneity and a strong geostrophic current near the South China Shelf slope form a nearly isolated water body south of the shelf (G. Wang et al., 2011). During El Niño-years thermohaline stratification gets intensified by higher evaporation in the northern SCS, with the result that a thermohaline boundary develops and deflects the flow of the cyclonic deep current (Figure 43).

Besides possible El Niño effects on sedimentation, the increase of Luzón derived material availability since 1988 can be an effect of the 1991 Pinatubo eruption. Since 1991 significant amounts of unconsolidated volcanic ashes cover the Luzón shelf, slopes and deep sea sediments stretching as far as west the Macclesfieldbank (Zhong Sha). These sediments facilitate the export of the Bucao River's REE-signal, which is characterized by a moderate LREE/HREE ratio very similar to that found in SCS-N. Nevertheless, the decrease of LREE/HREE ratios with depth and the clay mineral assemblages reaching SCS-N strongly insinuates a mixed signal from recent Luzón and Taiwan river sediments with increasingly more contribution from Luzón towards the bottom, conveyed by the cyclonic deep current.

Figure 40: Lithogenic matter fluxes are highest during winter monsoon, and generally higher during the non-ENSO moorings SCS-N03 and N04. Lithogenic matter fluxes and relative smectite abundances are higher in the deeper traps. Increasing Eu*, decreasing HREE/LREE and Zr/Sc indicate intensified contribution of Luzón derived material.
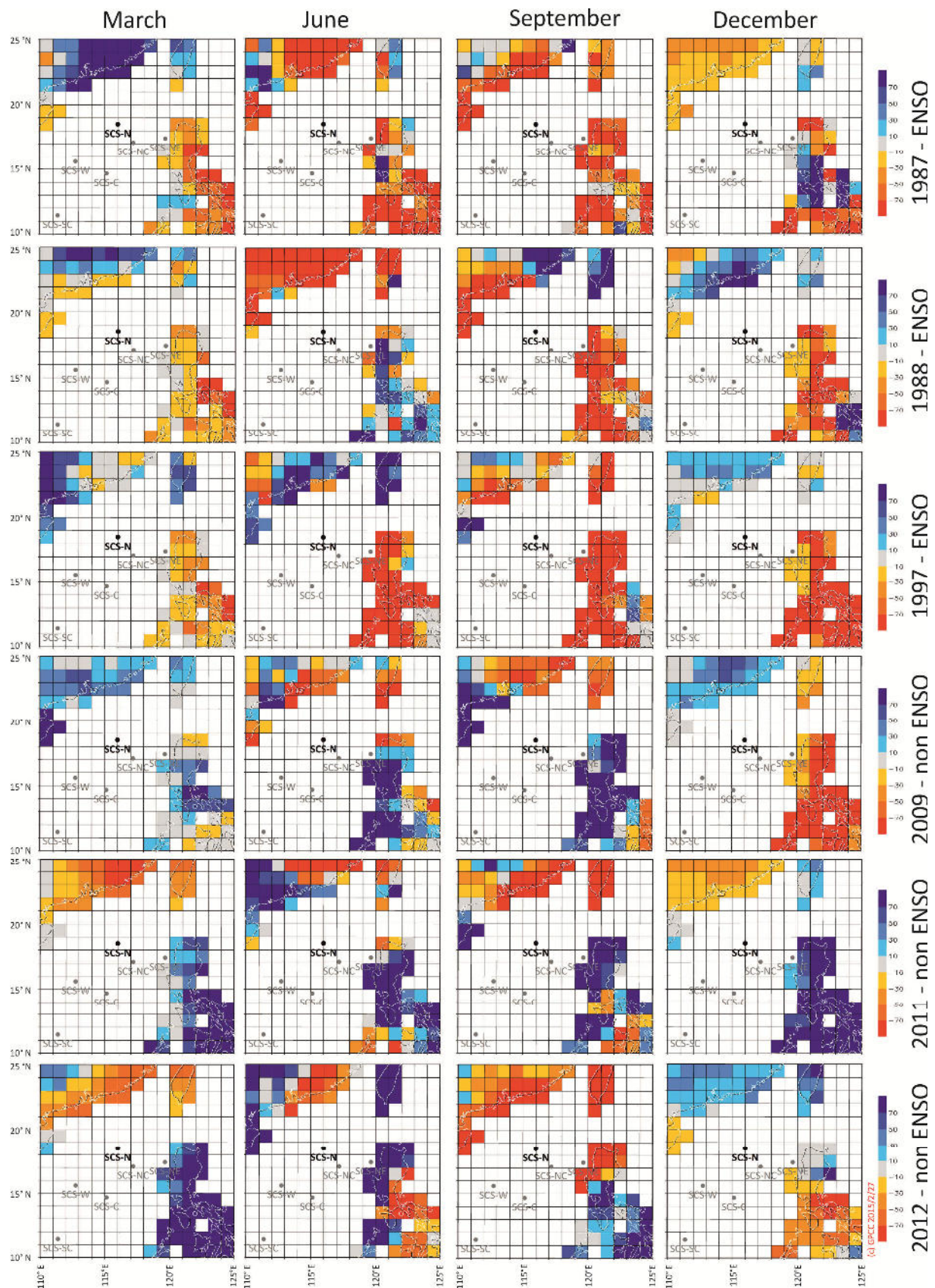
Figure 41: Precipitation deviations during El Niño years 1987/88 and 1997 and during non-ENSO years 2009, 2011 and 2012 (National Center for Atmospheric Research, 2014)**: During El Niño years precipitation is anomalously low on Luzón, producing a drier climate than during non-ENSO years, whereas precipitation on Taiwan and South China are higher or only moderately affected.**
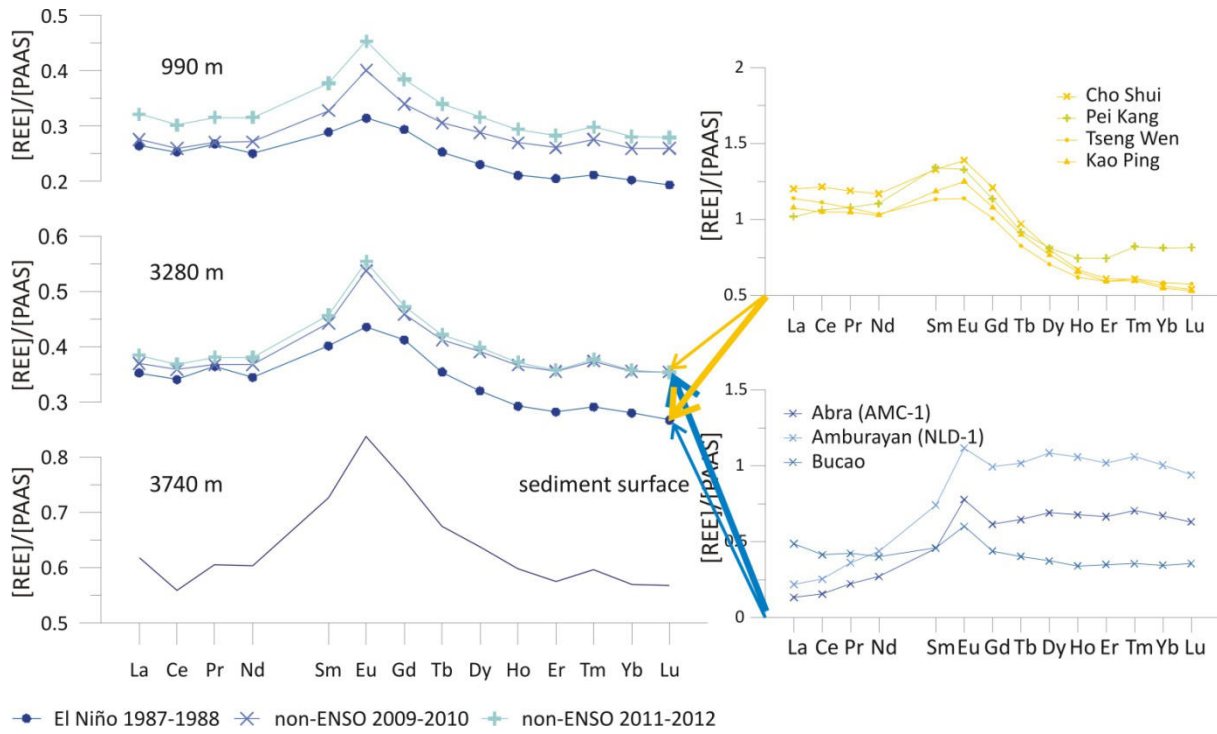
Figure 42: The contribution of materials from Luzón and Taiwan shifts from more contribution from Luzón during the non-ENSO years to more contribution from Taiwan during ENSO years. The underlying sediment adopts the non-ENSO signal in higher concentrations. The contribution of Pearl River material is not evident, but would also increase during ENSO-years.
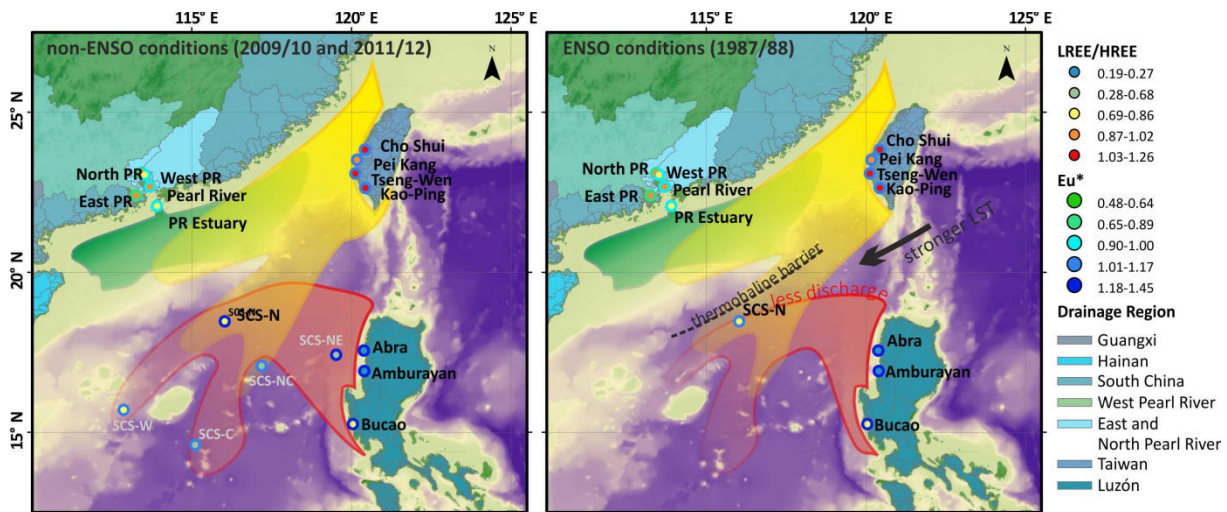
Figure 43: Sketch of the plumes carrying Luzón (red), Taiwanese (yellow) and Pearl River (green) derived material into the northern and central deep basin. During ENSO conditions a combination of less discharge from Luzón, a stronger LST and a possible thermohaline barrier along the South China Boundary Current cause, that the Luzón sediment plume barely reaches the traps at SCS-N.

6.5. Conclusions

Relative clay mineral abundances and Lanthanide elements show, that sinking particulate matter reaching station SCS-N (18.5°N/116°E) is always composed of a mixture of particles deriving mainly from Taiwan, Luzón and subordinately from the South China Rivers including the Pearl River. Trace element characteristics indicate that during ENSO-years 1987-1988, more material reached the trap from Taiwan than during non-ENSO-years 2009-2010 and 2011-2012, when material from Luzón dominated the contribution.

One reason for the change of contribution is less precipitation and therefore lower erosion and discharge rates during ENSO warm conditions in Luzón. Relatively, the erosion and discharge rates increase even further on Taiwan. Furthermore, cyclonic deep variation, which distributes SPM from Luzón, Taiwan and the Pearl River was weakened or deviated. We speculate that the enhanced Luzón Strait inflow plays a major role in weakening or deviation of the cyclonic deep current.

The signal found in the deep sea sediment resembles that of the cool condition non-ENSO years, which means, that overall, the impact of El Niño warm conditions is so finely resolved, that it does not affect the trace element signal of the upper 1 cm of sediment significantly.

Nevertheless, our results show the heavy impact of warm/cold condition changes on sinking particulate matters compositions. With an increasing trend of global warming, the warm conditions will occur more often and then change contribution to the sediment so it will also characterize the sediment. It seems probable, that warm/cold conditions on a larger time scale, like for example during glaciation events, which include longer termed changes in precipitation and surface temperature, will affect sedimentation processes and contribution. As the total environmental conditions are so fragile, oceanographic conditions and current routes must be inferred more cautiously from recent conditions to the past.

7. Conclusions and Outlook

The riverine sources around the South China Sea (SCS) are diverse, but only some of the smaller drainage basins, which drain specific lithologies, produce a recognizable clay mineralogical and geochemical signal that remains distinguishable in sinking particulate matter (SPM) (Figure 23). These are Taiwan, Luzón, Hainan and small coastal Rivers in South Vietnam, with their specific clay mineral assemblages, Europium anomaly and elemental ratios of LREE/HREE (Figure 32) and Zr/Sc (Figure 33). The larger major dischargers Mekong, Pearl River and Red River drain vast areas, which are composed of several different lithologies (Figure 31), which produce mixed clay mineral and trace element signals that are very similar to each other and therefore not well distinguishable.

Once the journey beyond the shelf margin starts, SPM is distributed in different layers of deep currents. Starting from Luzón, SPM with the Luzón signal fans up in the water column (Figure 1). Aggregates of smaller size or lower density and individual grains sink slower than bigger or denser ones, which makes them reach several different layers in the watercolumn. Differential settling during transport in pelagic surface waters further enriches suspension with smectite and finer grained particles. During specific months of planktonic blooms, small aggregates and individual grains from topmost water layers get scavenged and converted into faecal pellets, which can pass through the pycnocline. These add seasonal pulses of higher lithogenic matter fluxes to the main plume and deeper strata in general. Faecal pellets and aggregates preserve the slightly smectite enriched clay mineral and geochemical signal. As surface current velocities are mostly above the critical velocity for differential settling, the effect of should be of minor significance in pelagic waters. The main plume travels north- and downwards from Luzón towards the northern margin of the deep basin (Figure 28). Water and suspension mix with those coming from Taiwan, the South China shelf and Rivers. It gets deflected westwards by the westward along-slope currents in 1000 m depth and passes station SCS-N at 980 m to 3200 m depth (Figure 28). From there the signal is less distinctive, but apparently the plume forks around the Zhong Sha archipelago. One branch appears to pass north into the Xi Sha Trough, reaching SCS-W. Another branch passes southward, east of Zhong Sha, and reaches SCS-C in the central SCS mainly below 2300 m. The main plume moves around the shallow trap at station SCS-NC, where the material derives mostly from Taiwan (1400 m), but the lower trap (3500 m) is dominated by material from Luzón with minor contributions from Taiwan, which was probably transported there on a deep nepheloid layer (Figure 28).

The route of the main plume is temporally variable. During few weeks, variations of the Luzón signal indicate short-scaled temporal changes of the plume's peripheral reach in the western and central SCS. The plume of Luzón material shifts upwards, so that it reaches the middle trap at SCS-C and episodically fails to reach the deep trap (Figure 35), which could be caused by a short-termed weakening of deep circulation strength. The route also seems to be influenced by the El Niño Southern Oscillation (ENSO): During non-ENSO years 2009-2010 and 2011-2012 contribution of material from Luzón strongly affected the Lanthanide distribution pattern, LREE/HREE ratio and Europium anomaly (Figure 42), while during El Niño years 1987 and 1988 trace element variations clearly indicated significantly more contribution from Taiwanese Rivers. Rough comparison with a previous, unpublished study (Gerbich, 2001) suggests, that also clay mineral assemblages respond to environmental changes during El Niño years. The change in contribution could be caused by discharge-related variations of sediment availability or variations of the deep circulation, which may cause the Luzón-plume to miss station SCS-N. However, the effect of ENSO induced variations should be expected to be differ regionally within the SCS.

The southwestern basin of the SCS is not as deep as the northern and central basin. Deep circulation models often do not consider this part of the basin. Due to the lack of oceanographic information, the deduction of provenance is less reliable. Clay mineral and geochemical characteristics do not give many clues, as the major drainage basins are so similar in their sediment characteristics (Figure 23). Also, in this part of the basin, lithogenic matter fluxes are significantly higher in the deep traps (-1200 m) than in the shallow traps (-600 m) (Figure 26; Figure 27; Figure 28), which can only be caused by strong lateral advection. The high fluxes of lithogenic matter occur episodically, during the late intermonsoon phases, and are so much higher (+55-457%) (Figure 27), that they probably cannot have been caused by increased Mekong discharges alone. These extreme flux events must involve re-suspended sediments from the shelves and slopes, which could have been triggered by down-slope currents. Episodical changes in trace element properties at SCS-S (Figure 32) indicate more contribution from small southern Vietnamese drainage basins (Nha Trang, Ninh Hoa, Dinh, Long Song). At Station SCS-SC, material is generally enriched with smectite compared to SCS-S and -SW (Figure 29; Figure 28), but does not show any cyclic fluctuations. Apparently, material with different characteristics gets homogenized on the trajectory between SCS-S and -SW towards SCS-SC. The composition of sediments in the southwestern SCS is different from that of SPM (Figure 34) and appears to be mainly influenced by the high flux events that re-suspend and transport Sunda shelf material into the deep basin.

During most of the transversal route, clay minerals that detached from decaying aggregates are exposed to further differential settling. This segregation may be not as fast and effective as the differential settling in the estuaries, where clay minerals flocculate preferentially in response to salinity changes, but the duration of the transport should be long enough to promote a certain degree of smectite enrichment with increasing distance from the source. Clay mineral assemblages are relatively and absolutely enriched with smectite at all deep traps compared to the shallow traps. Greater water depth and longer transport distance increase the effect of differential settling. At the off-shore stations in the north-central basin, SCS-N and SCS-C, compositions of sediment below the traps mostly reflects the clay mineral and geochemical properties of SPM intercepted at the deep traps. Nevertheless, clay mineral assemblages are further enriched with smectite and general REE concentrations are higher (Figure 29). The stations closer to the shelf slope, SCS-SW and SCS-NE, are affected more severely by lateral advection below than the deep trap or by bedload (Figure 32), as their geochemical characteristics differ from the signals of SPM from the deep traps.

What do all of these findings about SPM transport in the marine environment mean for the interpretation of (detrital) sediment records?

The main mechanism to determine sediments composition, including the clay mineral and trace element properties, is the re-distribution by deep currents rather than surface currents, differential settling or even estuarine or terrestrial environmental changes. Which factor dominates, depends on oceanographic conditions, size and sediment yield of the sediment dischargers of a basin. Effectively, the farther off-shore the sediment, the more differentiation and mixing of several sources mask the original, drainage basin specific weathering signal presented by clay mineral assemblages. The location of cores suitable for weathering reconstructions should be as close as possible to the estuaries, because with longer transport, more variables like current direction, current velocity, discharge from various involved drainage basins, concentrations of re-suspended sediments, even eolian input and anthropogenic sediment displacement affect the reliability of the record. Overall,

the provenance signals are dominantly affected by marine environment factors rather than terrestrial environmental changes. Clay mineral and trace element signals in deep sea sediments mainly reflect (changes of) oceanographic conditions than variations in the terrestrial environment.

Clay mineral and trace element data from sinking particulate matter intercepted by sediment traps can give highly resolved insight to deep current routes and indications about their flow intensities. Sediment trap sampling campaigns with several simultaneous moorings, equipped with current meters could provide enough data to create time series and confirm the provenance estimations with in situ measured current data to help refine the existing current models. With these, statistical funnels and catchment areas of sediment traps should be modelled, which would greatly help to determine detrital particles' provenance.

8. Acknowledgements

9. References

Alibo, D.S., Nozaki, Y., 2000. Dissolved rare earth elements in the South China Sea: Geochemical characterization of the water masses. J. Geophys. Res. 105, 28771–28783.

Alldredge, A.L., Silver, M.W., 1988. Characteristics , Dynamics and Significance of Marine Snow. Prog. Oceanogr. 20, 41–82.

Amann, T., 2008. Primärproduktion und Advektion partikulärer Sinkstoffe im Tiefenwasserauftriebsgebiet vor Vietnam. Diplomarbeit (german), Universität Hamburg.

Aoki, S., 1976. Clay Mineral Distribution in Sediments of the Gulf of Thailand and the South China Sea. J. Oceanogr. Soc. Japan 32, 169–174.

Asper, V.L., 1987. Measuring the flux and sinking speed of marine snow aggregates. Deep. Res. 34, 1–17. doi:10.1016/0198-0149(87)90117-8

Asper, V.L., Deuser, W.G., Knauer, G.A., Lohrenz, S.E., 1992. Rapid coupling of sinking particle fluxes between surface and deep ocean waters. Nature 357, 670–672. doi:10.1038/nrd2468

Bailey, S.W., 1980. Structures of layer silicates, in: Brown, G. (Ed.), Crystal Structures of Clay Minerals and Their X-Ray Identification. Mineralogical Society of London, pp. 1–123.

Berner, R.A., 1971. Formation and alteration of Silica and Clay minerals, in: Principles of Chemical Sedimentology. McGraw-Hill, Inc, pp. 158–191.

Biscaye, P.E., 1965. Mineralogy and Sedimentation of Recent Deep-Sea Clay in the Atlantic Ocean and Adjacent Seas and Oceans. Geol. Soc. Am. Bull. 76, 803–832. doi:10.1130/0016-7606(1965)76[803:MASORD]2.0.CO;2

Blott, S.J., Pye, K., 2001. Technical communication Gradistat : A grain size distribution and statistics package for the analysis of unconsolidated sediments. Earth Surf. Process. Landforms 26, 1237–1248. doi:10.002/esp.261

Bonjean, F., Lagerloef, G.S.E., 2002. Diagnostic Model and Analysis of the Surface Currents in the Tropical Pacific Ocean. J. Phys. Oceanogr. 32, 2938–2954.

Boulay, S., Colin, C., Trentesaux, A., Clain, S., Liu, Z., Lauer-Leredde, C., 2007. Sedimentary responses to the Pleistocene climatic variations recorded in the South China Sea. Quat. Res. 68, 162–172. doi:10.1016/j.yqres.2007.03.004

Boulay, S., Colin, C., Trentesaux, A., Frank, N., Liu, Z., 2005. Sediment sources and East Asian monsoon intensity over the last 450 ky. Mineralogical and geochemical investigations on South China Sea sediments. Palaeogeogr. Palaeoclimatol. Palaeoecol. 228, 260–277. doi:10.1016/j.palaeo.2005.06.005

Brown, D., Alvarez-Marrón, J., Camanni, G., 2012. The structure of the central Taiwan mountain belt. Soc. Geológica Espana, Geo-Temas 13, 485–487.

Chamley, H., 1989. Clay Sedimentology. Springer.

Chao, S.-Y., Shaw, P.-T., Wu, S.Y., 1997. El Niño modulation of the South China Sea circulation. Prog. Oceanogr. 38, 51–93.

Chao, S.-Y., Shaw, P.-T., Wu, S.Y., 1996. Deep water ventilation in the South China Sea. Deep Sea Res. Part I 43, 445–466.

Chen, J., Wiesner, M.G., Wong, H.K., Zheng, L., Xu, L., Zheng, S., 1999. Vertical changes in POC flux and indicators of early degradation of organic matter in the South China Sea. Sci. China 42, 120–128.

Chen, P.Y., 1978. Minerals in bottom sediments of the South China Sea. Geol. Soc. Am. Bull. 89, 211–222. doi:10.1130/0016-7606(1978)89<211:MIBSOT>2.0.CO;2

Chu, P.C., Edmons, N.L., Fan, C., 1999. Dynamical Mechanisms for the South China Sea Seasonal Circulation and Thermohaline Variabilities. J. Phys. Oceanogr. 29, 2971–2989.

Clift, P.D., Plumb, A.R., 2008. The Asian Monsoon - Causes, History and Effects. Cambridge University Press.

Colin, C., Siani, G., Sicre, M.-A., Liu, Z., 2010. Impact of the East Asian monsoon rainfall changes on the erosion of the Mekong River basin over the past 25,000yr. Mar. Geol. 271, 84–92. doi:10.1016/j.margeo.2010.01.013

Eisma, D., 1986. Flocculation and de-flocculation of suspended matter in estuaries. Netherlands J. Sea Res. 20, 183–199. doi:10.1016/0077-7579(86)90041-4

Elderfield, H., Greaves, M.J., 1982. The rare earth elements in seawater. Nature 296, 214–219.

Fagel, N., Boës, X., 2008. Clay-mineral record in Lake Baikal sediments: The Holocene and Late Glacial transition. Palaeogeogr. Palaeoclimatol. Palaeoecol. 259, 230–243. doi:10.1016/j.palaeo.2007.10.009

Fagel, N., Hillaire-Marcel, C., Robert, C., 1997. Changes in the Western Boundary Undercurrents outflow since the Last Glacial Maxiumum, drom Smectite/Illite ratios in deep Labrador Sea sediments. Paleoceanography 12, 79–96.

Fang, W., Fang, G., Shi, P., Huang, Q., Xie, Q., 2002. Seasonal structures of upper layer circulation in the southern South China Sea from in situ observations. J. Geophys. Res. 107, 23–1 – 23–12. doi:10.1029/2002JC001343

Garbe-Schönberg, C.-D., 1993. Simultaneous determination of thirty-seven trace elements in twenty-eight international rock standards by ICP-MS. Geostand. Newsl. 17, 81–97.

Gaye, B., Wiesner, M.G., Lahajnar, N., 2009. Nitrogen sources in the South China Sea, as discerned from stable nitrogen isotopic ratios in rivers, sinking particles, and sediments. Mar. Chem. 114, 72–85. doi:10.1016/j.marchem.2009.04.003

Gerbich, C., 2001. Lithogener Partikelfluß im Südchinesischen Meer: Quellen, Transport und Sedimentation. Dissertation (german), Universität Hamburg.

Gibbs, R.J., 1977. Clay mineral segregation in the marine environment. J. Sediment. Petrol. 47, 237–243. doi:10.1306/212F713A-2B24-11D7-8648000102C1865D

Gibbs, R.J., 1968. Clay mineral mounting techniques for X-ray diffraction analysis; a discussion. J. Sediment. Res. 38, 242–244.

Gingele, F.X., De Deckker, P., 2004. Fingerprinting Australia's rivers with clay minerals and the application for the marine record of climate change. Aust. J. Earth Sci. 51, 339–348. doi:10.1111/j.1400-0952.2004.01061.x

Gingele, F.X., De Deckker, P., Hillenbrand, C.-D., 2001. Clay mineral distribution in surface sediments between Indonesia and NW Australia - source and transport by ocean currents. Mar. Geol. 179, 135–146.

Glos, M.F., 2002. Saisonale und regionale Variabilität des Partikelflusses im nordöstlichen und zentralen Südchinesischen Meer. Diplomarbeit (german), Universität Hamburg.

Goldstein, S.J., Jacobsen, S.B., 1988. Rare earth elements in river waters. Earth Planet. Sci. Lett. 89, 35–47.

Gordon, A.L., Huber, B. a., Metzger, E.J., Susanto, R.D., Hurlburt, H.E., Adi, T.R., 2012a. South China Sea throughflow impact on the Indonesian throughflow. Geophys. Res. Lett. 39, 7. doi:10.1029/2012GL052021

Gordon, A.L., Huber, B. a., Metzger, E.J., Susanto, R.D., Hurlburt, H.E., Adi, T.R., 2012b. South China Sea throughflow impact on the Indonesian throughflow. Geophys. Res. Lett. 39, 7. doi:10.1029/2012GL052021

Griffin, J.J., Windom, H., Goldberg, E.D., 1968. The distribution of clay minerals in the World Ocean. Deep. Res. 15, 433–459. doi:10.1016/0011-7471(68)90051-X

Hartmann, J., Moosdorf, N., 2012. The new global lithological map database GLiM: A representation of rock properties at the Earth surface. Geochemistry, Geophys. Geosystems 13, 37. doi:10.1029/2012GC004370

Hein, H., 2008. Vietnam Upwelling. Dissertation (english), Universität Hamburg.

Holtzapffel, T., 1985. Les mineraux argileux. Société géologique du Nord 136.

Honjo, S., 1980. Seasonality and Interaction of Biogenic and Lithogenic Particulate Flux at the Panama Basin. Science (80-.). 218, 883–884. doi:10.1126/science.218.4575.883

Honjo, S., Doherty, K.W., 1988. Large aperture time-series sediment traps: design, objectives, construction and appliance. Deep Sea Res. 35, 133–149.

Honjo, S., Manganini, S.J., Poppe, L.J., 1982. Sedimentation of lithogenic particles in the deep ocean. Mar. Geol. 50, 199–220. doi:10.1016/0025-3227(82)90139-6

Honnorez, J., 1981. The aging of the oceanic crust at low temperatures, in: C., E. (Ed.), The Oceanic Lithosphere. Wiley & Sons Ltd, pp. 525–587.

Huang, E., Tian, J., Steinke, S., 2011. Millennial-scale dynamics of the winter cold tongue in the southern South China Sea over the past 26ka and the East Asian winter monsoon. Quat. Res. 75, 196–204. doi:10.1016/j.yqres.2010.08.014

Jagodzinski, R., 2005. Petrography and geochemistry of surface sediments from Sunda and Vietnamese shelves (South China Sea). Ser. Geol.

Khim, B.K., Park, Y.A., 1992. Smectite as a Possible Source-Indicative Clay Mineral in the Yellow Sea. Geo-Marine Lett. 12, 228–231.

Kranck, K., 1973. Flocculation of suspended sediment in the Sea. Nature 246, 348–350.

Kuo, N., Zheng, Q., Ho, C., 2000. Satellite Observation of Upwelling along the Western Coast of the South China Sea. Remote Sens. Environ. 470, 463–470.

Lahajnar, N., Wiesner, M.G., Gaye, B., 2007. Fluxes of amino acids and hexosamines to the deep South China Sea. Deep Sea Res. Part I Oceanogr. Res. Pap. 54, 2120–2144. doi:10.1016/j.dsr.2007.08.009

Li, F., Li, L., Wang, X., Liu, C., 2002. Water Masses in the South China Sea and Water Exchange between the Pacific and the South China Sea. J. Ocean Univ. Qingdao 1, 19–24.

Li, J., Gao, J., Wang, Y., Bai, F., Cees, L., 2012. Distribution and dispersal pattern of clay minerals in surface sediments, eastern Beibu Gulf, South China Sea. Acta Oceanol. Sin. 31, 78–87.

Lin, I., Chen, J., Wong, G.T.F., Huang, C., Lien, C., 2007. Aerosol input to the South China Sea: Results from the MODerate Resolution Imaging Spectro-radiometer, the Quick Scatterometer, and the Measurements of Pollution in the Troposphere Sensor. Deep Sea Res. Part II 54, 1589–1601. doi:10.1016/j.dsr2.2007.05.013

Liu, J., Clift, P.D., Yan, W., Chen, Z., Chen, H., Xiang, R., Wang, D., 2014. Modern transport and deposition of settling particles in the northern South China Sea: Sediment trap evidence adjacent to Xisha Trough. Deep. Res. Part I 93, 145–155. doi:10.1016/j.dsr.2014.08.005

Liu, J., Xiang, R., Chen, Z., Chen, M., Yan, W., Zhang, L., Chen, H., 2013. Sources, transport and deposition of surface sediments from the South China Sea. Deep Sea Res. Part I Oceanogr. Res. 71, 92–102. doi:10.1016/j.dsr.2012.09.006

Liu, Z., Colin, C., Huang, W., Le, K.P., Tong, S., Chen, Z., Trentesaux, A., 2007a. Climatic and tectonic controls on weathering in south China and Indochina Peninsula: Clay mineralogical and geochemical investigations from the Pearl, Red, and Mekong drainage basins. Geochemistry, Geophys. Geosystems 8, n/a–n/a. doi:10.1029/2006GC001490

Liu, Z., Colin, C., Li, X., Zhao, Y., Tuo, S., Chen, Z., Siringan, F.P., Liu, J.T., Huang, C.-Y., You, C., Huang, K.-F., 2010a. Clay mineral distribution in surface sediments of the northeastern South China Sea and surrounding fluvial drainage basins: Source and transport. Mar. Geol. 277, 48–60. doi:10.1016/j.margeo.2010.08.010

Liu, Z., Colin, C., Trentesaux, A., Blamart, D., 2005. Clay mineral records of East Asian monsoon evolution during late Quaternary in the southern South China Sea. Sci. China Ser. D Earth Sci. 48, 84–92.

Liu, Z., Li, X., Colin, C., Ge, H., 2010b. A high-resolution clay mineralogical record in the northern South China Sea since the Last Glacial Maximum , and its time series provenance analysis. Chinese Sciene Bull. 55, 4058–4068. doi:10.1007/s11434-010-4149-5

Liu, Z., Trentesaux, A., Clemens, S.C., Colin, C., Wang, P., Huang, B., Boulay, S., 2003a. Clay mineral assemblages in the northern South China Sea: implications for East Asian monsoon evolution over the past 2 million years. Mar. Geol. 201, 133–146. doi:10.1016/S0025-3227(03)00213-5

Liu, Z., Trentesaux, A., Clemens, S.C., Wang, P., 2003b. Quaternary clay mineralogy in the northern South China Sea (ODP Site 1146). Sci. China Ser. D 46, 1223–1235. doi:10.1360/02yd0107

Liu, Z., Tuo, S., Colin, C., Liu, J.T., Huang, C.-Y., Selvaraj, K., Chen, C.-T.A., Zhao, Y., Siringan, F.P., Boulay, S., Chen, Z., 2008. Detrital fine-grained sediment contribution from Taiwan to the northern South China Sea and its relation to regional ocean circulation. Mar. Geol. 255, 149–155. doi:10.1016/j.margeo.2008.08.003

Liu, Z., Wang, H., Hantoro, W.S., Sathiamurthy, E., Colin, C., Zhao, Y., Li, J., 2012. Climatic and tectonic controls on chemical weathering in tropical Southeast Asia (Malay Peninsula, Borneo, and Sumatra). Chem. Geol. 291, 1–12. doi:10.1016/j.chemgeo.2011.11.015

Liu, Z., Zhao, Y., Colin, C., Siringan, F.P., Wu, Q., 2009. Chemical weathering in Luzon, Philippines from clay mineralogy and major-element geochemistry of river sediments. Appl. Geochemistry 24, 2195–2205. doi:10.1016/j.apgeochem.2009.09.025

Liu, Z., Zhao, Y., Colin, C., Stattegger, K., Wiesner, M., Chih-An, H., Zhang, Y., Li, X., Sompongchaiyakul, P., You, C., Huang, C., Liu, J.T., Siringan, F.P., Le, K.P., Sathiamurthy, E., Hantoro, W.S., Liu, J., Tuo, S., Zhou, S., He, Z., Wang, Y., Bunsomboonsakul, S., Li, Y., 2015. Source-to-Sink process of fluvial sediments in the South China Sea. Earth Sci. Rev. doi:10.1016/j.earscirev.2015.08.005

Liu, Z., Zhao, Y., Li, J., Colin, C., 2007b. Late Quaternary clay minerals off Middle Vietnam in the western South China Sea: Implications for source analysis and East Asian monsoon evolution. Sci. China Ser. D 50, 1674–1684. doi:10.1007/s11430-007-0115-8

Ma, J., Wei, G., Xu, Y., 2007. Mobilization and re-distribution of major and trace elements during extreme weathering of basalt in Hainan. Geochim. Cosmochim. Acta 71, 3223–3237. doi:10.1016/j.gca.2007.03.035

McCave, I.N., Manighetti, B., Robinson, S.G., 1995. Sortable silt an fine sediment size/composition slicing: Parameters for paleocurrent speed and paleoceanography. Paleoceanogrphy 10, 593–610.

McLennan, S.M., 1993. Weathering and global denudation. J. Geol. 101, 295–303.

McLennan, S.M., 1989. Rare earth elements in sedimentary rocks; influence of provenance and sedimentary processes. Rev. Mineral. Geochemistry 21, 169–200.

Milliman, J.D., Farnsworth, K., 2011. River discharge into the coastal ocean - A global synthesis, 1st ed. Cambridge University Press, Cambridge.

Millot, G., 1967. Les deux grandesvois de'l evoluion des silicates à la surface del'écorce terrestre. Rev. Quest. Sci. 138, 337–357.

Moffett, J.W., 1990. Microbially mediated cerium oxidation in sea water. Nature 345, 421–423.

Mortlock, R.A., Froehlich, P.N., 1989. A simple method for the rapid determination of biogenic opal in pelagic marine sediments. Deep. Res. 36, 1415–1426.

National Center for Atmospheric Research, 2014. The Climate Data Guide: GPCC: Global Precipitation Climatology Centre [WWW Document]. URL https://climatedataguide.ucar.edu/climate-data/gpcc-global-precipitation-climatology-centre

Naval Research Laboratory, 2014. Archive of the 1/12° Global HYCOM [WWW Document]. URL http://www7320.nrlssc.navy.mil/GLBhycom1-12/navo/arc_list_schinaspdcur.html

Okrusch, M., Matthes, S., 2009. Mineralogie, 8th ed. Springer Berlin / Heidelberg.

Oliveira, A., Rocha, F., Rodrigues, A., Jouanneau, J., Dias, A., Weber, O., 2002. Clay minerals from the sedimentary cover from the Northwest Iberian shelf. Prog. Oceanogr. 52, 233–247. doi:10.1016/S0079-6611(02)00008-3

Osipov, V.I., 2012. Density of clay minerals. Soil Mech. Found. Eng. 48, 231–240. doi:10.1007/s11204-012-9153-0

Peel, M.C., Finlayson, B.L., McMahon, T.A., 2007. Updated world map of the Köppen-Geiger climate classification. Hydrol. Earth Syst. Sci. 11, 1633–1644.

Petschick, R., 2002. MacDiff 4.2.6 [WWW Document]. URL www.geol-pal.uni-frankfurt.de/Staff/Homepages/Petschick/PDFs/MacDiff Manual E.pdf

Petschick, R., Kuhn, G., Gingele, F.X., 1996. Clay mineral distribution in surface sediments of the South Atlantic: Sources transport and relation to oceanography. Mar. Geol. 130, 203–229.

Piper, D.Z., 1974. Rare Earth Elements in the sedimentary cycle: a summary. Chem. Geol. 14, 285–304.

Porrenga, D.H., 1966. Clay minerals in recent sediments of the niger delta. Clays Clay Miner. 14, 221–233.

Pryor, W.A., 1975. Biogenic Sedimentation and Alteration of Argillaceous Sediments in Shallow Marine Environments. Geol. Soc. Am. Bull. 86, 1244–1254.

Qu, T., 2000. Upper-Layer Circulation in the South China Sea. J. Phys. Oceanogr. 30, 1450–1460. doi:10.1175/1520-0485(2000)030<1450:ULCITS>2.0.CO;2

Qu, T., Girton, J.B., Whitehead, J.A., 2006. Deepwater overflow through Luzon Strait. J. Geophys. Res. 111, 11. doi:10.1029/2005JC003139

Qu, T., Kim, Y.Y., Yaremchuck, M., Tozzuka, T., Ishida, A., Yamagata, T., 2004. Can Luzon Strait transport play a role in conveying the impact of ENSO to the South China Sea? J. Clim. 17, 3644–3657.

Rieger, M.J., 1995. Quellen, Transport und Sedimentation lithogener Partikel im nördlichen Südchinesischen Meer. Diplomarbeit (german), Universität Hamburg.

Rollinson, H., 1993. Using geochemical data: evaluation, presentation, interpretation. Longman, Harlow, Essex, UK.

Sarnthein, M., Pflaumann, U., Wang, P., Wong, H.K., 1994. Preliminary report in Report in Sonne-95 Cruise "Monitor Monsoon" to the South China Sea. Kiel.

Satterberg, J., Arnarson, T.S., Lessard, E.J., Keil, R.G., 2003. Sorption of organic matter from four phytoplankton species to montmorillonite, chlorite and kaolinite in seawater. Mar. Chem. 81, 11–18. doi:10.1016/S0304-4203(02)00136-6

Scheffer, F., Schachtschabel, P., Blume, H.-P., Hartge, K.-H., Schwertmann, U., 1982. Lehrbuch der Bodenkunde, 11th ed. Enke Verlag, Stuttgart.

Schimanski, A., 2002. Holocene Sedimentation on the Vietnamese Shelf: From Source to Sink. Christian Albrechts Universität Kiel.

Schröder, A.C., Wiesner, M.G., Liu, Z., n.d. Fluxes of clay minerals in the South China Sea. Earth Planet. Sci. Lett.

Shaw, P., Chao, S.-Y., Liu, K.-K., Pai, S.-C., Liu, C.-T., 1996. Winter upwelling off Luzon in the northeastern South China Sea. J. Geophys. Res. 101, 16435–16448. doi:10.1029/96JC01064

Shaw, P.-T., Chao, S.-Y., 1994. Surface circulation in the South China Sea. Deep Sea Res. Part I 41, 1663–1683.

Siegel, D.A., Deuser, W.G., 1997. Trajectories of sinking particles in the Sargasso Sea : modeling of statistical funnels above deep-ocean sediment traps. Deep. Res. Part I 44, 1519–1541. doi:10.1016/S0967-0637(97)00028-9

Steinke, S., Hanebuth, T.J.J., Vogt, C., Stattegger, K., 2008. Sea level induced variations in clay mineral composition in the southwestern South China Sea over the past 17,000 yr. Mar. Geol. 250, 199–210. doi:10.1016/j.margeo.2008.01.005

Stichel, T., 2007. Die Provenanz von Schelfsedimenten in der Süd-China-See vor der südöstlichen Küste Vietnams anhand von Spurenelementen & Neodym-Isotopen. Diplomarbeit (german), Christian-Albrechts-Universität, Kiel.

Stosch, H.-G., 2000. Geochemie der seltenen Erden.

Syvitski, J.P.M., 1980. Flocculation, agglomeration and zooplankton pelletization of suspended sediment in a Fjord receiving glacial meltwater, in: Fjord Oceanography. pp. 615–623.

Tang, Z., Wang, Y., 1993. The distribution characteristics of clay minerals in the northern South China Sea. Acta Oceanol. Sin. Sin. 12, 145–157.

Thiry, M., 2000. Palaeoclimatic interpretation of clay minerals in marine deposits: an outlook from the continental origin. Earth-Science Rev. 49, 201–221.

Trentesaux, A., Liu, Z., Colin, C., Boulay, S., Wang, P., 2003. Data Report: Pleistocene paleaoclimatic cyclicity of southern China: Clay mineral evidence recorded in the South China Sea (ODP Site 1146). Proc. Ocean Drill. Program. 184, 10.

Velde, B., 1995. Composition and mineralogy of clay minerals, in: Origin and Mineralogy of Clays. Springer, New York, pp. 8–42.

Wan, S., Jian, Z., 2014. Deep water exchange between the South China Sea and the Pacific since the last glacial period. Paleoceanography 1162–1178. doi:10.1002/2013PA002578

Wang, G., Xie, S.-P., Qu, T., Huang, R.X., 2011. Deep South China Sea circulation. Geophys. Res. Lett. 38, 6. doi:10.1029/2010GL046626

Wang, H., Liu, Z., Sathiamurthy, E., Colin, C., Li, J., Zhao, Y., 2011. Chemical weathering in Malay Peninsula and North Borneo: clay mineralogy and element geochemistry of river surface sediments. Sci. China Ser. D 54, 272–282. doi:10.1007/s11430-010-4158-x

Wang, L., Sarntheim, M., Erlenkeuser, H., 1999. East Asian monsoon cli-mate during the Late Pleistocene: High-resolution sediment records from the South China Sea. Mar. Geol. 156, 245–284.

Wang, P., Li, Q., Zhong, G., Tian, J., Liu, Z., Li, J., Wang, R., Yu, K., Zhao, J., Huang, W., Sun, X., Zhao, Q., Jian, Z., Zhao, M., 2009. The South China Sea, 1st ed. Springer.

Wang, S.-H., Hsu, N.C., Tsay, S., Lin, N., Sayer, A.M., Huang, S.-J., Lau, W.K.M., 2012. Can Asian dust trigger phytoplankton blooms in the oligotrophic northern South China Sea? Geophys. Res. Lett. 39, 1–6. doi:10.1029/2011GL050415

Wang, S.-H., Tsay, S.-C., Lin, N.-H., Hsu, N.C., Bell, S.W., Li, C., Ji, Q., Jeong, M.-J., Hansell, R.A., Welton, E.J., Holben, B.N., Sheu, G.-R., Chu, Y.-C., Chang, S.-C., Liu, J.-J., Chiang, W.-L., 2011. First detailed observations of long-range transported dust over the northern South China Sea. Atmos. Environ. 45, 4804–4808. doi:10.1016/j.atmosenv.2011.04.077

Waniek, J.J., Koeve, W., Prien, R.D., 2000. Trajectories of sinking particles and the catchment areas above sediment traps in the northeast Atlantic. J. Mar. Res. 58, 983–1006.

Whitehouse, U.G., Jeffrey, L.M., Debbrecht, J.D., 1960. Differential settling tendencies of clay minerals in saline waters. Seventh Natl. Conf. Clays Clay Miner. 1–79.

Wiesner, M.G., Wang, Y., Zheng, L., 1995. Fallout of volcanic ash to the deep South China Sea induced by the 1991 eruption of Mount Pinatubo (Philippines). Geology 23, 885–888. doi:10.1130/0091-7613(1995)023<0885

Wiesner, M.G., Wetzel, A., Catane, S.G., Listanco, E.L., Mirabueno, H.T., 2004. Grain size, areal thickness distribution and controls on sedimentation of the 1991 Mount Pinatubo tephra layer in the South China Sea. Bull. Volcanol. 66, 226–242. doi:10.1007/s00445-003-0306-x

Wiesner, M.G., Zheng, L., Wong, H.K., Wang, Y., Chen, W., 1996. Fluxes of Particulate Matter in the South China Sea, in: Ittekkot, V., Schäfer, P., Honjo, S., Depetris, P.T. (Eds.), Particle Flux in the Ocean. John Wiley & Sons Ltd, pp. 293–312.

Xie, Q., Xiao, J., Wang, D., Yu, Y., 2013. Analysis of deep-layer and bottom circulations in the South China Sea based on eight quasi-global ocean model outputs. Chinese Sci. Bull. 58, 4000–4011. doi:10.1007/s11434-013-5791-5

Xu, K., Milliman, J.D., Li, A., Liu, P.J., Kao, S.-J., Wan, S., 2009. Yangtze- and Taiwan-derived sediments on the inner shelf of East China Sea. Cont. Shelf Res. 29, 2240–2256. doi:10.1016/j.csr.2009.08.017

Xu, Z.X., Takeuchi, K., Ishidaira, H., 2004. Correlation between El Nino – Southern (ENSO) and precipitation in South-east Asia. Hydrol. Process. 18, 107–123. doi:10.1002/hyp.1315

Xuan, T.T., 2014. Transport und Sedimentation lithogener Sinkstoffe im Gebiet des Vietnam- und Sunda-Auftriebs (Südchinesisches Meer). Diplomarbeit (german), Universität Hamburg.

Zaric, S., 2001. Saisonale und regionale Variabilität der Partikelflüsse während des El Nino Ereignisses 1998/1999 im Südchinesischen Meer. Diplomarbeit (german), Universität Hamburg.

Zhang, C., Wang, L., 2001. Multi-element geochemistry of sediments from the Pearl River system, China. Appl. Geochemistry 16, 1251–1259. doi:10.1016/S0883-2927(01)00007-5

Zhang, C., Wang, L., Li, G., Dong, S., Yang, J., Wang, X., 2002. Grain size effect on multi-element concentrations in sediments from the intertidal flats of Bohai Bay, China. Appl. Geochemistry 17, 59–68. doi:10.1016/S0883-2927(01)00079-8

Zhao, Y., Liu, Z., Colin, C., Paterne, M., Siani, G., Cheng, X., Duchamp-Alphonse, S., Xie, X., 2011. Variations of the Nile suspended discharges during the last 1.75Myr. Palaeogeogr. Palaeoclimatol. Palaeoecol. 311, 230–241. doi:10.1016/j.palaeo.2011.09.001

Zhou, W., Chan, J.C.L., 2007. ENSO and the South China Sea summer monsoon onset. Int. J. Climatol. 27, 157–167. doi:10.1002/joc

10. Appendices

10.1. Timing, bulk fluxes and main components

10.1.1. SCS-N

ID	sample	interval start	interval end	duration	total	lithogen	lithogen	<2µm
				[d]	[mg/m²/d]	[mg/m²/d]	[%]	[%]
528	N01 SH01	10.09.1987	25.09.1987	15	39.76	15.03	37.80	
529	N01 SH02	25.09.1987	10.10.1987	15	15.72	3.54	22.49	
530	N01 SH03	10.10.1987	25.10.1987	15	28.81	8.88	30.82	
531	N01 SH04	25.10.1987	09.11.1987	15	11.47	11.46	99.91	
532	N01 SH05	09.11.1987	24.11.1987	15	166.13	88.71	53.40	
533	N01 SH06	24.11.1987	09.12.1987	15	119.19	71.12	59.67	
534	N01 SH07	09.12.1987	24.12.1987	15	113.84	43.83	38.50	
535	N01 SH08	24.12.1987	08.01.1988	15	119.74	45.87	38.30	
536	N01 SH09	08.01.1988	23.01.1988	15	179.70	76.39	42.51	
537	N01 SH10	23.01.1988	07.02.1988	15	118.04	49.48	41.92	
538	N01 SH11	07.02.1988	22.02.1988	15	114.00	41.97	36.82	
539	N01 SH12	22.02.1988	08.03.1988	15	94.09	29.73	31.60	
540	N01 SH13	08.03.1988	23.03.1988	15	41.55	15.22	36.63	
541	N01 DP01	10.09.1987	25.09.1987	15	48.46	24.44	50.44	
542	N01 DP02	25.09.1987	10.10.1987	15	75.34	50.05	66.44	
543	N01 DP03	10.10.1987	25.10.1987	15	84.14	48.53	57.68	
544	N01 DP04	25.10.1987	09.11.1987	15	98.97	46.46	46.94	
545	N01 DP05	09.11.1987	24.11.1987	15	106.72	50.39	47.22	
546	N01 DP06	24.11.1987	09.12.1987	15	86.86	46.57	53.62	
547	N01 DP07	09.12.1987	24.12.1987	15	65.44	27.07	41.37	
548	N01 DP08	24.12.1987	08.01.1988	15	35.26	5.72	16.23	
549	N01 DP09	08.01.1988	23.01.1988	15	55.95	15.84	28.30	
550	N01 DP10	23.01.1988	07.02.1988	15	85.82	41.17	47.97	
551	N01 DP11	07.02.1988	22.02.1988	15	108.87	53.94	49.54	
552	N01 DP12	22.02.1988	08.03.1988	15	111.70	61.60	55.15	
553	N01 DP13	08.03.1988	23.03.1988	15	52.55	28.22	53.71	
554	N02 SH01	13.04.1988	27.04.1988	14	99.28	54.58	54.98	
555	N02 SH02	27.04.1988	12.05.1988	15	89.16	51.67	57.95	
556	N02 SH03	12.05.1988	27.05.1988	15	79.27	48.12	60.70	
557	N02 SH04	27.05.1988	11.06.1988	15	117.50	64.14	54.59	
558	N02 SH05	11.06.1988	25.06.1988	14	121.17	69.92	57.70	
559	N02 SH06	25.06.1988	10.07.1988	15	107.11	59.44	55.49	
560	N02 SH07	10.07.1988	25.07.1988	14	90.63	50.22	55.41	
561	N02 SH08	25.07.1988	09.08.1988	15	44.18	18.32	41.47	
562	N02 SH09	09.08.1988	23.08.1988	14	42.95	12.13	28.24	
563	N02 SH10	23.08.1988	07.09.1988	15	33.35	8.09	24.26	
564	N02 SH11	07.09.1988	22.09.1988	15	32.93	11.88	36.08	
565	N02 SH12	22.09.1988	07.10.1988	15	27.27	10.27	37.66	
566	N02 SH13	07.10.1988	21.10.1988	14	18.67	8.56	45.85	
567	N03 SH01	27.06.2009	13.07.2009	16	73.44	16.02	21.82	
568	N03 SH02	13.07.2009	29.07.2009	16	82.52	15.57	18.86	
569	N03 SH03	29.07.2009	14.08.2009	16	90.87	22.41	24.67	
570	N03 SH04	14.08.2009	30.08.2009	16	97.22	12.95	13.32	
571	N03 SH05	30.08.2009	15.09.2009	16	45.37	6.45	14.21	
572	N03 SH06	15.09.2009	01.10.2009	16	56.86	12.00	21.10	
573	N03 SH07	01.10.2009	17.10.2009	16	75.55	9.39	12.43	
574	N03 SH08	17.10.2009	02.11.2009	16	102.88	21.67	21.06	
575	N03 SH09	02.11.2009	18.11.2009	16	202.30	62.66	30.97	
576	N03 SH10	18.11.2009	04.12.2009	16	280.64	125.34	44.66	
577	N03 SH11	04.12.2009	20.12.2009	16	294.74	54.51	18.49	
578	N03 SH12	20.12.2009	05.01.2010	16	181.86	59.73	32.84	

ID	sample	interval start	interval end	duration [d]	total [mg/m²/d]	lithogen [mg/m²/d]	lithogen [%]	<2µm [%]
579	N03 SH13	05.01.2010	21.01.2010	16	56.90	14.68	25.79	
580	N03 SH14	21.01.2010	06.02.2010	16	149.45	13.52	9.04	
581	N03 SH15	06.02.2010	22.02.2010	16	146.32	24.51	16.75	
582	N03 SH16	22.02.2010	10.03.2010	16	114.81	26.40	23.00	
583	N03 SH17	10.03.2010	26.03.2010	16	50.12	18.64	37.19	
584	N03 SH18	26.03.2010	11.04.2010	16	271.24	118.97	43.86	
585	N03 SH19	11.04.2010	27.04.2010	16	180.30	61.78	34.27	
586	N03 SH20	27.04.2010	13.05.2010	16	162.07	46.07	28.42	
587	N03 MD01	27.06.2009	13.07.2009	16	88.89	25.63	28.83	
588	N03 MD02	13.07.2009	29.07.2009	16	89.99	25.27	28.08	
589	N03 MD03	29.07.2009	14.08.2009	16	99.05	25.55	25.79	
590	N03 MD04	14.08.2009	30.08.2009	16	111.54	20.69	18.55	
591	N03 MD05	30.08.2009	15.09.2009	16	81.51	21.54	26.43	
592	N03 MD06	15.09.2009	01.10.2009	16	75.95	17.52	23.06	
593	N03 MD07	01.10.2009	17.10.2009	16	85.06	15.11	17.77	
594	N03 MD08	17.10.2009	02.11.2009	16	29.37	7.66	26.10	
595	N03 MD09	02.11.2009	18.11.2009	16	196.24	52.93	26.97	
596	N03 MD10	18.11.2009	04.12.2009	16	200.09	73.46	36.71	
597	N03 MD11	04.12.2009	20.12.2009	16	297.63	100.25	33.68	
598	N03 MD12	20.12.2009	05.01.2010	16	245.66	94.04	38.28	
599	N03 MD13	05.01.2010	21.01.2010	16	157.98	54.19	34.30	
600	N03 MD14	21.01.2010	06.02.2010	16	200.77	54.86	27.33	
601	N03 MD15	06.02.2010	22.02.2010	16	187.96	55.65	29.61	
602	N03 MD16	22.02.2010	10.03.2010	16	191.78	69.53	36.26	
603	N03 MD17	10.03.2010	26.03.2010	16	159.04	56.69	35.65	
604	N03 MD18	26.03.2010	11.04.2010	16	227.75	99.82	43.83	
605	N03 MD19	11.04.2010	27.04.2010	16	152.52	69.19	45.36	
606	N03 MD20	27.04.2010	13.05.2010	16	94.21	36.80	39.06	
607	N03 DP01	27.06.2009	13.07.2009	16	3.70	0.66	17.76	
608	N03 DP02	13.07.2009	29.07.2009	16	97.60	31.89	32.67	
609	N03 DP03	29.07.2009	14.08.2009	16	90.24	29.04	32.18	
610	N03 DP04	14.08.2009	30.08.2009	16	90.68	29.62	32.67	
611	N03 DP05	30.08.2009	15.09.2009	16	95.04	27.47	28.91	
612	N03 DP06	15.09.2009	01.10.2009	16	89.10	27.63	31.01	
613	N03 DP07	01.10.2009	17.10.2009	16	76.42	21.41	28.02	
614	N03 DP08	17.10.2009	02.11.2009	16	87.40	25.87	29.60	
615	N03 DP09	02.11.2009	18.11.2009	16	87.85	20.44	23.27	
616	N03 DP10	18.11.2009	04.12.2009	16	121.18	44.46	36.69	
617	N03 DP11	04.12.2009	20.12.2009	16	158.18	58.62	37.06	
618	N03 DP12	20.12.2009	05.01.2010	16	218.05	71.42	32.76	
618	N03 DP12	20.12.2009	05.01.2010	16	218.05	71.42	32.76	
619	N03 DP13	05.01.2010	21.01.2010	16	183.17	69.92	38.17	
620	N03 DP14	21.01.2010	06.02.2010	16	190.05	75.34	39.64	
621	N03 DP15	06.02.2010	22.02.2010	16	197.09	59.74	30.31	
622	N03 DP16	22.02.2010	10.03.2010	16	179.77	66.33	36.90	
623	N03 DP17	10.03.2010	26.03.2010	16	175.35	66.57	37.96	
624	N03 DP18	26.03.2010	11.04.2010	16	149.02	58.74	39.42	
625	N03 DP19	11.04.2010	27.04.2010	16	151.13	57.66	38.16	
626	N03 DP20	27.04.2010	13.05.2010	16	102.97	42.38	41.16	
627	N04 SH01	20.05.2011	05.06.2011	16	105.29	27.49	26.11	
628	N04 SH02	05.06.2011	21.06.2011	16	135.16	43.28	32.02	
629	N04 SH03	21.06.2011	07.07.2011	16	84.04	20.73	24.66	
630	N04 SH04	07.07.2011	23.07.2011	16	46.59	13.62	29.23	
631	N04 SH05	23.07.2011	08.08.2011	16	77.50	12.16	15.70	
632	N04 SH06	08.08.2011	24.08.2011	16	82.39	18.90	22.94	
633	N04 SH07	24.08.2011	09.09.2011	16	52.23	11.33	21.69	
634	N04 SH08	09.09.2011	25.09.2011	16	30.88	4.97	16.09	

Changes of clay mineral and trace element characteristics in the Deep South China Sea

ID	sample	interval start	interval end	duration	total	lithogen	lithogen	<2µm
				[d]	[mg/m²/d]	[mg/m²/d]	[%]	[%]
635	N04 SH09	25.09.2011	11.10.2011	16	138.32	62.82	45.42	
636	N04 SH10	11.10.2011	27.10.2011	16	150.40	38.28	25.45	
637	N04 SH11	27.10.2011	12.11.2011	16	161.57	44.81	27.73	
638	N04 SH12	12.11.2011	28.11.2011	16	250.14	64.22	25.67	
639	N04 SH13	28.11.2011	14.12.2011	16	109.96	21.47	19.52	
640	N04 SH14	14.12.2011	30.12.2011	16	190.92	18.73	9.81	
641	N04 SH15	30.12.2011	15.01.2012	16	195.72	38.90	19.88	
642	N04 SH16	15.01.2012	31.01.2012	16	297.36	101.68	34.20	
643	N04 SH17	31.01.2012	16.02.2012	16	109.88	27.61	25.13	
644	N04 SH18	16.02.2012	03.03.2012	16	134.01	33.33	24.87	
645	N04 SH19	03.03.2012	19.03.2012	16	159.43	47.36	29.71	
646	N04 SH20	19.03.2012	04.04.2012	16	178.66	68.25	38.20	
647	N04 MD01	20.05.2011	05.06.2011	16	147.98	47.82	32.31	
648	N04 MD02	05.06.2011	21.06.2011	16	177.90	62.30	35.02	
649	N04 MD03	21.06.2011	07.07.2011	16	139.75	52.78	37.77	
650	N04 MD04	07.07.2011	23.07.2011	16	71.90	29.29	40.74	
651	N04 MD05	23.07.2011	08.08.2011	16	105.22	30.56	29.04	
652	N04 MD06	08.08.2011	24.08.2011	16	83.99	28.68	34.15	
653	N04 MD07	24.08.2011	09.09.2011	16	101.32	34.12	33.68	
654	N04 MD08	09.09.2011	25.09.2011	16	96.32	33.45	34.73	
655	N04 MD09	25.09.2011	11.10.2011	16	118.31	46.40	39.22	
656	N04 MD10	11.10.2011	27.10.2011	16	260.96	85.19	32.65	
657	N04 MD11	27.10.2011	12.11.2011	16	129.34	53.83	41.62	
658	N04 MD12	12.11.2011	28.11.2011	16	175.71	61.28	34.88	
659	N04 MD13	28.11.2011	14.12.2011	16	165.23	51.56	31.20	
660	N04 MD14	14.12.2011	30.12.2011	16	196.80	46.85	23.81	
661	N04 MD15	30.12.2011	15.01.2012	16	164.44	46.58	28.32	
662	N04 MD16	15.01.2012	31.01.2012	16	180.93	57.50	31.78	
663	N04 MD17	31.01.2012	16.02.2012	16	299.91	108.03	36.02	
664	N04 MD18	16.02.2012	03.03.2012	16	200.92	68.20	33.94	
665	N04 MD19	03.03.2012	19.03.2012	16	134.53	50.54	37.57	
666	N04 MD20	19.03.2012	04.04.2012	16	135.68	52.30	38.55	
667	N04 DP-01	20.05.2011	05.06.2011	16	110.74	35.43	32.00	
668	N04 DP-02	05.06.2011	21.06.2011	16	134.79	47.75	35.42	
669	N04 DP-03	21.06.2011	07.07.2011	16	125.62	52.32	41.65	
670	N04 DP-04	07.07.2011	23.07.2011	16	87.39	33.01	37.77	
671	N04 DP-05	23.07.2011	08.08.2011	16	110.00	33.91	30.83	
672	N04 DP-06	08.08.2011	24.08.2011	16	66.04	19.79	29.97	
673	N04 DP-07	24.08.2011	09.09.2011	16	83.15	30.42	36.58	
674	N04 DP-08	09.09.2011	25.09.2011	16	84.41	29.17	34.56	
675	N04 DP-09	25.09.2011	11.10.2011	16	92.59	36.93	39.88	
676	N04 DP-10	11.10.2011	27.10.2011	16	165.41	53.08	32.09	
677	N04 DP-11	27.10.2011	12.11.2011	16	69.52	20.82	29.95	
678	N04 DP-12	12.11.2011	28.11.2011	16	150.42	57.87	38.48	
679	N04 DP-13	28.11.2011	14.12.2011	16	143.90	46.03	31.99	
680	N04 DP-14	14.12.2011	30.12.2011	16	151.39	35.65	23.55	
681	N04 DP-15	30.12.2011	15.01.2012	16	150.73	46.40	30.79	
682	N04 DP-16	15.01.2012	31.01.2012	16	160.55	45.67	28.44	
683	N04 DP-17	31.01.2012	16.02.2012	16	221.30	63.02	28.48	
684	N04 DP-18	16.02.2012	03.03.2012	16	163.19	52.92	32.43	
685	N04 DP-19	03.03.2012	19.03.2012	16	150.47	44.36	29.48	
686	N04 DP-20	19.03.2012	04.04.2012	16	168.06	23.09	13.74	

10.1.2. SCS-NE

ID	sample	interval start	interval end	duration	total	lithogen	organic	CaCO3	opal	lithogen	<2μm
				[d]	[mg/m²/d]		[%]	[%]	[%]	[%]	[%]
27	NE01 SH01	08.07.1998	26.07.1998	19	118.59	56.76	10.39	26.28	15.47	47.87	
28	NE01 SH02	27.07.1998	23.08.1998	28	69.10	30.13	11.75	27.59	17.06	43.60	
29	NE01 SH03	24.08.1998	20.09.1998	28	68.47	25.76	10.53	34.83	17.02	37.63	
30	NE01 SH04	21.09.1998	18.10.1998	28	191.18	101.18	7.21	22.37	17.50	52.93	
31	NE01 SH05	19.10.1998	15.11.1998	28	87.11	30.23	8.43	37.13	19.74	34.70	
32	NE01 SH06	16.11.1998	13.12.1998	28	35.65	13.46	9.96	32.12	20.18	37.75	
33	NE01 SH07	14.12.1998	10.01.1999	28	106.34	28.43	8.97	41.00	23.30	26.73	
34	NE01 SH08	11.01.1999	07.02.1999	28	99.59	24.66	8.38	39.59	27.27	24.76	
35	NE01 SH09	08.02.1999	07.03.1999	28	105.54	44.02	8.07	26.73	23.48	41.71	
36	NE01 SH10	08.03.1999	04.04.1999	28	119.53	53.72	9.18	24.29	21.58	44.95	
37	NE01 SH11	05.04.1999	30.04.1999	26	83.91	34.53	9.31	27.49	22.05	41.15	
38	NE01 MD01	08.07.1998	26.07.1998	19	95.18	42.32	7.02	30.94	17.58	44.47	
39	NE01 MD02	27.07.1998	23.08.1998	28	96.69	39.63	7.15	33.07	18.80	40.98	
40	NE01 MD03	24.08.1998	20.09.1998	28	82.40	32.86	8.04	32.10	19.99	39.88	
41	NE01 MD04	21.09.1998	18.10.1998	28	193.25	100.70	6.31	21.69	19.89	52.11	
42	NE01 MD05	19.10.1998	15.11.1998	28	136.25	53.06	6.76	34.04	20.26	38.94	
43	NE01 MD06	16.11.1998	13.12.1998	28	70.93	27.03	8.22	29.52	24.15	38.11	
44	NE01 MD07	14.12.1998	10.01.1999	28	116.47	31.32	7.61	43.22	22.28	26.89	
45	NE01 MD08	11.01.1999	07.02.1999	28	151.35	38.52	6.79	35.95	31.81	25.45	
46	NE01 MD09	08.02.1999	07.03.1999	28	179.67	90.61	5.38	23.38	20.81	50.43	
47	NE01 MD10	08.03.1999	04.04.1999	28	159.30	68.57	6.33	26.06	24.57	43.05	
48	NE01 MD11	05.04.1999	30.04.1999	26	47.12	17.95	5.80	37.29	18.81	38.10	
49	NE01 DP01	08.07.1998	26.07.1998	19	107.66	52.17	5.49	30.30	15.74	48.46	
50	NE01 DP02	27.07.1998	23.08.1998	28	64.48	35.66	7.63	17.30	19.77	55.30	
51	NE01 DP03	24.08.1998	20.09.1998	28	84.81	43.97	7.86	22.46	17.84	51.84	
52	NE01 DP04	21.09.1998	18.10.1998	28	193.75	104.70	6.20	23.25	16.51	54.04	
53	NE01 DP05	19.10.1998	15.11.1998	28	84.20	43.24	7.51	23.16	17.97	51.36	
54	NE01 DP06	16.11.1998	13.12.1998	28	87.18	39.42	6.50	29.56	18.72	45.21	
55	NE01 DP07	14.12.1998	10.01.1999	28	129.11	43.05	5.68	43.68	17.30	33.34	
56	NE01 DP08	11.01.1999	07.02.1999	28	179.05	57.31	5.26	37.18	25.55	32.01	
57	NE01 DP09	08.02.1999	07.03.1999	28	199.09	100.53	5.02	23.39	21.09	50.49	
58	NE01 DP10	08.03.1999	04.04.1999	28	130.88	65.79	5.83	22.82	21.08	50.27	
59	NE01 DP11	05.04.1999	30.04.1999	26	112.09	53.88	5.12	26.07	20.74	48.07	
60	NE02 SH01	15.05.1999	11.06.1999	28	148.25	33.21	0.00	33.61	36.95	22.40	
61	NE02 SH02	12.06.1999	09.07.1999	28	112.40	23.39	0.00	33.34	38.57	20.81	
62	NE02 SH03	10.07.1999	06.08.1999	28	122.24	26.91	0.00	32.94	37.43	22.02	
63	NE02 SH04	07.08.1999	03.09.1999	28	158.42	47.65	0.00	24.57	38.95	30.08	
64	NE02 SH05	04.09.1999	01.10.1999	28	89.83	22.37	0.00	28.45	39.89	24.90	
65	NE02 SH06	02.10.1999	29.10.1999	28	125.77	14.80	0.00	33.05	48.02	11.77	
66	NE02 SH07	30.10.1999	26.11.1999	28	127.14	10.57	0.00	34.87	49.03	8.32	
67	NE02 SH08	27.11.1999	24.12.1999	28	57.67	4.63	0.00	44.49	40.34	8.04	
68	NE03 DP01	15.05.1999	11.06.1999	28	68.79	22.77	0.00	23.36	39.51	33.09	
69	NE03 DP02	12.06.1999	09.07.1999	28	125.41	34.55	0.00	34.97	32.79	27.55	
70	NE03 DP03	10.07.1999	06.08.1999	28	87.66	26.49	0.00	26.35	38.34	30.22	
71	NE03 DP04	07.08.1999	03.09.1999	28	117.84	28.95	0.00	34.10	35.94	24.56	
72	NE03 DP05	04.09.1999	01.10.1999	28	119.51	36.66	0.00	24.05	38.89	30.68	
73	NE03 DP06	02.10.1999	29.10.1999	28	120.06	47.82	0.00	20.34	34.81	39.83	
74	NE03 DP07	30.10.1999	26.11.1999	28	102.15	26.03	0.00	28.79	39.96	25.48	
75	NE03 DP08	27.11.1999	24.12.1999	28	176.22	31.46	0.00	25.37	50.67	17.85	
76	NE03 DP09	25.12.1999	21.01.2000	28	194.53	28.71	0.00	29.86	48.14	14.76	
77	NE03 DP10	22.01.2000	18.02.2000	28	118.64	13.30	0.00	34.20	47.34	11.21	
78	NE03 DP11	19.02.2000	17.03.2000	28	120.98	4.90	0.00	42.39	46.75	4.05	
79	NE03 DP12	18.03.2000	14.04.2000	28	82.48	15.90	0.00	34.62	40.33	19.28	
80	NE03 DP13	15.04.2000	13.05.2000	28	116.15	33.48	0.00	27.59	38.17	28.82	

10.1.3. SCS-NC

ID	sample	interval start	interval end	duration	total	lithogen	organic	CaCO3	opal	lithogen	<2µm
				[d]	[mg/m²/d]	[mg/m²/d]	[%]	[%]	[%]	[%]	[%]
1	NC01 SH01	10.12.1996	05.01.1997	26	141.33	16.03	10.36	28.61	49.69	11.34	4.67
2	NC01 SH02	06.01.1997	01.02.1997	26	183.02	19.92	11.45	33.26	44.41	10.88	18.25
3	NC01 SH03	02.02.1997	28.02.1997	26	71.31	16.26	11.51	39.59	26.11	22.80	17.45
4	NC01 SH04	01.03.1997	27.03.1997	26	62.17	15.84	10.75	40.69	23.09	25.47	30.04
5	NC01 SH05	28.03.1997	23.04.1997	26	87.54	20.95	10.19	39.72	26.16	23.93	24.41
6	NC01 SH06	24.04.1997	20.05.1997	26	89.82	24.71	10.87	37.27	24.35	27.51	26.16
7	NC01 SH07	21.05.1997	16.06.1997	26	80.10	25.03	11.45	36.80	20.51	31.24	21.58
8	NC01 SH08	17.06.1997	14.07.1997	26	61.59	17.02	8.51	43.62	20.24	27.63	21.27
9	NC01 SH09	15.07.1997	10.08.1997	26	55.89	16.10	11.13	38.62	21.45	28.80	19.30
10	NC01 SH10	11.08.1997	06.09.1997	26	81.60	17.66	8.46	52.82	17.08	21.64	18.61
11	NC01 SH11	07.09.1997	03.10.1997	26	48.32	14.29	11.27	42.34	16.82	29.56	8.34
12	NC01 SH12	04.10.1997	30.10.1997	26	38.86	9.48	7.17	56.60	11.83	24.40	
13	NC01 SH13	31.10.1997	26.11.1998	26	86.19	30.06	11.41	42.34	11.37	34.88	
14	NC01 DP01	10.12.1996	05.01.1997	26	89.59	18.04	8.30	35.42	36.14	20.14	12.99
15	NC01 DP02	06.01.1997	01.02.1997	26	225.07	39.40	9.43	33.57	39.49	17.51	18.69
16	NC01 DP03	02.02.1997	28.02.1997	26	103.28	32.05	7.97	32.94	28.07	31.03	21.52
17	NC01 DP04	01.03.1997	27.03.1997	26	78.30	25.16	7.92	36.07	23.89	32.13	21.74
18	NC01 DP05	28.03.1997	20.05.1997	26	158.49	46.70	7.89	32.69	29.96	29.47	25.81
19	NC01 DP06	21.05.1997	16.06.1997	26	68.31	23.70	8.44	28.74	28.12	34.70	23.86
20	NC01 DP07	17.06.1997	14.07.1997	26	79.90	25.05	7.78	33.28	27.59	31.36	24.16
21	NC01 DP08	15.07.1997	10.08.1997	26	72.52	25.59	6.99	34.52	23.20	35.29	22.38
22	NC01 DP09	11.08.1997	06.09.1997	26	84.27	23.45	6.27	49.26	16.64	27.83	13.60
23	NC01 DP10	07.09.1997	03.10.1997	26	51.81	17.42	7.18	34.86	24.33	33.62	21.79
24	NC01 DP11	04.10.1997	30.10.1997	26	50.23	17.93	7.70	34.63	21.98	35.70	20.93
25	NC01 DP12	31.10.1997	26.11.1997	26	67.81	17.67	5.23	56.35	12.37	26.06	
26	NC01 DP13	27.11.1997			75.25	14.53	4.77	66.35	9.57	19.31	

10.1.4. SCS-C

ID	sample	interval start	interval end	duration	total	lithogen	organic	CaCO3	opal	lithogen	<2µm
				[d]	[mg/m²/d]	[mg/m²/d]	[%]	[%]	[%]	[%]	[%]
81	C01 SH01	01.12.1990	29.01.1991	59	91.41	17.55	7.50	50.44	22.80	19.20	
82	C01 SH02	29.01.1991	26.03.1991	56	22.86	4.67	10.67	48.95	19.86	20.43	
83	C01 SH03	26.03.1991	21.05.1991	56	22.21	4.62	9.37	71.63	16.07	20.80	
84	C01 SH04	21.05.1991	open		331040.50		0.00	0.00	0.00	0.00	
85	C01 DP01	29.12.1990	29.01.1991	31	90.07	16.76	6.49	46.47	28.41	18.61	
86	C01 DP02	29.01.1991	26.02.1991	28	96.31	17.41	5.78	53.56	22.57	18.08	
87	C01 DP03	26.02.1991	26.03.1991	28	73.66	18.73	6.41	39.90	28.27	25.43	
88	C01 DP04	26.03.1991	23.04.1991	28	65.91	21.40	8.12	29.98	29.42	32.47	
89	C01 DP05	23.04.1991	21.05.1991	28	132.00	36.60	5.23	46.94	20.10	27.73	
90	C01 DP06	21.05.1991	18.06.1991	28	15133.91		0.00	0.00	0.00	0.00	
91	C01 DP07	18.06.1991	16.07.1991	28	16767.34		0.00	0.00	0.00	0.00	
92	C01 DP08	16.07.1991	13.08.1991	28	17575.00		0.00		0.00	0.00	
93	C01 DP09	13.08.1991	10.09.1991	28	17593.22		0.00		0.00	0.00	
94	C01 DP10	10.09.1991	08.10.1991	28	17929.91		0.00		0.00	0.00	
95	C01 DP11	08.10.1991	05.11.1991	28	18198.62		0.00		0.00	0.00	
96	C01 DP12	05.11.1991	03.12.1991	28	17461.42		0.00		0.00	0.00	
97	C01 DP13	03.12.1991									
98	C02 SH01	20.03.1992	20.04.1992	31	73.27	21.81	9.17	31.84	29.22	29.77	
99	C02 SH02	21.04.1992	22.05.1992	31	76.35	21.51	8.37	35.76	27.69	28.17	
100	C02 SH03	23.05.1992	23.06.1992	31	73.72	17.12	8.16	40.11	28.50	23.22	
101	C02 SH04	24.06.1992	25.07.1992	31	168.66	34.94	11.70	30.25	37.34	20.72	
102	C02 SH05	26.07.1992	26.08.1992	31	63.71	13.59	7.15	41.90	29.62	21.33	
103	C02 SH06	27.08.1992	27.09.1992	31	93.73	19.96	8.83	44.67	25.21	21.30	
104	C02 SH07	28.09.1992	29.10.1992	31	68.04	13.71	8.24	46.17	25.44	20.15	

ID	sample	interval start	interval end	duration	total	lithogen	organic	CaCO3	opal	lithogen	<2μm
				[d]	[mg/m²/d]	[mg/m²/d]	[%]	[%]	[%]	[%]	[%]
105	C02 SH08	30.10.1992	30.11.1992	31	90.70	9.89	10.16	34.24	44.69	10.90	
106	C02 SH09	01.12.1992	01.01.1993	31	64.79	10.19	9.08	44.82	30.37	15.73	
107	C02 SH10	02.01.1993	02.02.1993	31	64.06	13.34	10.94	36.99	31.24	20.83	
108	C02 SH11	03.02.1993	06.03.1993	31	89.62	17.34	8.66	37.92	33.97	19.35	
109	C02 SH12	07.03.1993	07.04.1993	31	37.44	9.42	9.21	35.17	30.47	25.16	
110	C02 SH13	08.04.1993	09.05.1993	31	72.36	14.58	10.27	39.98	29.60	20.15	
111	C02 DP01	20.03.1992	20.04.1992	31	153.55	80.27	3.74	13.28	30.70	52.28	
112	C02 DP02	21.04.1992	22.05.1992	31	156.37	76.32	3.04	15.23	32.93	48.81	
113	C02 DP03	23.05.1992	23.06.1992	31	153.44	76.56	3.21	18.17	28.72	49.89	
114	C02 DP04	24.06.1992	25.07.1992	31	122.94	50.47	5.90	14.60	38.45	41.05	
115	C02 DP05	26.07.1992	26.08.1992	31	1.65	0.76	11.98	14.99	27.29	46.08	
116	C02 DP06	27.08.1992	27.09.1992	31	1.17		6.81	9.54	0.00	0.00	
117	C02 DP07	28.09.1992	29.10.1992	31	0.72	0.63	3.38	3.56	5.58	87.93	
118	C02 DP08	30.10.1992	30.11.1992	31	0.79	0.62	5.44	8.79	6.34	78.67	
119	C02 DP09	01.12.1992	01.01.1993	31	0.90	0.64	9.90	10.86	8.85	70.79	
120	C02 DP10	02.01.1993	02.02.1993	31	0.64		7.58	29.21	0.00	0.00	
121	C02 DP11	03.02.1993	06.03.1993	31	0.40		0.00	0.00	0.00	0.00	
122	C02 DP12	07.03.1993	07.04.1993	31	0.50		5.19	5.51	0.00	0.00	
123	C02 DP13	08.04.1993	09.05.1993	31	0.45	0.35	5.18	5.62	13.25	77.29	
124	C03 SH01	01.06.1993	28.06.1993	27	85.87	19.42	8.27	46.01	23.11	22.61	
125	C03 SH02	29.06.1993	26.07.1993	27	98.51	13.70	8.54	57.50	20.06	13.91	
126	C03 SH03	27.07.1993	23.08.1993	27	90.66	13.16	9.26	54.22	22.01	14.52	
127	C03 SH04	24.08.1993	20.09.1993	27	66.83	15.93	8.39	47.94	19.84	23.83	
128	C03 SH05	21.09.1993	18.10.1993	27	50.63	14.10	7.74	47.34	17.07	27.85	
129	C03 SH06	19.10.1993	15.11.1993	27	114.98	27.92	6.76	51.78	17.18	24.28	
130	C03 SH07	16.11.1993	13.12.1993	27	114.74	36.07	7.52	45.78	15.27	31.43	
131	C03 SH08	14.12.1993	10.01.1994	27	111.92	37.07	8.79	40.35	17.74	33.12	
132	C03 SH09	11.01.1994	07.02.1994	27	112.31	29.52	9.04	42.16	22.51	26.29	
133	C03 SH10	08.02.1994	07.03.1994	27	75.06	20.79	10.44	37.28	24.58	27.70	
134	C03 SH11	08.03.1994	04.04.1994	27	91.18	20.91	7.87	45.04	24.16	22.93	
135	C03 SH12	05.04.1994	02.05.1994	27	62.32	11.53	7.31	53.81	20.38	18.50	
136	C03 SH13	03.05.1994	31.05.1994	28	35.02	10.98	9.46	37.19	22.00	31.36	
137	C03 DP01										
138	C03 DP02										
139	C03 DP03	01.06.1993	26.07.1993	56	98.19	26.03	2.78	48.28	22.43	26.50	
139	C03 DP03	01.06.1993	26.07.1993	56	98.19	26.03	2.78	48.28	22.43	26.50	
140	C03 DP04	27.07.1993	23.08.1993	27	100.68	15.43	1.61	58.82	24.24	15.33	
141	C03 DP05	24.08.1993	20.09.1993	27	76.37	28.10	5.33	29.00	28.87	36.79	
142	C03 DP06	21.09.1993	18.10.1993	27	59.29	24.88	5.28	24.16	28.59	41.97	
143	C03 DP07	19.10.1993	15.11.1993	27	60.04	22.26	4.95	31.84	26.14	37.07	
144	C03 DP08	16.11.1993	13.12.1993	27	81.72	29.82	4.98	33.29	25.23	36.49	
145	C03 DP09	14.12.1993	10.01.1994	27	85.67	37.08	5.38	28.98	22.35	43.29	
145	C03 DP09	14.12.1993	10.01.1994	27	85.67	37.08	5.38	28.98	22.35	43.29	
146	C03 DP10	11.01.1994	07.02.1994	27	93.55	34.29	5.95	30.88	26.52	36.66	
147	C03 DP11	08.02.1994	07.03.1994	27	90.68	33.79	6.17	25.97	30.59	37.27	
148	C03 DP12	08.03.1994	04.04.1994	27	79.25	26.00	5.92	30.93	30.34	32.81	
149	C03 DP13	05.04.1994	02.05.1994	27	69.30	22.71	7.41	29.72	30.10	32.78	
150	C04 SH01	29.06.1994	26.07.1994	27	59.78	9.77	9.21	46.86	27.58	16.35	
151	C04 SH02	27.07.1994	23.08.1994	27	35.18	7.49	8.15	51.76	18.79	21.30	
152	C04 SH03	24.08.1994	20.09.1994	27	206.79	45.56	10.22	35.73	32.01	22.03	
153	C04 SH04	21.09.1994	18.10.1994	27	83.27	17.43	7.04	46.25	25.77	20.93	
154	C04 SH05	19.10.1994	15.11.1994	27	82.04	13.52	6.17	50.50	26.85	16.48	
155	C04 SH06	16.11.1994	13.12.1994	27	137.08	23.93	7.40	38.77	36.37	17.46	
156	C04 SH07	14.12.1994	10.01.1995	27	112.73	13.79	6.92	30.97	49.88	12.23	
157	C04 SH08	11.01.1995	07.02.1995	27	99.74	13.44	8.29	34.74	43.50	13.47	
158	C04 SH09	08.02.1995	07.03.1995	27	96.38	18.90	11.70	34.40	34.29	19.61	
159	C04 SH10	08.03.1995	04.04.1995	27	30.48	7.13	11.82	35.90	28.90	23.39	

Changes of clay mineral and trace element characteristics in the Deep South China Sea

ID	sample	interval start	interval end	duration	total	lithogen	organic	CaCO3	opal	lithogen	<2μm
				[d]	[mg/m²/d]	[mg/m²/d]	[%]	[%]	[%]	[%]	[%]
160	C04 SH11	05.04.1995	02.05.1995	27	63.82	13.30	12.43	38.22	28.51	20.84	
161	C04 MD01	01.06.1994	28.06.1994	27	71.12	12.82	8.58	48.54	24.85	18.03	
162	C04 MD02	29.06.1994	26.07.1994	27	65.60	12.41	7.21	43.75	30.13	18.91	
163	C04 MD03	27.07.1994	23.08.1994	27	79.85	16.02	7.39	44.73	27.82	20.06	
164	C04 MD04	24.08.1994	20.09.1994	27	135.40	35.34	9.50	33.90	30.50	26.10	
165	C04 MD05	21.09.1994	18.10.1994	27	95.23	30.04	6.99	32.99	28.48	31.55	
165	C04 MD05	21.09.1994	18.10.1994	27	95.23	30.04	6.99	32.99	28.48	31.55	
166	C04 MD06	19.10.1994	15.11.1994	27	88.20	28.44	7.38	39.28	21.09	32.25	
167	C04 MD07	16.11.1994	13.12.1994	27	109.74	19.05	6.43	36.11	40.10	17.36	
168	C04 MD08	14.12.1994	10.01.1995	27	106.34	21.82	5.99	33.96	39.52	20.52	
169	C04 MD09	11.01.1995	07.02.1995	27	102.63	18.75	6.12	36.60	39.01	18.27	
170	C04 MD10	08.02.1995	07.03.1995	27	79.78	15.60	6.98	33.30	40.17	19.55	
171	C04 MD11	08.03.1995	04.04.1995	27	62.43	14.83	6.94	32.10	37.20	23.76	
172	C04 MD12	05.04.1995	02.05.1995	27	50.08	8.47	7.67	32.96	42.47	16.91	
173	C04 DP01	01.06.1994	28.06.1994	27	52.28	14.34	5.70	41.91	24.95	27.43	
174	C04 DP02	29.06.1994	26.07.1994	27	61.67	17.90	6.35	33.66	30.96	29.03	
175	C04 DP03	27.07.1994	23.08.1994	27	77.34	19.26	4.50	47.13	23.47	24.90	
176	C04 DP04	24.08.1994	20.09.1994	27	107.14	26.12	8.02	32.83	34.77	24.38	
177	C04 DP05	21.09.1994	18.10.1994	27	77.49	23.37	5.97	32.36	31.51	30.16	
178	C04 DP06	19.10.1994	15.11.1994	27	76.51	24.04	6.02	33.61	28.96	31.42	
179	C04 DP07	16.11.1994	13.12.1994	27	53.23	12.88	8.36	32.82	34.62	24.20	
180	C04 DP08	14.12.1994	10.01.1995	27	73.35	19.20	5.92	31.36	36.55	26.17	
181	C04 DP09	11.01.1995	07.02.1995	27	90.26	20.13	5.28	30.11	42.31	22.30	
181	C04 DP09	11.01.1995	07.02.1995	27	90.26	20.13	5.28	30.11	42.31	22.30	
182	C04 DP10	08.02.1995	07.03.1995	27	85.66	22.80	5.33	26.90	41.15	26.61	
183	C04 DP11	08.03.1995	04.04.1995	27	61.54	17.96	5.71	25.27	39.83	29.19	
184	C04 DP12	05.04.1995	02.05.1995	27	16.09	4.35	7.81	25.74	39.41	27.04	
185	C05 SH01	01.06.1995	30.06.1995	29	52.94	11.70	9.63	34.29	33.98	22.10	
186	C05 SH02	01.07.1995	30.07.1995	29	72.14	18.81	9.53	36.17	28.22	26.08	
187	C05 SH03	31.07.1995	29.08.1995	29	57.40	15.88	9.75	30.93	31.67	27.66	
188	C05 SH04	30.08.1995	28.09.1995	29	48.65	15.04	9.82	24.80	34.47	30.91	
189	C05 SH05	29.09.1995	28.10.1995	29	41.16	10.42	8.59	35.09	31.01	25.32	
190	C05 SH06	29.10.1995	27.11.1995	29	45.47	11.17	9.65	34.60	31.19	24.56	
191	C05 SH07	28.11.1995	27.12.1995	29	96.76	19.82	10.07	32.04	37.41	20.49	
192	C05 SH08	28.12.1995	26.01.1996	29	177.53	28.84	8.32	27.80	47.64	16.24	
193	C05 SH09	27.01.1996	25.02.1996	29	130.76	28.87	8.55	29.26	40.11	22.08	
194	C05 SH10	26.02.1996	26.03.1996	29	102.40	22.34	7.86	36.11	34.22	21.81	
195	C05 SH11	27.03.1996	25.04.1996	29	69.59	15.09	9.35	34.46	34.50	21.69	
196	C05 SH12	26.04.1996	25.05.1996	29	69.28	16.73	10.78	29.54	35.54	24.14	
197	C05 SH13	26.05.1996	24.06.1996	29	51.49	13.99	10.27	25.86	36.71	27.16	
198	C05 DP01	01.06.1995	30.06.1995	29	115.83	24.24	7.26	32.04	39.77	20.93	
199	C05 DP02	01.07.1995	30.07.1995	29	106.43	27.57	7.74	25.56	40.80	25.90	
200	C05 DP03	31.07.1995	29.08.1995	29	176.87	51.45	9.28	22.81	38.81	29.09	
201	C05 DP04	30.08.1995	28.09.1995	29	78.09	24.68	7.85	23.61	36.94	31.60	
202	C05 DP05	29.09.1995	28.10.1995	29	52.11	12.83	7.48	30.76	37.15	24.62	
203	C05 DP06	29.10.1995	27.11.1995	29	105.90	32.47	7.80	25.68	35.86	30.66	
204	C05 DP07	28.11.1995	27.12.1995	29	4.26	3.89	3.68	1.87	3.06	91.39	
205	C05 DP08	28.12.1996	26.01.1996	29	0.70		0.00	0.00	0.00	0.00	
206	C05 DP09	27.01.1996	25.02.1996	29	8.19	2.59	7.99	28.12	32.27	31.61	
207	C05 DP10	26.02.1996	26.03.1996	29	0.86		0.00	0.00	0.00	0.00	
208	C05 DP11	27.03.1996	25.04.1996	29	2.95	1.04	8.91	24.23	31.51	35.36	
209	C05 DP12	26.04.1996	25.05.1996	29	4.18	1.42	8.33	22.73	34.94	33.99	
210	C05 DP13	26.05.1996	24.06.1996	29	0.48		0.00	0.00	0.00	0.00	
211	C06 SH01	10.12.1996	05.01.1997	26	65.35	13.12	9.23	44.60	26.09	20.08	27.31
212	C06 SH02	06.01.1997	01.02.1997	26	78.60	21.10	10.06	41.82	21.28	26.84	26.48
213	C06 SH03	02.02.1997	28.02.1997	26	76.04	21.57	10.52	37.91	23.19	28.37	18.19
214	C06 SH04	01.03.1997	27.03.1997	26	65.20	15.39	11.98	40.29	24.12	23.61	63.57

ID	sample	interval start	interval end	duration	total	lithogen	organic	CaCO3	opal	lithogen	<2µm
				[d]	[mg/m²/d]	[mg/m²/d]	[%]	[%]	[%]	[%]	[%]
215	C06 SH05	28.03.1997	23.04.1997	26	6.10	2.19	18.32	23.52	22.24	35.92	
216	C06 SH06	24.04.1997	20.05.1997	26	18.63	5.39	13.60	33.24	24.21	28.94	
217	C06 SH07	21.05.1997	16.06.1997	26	169.86	47.78	10.55	38.75	22.57	28.13	12.65
218	C06 SH08	17.06.1997	14.07.1997	26	59.62	14.53	10.25	45.46	19.91	24.38	7.56
219	C06 SH09	15.07.1997	10.08.1997	26	53.21	13.58	11.76	40.79	21.93	25.52	
220	C06 SH10	11.08.1997	06.09.1997	26	109.93	18.90	12.15	53.03	17.62	17.20	7.51
221	C06 SH11	07.08.1997	03.10.1997	26	59.25	11.02	10.53	54.88	16.00	18.59	5.29
222	C06 SH12	04.10.1997	30.10.1997	26	50.85	8.03	7.18	66.94	10.09	15.79	
223	C06 SH13	31.10.1997	26.11.1997	26	71.52	10.46	9.85	61.43	14.09	14.63	
224	C07 SH01	29.06.1998	26.07.1998	27	63.47	11.35	10.20	48.31	23.61	17.88	17.2
225	C07 SH02	27.07.1998	23.08.1998	27	57.66	8.83	8.46	53.96	22.26	15.32	21.4
226	C07 SH03	24.08.1998	20.09.1998	27	58.15	3.42	6.93	67.06	20.13	5.88	
227	C07 SH04	21.09.1998	18.10.1998	27	68.69	9.45	9.43	53.70	23.11	13.76	23.8
228	C07 SH05	19.10.1998	15.11.1998	27	68.82	11.85	10.44	47.38	24.96	17.22	15.5
229	C07 SH06	16.11.1998	13.12.1998	27	36.35	5.78	9.99	48.48	25.63	15.91	25.9
230	C07 SH07	14.12.1998	10.01.1999	27	50.63	7.33	6.89	58.03	20.59	14.49	27.1
231	C07 SH08	11.01.1999	07.02.1999	27	90.59	12.29	8.24	46.68	31.52	13.57	26.2
232	C07 SH09	08.02.1999	07.03.1999	27	89.94	9.34	9.92	53.91	25.78	10.39	29.3
233	C07 SH10	08.03.1999	04.04.1999	27	78.95	10.86	8.73	48.74	28.77	13.76	36.9
234	C07 SH11	05.04.1999		27							30.2
235	C07 DP01	29.06.1998	26.07.1998	27	50.22	12.48	7.40	43.91	23.83	24.86	16
236	C07 DP02	27.07.1998	23.08.1998	27	45.07	11.66	6.95	42.86	24.32	25.88	17.8
237	C07 DP03	24.08.1998	20.09.1998	27	55.43	16.53	6.29	41.99	21.90	29.82	14.9
238	C07 DP04	21.09.1998	18.10.1998	27	58.62	17.12	6.97	41.63	22.19	29.21	16.5
239	C07 DP05	19.10.1998	15.11.1998	27	57.51	16.85	7.52	39.84	23.33	29.30	21.7
240	C07 DP06	16.11.1998	13.12.1998	27	47.74	12.24	7.36	41.31	25.70	25.63	17.1
241	C07 DP07	14.12.1998	10.01.1999	27	46.14	13.52	6.56	41.37	22.78	29.29	19.5
242	C07 DP08	11.01.1999	07.02.1999	27	74.63	23.40	7.29	34.14	27.21	31.36	23.9
243	C07 DP09	08.02.1999	07.03.1999	27	81.72	24.78	7.26	32.08	30.32	30.33	20.2
244	C07 DP10	08.03.1999	04.04.1999	27	75.50	20.67	8.15	32.02	32.45	27.38	21.4

10.1.5. SCS-W

ID	sample	interval start	interval end	duration	total	lithogen	organic	CaCO3	opal	lithogen	<2µm
				[d]	[mg/m²/d]	[mg/m²/d]	[%]	[%]	[%]	[%]	[%]
488	W01 SH01	27.06.2009	13.07.2009	16	68.21	18.45	11.15	36.00	25.77	27.13	
489	W01 SH02	14.07.2009	29.07.2009	16	15.74	31.15	1.37	33.79	26.38	29.46	
490	W01 SH03	30.07.2009	14.08.2009	16	298.98	6.15	1.66	26.45	42.76	2.12	
491	W01 SH04	15.08.2009	30.08.2009	16	115.48	3.42	1.90	3.39	32.36	26.34	
492	W01 SH05	31.08.2009	15.09.2009	16	135.25	44.29	1.39	19.78	37.85	32.75	
493	W01 SH06	16.09.2009	01.10.2009	16	8.16	4.22	11.50	18.50	18.20	51.85	
494	W01 SH07	02.10.2009	17.10.2009	16	0.84						
495	W01 SH08	18.10.2009	02.11.2009	16	0.28						
496	W01 SH09	03.11.2009	18.11.2009	16	0.26						
497	W01 SH10	19.11.2009	04.12.2009	16	0.48						
498	W01 SH11	05.12.2009	20.12.2009	16	0.37						
499	W01 SH12	21.12.2009	05.01.2010	16	0.20						
500	W01 SH13	06.01.2010	21.01.2010	16	0.11						
501	W01 SH14	22.01.2010	06.02.2010	16	0.15						
502	W01 SH15	07.02.2010	22.02.2010	16	0.12						
503	W01 SH16	23.02.2010	10.03.2010	16	29.77						
504	W01 SH17	11.03.2010	26.03.2010	16	1.79	0.90	9.25	18.19	22.75	49.98	
505	W01 SH18	27.03.2010	11.04.2010	16	1.79	5.58	1.93	13.76	19.98	55.32	
506	W01 SH19	12.04.2010	27.04.2010	16	8.31	4.66	14.87	8.23	21.59	56.93	
507	W01 SH20	28.04.2010	13.05.2010	16	0.49						
508	W02 SH1	20.05.2011	04.06.2011	16	85.46	26.57	11.23	35.00	22.89	31.87	

509	W02 SH2	05.06.2011	20.06.2011	16	118.59	4.30	11.53	31.28	23.20	33.98	
510	W02 SH3	21.06.2011	06.07.2011	16	15.85	51.68	9.85	36.36	2.30	34.26	
511	W02 SH4	07.07.2011	22.07.2011	16	132.47	29.19	8.30	46.33	23.43	22.35	
512	W02 SH5	23.07.2011	07.08.2011	16	186.16	22.55	8.13	53.64	26.11	12.11	
513	W02 SH6	08.08.2011	23.08.2011	16	15.17	46.53	18.98	25.88	24.54	3.67	
514	W02 SH7	24.08.2011	08.09.2011	16	18.39	28.62	11.75	32.67	29.78	26.47	
515	W02 SH8	09.09.2011	24.09.2011	16	157.54	58.47	8.24	25.73	28.92	37.12	
516	W02 SH9	25.09.2011	10.10.2011	16	96.70	32.24	7.49	3.93	28.46	33.12	
517	W02 SH10	11.10.2011	26.10.2011	16	142.62	37.80	8.11	41.84	23.54	26.54	
518	W02 SH11	27.10.2011	11.11.2011	16	16.57	28.89	8.53	43.32	3.16	17.99	
519	W02 SH12	12.11.2011	27.11.2011	16	16.34	17.54	9.55	36.58	37.41	16.47	
520	W02 SH13	28.11.2011	13.12.2011	16	95.53	7.12	14.65	4.23	37.78	7.35	
521	W02 SH14	14.12.2011	29.12.2011	16	139.61	1.97	8.38	43.58	4.18	7.85	
522	W02 SH15	30.12.2011	14.01.2012	16	15.68	3.58	8.84	51.43	36.35	3.39	
523	W02 SH16	15.01.2012	30.01.2012	16	12.79	1.48	8.46	4.67	41.10	1.19	
524	W02 SH17	31.01.2012	15.02.2012	16	6.40	3.29	8.19	44.35	42.20	5.44	
525	W02 SH18	16.02.2012	02.03.2012	16	2.69						
526	W02 SH19	03.03.2012	18.03.2012	16	31.12	3.89	9.41	42.48	36.80	12.47	
527	W02 SH20	19.03.2012	04.04.2012	16	1.60						

10.1.6. SCS-SC

ID	sample	interval start	interval end	duration	total	lithogen	organic	CaCO3	opal	lithogen	<2μm
				[d]	[mg/m²/d]	[mg/m²/d]	[%]	[%]	[%]	[%]	[%]
245	SC01 SH01	10.05.2005	26.05.2005	17	38.38	13.94	11.80	36.73	15.84	36.39	
246	SC01 SH02	27.05.2005	12.06.2005	17	56.86	26.56	9.42	29.93	13.95	46.71	
247	SC01 SH03	13.06.2005	29.06.2005	17	197.94	126.28	6.40	16.44	13.50	63.67	
248	SC01 SH04	30.06.2005	16.07.2005	17	76.83	3.65	7.20	39.68	13.22	39.90	
249	SC01 SH05	17.07.2005	02.08.2005	17	115.12	54.96	8.89	29.13	14.19	47.79	
250	SC01 SH06	03.08.2005	19.08.2005	17	128.77	59.37	8.77	25.68	19.44	46.18	
251	SC01 SH07	20.08.2005	05.09.2005	17	0.78				21.47		
252	SC01 SH08	06.09.2005	22.09.2005	17	183.46	73.19	14.23	11.59	34.28	39.90	
253	SC01 SH09	23.09.2005	09.10.2005	17	2.89	1.53	14.77	14.92	18.18	53.26	
254	SC01 SH10	10.10.2005	26.10.2005	17	423.52	211.93	8.41	15.33	26.25	5.40	
255	SC01 SH11	27.10.2005	12.11.2005	17	241.43	127.43	6.76	17.66	22.89	52.77	
256	SC01 SH12	13.11.2005	29.11.2005	17	74.20	35.41	8.38	23.56	2.34	47.73	
257	SC01 SH13	30.11.2005	16.12.2005	17	165.29	14.99	5.75	16.85	14.69	63.52	
258	SC01 SH14	17.12.2005	02.01.2006	17	131.38	54.72	8.49	21.28	28.57	41.65	
259	SC01 SH15	03.01.2006	19.01.2006	17	43.29	98.88	1.83	13.55	53.14	22.99	
260	SC01 SH16	20.01.2006	05.02.2006	17	45.31	11.88	9.65	38.54	25.58	26.23	
261	SC01 SH17	06.02.2006	22.02.2006	17	15.50	3.67	8.98	36.98	25.55	29.69	
262	SC01 SH18	23.02.2006	11.03.2006	17	61.69	17.98	1.36	38.46	22.43	29.15	
263	SC01 SH19	12.03.2006	28.03.2006	17	273.33	99.89	9.12	36.29	18.33	36.25	
264	SC01 SH20	29.03.2006	14.04.2006	17	96.79	48.16	9.18	25.18	16.39	49.64	
265	SC01 DP01	10.05.2005	26.05.2005	17	153.50	78.20	6.92	22.62	19.48	5.97	
266	SC01 DP02	27.05.2005	12.06.2005	17	143.96	78.69	6.86	22.22	16.32	54.66	
267	SC01 DP03	13.06.2005	29.06.2005	17	194.58	123.22	5.75	16.14	14.79	63.33	
268	SC01 DP04	30.06.2005	16.07.2005	17	151.22	72.46	5.40	32.90	13.78	47.92	
269	SC01 DP05	17.07.2005	02.08.2005	17	125.85	67.14	5.98	26.12	14.54	53.36	
270	SC01 DP06	03.08.2005	19.08.2005	17	155.42	72.35	6.94	24.65	21.87	46.55	
271	SC01 DP07	20.08.2005	05.09.2005	17	348.77	17.43	8.59	1.82	31.73	48.87	
272	SC01 DP08	06.09.2005	22.09.2005	17	188.63	1.83	7.25	15.28	25.00	53.45	
273	SC01 DP09	23.09.2005	09.10.2005	17	255.93	13.77	6.48	13.88	28.37	51.26	
274	SC01 DP10	10.10.2005	26.10.2005	17	468.13	27.15	5.72	11.62	24.96	57.70	
275	SC01 DP11	27.10.2005	12.11.2005	17	23.59	126.39	5.57	15.57	16.79	62.89	
276	SC01 DP12	13.11.2005	29.11.2005	17	142.89	89.52	6.36	18.48	12.59	62.64	
277	SC01 DP13	30.11.2005	16.12.2005	17	352.14	23.97	4.81	13.65	16.20	65.34	
278	SC01 DP14	17.12.2005	02.01.2006	17	275.00	168.22	4.62	18.22	16.74	61.18	

ID	sample	interval start	interval end	duration	total	lithogen	organic	CaCO3	opal	lithogen	<2µm
				[d]	[mg/m²/d]	[mg/m²/d]	[%]	[%]	[%]	[%]	[%]
279	SC01 DP15	03.01.2006	19.01.2006	17	463.27	116.89	8.74	15.47	5.56	25.23	
280	SC01 DP16	20.01.2006	05.02.2006	17	164.18	61.78	6.59	29.48	26.34	37.63	
281	SC01 DP17	06.02.2006	22.02.2006	17	133.18	41.68	6.23	4.62	21.94	31.26	
282	SC01 DP18	23.02.2006	11.03.2006	17	112.25	39.65	7.82	32.92	23.94	35.32	
283	SC01 DP19	12.03.2006	28.03.2006	17	158.16	63.22	7.26	32.76	2.62	39.97	
284	SC01 DP20	29.03.2006	14.04.2006	17	184.98	85.24	7.23	25.39	21.33	46.78	
285	SC02 SH01	10.05.2006	26.05.2006	17	168.59	8.93	6.75	25.84	2.17	48.25	
286	SC02 SH02	27.05.2006	12.06.2006	17	21.21	77.28	7.95	3.82	22.82	38.45	
287	SC02 SH03	13.06.2006	29.06.2006	17	191.50	76.84	8.43	27.65	23.79	4.12	
288	SC02 SH04	30.06.2006	16.07.2006	17	147.92	64.32	8.37	24.69	23.84	43.48	
289	SC02 SH05	17.07.2006	02.08.2006	17	26.35	8.98	12.86	3.89	22.32	34.66	
290	SC02 SH06	03.08.2006	19.08.2006	17	0.79						
291	SC02 SH07	20.08.2006	05.09.2006	17	0.25						
292	SC02 SH08	06.09.2006	22.09.2006	17	0.95						
293	SC02 SH09	23.09.2006	09.10.2006	17	0.42						
294	SC02 SH10	10.10.2006	26.10.2006	17	0.76						
295	SC02 SH11	27.10.2006	12.11.2006	17	0.78						
296	SC02 SH12	13.11.2006	29.11.2006	17	0.60						
297	SC02 SH13	30.11.2006	16.12.2006	17	6.34	21.59	1.28	23.97	3.88	35.83	
298	SC02 SH14	17.12.2006	02.01.2007	17	1.23						
299	SC02 SH15	03.01.2007	19.01.2007	17	156.42	56.75	9.00	19.16	35.73	36.28	
300	SC02 SH16	20.01.2007	05.02.2007	17	8.96	3.49	9.85	24.11	27.35	39.00	
301	SC02 SH17	06.02.2007	22.02.2007	17	0.94						
302	SC02 SH18	23.02.2007	11.03.2007	17	0.28						
303	SC02 SH19	12.03.2007	28.03.2007	17	0.48						
304	SC02 SH20	29.03.2007	14.04.2007	17	0.56						
305	SC02 DP01	10.05.2006	26.05.2006	17	225.72	111.99	6.00	23.22	21.17	49.62	
306	SC02 DP02	27.05.2006	12.06.2006	17	246.47	132.43	6.22	2.32	19.72	53.73	
307	SC02 DP03	13.06.2006	29.06.2006	17	23.36	83.22	6.83	3.77	21.47	4.92	
308	SC02 DP04	30.06.2006	16.07.2006	17	158.82	7.64	6.78	24.99	23.74	44.48	
309	SC02 DP05	17.07.2006	02.08.2006	17	22.98	81.28	8.47	23.89	27.68	4.42	
310	SC02 DP06	03.08.2006	19.08.2006	17	191.17	67.56	6.26	29.18	29.38	35.34	
311	SC02 DP07	20.08.2006	05.09.2006	17	151.84	41.97	7.37	26.56	38.44	27.64	
312	SC02 DP08	06.09.2006	22.09.2006	17	222.75	43.67	8.18	19.48	53.33	19.67	
313	SC02 DP09	23.09.2006	09.10.2006	17	336.65	125.17	6.36	19.82	36.63	37.18	
314	SC02 DP10	10.10.2006	26.10.2006	17	23.64	86.71	5.66	24.18	27.58	42.58	
315	SC02 DP11	27.10.2006	12.11.2006	17	16.15	57.42	5.82	27.28	31.14	35.85	
316	SC02 DP12	13.11.2006	29.11.2006	17	12.37	42.76	6.41	26.30	31.77	35.53	
317	SC02 DP13	30.11.2006	16.12.2006	17	16.24	73.80	6.18	22.52	25.25	46.54	
318	SC02 DP14	17.12.2006	02.01.2007	17	241.87	125.67	5.39	2.73	21.93	51.96	
319	SC02 DP15	03.01.2007	19.01.2007	17	22.56	96.69	5.38	26.67	24.12	43.83	
320	SC02 DP16	20.01.2007	05.02.2007	17	152.15	79.89	5.37	24.62	17.52	52.53	
321	SC02 DP17	06.02.2007	22.02.2007	17	28.58	7.98	4.92	36.88	24.77	34.12	
322	SC02 DP18	23.02.2007	11.03.2007	17	121.26	45.94	6.86	25.25	3.13	37.88	
323	SC02 DP19	12.03.2007	28.03.2007	17	17.43	37.95	6.89	3.45	27.35	35.33	
324	SC02 DP20	29.03.2007	14.04.2007	17	111.92	47.19	7.22	27.83	22.79	42.17	

10.1.7. SCS-SW

ID	sample	interval start	interval end	duration	total	lithogen	organic	CaCO3	opal	lithogen	<2µm
				[d]	[mg/m²/d]	[mg/m²/d]	[%]	[%]	[%]	[%]	[%]
374	SW01 SH01	29.06.1998	23.08.1998		324.77	17.52	6.29	21.50	2.15	52.56	1.93
375	SW01 SH02	24.08.1998	20.09.1998		88.12	36.60	7.84	31.32	19.36	41.53	15.83
376	SW01 SH03	21.09.1998	18.10.1998		184.30	6.52	7.62	31.97	27.53	32.88	19.53
377	SW01 SH04	19.10.1998	15.11.1998		268.11	136.96	5.94	21.24	21.95	51.83	14.29
378	SW01 SH05	16.11.1998	13.12.1998		129.53	66.59	5.76	29.57	13.94	51.41	13.31

ID	sample	interval start	interval end	duration	total	lithogen	organic	CaCO3	opal	lithogen	<2μm
				[d]	[mg/m²/d]	[mg/m²/d]	[%]	[%]	[%]	[%]	[%]
379	SW01 SH06	14.12.1998	10.01.1999		289.14	176.62	4.65	21.00	13.27	61.85	12.67
380	SW01 SH07	11.01.1999	07.02.1999		53.98	34.48	3.61	17.95	1.88	67.56	1.70
381	SW01 SH08	08.02.1999	07.03.1999		514.77	343.86	4.59	18.77	1.38	66.80	14.66
382	SW01 SH09	08.03.1999	04.04.1999		122.99	52.44	8.92	23.86	24.58	42.63	2.17
383	SW01 SH10	05.04.1999	23.04.1999		62.50	15.64	8.55	4.88	25.38	25.23	17.19
384	SW02 DP02	15.05.1999	11.06.1999	28	2.66	99.63	8.12	17.84	25.16	49.65	
385	SW02 DP03	12.06.1999	09.07.1999	28	342.81	152.52	7.36	12.81	35.33	44.49	
386	SW04 SH01	10.06.2004	26.06.2004	16	5.33	9.62		49.14	18.11	19.12	
387	SW04 SH02	26.06.2004	12.07.2004	16	55.35	15.12		44.45	15.25	27.32	
388	SW04 SH03	12.07.2004	28.07.2004	16	8.40	24.00		38.19	18.32	29.74	
389	SW04 SH04	28.07.2004	13.08.2004	16	69.44	24.85		33.76	2.79	35.90	
390	SW04 SH05	13.08.2004	29.08.2004	16	53.15	34.65		17.75	9.26	65.26	
391	SW04 SH06	29.08.2004	14.09.2004	16	68.64	32.94		28.24	15.67	47.99	
392	SW04 SH07	14.09.2004	30.09.2004	16	276.77	138.69		14.99	24.66	5.24	
393	SW04 SH08	30.09.2004	16.10.2004	16	246.59	133.26		19.32	17.65	54.42	
394	SW04 SH09	16.10.2004	01.11.2004	16	26.88	8.75		44.28	9.22	3.38	
395	SW04 SH10	01.11.2004	17.11.2004	16	3.19	1.56		22.23	8.18	48.93	
396	SW04 SH11	17.11.2004	03.12.2004	16	8.34	3.28		4.83	7.63	39.39	
397	SW04 SH12	03.12.2004	19.12.2004	16	13.80	5.94		32.74	11.84	43.21	
398	SW04 SH13	19.12.2004	04.01.2005	16	4.16	1.98		27.23	12.22	47.52	
399	SW04 SH14	04.01.2005	20.01.2005	16	1.70			22.33			
400	SW04 SH15	20.01.2005	05.02.2005	16	229.96	115.23		23.53	18.27	5.38	
401	SW04 SH16	05.02.2005	21.02.2005	16	3.50	2.46		9.36	12.26	7.46	
402	SW04 SH17	21.02.2005	09.03.2005	16	2.98	2.11		1.35	11.85	7.97	
403	SW04 SH18	09.03.2005	25.03.2005	16	2.53	1.75		1.35	12.87	69.95	
404	SW04 SH19	25.03.2005	10.04.2005	16	5.52	3.85		24.39	11.93	55.91	
405	SW04 SH20	10.04.2005	26.04.2005	16	6.68	3.76		23.42	12.99	56.35	
406	SW04 SH21	26.04.2005			632.62	426.56		15.58	12.55	67.49	
407	SW04 DP01	10.06.2004	26.06.2004	16	129.75	52.73		26.48	21.35	4.64	
408	SW04 DP02	26.06.2004	12.07.2004	16	124.87	34.50		52.42	13.89	27.63	
409	SW04 DP03	12.07.2004	28.07.2004	16	21.57	5.32		61.36	7.73	24.66	
410	SW04 DP04	28.07.2004	13.08.2004	16	29.47	9.88		55.17	6.47	33.53	
411	SW04 DP05	13.08.2004	29.08.2004	16	45.25	286.46		15.56	1.35	7.69	
412	SW04 DP06	29.08.2004	14.09.2004	16	532.69	292.27		15.78	22.75	54.87	
413	SW04 DP07	14.09.2004	30.09.2004	16	36.87	1.24		19.89	37.66	28.37	
414	SW04 DP08	30.09.2004	16.10.2004	16	33.15	135.15		25.17	22.12	44.58	
414	SW04 DP08	30.09.2004	16.10.2004	16	33.15	135.15		25.17	22.12	44.58	
415	SW04 DP09	16.10.2004	01.11.2004	16	187.54	74.97		27.60	25.47	39.98	
416	SW04 DP10	01.11.2004	17.11.2004	16	144.00	49.69		27.19	29.38	34.57	
417	SW04 DP11	17.11.2004	03.12.2004	16	386.24	239.31		14.83	17.75	61.96	
418	SW04 DP12	03.12.2004	19.12.2004	16	494.90	317.74		15.58	15.58	64.23	
419	SW04 DP13	19.12.2004	04.01.2005	16	31.96	193.52		15.74	15.15	64.87	
420	SW04 DP14	04.01.2005	20.01.2005	16	397.33	271.52		13.58	12.98	68.34	
421	SW04 DP15	20.01.2005	05.02.2005	16	262.49	165.24		18.64	13.58	62.86	
422	SW04 DP16	05.02.2005	21.02.2005	16	446.86	31.34		15.24	12.98	67.43	
423	SW04 DP17	21.02.2005	09.03.2005	16	469.59	319.58		13.44	13.44	68.55	
424	SW04 DP18	09.03.2005	25.03.2005	16	1119.25	791.39		11.36	13.33	7.77	
425	SW04 DP19	25.03.2005	10.04.2005	16	1383.96	11.94		11.32	12.57	72.44	
426	SW04 DP20	10.04.2005	26.04.2005	16	357.53	217.72		17.27	16.62	6.89	
427	SW04 DP21	26.04.2005			85.24	42.45		21.15	2.94	49.80	
428	SW05 SH01	10.05.2005	26.05.2005	17	81.77	33.78	14.16	22.26	22.29	41.38	
429	SW05 SH02	27.05.2005	12.06.2005	17	55.18	31.15	7.52	15.94	16.11	61.39	
430	SW05 SH03	13.06.2005	29.06.2005	17	5.40	22.81	13.43	34.51	6.80	45.26	
431	SW05 SH04	30.06.2005	16.07.2005	17	489.56	247.32	8.28	12.52	28.69	5.52	
432	SW05 SH05	17.07.2005	02.08.2005	17	219.54	14.96	7.84	13.86	15.30	63.81	
433	SW05 SH06	03.08.2005	19.08.2005	17	78.82	54.87	5.45	13.99	11.83	69.62	
434	SW05 SH07	20.08.2005	05.09.2005	17	718.21	461.24	5.95	14.84	15.26	64.22	

ID	sample	interval start	interval end	duration	total	lithogen	organic	CaCO3	opal	lithogen	<2µm
				[d]	[mg/m²/d]	[mg/m²/d]	[%]	[%]	[%]	[%]	[%]
435	SW05 SH08	06.09.2005	22.09.2005	17	461.50	347.18	3.71	12.46	8.59	75.23	
436	SW05 SH09	23.09.2005	09.10.2005	17	4.14	13.24	15.51	27.16	24.80	32.99	
437	SW05 SH10	10.10.2005	26.10.2005	17	6.81	2.57	25.20	25.43	11.82	37.72	
438	SW05 SH11	27.10.2005	12.11.2005	17	4.67	2.25	24.85	15.25	12.62	48.51	
439	SW05 SH12	13.11.2005	29.11.2005	17	2.43	1.20	6.47	18.16	26.17	49.37	
440	SW05 SH13	30.11.2005	16.12.2005	17	0.20						
441	SW05 SH14	17.12.2005	02.01.2006	17	0.34						
442	SW05 SH15	03.01.2006	19.01.2006	17	0.15						
443	SW05 SH16	20.01.2006	05.02.2006	17	0.72						
444	SW05 SH17	06.02.2006	22.02.2006	17	0.16						
445	SW05 SH18	23.02.2006	11.03.2006	17	0.68						
446	SW05 SH19	12.03.2006	28.03.2006	17	0.24						
447	SW05 SH20	29.03.2006	14.04.2006	17	0.17						
448	SW06 SH01	10.05.2006	26.05.2006	17	118.86	54.45	7.61	27.85	18.72	45.88	
449	SW06 SH02	27.05.2006	12.06.2006	17	67.73	24.63	11.49	38.22	13.93	36.36	
450	SW06 SH03	13.06.2006	29.06.2006	17	174.26	73.22	7.75	24.95	26.14	42.18	
451	SW06 SH04	30.06.2006	16.07.2006	17	43.74	18.28	1.53	26.90	21.26	41.80	
452	SW06 SH05	17.07.2006	02.08.2006	17	125.78	46.53	1.80	17.80	35.14	37.00	
453	SW06 SH06	03.08.2006	19.08.2006	17	3.34	2.27	12.19	19.79		68.19	
454	SW06 SH07	20.08.2006	05.09.2006	17	87.47	46.93	9.29	15.19	21.88	53.65	
455	SW06 SH08	06.09.2006	22.09.2006	17	82.54	44.97	7.50	14.28	23.83	54.40	
456	SW06 SH09	23.09.2006	09.10.2006	17	15.37	9.43	8.14	12.33	18.15	61.38	
457	SW06 SH10	10.10.2006	26.10.2006	17	34.61	22.47	6.78	12.38	16.32	64.93	
458	SW06 SH11	27.10.2006	12.11.2006	17	13.93	8.75	6.75	14.86	15.70	62.75	
459	SW06 SH12	13.11.2006	29.11.2006	17	4.16	2.58	6.39	19.86	11.85	61.92	
460	SW06 SH13	30.11.2006	16.12.2006	17	6.87	4.67	6.95	12.63	12.50	67.94	
461	SW06 SH14	17.12.2006	02.01.2007	17	7.61	5.65	9.67	-0.51	16.59	74.26	
462	SW06 SH15	03.01.2007	19.01.2007	17	6.67	4.45	6.95	1.92	15.39	66.76	
463	SW06 SH16	20.01.2007	05.02.2007	17	18.62	12.48	7.29	1.70	15.39	66.70	
464	SW06 SH17	06.02.2007	22.02.2007	17	26.75	18.35	7.66	1.64	13.70	68.60	
465	SW06 SH18	23.02.2007	11.03.2007	17	26.81	17.62	5.98	12.77	15.55	65.79	
466	SW06 SH19	12.03.2007	28.03.2007	17	1.84	7.55	7.15	9.85	13.44	69.69	
467	SW06 SH20	29.03.2007	14.04.2007	17	56.29	36.94	6.37	14.13	13.87	65.64	
468	SW06 DP01	10.05.2006	26.05.2006	17	199.36	17.13	6.23	22.80	17.24	53.74	
469	SW06 DP02	27.05.2006	12.06.2006	17	145.21	8.64	8.39	21.43	14.65	55.53	
470	SW06 DP03	13.06.2006	29.06.2006	17	22.45	115.67	6.49	22.48	18.56	52.47	
471	SW06 DP04	30.06.2006	16.07.2006	17	173.73	86.78	7.59	2.11	22.35	49.95	
472	SW06 DP05	17.07.2006	02.08.2006	17	32.84	14.76	7.94	13.22	32.61	46.23	
473	SW06 DP06	03.08.2006	19.08.2006	17	725.14	391.84	6.69	13.29	26.66	54.36	
474	SW06 DP07	20.08.2006	05.09.2006	17	938.27	642.88	3.77	12.96	14.76	68.51	
475	SW06 DP08	06.09.2006	22.09.2006	17	269.52	161.17	5.43	16.69	18.47	59.86	
476	SW06 DP09	23.09.2006	09.10.2006	17	79.62	35.23	6.14	29.50	2.15	44.24	
477	SW06 DP10	10.10.2006	26.10.2006	17	38.96	1.69	5.86	46.28	2.42	27.45	
478	SW06 DP11	27.10.2006	12.11.2006	17	31.99	195.44	3.94	19.40	13.83	62.83	
479	SW06 DP12	13.11.2006	29.11.2006	17	282.61	171.41	9.58	17.00	13.33	6.64	
480	SW06 DP13	30.11.2006	16.12.2006	17	94.49	59.35	6.54	13.52	17.13	62.82	
481	SW06 DP14	17.12.2006	02.01.2007	17	16.80		5.48	14.95			
482	SW06 DP15	03.01.2007	19.01.2007	17							
483	SW06 DP16	20.01.2007	05.02.2007	17							
484	SW06 DP17	06.02.2007	22.02.2007	17							
485	SW06 DP18	23.02.2007	11.03.2007	17							
486	SW06 DP19	12.03.2007	28.03.2007	17							
487	SW06 DP20	29.03.2007	14.04.2007	17							

Changes of clay mineral and trace element characteristics in the Deep South China Sea

10.1.8. SCS-S

ID	sample	interval start	interval end	duration	total	lithogen	organic	CaCO3	opal	lithogen	<2μm
				[d]	[mg/m²/d]	[mg/m²/d]	[%]	[%]	[%]	[%]	[%]
325	S01 DP01	30.06.2003	16.07.2003		94.47	39.83	7.20	32.21	18.67	42.19	
326	S01 DP02	17.07.2003	02.08.2003		68.59	27.25	6.94	38.42	15.29	39.73	
327	S01 DP03	03.08.2003	19.08.2003		71.89	25.31	7.83	37.63	2.83	35.29	
328	S01 DP04	20.08.2003	05.09.2003		145.89	44.97	6.98	39.17	23.36	3.82	
329	S01 DP05	06.09.2003	22.09.2003		95.56	3.88	8.12	32.79	26.77	32.32	
330	S01 DP06	23.09.2003	09.10.2003		78.78	27.39	7.44	35.42	22.37	34.77	
331	S01 DP07	10.10.2003	26.10.2003		533.22	351.99	4.77	12.67	16.55	66.19	
332	S01 DP08	27.10.2003	12.11.2003		812.75	58.24	3.85	11.33	13.42	71.40	
333	S01 DP09	13.11.2003	29.11.2003		33.84	189.55	5.36	12.58	19.84	62.22	
334	S01 DP10	30.11.2003	16.12.2003		11.85	75.67	4.77	12.67	14.36	68.26	
335	S01 DP11	17.12.2003	02.01.2004		76.51	48.93	7.43	12.17	16.46	63.95	
336	S01 DP12	03.01.2004	19.01.2004		345.88	155.35	7.43	16.00	31.67	44.91	
337	S01 DP13	20.01.2004	05.02.2004		16.98	86.36	5.44	23.78	17.28	53.65	
338	S01 DP14	06.02.2004	22.02.2004		15.92	72.58	5.59	31.83	14.49	48.92	
339	S01 DP15	23.02.2004	10.03.2004		11.21	44.25	8.47	29.83	17.98	43.72	
340	S01 DP16	11.03.2004	27.03.2004		23.46	84.99	8.30	28.92	21.13	41.77	
341	S01 DP17	28.03.2004	13.04.2004		671.16	399.94	5.31	2.78	14.39	59.59	
342	S01 DP18	14.04.2004	30.04.2004		779.16	489.59	5.68	17.83	14.47	62.77	
343	S01 DP19	01.05.2004	17.05.2004		312.85	183.22	6.21	19.13	16.18	58.57	
344	S01 DP20	18.05.2004	03.06.2004		157.66	83.32	5.13	29.92	12.17	52.85	
345	S02 SH01	10.06.2004	25.06.2004		67.82	27.84	12.28	27.81	18.86	41.51	
346	S02 SH02	26.06.2004	11.07.2004		71.46	25.89	13.26	22.44	28.35	36.23	
347	S02 SH03	12.07.2004	27.07.2004		147.16	56.32	9.19	22.21	3.33	38.27	
348	S02 SH04	28.07.2004	12.08.2004		8.84	2.98	7.42	49.23	17.17	26.19	
349	S02 SH05	13.08.2004	28.08.2004		49.39	16.12	8.86	4.64	17.86	32.64	
350	S02 SH06	29.08.2004	13.09.2004		54.40	16.31	12.35	34.33	23.64	29.99	
351	S02 SH07	14.09.2004	29.09.2004		54.44	13.92	11.40	36.36	26.67	25.57	
352	S02 SH08	30.09.2004	15.10.2004		59.17	18.21	13.59	35.58	2.53	3.78	
353	S02 SH09	16.10.2004	31.10.2004		33.32	12.75	11.58	29.35	2.79	38.28	
354	S02 SH10	01.11.2004			1.79	56.33	7.48	18.86	17.77	55.89	
355	S02 DP01	10.06.2004	25.06.2004		14.92	52.84	8.28	23.12	18.51	5.37	
356	S02 DP02	26.06.2004	11.07.2004		193.73	97.36	7.43	18.56	23.78	5.26	
357	S02 DP03	12.07.2004	27.07.2004		172.58	72.34	7.75	21.13	29.22	41.92	
358	S02 DP04	28.07.2004	12.08.2004		129.75	45.68	7.52	34.85	22.94	35.15	
359	S02 DP05	13.08.2004	28.08.2004		75.87	24.79	9.82	32.68	25.74	31.76	
360	S02 DP06	29.08.2004	13.09.2004		93.30	35.33	7.15	28.44	26.94	37.55	
361	S02 DP07	14.09.2004	29.09.2004		83.93	38.59	12.29	23.39	18.59	45.98	
362	S02 DP08	30.09.2004	15.10.2004		117.87	53.97	7.60	22.32	24.39	45.79	
363	S02 DP09	16.10.2004	31.10.2004		166.61	82.65	6.37	23.44	2.58	49.69	
364	S02 DP10	01.11.2004	16.11.2004		1297.91	959.98	3.53	11.20	11.33	73.96	
365	S02 DP11	17.11.2004	02.12.2004		124.75	62.14	6.90	23.74	19.29	5.77	
366	S02 DP12	03.12.2004	18.12.2004		342.42	198.32	5.26	16.82	2.64	57.92	
367	S02 DP13	19.12.2004	03.01.2005		211.72	19.55	5.15	21.32	21.63	51.93	
368	S02 DP14	04.01.2005	19.01.2005		21.93	83.92	19.93	16.53	21.99	41.56	
369	S02 DP15	20.01.2005	04.02.2005		55.97	25.11	9.92	24.66	2.55	44.87	
370	S02 DP16	05.02.2005	20.02.2005		26.22	9.82	18.32	27.33	16.87	37.48	
371	S02 DP17	21.02.2005	08.03.2005		9.84	5.32	8.28	21.27	16.58	53.88	
372	S02 DP18	09.03.2005	24.03.2005		2.97	1.76	11.42	1.53	18.64	59.44	
373	S02 DP19	25.03.2005	06.04.2005		2.66	1.85	11.23	1.72	17.87	69.39	

10.2. Clay mineral abundances and fluxes

10.2.1. SCS-N

ID	Sample	<2µm	Sm	Chl	Ill	Kao	Flitho	f<2µm	fSm	FChl	fIll	fKao
				[%]						[mg/m²/d]		
528	N01 SH01											
529	N01 SH02											
530	N01 SH03											
531	N01 SH04											
532	N01 SH05											
533	N01 SH06											
534	N01 SH07											
535	N01 SH08											
536	N01 SH09											
537	N01 SH10											
538	N01 SH11											
539	N01 SH12											
540	N01 SH13											
541	N01 DP01											
542	N01 DP02											
543	N01 DP03											
544	N01 DP04											
545	N01 DP05											
546	N01 DP06											
547	N01 DP07											
548	N01 DP08											
549	N01 DP09											
550	N01 DP10											
551	N01 DP11											
552	N01 DP12											
553	N01 DP13											
554	N02 SH01											
555	N02 SH02											
556	N02 SH03											
557	N02 SH04											
558	N02 SH05											
559	N02 SH06											
560	N02 SH07											
561	N02 SH08											
562	N02 SH09											
563	N02 SH10											
564	N02 SH11											
565	N02 SH12											
566	N02 SH13											
567	N03 SH01		17.72		42.22	4.63	16.23					
568	N03 SH02		2.86		4.22	38.93	15.57					
569	N03 SH03		29.42		35.66	35.51	22.41					
570	N03 SH04		22.80		39.36	38.56	12.95					
571	N03 SH05		18.56		43.82	37.63	6.45					
572	N03 SH06		23.19		36.73		12.00					
573	N03 SH07											
574	N03 SH08		37.50		3.96	31.55	21.67					
575	N03 SH09	0.25	32.55		35.43	32.22	62.67	0.16	0.56		0.55	0.50
576	N03 SH10	0.25	31.79	22.47	37.30	8.76	125.34	0.31	0.99	0.70	0.11	0.27
577	N03 SH11	0.26	37.20	22.32	34.77	5.71	54.57	0.14	0.52	0.31	0.48	0.79
578	N03 SH12	0.30	33.12	27.78	35.75	4.70	59.73	0.17	0.57	0.47	0.63	0.77
579	N03 SH13		28.96	28.37	36.61	6.54	14.68					
580	N03 SH14		26.64	28.25	36.38	8.74	13.52					
581	N03 SH15	0.37	43.23	22.29	28.58	5.89	24.58	0.75	0.33	0.17	0.22	0.44

Changes of clay mineral and trace element characteristics in the Deep South China Sea

ID	Sample	<2µm	Sm	Chl	Ill	Kao	Flitho	f<2µm	fSm	FChl	fIll	fKao
				[%]						[mg/m²/d]		
582	N03 SH16	0.38	3.23	29.25	35.54	5.69	26.42	0.81	0.25	0.24	0.29	0.46
583	N03 SH17		24.68	24.66	43.91	6.75	18.64					
584	N03 SH18	0.27	2.60	25.29	5.76	3.48	118.97	0.31	0.64	0.78	0.16	0.16
585	N03 SH19		33.37	23.42	38.42	4.82	61.78					
586	N03 SH20	0.28	26.78	25.66	43.67	3.99	46.67	0.13	0.34	0.33	0.56	0.50
587	N03 MD01		3.29	24.58	36.38	8.75	25.63					
588	N03 MD02		29.21	24.65	37.43	8.75	25.27					
589	N03 MD03		22.19	26.85	4.89	1.80	25.55					
590	N03 MD04		25.98	23.82	38.79	11.41	2.69					
591	N03 MD05		28.84	24.23	38.38	8.55	21.54					
592	N03 MD06		29.98	24.16	37.45	8.48	17.52					
593	N03 MD07		21.70	27.44	41.46	9.41	15.11					
594	N03 MD08		36.59	21.23	36.64	6.12	7.66					
595	N03 MD09	0.30	35.41	19.38	36.53	8.68	52.93	0.16	0.56	0.34	0.57	0.14
596	N03 MD10	0.27	29.88	24.53	39.39	6.21	73.47	0.20	0.59	0.49	0.78	0.12
597	N03 MD11	0.28	3.15	23.16	39.75	6.94	1.25	0.28	0.84	0.64	0.12	0.19
598	N03 MD12	0.28	33.63	23.49	36.69	6.64	94.45	0.26	0.88	0.60	0.95	0.17
599	N03 MD13	0.29	21.35	22.60	47.89	8.47	54.19	0.16	0.33	0.35	0.75	0.13
600	N03 MD14	0.29	3.39	2.56	38.71	1.34	54.86	0.17	0.49	0.34	0.62	0.17
601	N03 MD15	0.36	42.95	5.79	31.91	2.68	55.65	0.17	0.74	0.86	0.54	0.34
602	N03 MD16	0.30	42.37	2.00	32.51	14.12	69.53	0.25	0.87	0.23	0.67	0.29
603	N03 MD17	0.28	4.88	22.69	31.52	4.93	56.69	0.16	0.66	0.37	0.58	0.79
604	N03 MD18	0.29	3.23	23.34	41.94	5.33	99.82	0.29	0.87	0.67	0.12	0.15
605	N03 MD19	0.27	25.88	26.24	44.45	3.52	69.19	0.18	0.48	0.48	0.82	0.65
606	N03 MD20	0.27	24.13	24.79	45.11	5.97	36.80	0.99	0.24	0.24	0.45	0.59
607	N03 DP01											
608	N03 DP02	0.35	33.16	22.17	34.69	9.98	31.89	0.97	0.32	0.22	0.34	0.98
609	N03 DP03	0.32	36.64	23.16	33.74	6.46	29.35	0.92	0.34	0.21	0.40	0.59
610	N03 DP04	0.33	33.28	23.14	34.68	8.98	29.62	0.90	0.30	0.28	0.31	0.87
611	N03 DP05	0.31	28.68	25.72	38.89	6.73	27.48	0.86	0.25	0.23	0.33	0.58
612	N03 DP06	0.33	32.74	23.86	36.17	7.30	27.63	0.97	0.29	0.21	0.33	0.66
613	N03 DP07		28.20	23.19	4.66	7.96	21.41					
614	N03 DP08		28.39	23.59	38.94	9.76	25.87					
615	N03 DP09		42.75	21.48	3.91	4.86	2.44					
616	N03 DP10	0.33	32.47	22.24	37.56	7.73	44.46	0.13	0.44	0.30	0.55	0.15
617	N03 DP11	0.29	4.75	2.18	33.83	5.24	58.62	0.17	0.69	0.34	0.57	0.89
618	N03 DP12	0.29	43.43	19.29	31.42	5.86	71.42	0.27	0.92	0.40	0.65	0.12
618	N03 DP12	0.29	44.52	18.45	3.64	6.40	71.42	0.27	0.92	0.38	0.63	0.13
619	N03 DP13	0.29	54.32	17.46	24.47	3.74	69.92	0.20	0.18	0.35	0.49	0.75
620	N03 DP14	0.27	41.19	21.29	31.98	5.53	75.34	0.21	0.83	0.43	0.64	0.11
621	N03 DP15	0.29	46.42	2.69	28.16	4.73	59.74	0.17	0.80	0.36	0.48	0.81
622	N03 DP16	0.30	45.17	21.19	28.56	5.83	66.33	0.20	0.89	0.42	0.57	0.17
623	N03 DP17	0.32	45.13	2.29	29.62	5.23	66.57	0.20	0.92	0.43	0.59	0.14
624	N03 DP18	0.31	44.43	2.18	3.99	5.28	58.74	0.18	0.81	0.37	0.56	0.97
625	N03 DP19	0.32	33.96	23.19	39.24	3.79	57.66	0.17	0.60	0.46	0.68	0.66
626	N03 DP20	0.28	29.45	22.19	42.27	6.33	42.38	0.12	0.35	0.26	0.50	0.75
627	N04 SH01		28.42	27.78	37.34	6.53	27.49					
628	N04 SH02	0.34	23.75	3.26	4.89	5.15	43.28	0.13	0.31	0.40	0.54	0.68
629	N04 SH03		13.58	28.63	47.74	1.47	2.73					
630	N04 SH04		21.53	25.45	45.12	8.37	13.62					
631	N04 SH05		27.62	25.86	4.26	6.26	12.16					
632	N04 SH06		24.12	27.38	41.93	6.61	18.91					
633	N04 SH07		25.13	22.86	42.51	9.58	11.33					
634	N04 SH08		9.93	31.96	5.42	7.74	4.97					
635	N04 SH09	0.23	3.94	21.32	41.27	6.47	62.83	0.14	0.44	0.35	0.59	0.92
636	N04 SH10	0.24	4.93	34.12	54.59	6.44	38.28	0.92	0.45	0.31	0.51	0.59
637	N04 SH11	0.26	3.55	21.19	42.59	5.66	44.87	0.11	0.34	0.24	0.48	0.63

ID	Sample	<2μm	Sm	Chl	Ill	Kao	Flitho	f<2μm	fSm	FChl	fIll	fKao
				[%]					[mg/m²/d]				
638	N04 SH12	0.27	18.24	27.85	49.42	4.50	64.22	0.17	0.32	0.47	0.84	0.77
639	N04 SH13		18.25	28.51	45.46	7.78	21.47					
640	N04 SH14		13.44	32.38	46.93	7.26	18.73					
641	N04 SH15	0.29	15.42	28.93	46.23	9.43	38.90	0.11	0.17	0.33	0.52	0.16
642	N04 SH16	0.26	32.65	24.34	37.20	5.87	11.68	0.26	0.85	0.64	0.97	0.15
643	N04 SH17	0.26	35.15	21.28	36.99	7.47	27.61	0.72	0.25	0.15	0.27	0.54
644	N04 SH18	0.28	28.20	25.24	37.78	8.77	33.33	0.93	0.26	0.23	0.35	0.81
645	N04 SH19	0.27	25.84	24.99	41.88	7.30	47.36	0.13	0.34	0.33	0.54	0.93
646	N04 SH20	0.27	28.44	24.97	38.54	8.84	68.25	0.18	0.51	0.45	0.70	0.15
647	N04 MD01	0.29	32.65	21.38	41.12	4.96	47.82	0.14	0.45	0.29	0.57	0.68
648	N04 MD02	0.32	25.97	26.29	42.97	4.78	62.30	0.19	0.49	0.49	0.87	0.90
649	N04 MD03	0.33	2.96	28.12	46.97	3.95	52.78	0.16	0.33	0.45	0.75	0.63
650	N04 MD04		29.45	22.78	41.52	6.25	29.29					
651	N04 MD05		21.27	26.17	45.16	7.56	3.56					
652	N04 MD06		23.97	27.17	42.53	6.32	28.68					
653	N04 MD07		26.92	23.62	42.99	6.46	34.12					
654	N04 MD08		24.90	23.53	46.77	4.82	33.45					
655	N04 MD09		28.98	24.42	4.85	5.75	46.43					
656	N04 MD10	0.27	25.38	26.00	44.67	3.95	85.20	0.23	0.58	0.60	0.13	0.97
657	N04 MD11		23.77	26.23	44.52	5.51	53.84					
658	N04 MD12	0.28	27.25	22.16	44.73	5.96	61.28	0.17	0.47	0.38	0.77	0.12
659	N04 MD13	0.27	32.56	21.57	4.68	5.27	51.56	0.14	0.46	0.34	0.57	0.73
660	N04 MD14	0.27	25.45	23.20	44.39	6.97	46.85	0.13	0.33	0.30	0.58	0.90
661	N04 MD15	0.29	27.50	23.73	43.17	5.67	46.58	0.13	0.37	0.32	0.58	0.76
662	N04 MD16	0.28	18.12	25.82	48.48	7.58	57.51	0.16	0.30	0.42	0.79	0.12
663	N04 MD17	0.26	33.97	23.48	37.58	5.50	18.27	0.28	0.97	0.67	0.16	0.16
664	N04 MD18	0.28	29.65	24.28	4.52	6.13	68.20	0.19	0.55	0.46	0.77	0.11
665	N04 MD19		32.29	23.73	36.45	7.53	5.54					
666	N04 MD20	0.28	33.80	23.25	38.55	5.17	52.33	0.15	0.48	0.34	0.56	0.76
667	N04 DP-01		28.27	23.66	41.47	6.66	35.43					
668	N04 DP-02	0.32	3.25	2.41	4.24	9.87	47.75	0.15	0.47	0.31	0.63	0.14
669	N04 DP-03		28.34	24.66	42.31	5.28	52.32					
670	N04 DP-04		25.45	25.97	42.33	6.33	33.55					
671	N04 DP-05		28.66	23.43	42.92	4.99	34.00					
672	N04 DP-06		26.69	25.47	4.20	7.74	19.79					
673	N04 DP-07		23.17	25.53	44.92	6.39	3.42					
674	N04 DP-08		25.38	23.87	45.23	5.52	29.17					
675	N04 DP-09		24.73	25.38	45.63	5.48	36.93					
676	N04 DP-10	0.29	23.98	27.28	43.99	4.76	53.76	0.15	0.36	0.41	0.67	0.73
677	N04 DP-11		2.75	26.17	46.62	6.47	2.82					
678	N04 DP-12	0.29	31.40	23.65	41.38	4.51	57.87	0.17	0.52	0.39	0.69	0.75
679	N04 DP-13		31.58	22.65	41.96	4.47	46.29					
680	N04 DP-14	0.30	24.67	24.65	44.85	5.83	35.65	0.14	0.26	0.26	0.47	0.65
681	N04 DP-15	0.30	25.68	24.85	44.83	4.65	46.45	0.13	0.35	0.34	0.65	0.63
682	N04 DP-16	0.29	24.21	27.17	42.76	6.70	45.67	0.13	0.32	0.36	0.56	0.89
683	N04 DP-17	0.27	31.61	23.33	41.65	3.45	63.28	0.17	0.55	0.43	0.72	0.59
684	N04 DP-18	0.28	23.53	3.38	4.98	5.18	52.92	0.15	0.34	0.44	0.60	0.76
685	N04 DP-19	0.28	23.92	24.19	44.23	7.67	44.36	0.12	0.30	0.30	0.55	0.95
686	N04 DP-20	0.27	33.55	22.88	37.29	6.36	23.91	0.63	0.21	0.14	0.24	0.42

10.2.2. SCS-NE

ID	Sample	<2μm	Sm	Chl	Ill	Kao	Flitho	f<2μm	fSm	FChl	fIll	fKao
				[%]					[mg/m²/d]				
31	NE01 SH05											
37	NE01 SH11		78.35	1.87	6.82	3.96	34.53					
36	NE01 SH10		79.35	12.47	4.34	3.84	53.72					

Changes of clay mineral and trace element characteristics in the Deep South China Sea

ID	Sample	<2µm	Sm	Chl	Ill	Kao	Flitho	f<2µm	fSm	FChl	fIll	fKao
			[%]					[mg/m²/d]				
35	NE01 SH09											
34	NE01 SH08		74.67	13.54	6.35	5.45	24.66					
32	NE01 SH06											
30	NE01 SH04		82.12	8.82	0.87	8.19	11.18					
29	NE01 SH03											
28	NE01 SH02											
27	NE01 SH01											
33	NE01 SH07											
44	NE01 MD07											
41	NE01 MD04		86.19	1.32	0.76	2.75	1.70					
48	NE01 MD11											
47	NE01 MD10		85.45	7.88	2.71	3.96	68.58					
46	NE01 MD09		84.56	11.30	2.42	2.57	9.67					
45	NE01 MD08											
42	NE01 MD05		85.20	1.39	1.76	2.83	53.57					
38	NE01 MD01											
40	NE01 MD03											
39	NE01 MD02											
43	NE01 MD06		81.17	1.69	3.83	4.34	27.37					
53	NE01 DP05		79.19	1.37	2.24	8.23	43.24					
59	NE01 DP11		86.21	6.74	2.64	4.41	53.88					
58	NE01 DP10		83.72	9.28	3.93	3.67	65.79					
57	NE01 DP09		84.68	6.88	2.63	5.85	1.53					
56	NE01 DP08		82.26	9.58	4.70	4.17	57.31					
54	NE01 DP06		82.89	9.33	3.43	4.77	39.42					
52	NE01 DP04		8.96	1.45	1.56	7.33	14.70					
51	NE01 DP03											
50	NE01 DP02											
49	NE01 DP01											
55	NE01 DP07		78.57	11.46	5.11	5.37	43.50					
62	NE02 SH03		77.45	14.12	4.95	3.59	26.92					
67	NE02 SH08		61.82	22.77	1.99	4.42	4.63					
66	NE02 SH07		7.83	18.38	8.00	3.14	1.57					
65	NE02 SH06		66.83	17.15	9.28	6.78	14.80					
61	NE02 SH02		8.68	13.22	4.36	1.88	23.39					
60	NE02 SH01		76.13	11.93	4.27	7.68	33.22					
63	NE02 SH04		82.46	1.46	2.55	4.95	47.65					
64	NE02 SH05		81.44	1.91	3.59	4.67	22.37					
72	NE03 DP05		79.92	11.60	4.43	4.53	36.67					
80	NE03 DP13											
79	NE03 DP12											
78	NE03 DP11											
77	NE03 DP10		68.32	15.69	9.69	6.30	13.34					
76	NE03 DP09		75.38	11.46	9.78	4.42	28.71					
75	NE03 DP08		78.72	11.99	5.91	4.27	31.46					
73	NE03 DP06		81.55	1.16	3.84	4.46	47.82					
71	NE03 DP04		75.57	13.25	4.66	6.52	28.95					
70	NE03 DP03		74.32	11.86	5.92	7.92	26.49					
69	NE03 DP02		8.40	9.23	4.35	6.25	34.55					
68	NE03 DP01		78.76	12.28	5.22	3.74	22.77					
74	NE03 DP07		78.40	12.62	5.22	4.32	26.35					

10.2.3. SCS-NC

ID	Sample	<2µm	Sm	Chl	Ill	Kao	Flitho	f<2µm	fSm	FChl	fIll	fKao
			[%]					[mg/m²/d]				
1	NC01 SH01	4.67	1.55	3.20	41.65	18.19	16.27	0.75	0.79	0.23	0.38	0.14
2	NC01 SH02	18.25	24.41	2.54	39.25	16.59	19.92	3.63	0.89	0.73	1.42	0.60

ID	Sample	<2µm	Sm	Chl	Ill	Kao	Flitho	f<2µm	fSm	FChl	fIll	fKao
				[%]					[mg/m²/d]			
3	NC01 SH03											
4	NC01 SH04											
5	NC01 SH05	24.48	31.22	25.25	32.33	11.22	2.95	5.11	1.60	1.29	1.65	0.57
6	NC01 SH06	26.16	14.46	3.47	46.49	8.58	24.78	6.46	0.93	1.97	3.51	0.55
7	NC01 SH07	21.59	27.45	27.42	38.58	6.57	25.26	5.48	1.48	1.49	2.83	0.35
8	NC01 SH08	21.27	21.46	23.51	42.86	12.96	17.21	3.62	0.78	0.85	1.52	0.47
9	NC01 SH09											
10	NC01 SH10											
11	NC01 SH11											
12	NC01 SH12											
13	NC01 SH13	19.25	34.58	28.19	32.25	4.99	3.62	5.77	2.00	1.63	1.86	0.29
14	NC01 DP01	12.99	4.47	23.73	27.34	8.54	18.41	2.34	0.95	0.56	0.65	0.27
15	NC01 DP02											
16	NC01 DP03	21.52	74.85	8.92	11.34	4.89	32.45	6.89	5.17	0.62	0.78	0.34
17	NC01 DP04	21.74	53.65	19.99	2.93	5.43	25.16	5.47	2.93	1.93	1.14	0.30
18	NC01 DP05	25.81	5.15	18.12	24.42	7.72	46.73	12.55	6.45	2.18	2.90	0.93
19	NC01 DP06											
20	NC01 DP07											
21	NC01 DP08	22.38	43.81	21.47	28.90	5.91	25.59	5.73	2.59	1.23	1.65	0.34
22	NC01 DP09											
23	NC01 DP10		43.72	2.67	26.35	9.26	17.42					
24	NC01 DP11											
25	NC01 DP12											
26	NC01 DP13											

10.2.4. SCS-C

ID	Sample	<2µm	Sm	Chl	Ill	Kao	Flitho	f<2µm	fSm	FChl	fIll	fKao
				[%]					[mg/m²/d]			
81	C01 SH01											
82	C01 SH02											
83	C01 SH03											
84	C01 SH04											
85	C01 DP01											
86	C01 DP02											
87	C01 DP03											
88	C01 DP04											
89	C01 DP05											
90	C01 DP06											
91	C01 DP07											
92	C01 DP08											
93	C01 DP09											
94	C01 DP10											
95	C01 DP11											
96	C01 DP12											
97	C01 DP13											
98	C02 SH01		23.85	19.92	4.63	16.93	21.81					
99	C02 SH02											
100	C02 SH03		35.42		64.58		17.12					
101	C02 SH04		9.52	25.89	5.86	13.73	34.94					
102	C02 SH05											
103	C02 SH06	0.23	2.61	23.93	42.72	13.39	19.96	0.46	0.95	0.20	0.19	0.61
104	C02 SH07											
105	C02 SH08											
106	C02 SH09											
107	C02 SH10											
108	C02 SH11											
109	C02 SH12											

Changes of clay mineral and trace element characteristics in the Deep South China Sea

ID	Sample	<2µm	Sm	Chl	Ill	Kao	Flitho	f<2µm	fSm	FChl	fIll	fKao
				[%]						[mg/m²/d]		
110	C02 SH13											
111	C02 DP01		54.37	11.56	25.24	8.85	8.27					
112	C02 DP02											
113	C02 DP03		52.95	15.23	26.83	5.74	76.56					
114	C02 DP04		28.12	19.26	37.19	15.43	5.47					
115	C02 DP05											
116	C02 DP06											
117	C02 DP07											
118	C02 DP08											
119	C02 DP09											
120	C02 DP10											
121	C02 DP11											
122	C02 DP12											
123	C02 DP13											
124	C03 SH01		35.34	16.88	33.16	14.78	19.42					
125	C03 SH02		34.57	23.75	38.22	3.45	13.70					
126	C03 SH03		21.43	28.51	4.98	9.78	13.16					
127	C03 SH04		29.39	2.44	37.23	12.95	15.93					
128	C03 SH05											
129	C03 SH06		44.85	11.63	28.67	14.85	27.92					
130	C03 SH07		39.20	18.44	28.43	14.17	36.66					
131	C03 SH08		43.88	16.90	25.36	13.85	37.72					
132	C03 SH09		3.46	19.55	35.15	14.89	29.52					
133	C03 SH10		3.61	23.64	32.66	14.00	2.79					
134	C03 SH11		26.28	2.64	39.24	13.83	2.96					
135	C03 SH12		29.65	2.83	35.41	14.11	11.53					
136	C03 SH13											
137	C03 DP01											
138	C03 DP02											
139	C03 DP03	0.19	5.59	14.34	24.79	1.82	26.26	0.49	0.25	0.79	0.12	0.53
139	C03 DP03		5.59	14.34	24.79	1.82	26.26					
140	C03 DP04		42.59	18.76	28.65	10.00	15.44					
141	C03 DP05		52.12	15.67	23.48	8.73	28.97					
142	C03 DP06		46.86	17.82	28.40	8.43	24.88					
143	C03 DP07		48.71	13.55	26.76	11.62	22.26					
144	C03 DP08		44.12	14.94	3.36	1.58	29.82					
145	C03 DP09	0.20	49.49	16.54	24.51	9.46	37.83	0.74	0.37	0.12	0.18	0.76
145	C03 DP09		49.49	16.54	24.51	9.46	37.83					
146	C03 DP10		44.57	17.53	28.73	9.17	34.29					
147	C03 DP11		5.87	16.58	22.55	1.62	33.79					
148	C03 DP12											
149	C03 DP13		47.34	15.81	25.20	11.65	22.71					
150	C04 SH01											
151	C04 SH02											
152	C04 SH03		22.22	29.27	38.69	1.17	45.56					
153	C04 SH04											
154	C04 SH05		34.28	24.12	29.24	12.68	13.53					
155	C04 SH06											
156	C04 SH07		42.86	17.14	24.36	15.96	13.79					
157	C04 SH08		38.78	21.27	26.62	13.34	13.44					
158	C04 SH09		31.17	18.83	33.73	17.19	18.90					
159	C04 SH10											
160	C04 SH11											
161	C04 MD01		22.61	23.47	41.42	12.49	12.83					
162	C04 MD02											
163	C04 MD03		41.88	19.98	28.98	1.67	16.18					
164	C04 MD04		43.69	2.79	24.82	1.79	35.34					

ID	Sample	<2μm	Sm	Chl	Ill	Kao	Flitho	f<2μm	fSm	FChl	fIll	fKao
					[%]					[mg/m²/d]		
165	C04 MD05		49.00	12.86	22.89	15.34	3.43					
165	C04 MD05	0.22	49.00	12.86	22.89	15.34	3.43	0.67	0.33	0.86	0.15	0.12
166	C04 MD06		35.25	19.14	3.98	14.64	28.44					
167	C04 MD07		42.69	14.60	26.43	16.28	19.53					
168	C04 MD08		36.88	24.69	24.17	15.13	21.82					
169	C04 MD09		42.32	17.92	26.83	12.94	18.75					
170	C04 MD10		38.70	21.97	27.87	12.85	15.60					
171	C04 MD11											
172	C04 MD12											
173	C04 DP01		39.83	17.88	32.42	9.87	14.34					
174	C04 DP02		51.52	15.45	24.77	8.66	17.92					
175	C04 DP03		53.39	15.44	22.95	8.35	19.26					
176	C04 DP04		39.58	17.37	31.13	12.45	26.12					
177	C04 DP05		5.36	13.78	24.77	11.23	23.38					
178	C04 DP06		4.61	19.56	28.35	11.53	24.38					
179	C04 DP07											
180	C04 DP08		37.21	21.46	27.29	14.43	19.20					
181	C04 DP09	0.25	5.19	16.17	21.43	12.23	2.13	0.50	0.25	0.87	0.17	0.65
181	C04 DP09		5.19	16.17	21.43	12.23	2.13					
182	C04 DP10		57.99	12.63	19.59	1.33	22.80					
183	C04 DP11		42.18	19.37	25.76	12.69	17.97					
184	C04 DP12											
185	C05 SH01											
186	C05 SH02											
187	C05 SH03											
188	C05 SH04											
189	C05 SH05											
190	C05 SH06											
191	C05 SH07											
192	C05 SH08											
193	C05 SH09											
194	C05 SH10											
195	C05 SH11											
196	C05 SH12											
197	C05 SH13											
198	C05 DP01											
199	C05 DP02											
200	C05 DP03											
201	C05 DP04											
202	C05 DP05											
203	C05 DP06											
204	C05 DP07											
205	C05 DP08											
206	C05 DP09											
207	C05 DP10											
208	C05 DP11											
209	C05 DP12											
210	C05 DP13											
211	C06 SH01											
212	C06 SH02	26.48	18.43	25.34	41.42	14.82	22.00	5.59	1.30	1.42	2.31	0.83
213	C06 SH03	18.19	28.33	22.24	32.85	16.82	21.57	3.92	1.11	0.86	1.29	0.66
214	C06 SH04											
215	C06 SH05											
216	C06 SH06											
217	C06 SH07	12.65	37.87	23.23	27.97	11.74	47.78	6.42	2.25	1.44	1.69	0.77
218	C06 SH08											
219	C06 SH09											
220	C06 SH10											

ID	Sample	<2µm	Sm	Chl	Ill	Kao	Flitho	f<2µm	fSm	FChl	fIll	fKao
				[%]						[mg/m²/d]		
221	C06 SH11											
222	C06 SH12											
223	C06 SH13											
224	C07 SH01	17.17	43.90	22.11	25.86	8.94	11.35	1.95	0.86	0.44	0.49	0.17
225	C07 SH02	21.36	36.88	22.54	3.83	9.77	8.83	1.89	0.70	0.43	0.58	0.18
226	C07 SH03		29.15	22.12	34.38	14.36	3.42					
227	C07 SH04	23.81	38.93	19.16	3.17	11.74	9.45	2.26	0.88	0.43	0.68	0.26
228	C07 SH05	15.50	38.27	23.69	27.74	1.31	11.85	1.84	0.73	0.44	0.60	0.19
229	C07 SH06											
230	C07 SH07											
231	C07 SH08	26.18	27.60	19.53	33.64	19.71	12.30	3.22	0.89	0.61	1.82	0.63
232	C07 SH09	29.34	29.63	2.44	35.24	14.69	9.34	2.75	0.81	0.56	0.97	0.43
233	C07 SH10	36.93	33.29	26.73	3.74	9.90	1.86	4.11	1.34	1.46	1.23	0.40
234	C07 SH11	3.20	26.76	22.70	37.18	13.36						
235	C07 DP01											
236	C07 DP02											
237	C07 DP03	14.88	34.99	15.82	33.88	15.31	16.53	2.46	0.87	0.39	0.83	0.38
238	C07 DP04	16.47	39.58	21.96	29.65	8.81	17.12	2.82	1.12	0.62	0.84	0.25
239	C07 DP05	21.68	37.24	19.62	31.43	11.72	16.85	3.65	1.36	0.72	1.15	0.43
240	C07 DP06	17.13	37.48	19.56	29.95	13.13	12.24	2.96	0.78	0.42	0.63	0.28
241	C07 DP07											
242	C07 DP08	23.85	35.46	2.77	33.89	9.88	23.44	5.58	1.98	1.16	1.89	0.55
243	C07 DP09	2.20	44.34	18.95	25.92	11.68	24.78	5.64	2.22	0.96	1.30	0.58
244	C07 DP10	21.41	38.59	19.72	3.74	1.95	2.67	4.43	1.78	0.87	1.36	0.48

10.2.5. SCS-W

ID	Sample	<2µm	Sm	Chl	Ill	Kao	Flitho	f<2µm	fSm	FChl	fIll	fKao
				[%]						[mg/m²/d]		
488	W01 SH01											
489	W01 SH02											
490	W01 SH03											
491	W01 SH04											
492	W01 SH05											
493	W01 SH06											
494	W01 SH07											
495	W01 SH08											
496	W01 SH09											
497	W01 SH10											
498	W01 SH11											
499	W01 SH12											
500	W01 SH13											
501	W01 SH14											
502	W01 SH15											
503	W01 SH16											
504	W01 SH17											
505	W01 SH18											
506	W01 SH19											
507	W01 SH20											
508	W02 SH1		22.95	21.79	37.35	17.96	26.57					
509	W02 SH2	0.27	32.24	22.96	33.94	11.73	4.30	0.11	0.36	0.24	0.37	0.13
510	W02 SH3											
511	W02 SH4											
512	W02 SH5		5.17	23.66	47.43	23.73	22.55					
513	W02 SH6	0.27	1.75	25.75	43.85	19.64	46.53	0.13	0.13	0.32	0.55	0.25
514	W02 SH7		11.77	24.32	43.28	2.92	28.62					
515	W02 SH8	0.26	38.85	22.97	26.59	12.47	58.47	0.15	0.58	0.33	0.40	0.19
516	W02 SH9	0.25	35.66	18.88	3.97	14.59	32.24	0.77	0.27	0.15	0.24	0.11

ID	Sample	<2µm	Sm	Chl	Ill	Kao	Flitho	f<2µm	fSm	FChl	fIll	fKao
				[%]				[mg/m²/d]				
517	W02 SH10	0.26	27.98	22.98	35.55	13.57	37.80	0.97	0.27	0.22	0.34	0.13
518	W02 SH11		34.37	24.45	28.79	12.38	28.89					
519	W02 SH12		44.83	17.16	23.82	14.20	17.54					
520	W02 SH13		21.71	23.51	36.66	18.12	7.12					
521	W02 SH14		13.13	24.38	48.60	13.89	1.97					
522	W02 SH15		17.91	25.39	39.84	16.89	3.58					
523	W02 SH16		15.82	23.85	43.93	17.16	1.48					
524	W02 SH17											
525	W02 SH18											
526	W02 SH19											
527	W02 SH20											

10.2.6. SCS-SC

ID	Sample	<2µm	Sm	Chl	Ill	Kao	Flitho	f<2µm	fSm	FChl	fIll	fKao
				[%]				[mg/m²/d]				
245	SC01 SH01											
246	SC01 SH02											
247	SC01 SH03											
248	SC01 SH04											
249	SC01 SH05											
250	SC01 SH06											
251	SC01 SH07											
252	SC01 SH08											
253	SC01 SH09											
254	SC01 SH10	0.29	46.54	15.78	2.89	16.79	211.93	0.68	0.28	0.96	0.13	0.12
255	SC01 SH11											
256	SC01 SH12											
257	SC01 SH13											
258	SC01 SH14											
259	SC01 SH15	0.28	11.67	21.72	45.12	21.49	98.88	0.28	0.32	0.63	0.13	0.60
260	SC01 SH16											
261	SC01 SH17											
262	SC01 SH18											
263	SC01 SH19		41.76	15.84	25.25	17.98	99.89					
264	SC01 SH20											
265	SC01 DP01											
266	SC01 DP02											
267	SC01 DP03											
268	SC01 DP04											
269	SC01 DP05											
270	SC01 DP06											
271	SC01 DP07	0.28	4.97	16.87	24.48	17.74	17.43	0.48	0.20	0.83	0.12	0.85
272	SC01 DP08											
273	SC01 DP09											
274	SC01 DP10	0.27	52.42	12.93	19.28	15.42	27.15	0.73	0.39	0.94	0.14	0.11
275	SC01 DP11		55.14	12.61	17.48	14.77	126.39					
276	SC01 DP12											
277	SC01 DP13											
278	SC01 DP14											
279	SC01 DP15	0.28	17.77	26.75	32.18	23.37	116.89	0.33	0.58	0.87	0.15	0.76
280	SC01 DP16											
281	SC01 DP17											
282	SC01 DP18											
283	SC01 DP19											
284	SC01 DP20											
285	SC02 SH01	0.34	48.16	11.82	22.88	17.14	8.93	0.25	0.12	0.30	0.56	0.42
286	SC02 SH02											

ID	Sample	<2µm	Sm	Chl	Ill	Kao	Flitho	f<2µm	fSm	FChl	fIll	fKao
				[%]					[mg/m²/d]			
287	SC02 SH03	0.29	51.84	12.80	18.41	16.95	76.84	0.22	0.11	0.28	0.47	0.37
288	SC02 SH04	0.37	51.59	14.58	2.73	13.76	64.32	0.20	0.12	0.29	0.40	0.27
289	SC02 SH05											
290	SC02 SH06											
291	SC02 SH07											
292	SC02 SH08											
293	SC02 SH09											
294	SC02 SH10											
295	SC02 SH11											
296	SC02 SH12											
297	SC02 SH13											
298	SC02 SH14											
299	SC02 SH15	0.39	49.78	13.87	19.92	16.43	56.75	0.18	0.87	0.24	0.35	0.29
300	SC02 SH16											
301	SC02 SH17											
302	SC02 SH18											
303	SC02 SH19											
304	SC02 SH20											
305	SC02 DP01	0.32	53.98	11.55	19.90	14.66	111.99	0.35	0.19	0.42	0.69	0.51
306	SC02 DP02	0.39	53.44	11.54	19.61	15.43	132.43	0.50	0.22	0.47	0.83	0.63
307	SC02 DP03	0.32	53.74	11.68	18.95	15.69	83.22	0.26	0.14	0.34	0.50	0.46
308	SC02 DP04	0.30	51.61	11.23	2.39	17.32	7.64	0.29	0.17	0.23	0.43	0.36
309	SC02 DP05	0.32	56.59	12.84	17.51	13.57	81.28	0.25	0.14	0.32	0.43	0.32
310	SC02 DP06	0.29	53.65	12.50	18.66	15.19	67.56	0.20	0.17	0.25	0.37	0.32
311	SC02 DP07	0.29	51.70	3.97	2.18	24.16	41.97	0.13	0.62	0.48	0.24	0.29
312	SC02 DP08	0.34	73.22	7.72	11.42	7.64	43.67	0.15	0.19	0.11	0.17	0.11
313	SC02 DP09	0.32	52.60	11.37	18.84	17.19	125.17	0.47	0.21	0.46	0.77	0.70
314	SC02 DP10	0.29	55.97	12.50	17.75	13.78	86.71	0.25	0.15	0.31	0.45	0.35
315	SC02 DP11	0.27	47.98	14.45	22.84	14.74	57.42	0.15	0.74	0.22	0.35	0.23
316	SC02 DP12		56.16	12.45	17.14	14.25	42.76					
317	SC02 DP13	0.32	5.72	13.23	19.62	16.46	73.80	0.24	0.12	0.32	0.47	0.39
318	SC02 DP14	0.30	49.44	12.34	2.80	17.58	125.67	0.38	0.19	0.46	0.78	0.66
319	SC02 DP15	0.30	54.68	11.53	19.80	14.60	96.69	0.29	0.16	0.33	0.57	0.42
320	SC02 DP16	0.28	49.92	13.67	21.78	15.39	79.89	0.22	0.11	0.29	0.48	0.34
321	SC02 DP17	0.28	54.17	12.57	18.95	14.31	7.98	0.20	0.16	0.25	0.37	0.28
322	SC02 DP18		48.65	15.64	21.46	14.83	45.94					
323	SC02 DP19		48.66	15.45	21.55	14.38	37.95					
324	SC02 DP20		54.73	13.22	19.23	13.55	47.19					

10.2.7. SCS-SW

ID	Sample	<2µm	Sm	Chl	Ill	Kao	Flitho	f<2µm	fSm	FChl	fIll	fKao
				[%]					[mg/m²/d]			
374	SW01 SH01	1.93	56.49	12.87	15.95	14.76	17.52	18.64	1.53	2.39	2.97	2.75
375	SW01 SH02	15.83	42.12	15.88	24.42	17.57	36.60	5.79	2.44	0.92	1.41	1.18
376	SW01 SH03											
377	SW01 SH04	14.29	43.71	15.58	22.87	17.84	136.96	19.57	8.56	3.48	4.48	3.49
378	SW01 SH05	13.31	54.73	11.93	19.13	14.29	66.59	8.86	4.86	1.58	1.70	1.26
379	SW01 SH06	0.28	61.29	1.67	15.12	13.22	176.62	0.49	0.33	0.53	0.74	0.64
380	SW01 SH07	0.25	65.36	1.13	12.82	11.71	34.48	0.86	0.56	0.87	0.12	0.11
381	SW01 SH08	14.66	67.78	8.48	11.48	12.27	343.86	5.42	34.17	4.27	5.79	6.18
382	SW01 SH09	0.38	55.74	13.48	17.49	13.29	52.44	0.16	0.88	0.21	0.28	0.30
383	SW01 SH10											
384	SW02 DP02											
385	SW02 DP03											
386	SW04 SH01											
387	SW04 SH02											
388	SW04 SH03		13.75	23.63	41.72	2.95	24.00					

ID	Sample	<2μm	Sm	Chl	Ill	Kao	Flitho	f<2μm	fSm	FChl	fIll	fKao
					[%]					[mg/m²/d]		
389	SW04 SH04		27.85	24.33	32.43	15.39	24.85					
390	SW04 SH05											
391	SW04 SH06		31.16	25.42	3.32	13.40	32.94					
392	SW04 SH07	0.25	49.73	13.98	17.58	18.72	138.69	0.35	0.17	0.49	0.61	0.65
393	SW04 SH08	0.26	41.36	15.43	24.15	19.17	133.26	0.35	0.14	0.53	0.84	0.66
394	SW04 SH09											
395	SW04 SH10											
396	SW04 SH11											
397	SW04 SH12											
398	SW04 SH13											
399	SW04 SH14											
400	SW04 SH15	0.29	51.83	13.26	18.50	16.41	115.23	0.33	0.17	0.44	0.61	0.55
401	SW04 SH16											
402	SW04 SH17											
403	SW04 SH18											
404	SW04 SH19											
405	SW04 SH20											
406	SW04 SH21	0.36	65.30	9.49	11.35	13.87	426.56	1.55	1.11	0.15	0.18	0.21
407	SW04 DP01		35.55	17.75	28.49	18.25	52.73					
408	SW04 DP02		47.68	16.53	24.13	11.68	34.50					
409	SW04 DP03											
410	SW04 DP04											
411	SW04 DP05	0.28	69.95	8.55	1.33	11.22	286.46	0.60	0.42	0.59	0.62	0.67
412	SW04 DP06	0.22	53.38	14.43	18.25	13.95	292.27	0.65	0.35	0.93	0.12	0.94
413	SW04 DP07											
414	SW04 DP08		39.76	19.39	25.12	16.77	135.15					
414	SW04 DP08	0.25	39.76	19.39	25.12	16.77	135.15	0.34	0.13	0.65	0.86	0.57
415	SW04 DP09		64.37	1.77	13.96	1.96	74.97					
416	SW04 DP10		44.65	17.59	23.92	13.84	49.69					
417	SW04 DP11	0.35	54.47	13.97	2.44	11.52	239.31	0.73	0.40	0.12	0.15	0.84
418	SW04 DP12	0.30	45.32	15.28	21.73	17.68	317.74	0.94	0.43	0.14	0.24	0.17
419	SW04 DP13	0.27	57.41	11.22	16.76	14.63	193.52	0.52	0.30	0.58	0.88	0.76
420	SW04 DP14	0.22	54.53	12.15	18.62	14.70	271.52	0.70	0.33	0.75	0.11	0.90
421	SW04 DP15	0.26	59.23	11.13	15.53	14.11	165.24	0.42	0.25	0.47	0.66	0.60
422	SW04 DP16	0.27	6.41	1.76	15.14	13.68	31.34	0.81	0.49	0.88	0.12	0.11
423	SW04 DP17	0.28	52.95	12.29	19.25	15.55	319.58	0.89	0.47	0.19	0.17	0.14
424	SW04 DP18	0.33	61.32	1.99	14.43	13.25	791.39	2.54	1.56	0.28	0.37	0.34
425	SW04 DP19	0.28	62.43	11.41	11.81	14.35	11.94	2.76	1.72	0.32	0.33	0.40
426	SW04 DP20											
427	SW04 DP21		5.96	13.21	19.00	16.84	42.45					
428	SW05 SH01											
429	SW05 SH02	0.27	58.77	1.47	14.62	16.14	31.15	0.84	0.49	0.87	0.12	0.13
430	SW05 SH03											
431	SW05 SH04	0.23	49.76	14.46	17.58	19.13	247.32	0.56	0.29	0.79	0.96	0.18
432	SW05 SH05	0.27	56.89	11.59	16.46	15.73	14.96	0.38	0.22	0.44	0.62	0.57
433	SW05 SH06		58.83	11.28	16.74	13.14	54.87					
434	SW05 SH07	0.26	59.76	1.15	14.48	15.61	461.24	1.19	0.71	0.12	0.17	0.19
435	SW05 SH08	0.23	61.88	1.72	13.26	14.14	347.18	0.84	0.50	0.86	0.16	0.11
436	SW05 SH09											
437	SW05 SH10											
438	SW05 SH11											
439	SW05 SH12											
440	SW05 SH13											
441	SW05 SH14											
442	SW05 SH15											
443	SW05 SH16											
444	SW05 SH17											
445	SW05 SH18											

Changes of clay mineral and trace element characteristics in the Deep South China Sea

ID	Sample	<2µm	Sm	Chl	Ill	Kao	Flitho	f<2µm	fSm	FChl	fIll	fKao
				[%]					[mg/m²/d]			
446	SW05 SH19											
447	SW05 SH20											
448	SW06 SH01		57.86	12.51	16.70	13.73	54.45					
449	SW06 SH02		41.97	16.12	25.82	16.87	24.63					
450	SW06 SH03	0.30	4.93	16.99	25.87	16.22	73.22	0.21	0.87	0.36	0.56	0.35
451	SW06 SH04											
452	SW06 SH05	0.34	58.15	12.44	14.44	14.97	46.53	0.16	0.91	0.20	0.23	0.24
453	SW06 SH06											
454	SW06 SH07		54.62	11.78	17.17	16.43	46.93					
455	SW06 SH08		45.36	14.99	23.38	16.28	44.97					
456	SW06 SH09											
457	SW06 SH10											
458	SW06 SH11											
459	SW06 SH12											
460	SW06 SH13											
461	SW06 SH14											
462	SW06 SH15											
463	SW06 SH16											
464	SW06 SH17											
465	SW06 SH18											
466	SW06 SH19											
467	SW06 SH20											
468	SW06 DP01	0.32	48.76	13.62	21.74	15.88	17.13	0.32	0.16	0.44	0.73	0.51
469	SW06 DP02											
470	SW06 DP03											
471	SW06 DP04	0.29	48.35	14.46	21.73	15.52	86.78	0.26	0.12	0.37	0.56	0.40
472	SW06 DP05	0.29	53.22	11.85	16.44	18.69	14.76	0.41	0.22	0.49	0.68	0.77
473	SW06 DP06	0.27	54.64	12.33	17.82	15.25	391.84	1.65	0.58	0.14	0.19	0.16
474	SW06 DP07	0.22	68.23	1.53	1.85	1.40	642.88	1.44	0.99	0.15	0.16	0.15
475	SW06 DP08	0.24	6.18	11.93	15.87	12.47	161.17	0.39	0.23	0.46	0.62	0.47
476	SW06 DP09											
477	SW06 DP10											
478	SW06 DP11	0.29	68.63	8.88	11.18	11.32	195.44	0.56	0.39	0.50	0.63	0.64
479	SW06 DP12	0.24	52.85	13.28	19.55	14.32	171.41	0.46	0.21	0.54	0.79	0.58
480	SW06 DP13											
481	SW06 DP14											
482	SW06 DP15											
483	SW06 DP16											
484	SW06 DP17											
485	SW06 DP18											
486	SW06 DP19											
487	SW06 DP20											

10.2.8. SCS-S

ID	Sample	<2µm	Sm	Chl	Ill	Kao	Flitho	f<2µm	fSm	FChl	fIll	fKao
				[%]					[mg/m²/d]			
325	S01 DP01		5.64	13.59	2.85	14.93	39.83					
326	S01 DP02											
327	S01 DP03		42.18	16.24	25.96	15.63	25.31					
328	S01 DP04		36.34	17.35	27.54	18.82	44.97					
329	S01 DP05											
330	S01 DP06		4.63	15.68	24.94	19.62	27.39					
331	S01 DP07	0.32	46.54	13.74	21.94	17.78	351.99	1.14	0.53	0.16	0.25	0.23
332	S01 DP08	0.28	5.33	13.23	18.40	18.40	58.24	1.70	0.81	0.21	0.30	0.29
333	S01 DP09	0.28	54.20	12.68	16.84	16.32	189.55	0.54	0.29	0.68	0.94	0.88
334	S01 DP10		47.94	13.82	2.54	17.75	75.67					
335	S01 DP11		46.39	14.32	21.75	17.54	48.93					

ID	Sample	<2µm	Sm	Chl	Ill	Kao	Flitho	f<2µm	fSm	FChl	fIll	fKao
				[%]						[mg/m²/d]		
336	S01 DP12		33.65	17.77	28.20	2.45	155.35					
337	S01 DP13	0.26	49.66	12.77	21.19	16.38	86.36	0.23	0.11	0.29	0.48	0.37
338	S01 DP14	0.30	49.25	13.85	2.73	16.18	72.58	0.21	0.15	0.30	0.44	0.35
339	S01 DP15		5.00	16.23	27.24	15.54	44.25					
340	S01 DP16	0.32	4.34	14.94	26.18	18.54	84.99	0.26	0.13	0.38	0.67	0.48
341	S01 DP17	0.32	48.46	13.76	2.77	17.42	399.94	1.27	0.62	0.17	0.26	0.22
342	S01 DP18	0.33	5.77	13.76	17.90	17.57	489.59	1.59	0.89	0.22	0.29	0.28
343	S01 DP19	0.32	5.92	13.00	19.18	17.73	183.22	0.59	0.30	0.77	0.11	0.15
344	S01 DP20	0.32	52.50	13.29	19.63	15.64	83.32	0.25	0.13	0.33	0.48	0.39
345	S02 SH01		26.34	23.35	35.35	14.96	27.84					
346	S02 SH02		26.68	18.55	31.42	23.77	25.89					
347	S02 SH03	0.25	45.68	14.85	22.15	17.33	56.32	0.14	0.65	0.22	0.31	0.25
348	S02 SH04		41.15	14.20	27.38	17.27	2.98					
349	S02 SH05		36.87	15.24	3.46	17.44	16.12					
350	S02 SH06		26.78	18.16	34.51	2.54	16.31					
351	S02 SH07		3.32	19.27	3.99	19.42	13.92					
352	S02 SH08		16.57	2.89	4.53	22.13	18.21					
353	S02 SH09											
354	S02 SH10		52.96	11.48	19.36	17.62	56.33					
355	S02 DP01		44.88	15.74	24.26	15.13	52.84					
356	S02 DP02	0.29	5.25	15.23	19.78	15.67	97.36	0.29	0.14	0.44	0.55	0.45
357	S02 DP03	0.33	59.51	1.33	16.64	13.51	72.34	0.22	0.13	0.22	0.36	0.29
358	S02 DP04		47.46	15.67	21.69	15.17	45.68					
359	S02 DP05		38.37	18.69	27.55	15.40	24.79					
360	S02 DP06											
361	S02 DP07		19.47	23.38	39.11	18.52	38.59					
362	S02 DP08		51.19	13.83	19.53	15.45	53.97					
363	S02 DP09	0.39	53.98	13.15	18.84	14.36	82.65	0.26	0.14	0.34	0.48	0.36
364	S02 DP10	0.25	61.40	1.86	14.27	13.56	959.98	2.43	1.49	0.26	0.35	0.33
365	S02 DP11	0.26	55.84	12.48	18.45	13.28	62.14	0.16	0.91	0.24	0.40	0.22
366	S02 DP12	0.29	53.56	13.85	16.72	15.92	198.32	0.57	0.33	0.79	0.95	0.93
367	S02 DP13	0.30	56.17	11.94	16.37	15.52	19.55	0.32	0.18	0.39	0.53	0.54
368	S02 DP14	0.29	15.64	25.20	35.99	23.18	83.92	0.25	0.39	0.62	0.89	0.57
369	S02 DP15											
370	S02 DP16											
371	S02 DP17											
372	S02 DP18											
373	S02 DP19											

10.3. Lanthanides

10.3.1. SCS-N

Sample	La PAAS	Ce PAAS	Pr PAAS	Nd PAAS	Sm PAAS	Eu PAAS	Gd PAAS	Tb PAAS	Dy PAAS	Ho PAAS	Er PAAS	Tm PAAS	Yb PAAS	Lu PAAS
N01 SH05	0.480	0.466	0.483	0.445	0.493	0.516	0.479	0.400	0.356	0.322	0.312	0.321	0.307	0.294
N01 SH06	0.667	0.640	0.625	0.591	0.658	0.653	0.603	0.533	0.513	0.470	0.535	0.502	0.609	0.469
N01 SH06	0.539	0.518	0.547	0.508	0.572	0.606	0.558	0.481	0.430	0.388	0.380	0.392	0.373	0.356
N01 SH07	0.288	0.281	0.291	0.270	0.313	0.331	0.315	0.267	0.243	0.219	0.216	0.221	0.213	0.208
N01 SH08	0.415	0.386	0.390	0.382	0.469	0.457	0.445	0.398	0.392	0.384	0.374	0.381	0.360	0.343
N01 SH08	0.185	0.175	0.187	0.175	0.207	0.228	0.218	0.191	0.174	0.160	0.156	0.164	0.153	0.143
N01 SH09	0.255	0.246	0.237	0.229	0.264	0.256	0.251	0.228	0.243	0.215	0.220	0.229	0.243	0.231
N01 SH09	0.138	0.129	0.140	0.133	0.160	0.184	0.175	0.157	0.146	0.137	0.133	0.138	0.132	0.127
N01 SH10	0.223	0.209	0.213	0.206	0.243	0.258	0.234	0.225	0.231	0.204	0.218	0.221	0.224	0.223
N01 SH10	0.156	0.144	0.160	0.154	0.187	0.221	0.202	0.174	0.163	0.151	0.144	0.149	0.142	0.136
N01 SH11	0.387	0.494	0.351	0.334	0.380	0.399	0.379	0.360	0.356	0.352	0.369	0.425	0.399	0.404
N01 SH11	0.173	0.165	0.174	0.167	0.199	0.227	0.211	0.188	0.176	0.164	0.158	0.160	0.159	0.149

Changes of clay mineral and trace element characteristics in the Deep South China Sea

Sample	La PAAS	Ce PAAS	Pr PAAS	Nd PAAS	Sm PAAS	Eu PAAS	Gd PAAS	Tb PAAS	Dy PAAS	Ho PAAS	Er PAAS	Tm PAAS	Yb PAAS	Lu PAAS
N01 SH12	0.152	0.145	0.156	0.149	0.179	0.200	0.190	0.164	0.152	0.142	0.138	0.144	0.139	0.133
N01 DP02	0.523	0.490	0.499	0.481	0.554	0.550	0.523	0.451	0.455	0.425	0.436	0.417	0.430	0.424
N01 DP03	0.511	0.491	0.499	0.479	0.570	0.551	0.573	0.498	0.490	0.447	0.462	0.440	0.469	0.444
N01 DP04	0.614	0.603	0.620	0.588	0.680	0.761	0.712	0.689	0.686	0.613	0.681	0.708	0.727	0.670
N01 DP05	0.697	0.716	0.678	0.649	0.773	0.799	0.790	0.722	0.863	0.614	0.666	0.766	0.764	0.701
N01 DP05	0.393	0.381	0.403	0.383	0.442	0.477	0.444	0.377	0.338	0.304	0.295	0.304	0.291	0.275
N01 DP06	0.669	0.645	0.644	0.611	0.698	0.727	0.668	0.604	0.580	0.525	0.506	0.552	0.559	0.523
N01 DP06	0.500	0.484	0.515	0.485	0.556	0.595	0.558	0.471	0.423	0.383	0.370	0.382	0.361	0.347
N01 DP07	0.227	0.215	0.232	0.220	0.263	0.290	0.272	0.231	0.207	0.189	0.178	0.187	0.181	0.172
N01 DP10	0.807	0.723	0.708	0.660	0.720	0.719	0.670	0.561	0.563	0.526	0.538	0.557	0.587	0.500
N01 DP11	0.184	0.209	0.177	0.164	0.201	0.239	0.233	0.194	0.181	0.174	0.170	0.185	0.170	0.174
N01 DP12	0.398	0.384	0.391	0.377	0.440	0.436	0.446	0.416	0.416	0.371	0.397	0.404	0.411	0.392
N02 DP02	0.476	0.446	0.455	0.431	0.489	0.532	0.450	0.407	0.395	0.354	0.357	0.387	0.366	0.365
N02 DP03	0.648	0.635	0.638	0.602	0.755	0.750	0.699	0.617	0.636	0.604	0.576	0.557	0.563	0.545
N02 DP04	0.548	0.523	0.532	0.502	0.577	0.584	0.594	0.512	0.529	0.494	0.488	0.477	0.461	0.438
N02 DP05	0.336	0.326	0.350	0.330	0.389	0.430	0.411	0.360	0.326	0.300	0.291	0.300	0.290	0.277
N02 DP06	0.301	0.291	0.312	0.296	0.345	0.379	0.367	0.321	0.298	0.274	0.267	0.274	0.267	0.253
N02 DP07	0.361	0.348	0.375	0.355	0.416	0.443	0.424	0.367	0.329	0.304	0.291	0.300	0.291	0.278
N03 SH01	0.225	0.208	0.218	0.221	0.276	0.356	0.297	0.271	0.259	0.244	0.235	0.244	0.229	0.232
N03 SH02	0.258	0.239	0.251	0.251	0.311	0.393	0.327	0.294	0.278	0.259	0.249	0.262	0.244	0.246
N03 SH03	0.262	0.246	0.258	0.257	0.315	0.394	0.329	0.297	0.280	0.261	0.249	0.266	0.248	0.244
N03 SH04	0.151	0.140	0.146	0.147	0.184	0.239	0.201	0.186	0.174	0.164	0.159	0.168	0.157	0.161
N03 SH05	0.202	0.189	0.199	0.203	0.254	0.336	0.276	0.250	0.239	0.224	0.214	0.221	0.209	0.210
N03 SH06	0.226	0.212	0.222	0.226	0.279	0.356	0.297	0.265	0.249	0.234	0.224	0.236	0.219	0.218
N03 SH08	0.183	0.172	0.179	0.181	0.225	0.285	0.237	0.218	0.209	0.199	0.191	0.207	0.194	0.194
N03 SH09	0.341	0.321	0.332	0.330	0.391	0.463	0.402	0.362	0.340	0.316	0.306	0.325	0.303	0.302
N03 SH10	0.513	0.489	0.502	0.496	0.580	0.653	0.572	0.501	0.465	0.425	0.408	0.434	0.406	0.400
N03 SH11	0.226	0.214	0.222	0.223	0.270	0.333	0.285	0.259	0.250	0.237	0.229	0.244	0.231	0.234
N03 SH12	0.306	0.290	0.301	0.305	0.364	0.442	0.377	0.340	0.328	0.308	0.302	0.321	0.308	0.308
N03 SH13	0.277	0.263	0.277	0.279	0.339	0.420	0.346	0.308	0.287	0.267	0.256	0.269	0.253	0.254
N03 SH14	0.119	0.111	0.119	0.121	0.155	0.205	0.171	0.157	0.153	0.146	0.143	0.158	0.146	0.151
N03 Sh15	0.177	0.166	0.177	0.182	0.233	0.309	0.257	0.238	0.232	0.222	0.216	0.231	0.217	0.219
N03 SH16	0.203	0.190	0.202	0.206	0.259	0.340	0.278	0.256	0.247	0.231	0.226	0.239	0.224	0.226
N03 SH17	0.330	0.313	0.326	0.329	0.396	0.477	0.405	0.359	0.337	0.316	0.306	0.324	0.311	0.310
N03 SH18	0.530	0.501	0.513	0.505	0.581	0.658	0.579	0.514	0.482	0.447	0.435	0.462	0.442	0.438
N03 SH19	0.415	0.392	0.409	0.403	0.475	0.553	0.476	0.423	0.390	0.361	0.348	0.362	0.342	0.341
N03 SH20	0.296	0.279	0.290	0.291	0.348	0.415	0.346	0.300	0.278	0.258	0.250	0.262	0.247	0.247
N03 MD02	0.305	0.287	0.304	0.305	0.376	0.467	0.394	0.353	0.333	0.309	0.298	0.318	0.297	0.299
N03 MD03	0.335	0.319	0.332	0.332	0.406	0.505	0.423	0.381	0.362	0.335	0.324	0.341	0.320	0.318
N03 MD04	0.242	0.231	0.241	0.245	0.300	0.389	0.326	0.298	0.286	0.270	0.261	0.275	0.258	0.260
N03 MD11	0.354	0.336	0.348	0.346	0.412	0.488	0.422	0.376	0.356	0.330	0.321	0.339	0.320	0.316
N03 MD13	0.394	0.374	0.389	0.387	0.462	0.554	0.471	0.424	0.400	0.375	0.362	0.377	0.359	0.358
N03 MD14	0.262	0.246	0.259	0.263	0.325	0.403	0.344	0.311	0.299	0.280	0.270	0.285	0.266	0.271
N03 MD15	0.300	0.284	0.299	0.303	0.370	0.471	0.394	0.354	0.340	0.319	0.309	0.328	0.311	0.311
N03 MD16	0.311	0.294	0.310	0.309	0.372	0.458	0.388	0.351	0.332	0.313	0.302	0.321	0.304	0.305
N03 MD17	0.397	0.377	0.393	0.395	0.476	0.587	0.492	0.446	0.422	0.397	0.385	0.400	0.383	0.383
N03 DP02	0.372	0.357	0.368	0.371	0.447	0.551	0.466	0.420	0.396	0.373	0.360	0.371	0.357	0.355
N03 DP03	0.385	0.374	0.386	0.390	0.471	0.577	0.484	0.437	0.412	0.382	0.366	0.381	0.365	0.366
N03 DP04	0.380	0.367	0.379	0.379	0.457	0.561	0.481	0.430	0.407	0.379	0.367	0.383	0.361	0.360
N03 MD10	0.367	0.361	0.364	0.368	0.445	0.549	0.466	0.421	0.403	0.375	0.362	0.384	0.361	0.366
N03 DP11	0.427	0.416	0.424	0.422	0.503	0.607	0.523	0.469	0.445	0.415	0.400	0.418	0.404	0.398
N03 DP12	0.368	0.358	0.365	0.365	0.437	0.523	0.444	0.401	0.380	0.359	0.344	0.366	0.347	0.343
N03 DP15	0.339	0.326	0.336	0.338	0.408	0.496	0.427	0.384	0.363	0.342	0.332	0.352	0.334	0.335
N03 DP16	0.347	0.335	0.345	0.347	0.425	0.524	0.441	0.396	0.375	0.353	0.345	0.359	0.338	0.342
N04 SH03	0.267	0.250	0.264	0.268	0.330	0.422	0.347	0.312	0.296	0.275	0.266	0.280	0.264	0.262
N04 SH04	0.300	0.282	0.294	0.297	0.362	0.463	0.378	0.337	0.315	0.297	0.285	0.302	0.281	0.284
N04 SH05	0.223	0.210	0.221	0.224	0.274	0.347	0.285	0.254	0.236	0.223	0.215	0.226	0.210	0.209
N04 SH06	0.227	0.211	0.223	0.226	0.282	0.370	0.303	0.269	0.256	0.240	0.231	0.244	0.228	0.230

Sample	La PAAS	Ce PAAS	Pr PAAS	Nd PAAS	Sm PAAS	Eu PAAS	Gd PAAS	Tb PAAS	Dy PAAS	Ho PAAS	Er PAAS	Tm PAAS	Yb PAAS	Lu PAAS
N04 SH09	0.560	0.532	0.551	0.542	0.627	0.706	0.614	0.532	0.486	0.444	0.423	0.440	0.419	0.409
N04 SH10	0.275	0.256	0.269	0.268	0.317	0.365	0.317	0.275	0.254	0.235	0.230	0.243	0.230	0.234
N04 SH11	0.410	0.386	0.400	0.398	0.465	0.535	0.463	0.404	0.373	0.342	0.330	0.345	0.329	0.325
N04 SH17	0.310	0.290	0.305	0.304	0.366	0.428	0.371	0.330	0.306	0.286	0.277	0.292	0.278	0.276
N04 SH18	0.328	0.305	0.320	0.319	0.380	0.459	0.387	0.344	0.316	0.293	0.281	0.298	0.277	0.277
N04 SH19	0.315	0.294	0.308	0.308	0.368	0.441	0.379	0.343	0.325	0.303	0.292	0.308	0.290	0.287
N04 MD03	0.393	0.369	0.385	0.386	0.461	0.557	0.480	0.433	0.408	0.380	0.364	0.387	0.366	0.367
N04 MD04	0.387	0.366	0.384	0.384	0.461	0.564	0.482	0.438	0.416	0.393	0.376	0.395	0.379	0.375
N04 MD05	0.340	0.322	0.336	0.336	0.410	0.498	0.426	0.380	0.360	0.338	0.325	0.343	0.325	0.327
N04 MD06	0.344	0.324	0.339	0.341	0.412	0.513	0.429	0.383	0.359	0.336	0.321	0.337	0.318	0.316
N04 MD18	0.394	0.367	0.386	0.384	0.455	0.537	0.468	0.415	0.386	0.358	0.343	0.359	0.341	0.335
N04 MD19	0.394	0.368	0.388	0.387	0.460	0.549	0.473	0.423	0.398	0.372	0.357	0.375	0.357	0.354
N04 DP03	0.416	0.398	0.411	0.410	0.492	0.593	0.502	0.450	0.424	0.396	0.383	0.406	0.384	0.380
N04 DP04	0.427	0.411	0.424	0.422	0.509	0.623	0.527	0.466	0.442	0.411	0.395	0.417	0.392	0.389
N04 DP05	0.354	0.343	0.351	0.352	0.424	0.521	0.439	0.391	0.370	0.346	0.331	0.347	0.329	0.323
N04 DP06	0.349	0.337	0.348	0.349	0.423	0.525	0.447	0.402	0.381	0.361	0.351	0.369	0.351	0.349
N04 DP18	0.412	0.392	0.407	0.405	0.480	0.568	0.496	0.445	0.416	0.387	0.369	0.390	0.371	0.368
N04 DP19	0.350	0.332	0.347	0.347	0.415	0.495	0.425	0.377	0.356	0.334	0.320	0.335	0.320	0.313

10.3.2. SCS-NE

Sample	La PAAS	Ce PAAS	Pr PAAS	Nd PAAS	Sm PAAS	Eu PAAS	Gd PAAS	Tb PAAS	Dy PAAS	Ho PAAS	Er PAAS	Tm PAAS	Yb PAAS	Lu PAAS
NE02 SH01	0.149	0.168	0.181	0.201	0.317	0.441	0.401	0.403	0.429	0.409	0.409	0.427	0.420	0.401
NE02 SH02	0.153	0.172	0.178	0.189	0.278	0.377	0.347	0.329	0.340	0.324	0.321	0.339	0.321	0.313
NE02 SH03	0.153	0.172	0.169	0.176	0.249	0.333	0.307	0.289	0.299	0.285	0.281	0.284	0.280	0.277
NE02 SH04	0.158	0.158	0.163	0.163	0.220	0.310	0.270	0.256	0.268	0.255	0.254	0.266	0.256	0.258
NE02 SH05	0.136	0.143	0.142	0.144	0.196	0.265	0.236	0.224	0.232	0.219	0.214	0.227	0.216	0.218
NE02 SH06	0.168	0.186	0.177	0.183	0.249	0.331	0.300	0.281	0.287	0.273	0.267	0.281	0.263	0.259
NE02 SH07	0.128	0.137	0.137	0.141	0.194	0.257	0.242	0.225	0.231	0.216	0.214	0.222	0.216	0.209
NE02 SH08	0.112	0.117	0.118	0.121	0.164	0.217	0.204	0.199	0.196	0.185	0.184	0.181	0.174	0.175
NE02 SH09	0.116	0.132	0.135	0.146	0.216	0.299	0.266	0.263	0.277	0.265	0.264	0.273	0.262	0.257
NE02 SH10	0.143	0.160	0.167	0.181	0.261	0.363	0.322	0.309	0.314	0.299	0.296	0.302	0.297	0.279
NE02 SH11	0.143	0.150	0.158	0.166	0.230	0.314	0.290	0.270	0.278	0.264	0.266	0.271	0.255	0.252
NE01 MD04	0.171	0.182	0.188	0.188	0.258	0.363	0.316	0.302	0.300	0.286	0.279	0.298	0.298	0.285
NE01 MD06	0.177	0.183	0.194	0.195	0.262	0.348	0.313	0.292	0.284	0.271	0.265	0.273	0.263	0.256
NE01 MD09	0.172	0.185	0.214	0.229	0.342	0.498	0.424	0.418	0.421	0.404	0.396	0.417	0.399	0.383
NE01 DP04	0.146	0.143	0.163	0.167	0.235	0.328	0.284	0.274	0.272	0.261	0.256	0.271	0.269	0.264
NE01 DP06	0.119	0.122	0.133	0.132	0.178	0.237	0.213	0.200	0.197	0.190	0.184	0.188	0.185	0.183
NE01 DP09	0.194	0.207	0.236	0.248	0.359	0.506	0.434	0.427	0.426	0.404	0.396	0.415	0.408	0.387

10.3.3. SCS-NC

Sample	La PAAS	Ce PAAS	Pr PAAS	Nd PAAS	Sm PAAS	Eu PAAS	Gd PAAS	Tb PAAS	Dy PAAS	Ho PAAS	Er PAAS	Tm PAAS	Yb PAAS	Lu PAAS
NC01 SH04	0.204	0.212	0.204	0.201	0.250	0.287	0.283	0.253	0.252	0.234	0.230	0.235	0.221	0.216

10.3.4. SCS-C

Sample	La PAAS	Ce PAAS	Pr PAAS	Nd PAAS	Sm PAAS	Eu PAAS	Gd PAAS	Tb PAAS	Dy PAAS	Ho PAAS	Er PAAS	Tm PAAS	Yb PAAS	Lu PAAS
C02 SH01	0.227	0.292	0.221	0.202	0.228	0.254	0.265	0.224	0.212	0.189	0.208	0.202	0.179	0.188
C02 SH02	0.262	0.346	0.245	0.233	0.278	0.300	0.282	0.254	0.244	0.221	0.237	0.226	0.211	0.210
C02 SH03	0.165	0.227	0.146	0.131	0.141	0.178	0.130	0.129	0.124	0.110	0.111	0.106	0.112	0.102
C02 SH04	0.111	0.142	0.104	0.103	0.130	0.139	0.108	0.109	0.113	0.101	0.105	0.088	0.111	0.105
C02 SH05	0.287	0.347	0.267	0.252	0.298	0.348	0.310	0.272	0.270	0.235	0.261	0.253	0.244	0.235
C02 SH06	0.198	0.260	0.197	0.188	0.234	0.255	0.259	0.211	0.206	0.198	0.203	0.179	0.179	0.176
C02 SH07	0.195	0.252	0.196	0.182	0.229	0.233	0.240	0.215	0.217	0.197	0.194	0.218	0.180	0.163
C02 SH08	0.063	0.075	0.059	0.055	0.064	0.091	0.077	0.070	0.076	0.068	0.057	0.062	0.070	0.075
C02 SH09	0.174	0.217	0.168	0.160	0.220	0.193	0.198	0.189	0.175	0.168	0.161	0.172	0.159	0.170
C02 SH10	0.166	0.192	0.160	0.152	0.187	0.216	0.200	0.188	0.179	0.155	0.185	0.174	0.165	0.158
C02 SH11	0.191	0.199	0.178	0.170	0.218	0.204	0.228	0.209	0.194	0.166	0.190	0.187	0.191	0.160

Changes of clay mineral and trace element characteristics in the Deep South China Sea

Sample	La PAAS	Ce PAAS	Pr PAAS	Nd PAAS	Sm PAAS	Eu PAAS	Gd PAAS	Tb PAAS	Dy PAAS	Ho PAAS	Er PAAS	Tm PAAS	Yb PAAS	Lu PAAS
C02 SH12	0.239	0.266	0.231	0.217	0.268	0.305	0.297	0.255	0.247	0.235	0.219	0.227	0.186	0.201
C02 SH13	0.209	0.296	0.210	0.199	0.234	0.311	0.244	0.259	0.229	0.197	0.249	0.212	0.203	0.185
C03 SH01	0.152	0.236	0.145	0.140	0.173	0.193	0.191	0.166	0.161	0.146	0.156	0.147	0.155	0.156
C03 SH02	0.087	0.153	0.087	0.082	0.093	0.112	0.131	0.101	0.093	0.077	0.100	0.083	0.092	0.101
C03 SH03	0.116	0.170	0.114	0.112	0.136	0.151	0.145	0.129	0.131	0.125	0.129	0.132	0.124	0.135
C03 SH04	0.165	0.195	0.158	0.153	0.182	0.200	0.190	0.180	0.179	0.168	0.167	0.176	0.162	0.172
C03 SH05	0.205	0.256	0.199	0.194	0.251	0.281	0.276	0.246	0.252	0.230	0.236	0.211	0.224	0.217
C03 SH06	0.210	0.248	0.205	0.200	0.237	0.235	0.262	0.239	0.219	0.210	0.207	0.204	0.183	0.190
C03 SH07	0.293	0.320	0.281	0.273	0.322	0.329	0.349	0.304	0.289	0.256	0.262	0.272	0.255	0.255
C03 SH08	0.257	0.291	0.248	0.233	0.269	0.290	0.369	0.282	0.270	0.259	0.381	0.269	0.268	0.277
C03 SH09	0.212	0.242	0.207	0.203	0.245	0.251	0.259	0.227	0.216	0.198	0.213	0.210	0.193	0.184
C03 SH10	0.210	0.252	0.209	0.199	0.242	0.255	0.272	0.237	0.226	0.205	0.219	0.201	0.215	0.210
C03 SH11	0.181	0.211	0.170	0.163	0.199	0.221	0.216	0.195	0.196	0.171	0.184	0.174	0.161	0.186
C03 SH12	0.123	0.148	0.117	0.112	0.145	0.165	0.162	0.144	0.140	0.129	0.135	0.122	0.135	0.135
C03 SH13	0.132	0.162	0.129	0.128	0.156	0.184	0.175	0.161	0.151	0.146	0.142	0.161	0.146	0.148
C04 SH01	0.175	0.205	0.166	0.166	0.199	0.223	0.217	0.197	0.191	0.184	0.196	0.188	0.180	0.182
C04 SH02	0.135	0.171	0.143	0.138	0.169	0.171	0.186	0.170	0.154	0.147	0.146	0.118	0.142	0.155
C04 SH03	0.163	0.184	0.159	0.155	0.194	0.209	0.198	0.188	0.182	0.169	0.174	0.173	0.171	0.169
C04 SH04	0.149	0.160	0.142	0.137	0.163	0.195	0.200	0.184	0.174	0.171	0.178	0.178	0.183	0.190
C04 SH05	0.148	0.164	0.151	0.144	0.182	0.201	0.208	0.195	0.181	0.182	0.172	0.177	0.185	0.197
C04 SH06	0.118	0.129	0.117	0.113	0.148	0.158	0.157	0.171	0.167	0.150	0.149	0.173	0.170	0.184
C04 SH07	0.130	0.151	0.123	0.117	0.155	0.141	0.147	0.151	0.127	0.126	0.118	0.105	0.112	0.114
C04 SH08	0.134	0.154	0.131	0.122	0.158	0.152	0.190	0.149	0.157	0.148	0.141	0.111	0.144	0.147
C04 SH09	0.140	0.152	0.135	0.130	0.153	0.186	0.167	0.157	0.163	0.138	0.138	0.135	0.143	0.162
C04 SH10	0.203	0.225	0.205	0.194	0.247	0.272	0.257	0.232	0.228	0.204	0.217	0.210	0.189	0.204
C04 SH11	0.168	0.191	0.167	0.158	0.197	0.222	0.221	0.193	0.206	0.193	0.184	0.205	0.181	0.177
C04 MD01	0.153	0.177	0.150	0.139	0.172	0.165	0.173	0.166	0.166	0.153	0.147	0.153	0.152	0.153
C04 MD02	0.223	0.262	0.218	0.200	0.245	0.252	0.251	0.244	0.239	0.214	0.219	0.229	0.219	0.216
C04 MD03	0.156	0.183	0.152	0.139	0.173	0.174	0.175	0.159	0.164	0.147	0.142	0.153	0.153	0.157
C04 MD04	0.425	0.433	0.430	0.398	0.492	0.493	0.500	0.452	0.435	0.390	0.397	0.397	0.398	0.395
C04 MD05	0.274	0.303	0.269	0.245	0.308	0.314	0.304	0.272	0.267	0.250	0.253	0.255	0.256	0.267
C04 MD06	0.187	0.216	0.193	0.189	0.230	0.266	0.248	0.236	0.241	0.203	0.227	0.236	0.222	0.248
C04 MD07	0.149	0.170	0.155	0.148	0.188	0.212	0.212	0.203	0.191	0.173	0.185	0.194	0.177	0.217
C04 MD08	0.167	0.188	0.164	0.156	0.194	0.179	0.186	0.170	0.173	0.153	0.149	0.151	0.154	0.164
C04 MD09	0.181	0.196	0.176	0.164	0.205	0.196	0.198	0.188	0.178	0.159	0.162	0.163	0.177	0.168
C04 MD10	0.208	0.227	0.200	0.187	0.227	0.224	0.229	0.214	0.208	0.184	0.191	0.189	0.189	0.190
C04 MD11	0.230	0.255	0.224	0.208	0.249	0.241	0.240	0.231	0.232	0.212	0.204	0.221	0.204	0.211
C04 DP01	0.133	0.155	0.132	0.128	0.160	0.204	0.182	0.172	0.164	0.156	0.154	0.177	0.166	0.181
C04 DP02	0.236	0.283	0.238	0.219	0.280	0.340	0.303	0.289	0.278	0.258	0.279	0.289	0.300	0.305
C04 DP03	0.182	0.208	0.180	0.166	0.212	0.227	0.220	0.211	0.202	0.195	0.197	0.186	0.202	0.211
C04 DP04	0.275	0.305	0.261	0.240	0.295	0.299	0.296	0.276	0.271	0.254	0.256	0.265	0.257	0.264
C04 DP05	0.235	0.275	0.234	0.222	0.274	0.310	0.297	0.284	0.285	0.269	0.283	0.268	0.292	0.315
C04 DP06	0.240	0.275	0.240	0.221	0.259	0.311	0.307	0.305	0.294	0.269	0.262	0.305	0.284	0.299
C04 DP07	0.193	0.218	0.188	0.181	0.223	0.261	0.237	0.228	0.237	0.227	0.219	0.232	0.234	0.261
C04 DP08	0.291	0.321	0.284	0.262	0.313	0.299	0.314	0.290	0.276	0.248	0.249	0.257	0.259	0.265
C04 DP09	0.213	0.238	0.214	0.204	0.257	0.277	0.266	0.259	0.247	0.231	0.248	0.249	0.256	0.270
C04 DP10	0.261	0.288	0.252	0.234	0.282	0.279	0.273	0.260	0.257	0.226	0.229	0.245	0.241	0.246
C04 DP11	0.211	0.239	0.209	0.200	0.245	0.275	0.259	0.265	0.256	0.225	0.236	0.243	0.251	0.273
C04 DP12	0.109	0.140	0.123	0.120	0.170	0.179	0.186	0.160	0.151	0.127	0.125	0.127	0.136	0.136
C05 SH01	0.200	0.220	0.201	0.191	0.252	0.260	0.261	0.250	0.250	0.226	0.231	0.236	0.250	0.243
C05 SH02	0.181	0.203	0.186	0.177	0.222	0.267	0.259	0.231	0.228	0.221	0.219	0.232	0.235	0.235
C05 SH03	0.207	0.230	0.211	0.199	0.251	0.256	0.278	0.272	0.264	0.244	0.243	0.265	0.245	0.251
C05 SH04	0.215	0.245	0.214	0.208	0.253	0.275	0.300	0.280	0.262	0.245	0.230	0.272	0.265	0.281
C05 SH05	0.188	0.225	0.198	0.189	0.245	0.281	0.272	0.247	0.236	0.229	0.232	0.240	0.245	0.254
C05 SH06	0.176	0.202	0.180	0.174	0.213	0.242	0.250	0.235	0.235	0.210	0.224	0.233	0.222	0.246
C05 SH07	0.117	0.131	0.122	0.114	0.151	0.178	0.169	0.158	0.161	0.149	0.150	0.169	0.171	0.169
C05 SH08	0.102	0.111	0.103	0.099	0.146	0.153	0.152	0.136	0.129	0.129	0.146	0.138	0.150	0.167
C05 SH09	0.114	0.123	0.116	0.109	0.147	0.165	0.169	0.152	0.149	0.141	0.148	0.152	0.158	0.162

Sample	La PAAS	Ce PAAS	Pr PAAS	Nd PAAS	Sm PAAS	Eu PAAS	Gd PAAS	Tb PAAS	Dy PAAS	Ho PAAS	Er PAAS	Tm PAAS	Yb PAAS	Lu PAAS
C05 SH10	0.147	0.164	0.156	0.150	0.198	0.210	0.198	0.194	0.187	0.175	0.179	0.185	0.201	0.209
C05 SH11	0.122	0.143	0.131	0.127	0.167	0.190	0.186	0.170	0.166	0.158	0.163	0.179	0.169	0.179
C05 SH12	0.167	0.189	0.168	0.161	0.220	0.240	0.222	0.220	0.233	0.199	0.211	0.226	0.212	0.242
C05 SH13	0.159	0.185	0.164	0.159	0.208	0.237	0.229	0.225	0.214	0.203	0.210	0.203	0.217	0.237
C07 SH01	0.245	0.242	0.239	0.235	0.287	0.326	0.322	0.286	0.279	0.254	0.247	0.248	0.235	0.230
C07 SH02	0.227	0.237	0.225	0.222	0.282	0.324	0.322	0.288	0.276	0.254	0.251	0.257	0.240	0.235
C07 SH03	0.153	0.161	0.153	0.151	0.195	0.221	0.218	0.191	0.190	0.175	0.170	0.172	0.163	0.157
C07 SH04	0.170	0.168	0.167	0.163	0.204	0.230	0.231	0.204	0.202	0.188	0.179	0.179	0.171	0.168
C07 SH05	0.144	0.150	0.142	0.140	0.178	0.194	0.197	0.173	0.171	0.156	0.153	0.150	0.145	0.143
C07 SH06	0.209	0.219	0.206	0.202	0.255	0.284	0.289	0.251	0.248	0.227	0.221	0.223	0.203	0.209
C07 SH07	0.191	0.196	0.183	0.175	0.214	0.228	0.234	0.203	0.197	0.179	0.173	0.169	0.163	0.159
C07 SH08	0.180	0.183	0.177	0.171	0.208	0.219	0.220	0.194	0.189	0.172	0.164	0.167	0.157	0.157
C07 SH09	0.196	0.202	0.191	0.180	0.221	0.232	0.255	0.212	0.206	0.187	0.191	0.195	0.186	0.179
C07 SH10	0.226	0.229	0.219	0.208	0.251	0.265	0.275	0.235	0.233	0.211	0.206	0.205	0.195	0.192
C07 SH11	0.208	0.205	0.206	0.197	0.245	0.259	0.264	0.234	0.230	0.214	0.204	0.214	0.196	0.189

10.3.5. SCS-W

Sample	La PAAS	Ce PAAS	Pr PAAS	Nd PAAS	Sm PAAS	Eu PAAS	Gd PAAS	Tb PAAS	Dy PAAS	Ho PAAS	Er PAAS	Tm PAAS	Yb PAAS	Lu PAAS
W02 SH01	0.390	0.369	0.377	0.373	0.440	0.504	0.448	0.402	0.379	0.350	0.336	0.351	0.332	0.326
W02 SH02	0.462	0.440	0.449	0.443	0.520	0.591	0.522	0.472	0.444	0.408	0.389	0.403	0.382	0.373
W02 SH05	0.509	0.488	0.495	0.483	0.563	0.622	0.564	0.513	0.481	0.437	0.421	0.447	0.418	0.408
W02 SH06	0.349	0.336	0.342	0.336	0.396	0.444	0.398	0.356	0.331	0.304	0.291	0.306	0.288	0.285
W02 SH07	0.413	0.393	0.404	0.398	0.468	0.526	0.472	0.419	0.387	0.356	0.342	0.354	0.332	0.328
W02 SH08	0.554	0.531	0.542	0.531	0.621	0.685	0.623	0.549	0.511	0.467	0.448	0.467	0.437	0.431
W02 SH09	0.534	0.511	0.520	0.511	0.595	0.670	0.599	0.538	0.501	0.462	0.443	0.457	0.432	0.426
W02 SH10	0.339	0.311	0.328	0.328	0.392	0.454	0.408	0.365	0.344	0.320	0.303	0.323	0.297	0.298
W02 SH11	0.307	0.287	0.298	0.295	0.352	0.414	0.364	0.327	0.309	0.288	0.276	0.290	0.272	0.268
W02 SH12	0.294	0.284	0.286	0.283	0.343	0.417	0.355	0.322	0.301	0.280	0.268	0.281	0.269	0.269
W02 SH13	0.208	0.200	0.204	0.204	0.253	0.324	0.274	0.247	0.236	0.222	0.213	0.221	0.208	0.208
W02 SH14	0.186	0.168	0.180	0.181	0.225	0.293	0.247	0.224	0.214	0.202	0.194	0.202	0.190	0.192
W02 SH15	0.189	0.175	0.183	0.184	0.228	0.292	0.246	0.224	0.214	0.200	0.193	0.201	0.189	0.193
W02 SH16	0.210	0.195	0.204	0.202	0.246	0.309	0.262	0.239	0.227	0.212	0.206	0.213	0.203	0.205

10.3.6. SCS-SC

No data

10.3.7. SCS-SW

Sample	La PAAS	Ce PAAS	Pr PAAS	Nd PAAS	Sm PAAS	Eu PAAS	Gd PAAS	Tb PAAS	Dy PAAS	Ho PAAS	Er PAAS	Tm PAAS	Yb PAAS	Lu PAAS
SW01 SH01	0.659	0.651	0.642	0.604	0.702	0.680	0.686	0.601	0.579	0.504	0.503	0.506	0.495	0.463
SW01 SH02	0.507	0.509	0.494	0.466	0.543	0.544	0.549	0.479	0.461	0.414	0.403	0.411	0.388	0.377
SW01 SH03	0.419	0.424	0.409	0.386	0.450	0.444	0.448	0.396	0.383	0.337	0.330	0.340	0.329	0.308
SW01 SH04	0.656	0.660	0.642	0.606	0.702	0.683	0.689	0.619	0.584	0.506	0.491	0.503	0.482	0.459
SW01 SH05	0.592	0.590	0.575	0.546	0.628	0.619	0.631	0.556	0.539	0.473	0.473	0.473	0.442	0.424
SW01 SH06	0.780	0.773	0.758	0.710	0.815	0.799	0.821	0.703	0.679	0.593	0.568	0.584	0.631	0.527
SW01 SH07	0.873	0.869	0.854	0.804	0.930	0.912	0.910	0.787	0.753	0.656	0.654	0.667	0.655	0.603
SW01 SH08	0.927	0.925	0.910	0.857	0.996	0.975	0.961	0.835	0.796	0.695	0.689	0.713	0.684	0.639
SW01 SH09	0.493	0.492	0.480	0.455	0.530	0.525	0.534	0.484	0.453	0.400	0.390	0.395	0.390	0.367
SW01 SH10	0.247	0.248	0.240	0.228	0.269	0.271	0.276	0.243	0.237	0.210	0.207	0.204	0.199	0.186

10.3.8. SCS-S

Sample	La PAAS	Ce PAAS	Pr PAAS	Nd PAAS	Sm PAAS	Eu PAAS	Gd PAAS	Tb PAAS	Dy PAAS	Ho PAAS	Er PAAS	Tm PAAS	Yb PAAS	Lu PAAS
S01 SH03	0.399	0.404	0.405	0.375	0.432	0.445	0.438	0.372	0.335	0.301	0.289	0.300	0.285	0.268
S01 SH04	0.345	0.347	0.350	0.324	0.375	0.382	0.373	0.324	0.290	0.266	0.263	0.262	0.256	0.245
S01 SH08	0.942	0.929	0.964	0.892	1.006	1.018	0.975	0.845	0.743	0.660	0.628	0.650	0.627	0.588
S01 SH12	0.458	0.452	0.462	0.429	0.491	0.454	0.482	0.417	0.371	0.335	0.324	0.340	0.331	0.318

Changes of clay mineral and trace element characteristics in the Deep South China Sea

S01 SH17	0.806	0.797	0.820	0.756	0.861	0.873	0.846	0.754	0.675	0.605	0.582	0.602	0.576	0.538
S01 SH18	7.032	7.506	8.122	6.133	7.498	4.751	7.267	6.542	6.006	5.436	5.380	5.831	5.801	5.705
S01 SH18	0.822	0.816	0.839	0.760	0.870	0.557	0.858	0.740	0.662	0.599	0.581	0.599	0.576	0.518
S01 SH19	0.774	0.761	0.787	0.716	0.816	0.835	0.800	0.705	0.637	0.571	0.546	0.566	0.544	0.514

10.4. Element ratios

10.4.1. SCS-N

Sample	LREE	MREE	HREE	Eu*	La/Lu	LREE/HREE	Zr/10	Zr/Sc
N01 SH05	1.874	1.887	1.911	1.062	1.633	0.981	4.153	
N01 SH06	2.523	2.446	3.097	1.035	1.424	0.815	6.794	
N01 SH06	2.112	2.217	2.320	1.072	1.514	0.911	4.386	
N01 SH07	1.130	1.226	1.320	1.053	1.387	0.856	2.153	
N01 SH08	1.572	1.770	2.234	1.001	1.209	0.704	3.937	
N01 SH08	0.722	0.844	0.952	1.075	1.290	0.759	1.588	
N01 SH09	0.966	0.999	1.382	0.993	1.103	0.699	2.990	
N01 SH09	0.539	0.675	0.814	1.100	1.083	0.663	1.429	
N01 SH10	0.851	0.960	1.321	1.081	1.003	0.645	2.735	
N01 SH10	0.615	0.785	0.883	1.134	1.153	0.697	1.140	
N01 SH11	1.565	1.519	2.305	1.051	0.956	0.679	5.689	
N01 SH11	0.679	0.826	0.966	1.108	1.157	0.702	1.461	
N01 SH12	0.601	0.733	0.848	1.082	1.147	0.709	1.258	
N01 DP02	1.993	2.079	2.586	1.021	1.234	0.771	5.467	
N01 DP03	1.979	2.192	2.752	0.964	1.151	0.719	5.280	
N01 DP04	2.425	2.842	4.084	1.095	0.916	0.594	14.224	
N01 DP05	2.739	3.084	4.373	1.022	0.994	0.626	12.196	
N01 DP05	1.559	1.740	1.807	1.078	1.426	0.863	2.932	
N01 DP06	2.569	2.697	3.245	1.064	1.279	0.792	6.929	
N01 DP06	1.983	2.181	2.267	1.068	1.439	0.875	3.597	
N01 DP07	0.893	1.056	1.114	1.086	1.315	0.802	1.560	
N01 DP10	2.899	2.671	3.271	1.035	1.614	0.886	7.640	
N01 DP11	0.735	0.867	1.055	1.099	1.060	0.696	1.884	
N01 DP12	1.551	1.738	2.391	0.984	1.015	0.649	4.522	
N02 DP02	1.809	1.878	2.224	1.134	1.304	0.813	4.691	
N02 DP03	2.523	2.822	3.480	1.032	1.190	0.725	7.866	
N02 DP04	2.104	2.267	2.886	0.997	1.250	0.729	5.862	
N02 DP05	1.343	1.590	1.784	1.076	1.212	0.753	2.699	
N02 DP06	1.200	1.411	1.634	1.066	1.189	0.735	2.475	
N02 DP07	1.438	1.650	1.793	1.056	1.297	0.802	2.651	
N03 SH01	0.872	1.201	1.443	1.244	0.968	0.604	1.925	4.916
N03 SH02	0.999	1.326	1.539	1.231	1.048	0.649	2.076	4.530
N03 SH03	1.023	1.334	1.548	1.223	1.072	0.661	2.141	4.698
N03 SH04	0.584	0.810	0.983	1.240	0.937	0.593	1.389	5.234
N03 SH05	0.793	1.116	1.316	1.266	0.963	0.603	1.659	4.539
N03 SH06	0.887	1.197	1.380	1.237	1.037	0.643	1.715	4.336
N03 SH08	0.715	0.965	1.193	1.234	0.945	0.599	1.666	4.322
N03 SH09	1.323	1.618	1.892	1.168	1.128	0.699	2.981	4.625
N03 SH10	2.000	2.307	2.538	1.134	1.280	0.788	4.150	4.771
N03 SH11	0.885	1.147	1.425	1.199	0.964	0.621	2.104	3.899
N03 SH12	1.202	1.522	1.874	1.193	0.995	0.641	2.980	4.010
N03 SH13	1.096	1.412	1.586	1.225	1.091	0.691	2.892	4.768
N03 SH14	0.469	0.688	0.896	1.254	0.792	0.524	1.266	4.038
N03 Sh15	0.702	1.037	1.337	1.261	0.805	0.525	1.879	3.690
N03 SH16	0.801	1.133	1.394	1.265	0.897	0.575	1.796	3.424
N03 SH17	1.299	1.638	1.903	1.192	1.064	0.682	3.069	4.326
N03 SH18	2.049	2.332	2.705	1.135	1.210	0.757	4.555	4.622
N03 SH19	1.619	1.926	2.145	1.164	1.217	0.755	3.350	4.263
N03 SH20	1.155	1.408	1.543	1.196	1.196	0.749	2.097	3.479

Sample	LREE	MREE	HREE	Eu*	La/Lu	LREE/HREE	Zr/10	Zr/Sc
N03 MD02	1.201	1.589	1.854	1.213	1.021	0.648	2.581	4.520
N03 MD03	1.317	1.715	1.999	1.218	1.053	0.659	2.709	4.375
N03 MD04	0.958	1.314	1.610	1.242	0.928	0.595	2.176	4.362
N03 MD11	1.384	1.699	1.982	1.170	1.120	0.698	3.003	4.237
N03 MD13	1.545	1.911	2.231	1.188	1.101	0.692	3.323	4.177
N03 MD14	1.030	1.383	1.672	1.205	0.967	0.616	2.325	4.006
N03 MD15	1.186	1.589	1.918	1.232	0.964	0.618	2.737	3.860
N03 MD16	1.223	1.570	1.877	1.206	1.019	0.652	2.820	3.888
N03 MD17	1.562	2.001	2.370	1.213	1.037	0.659	3.594	4.120
N03 DP02	1.468	1.883	2.213	1.207	1.046	0.663	3.263	4.620
N03 DP03	1.535	1.969	2.273	1.208	1.053	0.676	3.112	4.159
N03 DP04	1.505	1.930	2.256	1.196	1.056	0.667	3.266	4.561
N03 MD10	1.461	1.881	2.251	1.204	1.003	0.649	3.407	4.348
N03 DP11	1.689	2.102	2.480	1.182	1.073	0.681	3.782	4.360
N03 DP12	1.455	1.806	2.139	1.188	1.070	0.680	3.309	4.156
N03 DP15	1.339	1.715	2.058	1.187	1.014	0.651	3.125	4.391
N03 DP16	1.374	1.786	2.113	1.211	1.015	0.650	3.050	3.882
N04 SH03	1.048	1.411	1.643	1.247	1.018	0.638	2.118	3.852
N04 SH04	1.172	1.540	1.765	1.252	1.055	0.664	2.358	3.932
N04 SH05	0.878	1.159	1.317	1.244	1.071	0.666	1.814	4.351
N04 SH06	0.888	1.224	1.430	1.265	0.985	0.621	1.758	4.014
N04 SH09	2.184	2.478	2.621	1.138	1.370	0.833	4.231	4.608
N04 SH10	1.068	1.275	1.426	1.152	1.172	0.749	2.149	4.191
N04 SH11	1.595	1.868	2.043	1.153	1.260	0.781	3.088	4.119
N04 SH17	1.208	1.496	1.714	1.161	1.124	0.705	2.609	4.271
N04 SH18	1.271	1.569	1.742	1.195	1.184	0.730	2.465	4.052
N04 SH19	1.225	1.531	1.805	1.179	1.098	0.679	2.805	4.775
N04 MD03	1.533	1.930	2.272	1.185	1.070	0.675	3.489	4.588
N04 MD04	1.521	1.945	2.334	1.196	1.033	0.652	3.498	4.604
N04 MD05	1.334	1.714	2.018	1.192	1.043	0.661	2.790	4.219
N04 MD06	1.348	1.738	1.987	1.221	1.089	0.678	2.715	4.114
N04 MD18	1.530	1.875	2.121	1.165	1.175	0.721	3.140	4.442
N04 MD19	1.538	1.906	2.213	1.177	1.112	0.695	3.327	4.616
N04 DP03	1.634	2.037	2.374	1.194	1.092	0.688	3.609	4.371
N04 DP04	1.683	2.125	2.446	1.203	1.096	0.688	3.495	4.167
N04 DP05	1.401	1.775	2.046	1.207	1.096	0.685	2.890	4.031
N04 DP06	1.383	1.797	2.162	1.208	1.001	0.640	3.157	4.497
N04 DP18	1.617	1.988	2.300	1.164	1.122	0.703	3.642	4.885
N04 DP19	1.376	1.713	1.979	1.179	1.119	0.695	2.965	4.618

10.4.2. SCS-NE

Sample	LREE	MREE	HREE	Eu*	La/Lu	LREE/HREE	Zr/10	Zr/Sc
NE02 SH01	0.699	1.563	2.496	1.228	0.371	0.280	3.039	2.490
NE02 SH02	0.692	1.330	1.958	1.208	0.489	0.354	2.346	2.774
NE02 SH03	0.670	1.178	1.706	1.200	0.553	0.393	2.192	2.913
NE02 SH04	0.643	1.056	1.556	1.266	0.614	0.413	2.417	1.848
NE02 SH05	0.565	0.921	1.325	1.225	0.626	0.426	1.866	2.491
NE02 SH06	0.715	1.161	1.631	1.207	0.650	0.438	2.083	2.623
NE02 SH07	0.543	0.917	1.307	1.177	0.611	0.415	1.625	2.604
NE02 SH08	0.468	0.783	1.096	1.179	0.638	0.427	1.320	2.723
NE02 SH09	0.529	1.043	1.599	1.245	0.452	0.331	1.943	2.599
NE02 SH10	0.652	1.254	1.786	1.246	0.513	0.365	2.100	2.394
NE02 SH11	0.618	1.104	1.587	1.210	0.567	0.389	1.836	2.796
NE01 MD04	0.730	1.238	1.746	1.266	0.602	0.418	2.639	1.629
NE01 MD06	0.749	1.216	1.613	1.208	0.689	0.464	2.133	2.237
NE01 MD09	0.800	1.682	2.420	1.300	0.448	0.331	3.097	2.006
NE01 DP04	0.619	1.121	1.593	1.261	0.552	0.388	2.355	1.750
NE01 DP06	0.506	0.828	1.127	1.213	0.652	0.449	1.642	2.037

NE01 DP09	0.885	1.725	2.435	1.276	0.501	0.363	3.157	2.382

10.4.3. SCS-NC

Sample	LREE	MREE	HREE	Eu*	La/Lu	LREE/HREE	Zr/10	Zr/Sc
NC01 SH04	0.822	1.072	1.388	1.078	0.946	0.592	1.693	4.678

10.4.4. SCS-C

Sample	LREE	MREE	HREE	Eu*	La/Lu	LREE/HREE	Zr/10	Zr/Sc
C02 SH01	0.942	0.971	1.178	1.033	1.202	0.799	2.670	
C02 SH02	1.086	1.114	1.350	1.070	1.246	0.804	2.679	
C02 SH03	0.669	0.578	0.665	1.309	1.614	1.006	1.530	
C02 SH04	0.459	0.486	0.624	1.172	1.050	0.737	1.242	
C02 SH05	1.152	1.229	1.499	1.145	1.220	0.769	2.920	
C02 SH06	0.843	0.959	1.141	1.036	1.126	0.739	1.965	
C02 SH07	0.826	0.916	1.169	0.995	1.197	0.707	1.956	
C02 SH08	0.251	0.302	0.408	1.288	0.837	0.616	0.669	
C02 SH09	0.720	0.799	1.006	0.921	1.024	0.716	1.696	
C02 SH10	0.671	0.792	1.016	1.118	1.047	0.660	1.791	
C02 SH11	0.738	0.860	1.089	0.913	1.193	0.678	1.837	
C02 SH12	0.953	1.125	1.315	1.079	1.185	0.725	2.622	
C02 SH13	0.915	1.048	1.275	1.303	1.131	0.718	2.217	
C03 SH01	0.672	0.724	0.921	1.062	0.973	0.730	1.555	
C03 SH02	0.409	0.437	0.545	0.999	0.861	0.751	0.921	
C03 SH03	0.512	0.561	0.777	1.071	0.860	0.659	1.424	
C03 SH04	0.671	0.753	1.025	1.078	0.962	0.654	1.547	
C03 SH05	0.854	1.054	1.369	1.064	0.943	0.624	1.852	
C03 SH06	0.863	0.974	1.213	0.944	1.102	0.711	1.901	
C03 SH07	1.167	1.304	1.588	0.981	1.151	0.735	2.565	
C03 SH08	1.029	1.210	1.725	0.908	0.928	0.597	3.416	
C03 SH09	0.863	0.982	1.214	0.998	1.153	0.711	1.934	
C03 SH10	0.870	1.007	1.275	0.992	1.000	0.682	2.022	
C03 SH11	0.725	0.831	1.072	1.068	0.975	0.676	1.857	
C03 SH12	0.500	0.616	0.795	1.071	0.910	0.629	1.253	
C03 SH13	0.551	0.676	0.894	1.114	0.896	0.616	1.262	
C04 SH01	0.711	0.835	1.121	1.073	0.957	0.634	1.620	
C04 SH02	0.587	0.696	0.862	0.966	0.871	0.681	1.431	
C04 SH03	0.661	0.789	1.038	1.067	0.964	0.637	1.671	
C04 SH04	0.588	0.742	1.073	1.078	0.784	0.548	1.519	0.948
C04 SH05	0.607	0.787	1.094	1.029	0.751	0.555	1.543	0.881
C04 SH06	0.477	0.634	0.992	1.036	0.641	0.481	1.211	0.774
C04 SH07	0.521	0.594	0.702	0.933	1.141	0.742	1.164	
C04 SH08	0.541	0.649	0.849	0.875	0.911	0.637	1.313	
C04 SH09	0.556	0.662	0.880	1.161	0.861	0.632	1.344	
C04 SH10	0.827	1.008	1.251	1.077	0.997	0.661	1.966	
C04 SH11	0.684	0.834	1.146	1.060	0.950	0.597	1.581	
C04 MD01	0.619	0.675	0.923	0.957	1.002	0.670	1.258	4.771
C04 MD02	0.904	0.992	1.335	1.015	1.034	0.677	1.766	5.128
C04 MD03	0.629	0.680	0.916	0.999	0.992	0.687	1.278	5.193
C04 MD04	1.686	1.938	2.413	0.994	1.077	0.699	4.517	6.272
C04 MD05	1.092	1.199	1.548	1.026	1.028	0.706	2.379	4.565
C04 MD06	0.786	0.980	1.376	1.114	0.756	0.571	2.191	1.313
C04 MD07	0.621	0.816	1.137	1.061	0.688	0.546	1.614	0.965
C04 MD08	0.675	0.728	0.945	0.940	1.016	0.715	1.325	4.607
C04 MD09	0.717	0.786	1.008	0.972	1.081	0.712	1.444	4.684
C04 MD10	0.822	0.893	1.150	0.982	1.095	0.715	1.676	5.053
C04 MD11	0.916	0.961	1.284	0.987	1.088	0.713	1.796	5.414
C04 DP01	0.548	0.718	0.998	1.191	0.737	0.549	1.659	0.970
C04 DP02	0.975	1.212	1.708	1.163	0.775	0.571	2.980	1.689
C04 DP03	0.735	0.869	1.193	1.050	0.865	0.616	2.167	1.610

Sample	LREE	MREE	HREE	Eu*	La/Lu	LREE/HREE	Zr/10	Zr/Sc
C04 DP04	1.080	1.165	1.567	1.012	1.043	0.689	2.441	5.518
C04 DP05	0.967	1.166	1.713	1.086	0.745	0.565	3.247	1.612
C04 DP06	0.975	1.181	1.713	1.098	0.804	0.569	3.064	1.489
C04 DP07	0.780	0.948	1.410	1.134	0.739	0.553	2.346	1.410
C04 DP08	1.157	1.215	1.554	0.956	1.097	0.745	2.647	5.150
C04 DP09	0.870	1.060	1.500	1.060	0.790	0.580	2.601	1.567
C04 DP10	1.036	1.094	1.444	1.006	1.062	0.717	2.481	5.221
C04 DP11	0.859	1.044	1.484	1.091	0.773	0.579	2.560	1.389
C04 DP12	0.493	0.695	0.801	1.003	0.803	0.615	0.496	0.317
C05 SH01	0.812	1.024	1.435	1.013	0.823	0.566	2.100	1.392
C05 SH02	0.747	0.980	1.370	1.108	0.773	0.546	1.866	1.172
C05 SH03	0.847	1.058	1.512	0.967	0.824	0.560	2.096	1.205
C05 SH04	0.883	1.108	1.554	0.996	0.766	0.568	2.179	1.249
C05 SH05	0.800	1.045	1.437	1.087	0.741	0.557	2.016	1.037
C05 SH06	0.732	0.940	1.370	1.046	0.716	0.534	1.832	1.178
C05 SH07	0.482	0.656	0.968	1.109	0.688	0.498	1.224	0.878
C05 SH08	0.415	0.587	0.858	1.025	0.612	0.483	1.076	0.734
C05 SH09	0.462	0.634	0.910	1.043	0.701	0.508	1.207	0.921
C05 SH10	0.617	0.800	1.136	1.058	0.701	0.543	1.644	1.084
C05 SH11	0.523	0.713	1.014	1.076	0.685	0.516	1.341	0.962
C05 SH12	0.685	0.902	1.324	1.084	0.688	0.517	1.826	1.177
C05 SH13	0.667	0.898	1.284	1.084	0.671	0.519	1.848	0.943
C07 SH01	0.962	1.220	1.495	1.070	1.065	0.643	1.770	5.344
C07 SH02	0.910	1.215	1.511	1.074	0.967	0.602	1.679	5.240
C07 SH03	0.618	0.825	1.027	1.073	0.974	0.602	1.142	5.259
C07 SH04	0.668	0.870	1.088	1.057	1.008	0.614	1.226	5.064
C07 SH05	0.576	0.742	0.919	1.037	1.003	0.627	1.037	5.209
C07 SH06	0.836	1.080	1.332	1.044	0.999	0.628	1.477	5.508
C07 SH07	0.745	0.878	1.041	1.017	1.202	0.716	1.318	5.439
C07 SH08	0.711	0.841	1.006	1.022	1.147	0.707	1.305	5.375
C07 SH09	0.768	0.920	1.143	0.975	1.097	0.672	1.739	6.353
C07 SH10	0.883	1.026	1.243	1.010	1.175	0.710	1.688	5.496
C07 SH11	0.816	1.002	1.248	1.015	1.104	0.654	1.245	4.656

10.4.5. SCS-W

Sample	LREE	MREE	HREE	Eu*	La/Lu	LREE/HREE	Zr/10	Zr/Sc
W02 SH01	1.509	1.794	2.073	1.135	1.196	0.728	3.318	5.635
W02 SH02	1.794	2.106	2.398	1.135	1.240	0.748	3.875	5.621
W02 SH05	1.975	2.262	2.613	1.104	1.246	0.756	4.495	6.030
W02 SH06	1.363	1.593	1.806	1.119	1.227	0.755	2.922	5.681
W02 SH07	1.608	1.885	2.100	1.119	1.258	0.766	3.239	5.305
W02 SH08	2.158	2.478	2.761	1.102	1.285	0.782	4.624	5.808
W02 SH09	2.076	2.403	2.721	1.121	1.252	0.763	4.622	6.021
W02 SH10	1.305	1.618	1.885	1.134	1.137	0.693	2.751	5.524
W02 SH11	1.187	1.457	1.704	1.156	1.144	0.697	2.558	5.532
W02 SH12	1.147	1.436	1.669	1.194	1.096	0.687	2.487	5.284
W02 SH13	0.816	1.097	1.307	1.232	1.001	0.624	1.738	5.235
W02 SH14	0.715	0.990	1.195	1.240	0.971	0.599	1.449	4.777
W02 SH15	0.732	0.990	1.190	1.231	0.982	0.615	1.531	5.011
W02 SH16	0.811	1.057	1.267	1.216	1.021	0.640	1.799	5.300

10.4.6. SCS-SC

No data

10.4.7. SCS-SW

Sample	LREE	MREE	HREE	Eu*	La/Lu	LREE/HREE	Zr/10	Zr/Sc
SW01 SH01	2.556	2.669	3.050	0.979	1.425	0.838	2.408	3.176
SW01 SH02	1.975	2.115	2.454	0.996	1.346	0.805	1.539	2.658

SW01 SH03	1.637	1.738	2.027	0.988	1.362	0.808	1.517	3.010
SW01 SH04	2.563	2.692	3.025	0.981	1.427	0.847	4.733	6.272
SW01 SH05	2.304	2.433	2.823	0.983	1.398	0.816	4.909	6.478
SW01 SH06	3.021	3.139	3.581	0.977	1.481	0.844	6.421	6.942
SW01 SH07	3.400	3.538	3.988	0.991	1.447	0.852	6.952	7.947
SW01 SH08	3.619	3.767	4.217	0.996	1.451	0.858	7.288	7.521
SW01 SH09	1.920	2.073	2.395	0.987	1.344	0.802	3.891	6.437
SW01 SH10	0.964	1.060	1.245	0.995	1.326	0.774	1.837	5.476

10.4.8. SCS-S

Sample	LREE	MREE	HREE	Eu*	La/Lu	LREE/HREE	Zr/10	Zr/Sc
S01 SH03	1.583	1.688	1.778	1.024	1.488	0.890	3.119	
S01 SH04	1.365	1.454	1.582	1.021	1.409	0.863	2.750	
S01 SH08	3.726	3.843	3.895	1.027	1.602	0.957	8.908	
S01 SH12	1.801	1.844	2.019	0.935	1.437	0.892	8.017	
S01 SH17	3.179	3.335	3.578	1.023	1.497	0.888	8.094	
S01 SH18	28.793	26.058	34.160	0.644	1.233	0.843	72.312	
S01 SH18	9.795	33.044	30.878	36.078	8.388	8.330	8.563	7.762
S01 SH19	3.038	3.156	3.377	1.033	1.505	0.899	7.320	

10.5. Figures

10.6. Abbreviations

Abbreviation	Meaning
Amp	Amphibole
Ce	Cerium
Chl	Chlorite
Cpx	Clinopyroxene
Dy	Dysprosium
ENSO	El Niño Southern Oscillation
Er	Erbium
Eu	Europium
Eu*	Europium Anomaly
Gd	Gadolinium
Grt	Garnet
Ho	Holmium
HREE	Heavy Rare Earth Elements (Dy, Ho, Er, Tm, Yb, Lu)
Ill	Illite
Kao	Kaolinite
La	Lanthanum
LREE	Light Rare Earth Elements (La, Ce, Pr, Nd)
Lu	Lutetium
meq	Molecular equivalent
MREE	Middle Rare Earth Elements (Sm, Eu, Gd, Tb)
Nd	Neodymium
Opx	Orthopyroxene
Pr	Praesodymium
REE	Rare Earth Elements
Sc	Scandium
SCS	South China Sea
Sm	Samarium
Sm	Smectite (only in Tables)
SPM	sinking particulate matter
Tb	Terbium
Tm	Thulium
TSS	Total Suspended Solids
XRD	X-Ray Diffractography
Yb	Ytterbium
Zr	Zirconium

10.7.   Publications and Contributions

10.7.1. Publications

Date	Title	Platform
14.11.2012	'Recent trace element patterns in lithogenic matter in the SCS and what they tell about oceanography' Talk	Flused
13.11.2012	'Recent trace element patterns in lithogenic matter in the SCS and what they tell about oceanography' Poster	Flused
Sept. 2013	'Sources, transport and deposition of lithogenic matter in the South China Sea' Talk	GeoTübingen
12.02.2015	,SO-220 Leg 1 - Partikelfluss im nördlichen Südchinesischen Meer' Talk	Sonne workshop
Published (accepted: 01.08.2015)	'Fluxes of clay minerals in the South China Sea' A. Schröder, M. Wiesner, Z. Liu DOI: 10.1016/j.epsl.2015.08.001	Earth and Planetary Science Letters Issue: 430 Pages: 30-42
In preparation	'Regional diversity of geochemistry in the deep South China Sea' A. Schröder, D. Garbe-Schönberg, Z. Liu, M. Wiesner Manuscript	Marine Chemistry (intended)
In preparation	'ENSO-variations of trace elements in the northern SCS' A. Schröder, Z. Liu, M. Wiesner Manuscript	Deep Sea Research (intended)

10.7.2. Own contributions

- all clay mineral analyses except N01 and N02, with great support from Dr. Yanli Li.
- data management
- ArcGIS and Access database
- review of previous unpublished studies
- all texts except Chapters 4.1.1., 4.1.2 and parts of 2.4., which were written by Dr. Martin Wiesner
- all figures, including all GIS maps, unless cited else.

10.8.   Curriculum Vitae

Family name	Schröder
Maiden name	Heddaeus–Espenschied
Given name	Annette Cornelia
Date of birth	02. April 1985, Hamburg, Germany
Nationality	german
Family status	Married, 02.11.2013

Education

2013 January - 2015 August	Data management, evaluation, visualization, writing	University of Hamburg
2011 September - 2013 January	Admission PhD Tongji University, scientific, language and social studies, field- (SO-220) and laboratory work	Tongji University
2011 April - 2011 July	Admission Promotion Hamburg University, organization, administrative preparations, language and literature studies	University of Hamburg
2011 March	Graduation Diplom Geology-Paleontology Grade: ‚very good‘ (MSc)	
2010 October	Diplom Thesis part II, geological mapping: „Geologische Kartierung eines Abschnitts des nordwestlichen Ebbe Antiklinoriums (Rheinisches Schiefergebirge, Devon): Kartiergebiet Jubach-Talsperre (4811 Meinerzhagen)" (german, unpublished)	
2010 August	Diplom thesis part I „Rekonstruktion der Oberflächentemperatur des östlichen Mittelmeers zur Zeit des S1-Sapropels (Holozän) anhand des $U^{k'}_{37}$" (german, unpublished)	
2008 April – 2011 March	Geology-Palaeontology (Diplom)	University of Hamburg
2007 September - 2008 March	Geology (BSc/ MSc) ERASMUS Programm	Universidad de Granada, Spain
2007 September	Vordiplom: 1.4 (eq. BSc)	
2004 October - 2007 September	Geology-Paleontology (Diplom)	University of Hamburg
2004 June	Abitur: 2.1	

Conferences/Workshops:

January 2012	IODP	staff
March 2012	Intercoh	audience
September 2013	GeoTübingen 2013	Oral presentation
September 2014	Middle European Claymineral Conference	audience
February 2015	Sonne Workshop	Oral presentation

Practical experience:

2013 May - 2014 December	Input of geological data into the database of the agency for urban development and environment (BSU)	BGW (Office for applied geosciences)
2013 April - 2013 September 2014 April - 2014 September	Assistant teacher BSc mapping course Rheinisches Schiefergebirge	IfGeo
2010 November - 2010 December	anorganic laboratory, Dissolved Organic Material	IfBM
2009 April - 2010 May	anorganic laboratory TOC, C/N organic laboratory Alkenone - Analysis	IfBM
2009 April - 2009 July	Assistant teacher "Mathematics in geosciences" (Diplom/MSc)	IfBM
2009 January - 2009 February	MSM-10/3 Gas Chromatography dissolved gas in sea water	Research Vessel Maria S. Merian IfBM
2008 May - 2008 October	Input of well logs an lithology	RWE – Dea (Rheinwestfälische Energie)